ABSTRACT

Title of Document: INFLUENCE OF ANGLE OF INCIDENCE ON THE SEISMIC DEMANDS FOR INELASTIC STRUCTURES SUBJECTED TO BI-DIRECTIONAL GROUND MOTIONS

Antonio Bruno Rigato, Doctor of Philosophy, 2007

Directed By: Assistant Professor Ricardo A. Medina, Department of Civil Engineering and Environmental Engineering

This study investigated the influence that angle of incidence of applied bi-directional ground motions had on several engineering demand parameters (EDPs) for inelastic structures. The EDPs of interest in this study were peak drift, peak ductility, and peak slab rotation demands. The structural models had various degrees of inelasticity, plan irregularities, 5% damping ratios, and fundamental periods that ranged from 0.2 seconds to 2.0 seconds. This work utilized suites of ground motions recorded on stiff soils and on rock. The critical angle (the angle of incidence at which an EDP achieves a maximum) for a given EDP and bi-directional ground motion was found to occur at virtually any angle of incidence. For a given bi-directional ground motion and given fundamental period, the critical angle was found to vary unpredictably with increasing degree of inelasticity. The results also indicated that, on average, applying bi-directional ground motions only along the principal axes of an inelastic building

underestimated the peak deformation demands when compared to those obtained at other ground motion angles of incidence. For a given degree of inelasticity, the average ratio of peak deformation responses based on all angles of incidence to the peak deformation response when the ground motion components were applied along the principal building orientations increased with fundamental period of vibration. Specifically, the results from this study indicated that for small and moderate degrees of inelasticity, average values for maximum inelastic deformation demands relative to the principal orientation ranged from 1.1 to 1.8 (for fundamental periods ranging from 0.2 seconds to 2.0 seconds). In addition, the standard deviations of such ratios are typically on the order of 0.15 to 0.8 which can be approximated by the standard deviation of the spectral ground motion component ratios. In this context, spectral component ratios refer to the ratio of spectral horizontal component accelerations at the fundamental period of the structure. A statistical analysis of the results also demonstrated that these ratios of peak deformation demands are weakly dependent on moment magnitude and distance for ground motions and structural systems with characteristics consistent with those used in this study.

INFLUENCE OF ANGLE OF INCIDENCE ON THE SEISMIC DEMANDS FOR INELASTIC STRUCTURES SUBJECTED TO BI-DIRECTIONAL GROUND MOTIONS

By

Antonio Bruno Rigato

Dissertation submitted to the Faculty of the Graduate School of the
University of Maryland, College Park, in partial fulfillment
of the requirements for the degree of
Doctor of Philosophy
2007

Advisory Committee:
Assistant Professor Ricardo A. Medina, Chair
Research Professor Chung C. Fu
Professor Amde M. Amde
Professor Darryll J. Pines
Professor M. Sherif Aggour

Dedication

To my loving wife Melissa, and my parents Sergio and Lucia.

Acknowledgements

First and foremost, I sincerely thank Professor Ricardo A. Medina for all his technical help, advice, guidance and patience during these last few years which has culminated into this document. I greatly appreciate his effort.

I would also like to thank the committee members and fellow office mates Ragu Sankaranarayanan and Kyungha Park for their comments, suggestions and support throughout the Ph.D. process.

In addition, I thank all the teachers, friends, and relatives who have supported and encouraged me throughout the years.

List of Tables

List of Figures

Chapter 1 Introduction

For structures that consider seismic loads in the design process, one of the challenges that the designer faces is the lack of prior knowledge regarding the direction at which these seismic loads will occur. Because of uncertainty in the estimation of local site conditions as well as uncertainties in the location of the epicenter and the wave propagation characteristics of the next seismic event, it is reasonable to assume that the seismic loads from a future seismic event can be applied at any direction relative to the structure in question. Given these uncertainties, the critical angle of incidence (critical angle), i.e., the angle at which the structural response achieves a maximum for a given seismic demand parameter, becomes of interest to the engineer. To accommodate these directional effects, several combination rules such as the 30%-100%, 40%-100% and other methods such as SRSS methods have been developed and allow the engineer to conduct an analysis based primarily on horizontal components of ground motion that are applied such that they coincide with the principal building orientations. While these rules have various pros such as ease of use, and cons such as not always producing conservative results as previous work has illustrated (Wilson, Suhawardy, and Habibullah 1995; MacRae Mattheis 2000), they are used extensively in practice. A major limitation of these methods is that, strictly speaking, they are confined to elastic analyses even if it is widely believed that structures can be expected to behave inelastically during a major seismic event.

MOTIVATION AND OBJECTIVE

Many of the combination rules are based on seismic components (2 lateral and one vertical) which are cross-correlated; however, according to Penzien and Watabe (Penzien and Watabe 1975) a set of principal axes at which these components can be considered uncorrelated for a given time interval exists. Much of the earliest work toward the determination of the critical angle has laid its foundations upon this model, and the use of the response spectrum method that utilizes responses corresponding to these principal axes. While more accurate procedures exist for determining the critical response for the elastic case (Athanatopoulou 2005), that provide the critical angle of response based on the results of a time-history analysis conducted for each individual component of the ground motion, methods such as the 30%-100% combination rules are still widely used, but similar methods are lacking with regards to the inelastic case.

In addition, the majority of studies that examine torsional effects induced by non-co-centric locations of mass, strength and rigidity, often do so with seismic loads applied along the principal building orientations. These two angles, i.e., 0^{o} and 90^{o}, are the angles of incidence traditionally used to evaluate seismic demand parameters (Goel 1997; Tso and Smith 1999; Humar and Kumar 1999; Fajfar 2005). It is still unclear as to how much of a role angle of incidence has on the estimation of demands for asymmetric structures with varying degrees of inelasticity and fundamental periods of vibration. Given that a significant portion of damage experienced by asymmetric structures is believed to be caused by torsion (Tso and Smith 1999; Aziminejad and Moghadam 2005) and the relatively small amount of information known with regards to angle of incidence for inelastic structures, the need for systematic studies that address the influence of angle of incidence, ground motion input, structural configuration (location of center of strength, mass and rigidity), and fundamental period for the *inelastic* response of structures is apparent. The purpose of this study was to examine the response of several engineering demand parameters (EDPs) observed for several asymmetric and symmetric structures with various structural configurations subjected to ground motion inputs which had varying angles of incidence. More specifically, it was hypothesized that the critical response for an inelastic structure was not obtained when the ground motions were applied along the principal orientations. The quantification of maximum demands relative to the principal building orientation was also a focus of this study because this quantification provides a measure of how much inaccuracy was introduced into the analysis (if any) when the analysis was based solely on this orientation.

PREVIOUS RESEARCH ON ANGLE OF INCIDENCE

This section provides a more comprehensive summary of previous research work on the evaluation of critical angle and torsional demands brought on by seismic loads. Work regarding angle of incidence was summarized first, followed by work that dealt primarily with torsional demands.

As stated in the previous section, Penzien and Watabe (Penzien and Watabe 1975) found that an orthogonal set of principal directions for three seismic components (2 lateral and one vertical) exists in which components are not correlated with respect to time. Some of the earliest work which dealt with building orientation and an inelastic structure by Franklin and Volker (Franklin and Volker 1982), briefly highlighted the underestimation of seismic loads for an inelastic time history using one ground motion, which was applied at the principal building orientations and at one additional angle of incidence. Wilson and Button (Wilson and Button 1982) proposed an approach that utilized the response spectrum method to calculate the critical angle and the resulting critical response. This method was limited in that it did not account for the correlation of the seismic components if they were to be applied along the principal orientation of the structure, which did not necessarily coincide with the principal directions of the ground motion itself (Lopez and Torres 1997).

Wilson et al. (Wilson E.L., Suhawardy I. and Habibullah A. 1995) in an effort to display the shortcomings of the 30%-100% and 40%-100% combination rules improved upon this earlier method. In this paper, the author provided a closed-form solution to determine the critical angle of response for an elastic, asymmetric structure for seismic loads that were based on a ground motion spectrum that described both components of the ground motion that were assumed to be statistically independent. The proposed formula did not depend on angle of incidence when the two seismic component inputs had the same spectra, nor did it depend on the ratio of the spectral components if the second component was a fraction of the primary one.

Fernandez-Davila et al. (Fernandez-Davilla I., Cominetti S. and Cruz E.F 2000) compared different methodologies such as the 30%-100% combination rule and

SRSS method in determining the maximum response of an elastic 5-storey structure when one and two seismic components of ground motion were applied at various angles of incidence. Their results also demonstrated that the SRSS and 30%-100% combination rule can underestimate the maximum response. MacRae and Mattheis (MacRae and Mattheis 2000) investigated the effect of angle of incidence on seismic demands of a multi-storey steel structure exposed to near-fault ground motions with one degree of inelasticity, and negligible torsion. This work also provided some shortcomings of the 30%-100%, 40%-100% and absolute combination rules and the SRSS method. Khoshnoudian & Poursha (Khoshnoudian & Poursha 2004) examined 5-storey structures and evaluated the elastic and inelastic response of these structures. They found that the angle at which the maximum inelastic response occurs for a given ground motion was not necessarily the same angle at which the maximum elastic response occurs. As mentioned previously, Athanatopoulou (Athanatopoulou 2005) provided a closed form solution for the critical angle of response based on the results of a time-history analysis conducted for each individual component of the ground motion that was independent of the correlation of ground motion components.

With regards to torsion, several researchers (Tso and Smith 1999; Ghersi and Rossi 2001) have investigated the capability of various code provisions to minimize seismic demands in torsionally unbalanced structures (TUB). These studies examined single-storey structures with various configurations of structural elements which acted in series or in parallel, with varying locations of mass, strength, and stiffness. The ground motions utilized in these studies generally consisted of a relatively small set of orthogonal horizontal seismic components pairs applied only along the principal axes of the structure (Tso and Smith 1999; Ghersi and Rossi 2001; Goel 1997). Tezcan and Alhan (Tezcan and Alhan 2001) considered angle of incidence in their study of torsional effects and examined three additional orientations beyond the principal building orientations for a 5-storey structure, with one degree of inelasticity. Other orientations at which these ground motions could be applied were not a focus of these studies, nor was the dependence of seismic demands on the degree of inelasticity of the building.

Now that the problem and objective of this work have been introduced, the rest of this work is briefly outlined as follows: Chapter 2 explains the methodology, describes the single-storey base case model (TUB1) which allows for torsional effects as well as all additional models examined, and details the ground motion sets utilized. Seismic demand evaluation of drift, ductilities, and slab rotation demands for model (TUB1) and model TB (a single storey model that does not have torsional effects) are examined in Chapter 3. In addition, the effect of ground motion frequency content on the critical response was examined as well as looking at ductility demands that occur at a given angle of incidence vs. the demands that occur at a principal building orientation from a performance based design point of view. Evaluation of the sensitivity of the response to mass, plan irregularity (such as off-center strength and stiffness), and number of stories was the focus of Chapter 4. Chapter 5 examines the statistical correlation of various parameters such as fundamental period to the seismic demands observed in the previous chapters in an effort to determine which of these parameters contributes to the increase or decrease of maximum response relative to the principal building orientation, and to quantify the scatter observed in the results.

Finally, Chapter 6 provides a summary of the main conclusions obtained from this work.

Chapter 2 Structural Models, Methodology, and Ground Motions

INTRODUCTION

With the intent of determining how parameters such as center of strength (CS), center of rigidity (CR), center of mass (CM), and frequency content affect the response of EDPs as a function of angle of incidence, a description of the models that were used to facilitate any difference in response due to these entities was first detailed. Specifically, four single-storey structures and a 3-storey structure were described, along with the general methodology used to quantify seismic demands. The section that follows described the characteristics of the ground motions to which the models were subjected to, and lastly, the EDPs used throughout this work were defined. While this section does not have any specific conclusions or observations that contribute directly to the objective of this work, it does summarize all the models and ground motions for easy reference.

DESCRIPTION OF THE BASE CASE MODEL, TUB1 AND TUB1*

The base case model to which all other models in this work were developed from, was a single-storey structure as shown in Figure 2.1. This was an asymmetric structure with off-centered mass equal to 14.4 kips in weight with co-centric centers of strength and rigidity located at the geometric center of the roof. The location of the center of mass was chosen as to induce torsion in the structure at any angle of incidence. Columns 1 through 4 had the same stiffness and were modeled in the computer program SAP2000 (Computers and Structures Inc., 2007). The column stiffness of the structures was tuned to achieve fundamental periods (seconds) of 0.2 s, 0.3 s, 0.4 s, 0.5 s, 1.0 s and 2.0 s and the columns were assumed to have had negligible mass. The roof was modeled as a rigid diaphragm with columns that were fixed at their base. Inelasticity was modeled by plastic hinges, located at the column ends characterized with a bi-linear hysteretic behavior with 3% post yield strain hardening. With regards to damping, 5% was assumed for the 1st and 3rd modes. The remaining models detailed in this work and their relationship to the base case are shown schematically in Figure 2.2.

Model TUB1* differs from model TUB1 in that the amount of mass in the model was thirty times that of model TUB1, and also had much stiffer columns and larger column plastic moments for a given fundamental period. This model was generated to investigate the effect that a larger mass had on critical response. As a comparison of models utilized in previous work, the model used by Lopez and Torres (Lopez and Torres 1997) was a four columned single-storey structure with rectangular plan, and with less mass than that of TUB1* but greater than that of model TUB1, with dimensions that were typically larger, but with a smaller moment arm to induce torsion.

STRUCTURAL MODEL WITHOUT TORSION (TB)

The first in a series of significantly differently configured models with respect to the TUB1 model was the TB model. This single-storey structure illustrated in

Figure 2.3 differs from the TUB1 model in that it had co-centric centers of strength, rigidity, and mass. Schematically, it resembled the TUB1 model with the exception that the off-centered mass was placed at the geometric center of the structure at roof level rather than an offset location with mass equal to 14.4 kips in weight, and was meant to represent a structure that had negligible torsional effects. Similarly to the TUB1 model, 5% damping was assumed for the 1st and 3rd modes and inelasticity was modeled by plastic hinges, located at the column ends which had bi-linear behavior with 3% post yield strain hardening. Like model TUB1, Columns 1-4 all had the same stiffness; however, they were more flexible than their TUB1 counterparts for a given fundamental period. Regarding fundamental periods, the same periods as per the TUB1 models were examined: 0.2 s, 0.3 s, 0.4 s, 0.5 s, 1.0 s and 2.0 s. Like the TUB1 model, a rigid diaphragm assumption of the roof was utilized.

STRUCTURAL MODEL WITH OFFSET STRENGTH AND RIGIDITY (TUB2)

The 3rd of four single-storey structures detailed in this work was model TUB2 which had co-centric centers of strength and rigidity offset relative to the center off mass, which was located at the geometric center of the roof as illustrated in Figure 2.4. The weight in the model equaled 14.4 kips and had also been placed at roof level. A rigid diaphragm assumption of the roof was utilized. The locations of strength and rigidity had been placed at this location so that the moment arm that induces torsion was similar to the TUB3 model (detailed below) but with a different structural configuration. All columns had the same plastic moment capacity; however, one row of columns (Columns 3 and 4) has had its plastic moments slightly increased about one axis to shift the center of strength. The center of rigidity was shifted similarly by having the stiffness of one row of columns (Columns 3 and 4) increased in one direction such that the fundamental period of 0.2 s 1.0 s and 2.0 s were achieved. Similarly to the TUB1 and TB models, 5% damping was assumed for the 1st and 3rd modes and inelasticity was modeled by plastic hinges located at the column ends with a bi-linear hysteretic behavior with 3% post yield strain hardening.

STRUCTURAL MODEL WITH A 'BALANCED CONDITION' (TUB3)

The last single-storey structure model examined in this work that also considered torsional effects via offset strength and rigidity rather than mass, was model TUB3 displayed in Figure 2.5. This model exhibited the configuration used by Tso and Smith (Tso and Smith 1999; Myslmaj and Tso 2001; Myslimaj and Tso 2005) with regards to the "balanced condition". That is, the configuration where the center of strength lies on one side with respect to the center of mass, and the center of rigidity lies on the opposing side of the center of mass and rigidity. The balanced condition is a configuration in which torsional effects should be reduced according to Tso and Smith and Myslmaj and Tso (Tso and Smith 1999; Myslmaj and Tso 2001; Myslimaj and Tso 2005), when compared to a mass-strength-rigidity configuration such as that of model TUB2. Like the TUB2 model, the TUB3 model had plastic moment values assigned to hinges for a particular direction, rather than the same value assigned to both X&Y directions for all columns. Since non co-centric centers of strength and stiffness were desired, plastic moments for the more flexible column line (columns 3-4) were increased in the Y-direction (moments about the X-axis) until the configuration of mass strength and rigidity in Figure 2.5 was achieved. Fundamental periods of 0.2 s, 1.0 s and 2.0 s were examined utilizing 5% damping for the first and 3^{rd} modes, and inelasticity modeled by plastic hinges, located at the column ends with bi-linear hysteretic behavior with 3% post yield strain hardening.

3-STOREY STRUCTURAL MODEL

While the majority of this work dealt with the single-storey structures, this model intended to provide preliminary quantification of the effect that multiple stories had with regards to critical angle. Since the configuration of a multi-storey structure can vary greatly, and a comparison to a single-storey structure previously outlined was desired, the configuration of the 3-storey model shown in Figure 2.6 was modeled similarly to the TUB1 model. In this model, each floor had the same amount of mass equal to 14.4 kips worth in weight, which was equal to the amount of mass used in models TUB1, TB, TUB2 and TUB3. On a per floor basis, this mass was offset at the same location as the TUB1 model. The plastic hinges in this model were located near column ends as per previous models and had bi-linear hysteretic behavior with 3% post yield strain hardening and 5% damping for the 1st and 3^{rd} modes. Fundamental periods of 1.0 s and 2.0 s were examined. Slab rotations, ductilities, and drift demands were calculated on a per floor basis.

Distribution of Lateral Strength

Thus far, the general characteristics of the structural models have been discussed, but there has been little discussion as to how plastic moments values were assigned. These plastic moment values were calculated via the modal response spectrum analysis procedure in the IBC 2006 (ICC 2006). Equivalent lateral forces based on modal properties of the structure and the design spectrum shown in Figure 2.7 were calculated and then applied to the center of mass of the structure in a separate linear elastic static analysis. For this calculation only the first two modes were considered, for they corresponded to a cumulative mass participation of at least 90% as stated in article 1618.2 of the IBC. The equations used in determining the value assigned to the plastic hinges are as follows:

Modal base shear:

$$V_m = C_{sm}.\overline{W}_m \tag{2.1}$$

Where

V_m = The total design lateral force or shear at the base in the mth mode

$\overline{W}_m$ = The effective modal gravity

C_{sm} = Model seismic coefficient defined by:

$$C_{sm} = \frac{S_{am}}{\frac{R}{I_E}} \tag{2.2}$$

With:

S_{am} = Modal design spectral response acceleration at period T_m

I_E = Occupancy importance factor which was set to 1.0 throughout this study

R = Response modification factor, similar to R_d in this study and elaborated in the following sections.

Once C_{sm} has been determined and substituted into equation 2.1, the modal force was determined via equation 16-55 of the IBC:

$$F_{xm} = C_{vxm} V_m \tag{2.3}$$

Where:

C_{vxm} = The vertical distribution factor in the mth mode defined by equation 16-56 of the IBC:

$$C_{vxm} = \frac{w_x \phi_{xm}}{\sum_{i=1}^{n} w_i \phi_{im}} \tag{2.4}$$

Where:

w_i , w_x = The portion of the total gravity load of the building, W, located or assigned to level i or x

and:

ϕ_{im} = The displacement amplitude at the ith level of the building when vibrating in its mth mode

ϕ_{xm} = The displacement amplitude at the xth level of the building when vibrating in its mth mode

Solving 2.3 via 2.4 and 2.1 yielded the modal forces to be applied at the center of mass of the structure. Since modal forces along the X-direction and Y- direction could be positive or negative, all combinations of these forces were applied along the

X and Y axis as to induce the maximum moment demands in the columns. The maximum moment observed in this linear elastic static analysis at any plastic hinge location was the value assigned as the plastic moment to all hinges on a per floor basis for all models with the exception of models TUB2 and TUB3 were which modified slightly as described previously. The design spectrum used for all models in this work which yields S_{am} at T_m of interest in the above equations was for a location along coastal California and is illustrated in Figure 2.7.

Quantification of Global Strength

Unless explicitly stated, all the models used in this work had plastic moments determined in the preceding paragraphs pertaining to a relative design intensity (R_d) value equal to one. The parameter R_d was defined by the ratio of the ground motion intensity to the design lateral force (V_d) in the structure divided by the weight of the structure (W):

$$R_d = \frac{\frac{S_a(T_1)}{g}}{\frac{V_d}{W}} \qquad (2.5)$$

As mentioned previously, R_d as defined above was the variable used in place of R in equation 2.2. In the analysis process, all records were scaled to the same pseudo-spectral acceleration at the first mode period of the structure, $S_a(T_1)/g$. To produce various inelastic results from the aforementioned models, a fraction of the plastic moment value relative to $R_d = 1$ was used during inelastic analyses. R_d values of 1, 2, 4 and 6 were used for all models for each fundamental period of interest. For instance, $R_d = 2$ indicates that the plastic moment in the model will only need to be half of the value required for $R_d = 1$. In addition, an elastic case (i.e., with infinitely strong columns) was created for all models and for each fundamental period examined. Results from the elastic case were used to quantify how the critical response changed with angle of incidence and degree of inelasticity and helped explain certain phenomena such as the decrease of inelastic slab rotations relative to elastic slab rotations explained in subsequent chapters. For all models, the effects of gravity load moments, P-M interaction, soil interaction and P-delta were not taken into consideration.

ANALYSIS METHODOLOGY

In an effort to determine the angle of incidence at which the EDPs detailed in the following section achieve a maximum for a given ground motion, time history analyses using ground motion pairs of orthogonal components were conducted at increasing 5^o increments counter clockwise relative to the X-axis of the structure (see Figure 2.1). The seismic loads were applied between 0^o and 180^o since the remaining orientations from 185^o to 360^o produced duplicate values due to symmetry. The results at 180^o were identical to those produced at 0^o but were included for completeness. Thus, a total of 37 orientations were considered per ground motion pair. With regards to quantities recorded during the time history analyses, ductility, slab rotations, drift, displacements, axial forces, moments and shear forces were recorded.

Engineering Demand Parameters

The common engineering demand parameters examined in this study were column displacement ductility ratios, slab rotations, and column drift ratios. In this context, column displacement ductility ratio (ductility) was defined as the displacement observed at the top of the column normalized by its yield displacement which provides a measure of structural damage. Column drift ratios (drift) were defined as the displacement observed at the top of the column normalized by the column height and provide an additional measure of structural damage as well as a measure of nonstructural damage. Slab rotations indicate the degree of torsion experienced by the structure. With respect to ductility, the maximum ductility (upper bound value) observed at any particular column and the average ductility of all columns for a particular direction such as in the X or Y was utilized. Average ductility was considered to be a global measure of damage. Graphical representations of the EDPs are shown in Figure 2.8.

GROUND MOTION SCALING AND FREQUENCY CONTENT

With regards to ground motion record scaling for a given ground motion pair, one of the two components was classified as either being a major component or a minor component based on its peak ground acceleration (PGA) value. The one with the highest PGA was considered to be the major component, while the other was labeled as the minor component. Where the grey lines are individual records and the black line was their mean, Figure 2.9 is an example of the major component scaled to a $S_a(T_1)/g$ value of 1.0 at 0.5 s as per the design spectrum of Figure 2.7. However, this definition did not ensure that the $S_a(T_1)/g$ value of the major component was larger than that of the minor component. For instance, at 0.5 s, 7 of the 39 records had larger $S_a(T_1)/g$ values for the minor component than for the major component as shown in Figure 2.10. It was also noted from Figures 2.9 and 2.10 that for periods away from $S_a(T_1)/g$, $S_a(T)/g$ varies greatly, and contributes a great deal to the scatter of the results yet to be discussed. With the major and minor components scaled, the major component was applied at various angles of incidence, α, while the minor component was applied at an angle of $\alpha + 90^{o}$ with respect to the x-axis as shown in Figure 2.1.

Site Class D Ground Motions

The first set of ground motions described in this work to which all models were subjected to, consisted of 39 non-near fault ground motion records each with two horizontal components obtained from the PEER strong motion database (http://peer.berkeley.edu/smcat/). This suite of ground motions were recorded on stiff soil sites (NEHRP site class D) which were at least 13 km away from the fault rupture zone but occurred within 60 km of the site [15]. The ground motions had moment magnitudes between 6.5 and 6.9 and had similar frequency content (Medina 2002). Table 2.1 provides basic characteristics of the specific ground motions in this suite.

Site Class AB Ground Motions

The second set of ground motions which will aid in examining the influence that frequency content had on the critical response consists of 37 ground motion pairs recorded on NEHRP site class A and B (AB) and were also obtained from the PEER strong motion database. These ground motions had moment magnitudes between 5.7 and 7.3 and were recorded at least 9 km from the fault rupture zone on sites that are considered to be "rock". Table 2.2 provides additional information and summarizes the characteristics of these ground motions.

Near Fault Ground Motions

Preliminary investigations were done for a set of near-fault ground motions with 2 horizontal components. The set of near-fault ground motions is described in Table 2.3 and was labeled as the "nearby set" in the thesis of Nico Luco [Luco 2002]. All but three of the set of 75 ground motions were events that occurred in California and all ground motions were recorded on NEHRP site class C and D, and were typically recorded at distances less than 15.5 km from the fault rupture zone. For this set of records, the fault normal component was considered the major component, while the minor was considered the fault parallel component. Additional details can be found in Luco 2002.

SUMMARY

This chapter described the models, outlined the methodology, defined the EDPs used to characterize the influence of critical response, and described the ground motions used in this study. Four, single-storey structures (models TUB1, TB, TUB2 and TUB3) and a 3-storey structure were detailed, the assignment of lateral strength was outlined, and the definition of inelasticity used in these models was made. The

EDPs used throughout this work were defined as column displacement ductility ratios (ductility), slab rotations, and column drift ratios (drift). Three ground motions sets were also detailed and the scaling of their corresponding components of which two non-near-fault sets were used extensively (site D and site AB ground motions) was explained. The near-fault ground motion set described was used primarily for preliminary work on the effect that forward directivity ground motions had on the critical response for a given EDP.

Event	Year	Moment Magnitude	Station	Closest distance (km)	PGA (g) Major Component	PGA (g) Minor Component
Imperial Valley	1979	6.5	Calipatria Fire station	23.8	0.128	0.078
Imperial Valley	1979	6.5	Chihuahua	28.7	0.27	0.254
Imperial Valley	1979	6.5	Compuertas	32.6	0.186	0.147
Imperial Valley	1979	6.5	El Centro Array #1	15.5	0.139	0.134
Imperial Valley	1979	6.5	El Centro Array #12	18.2	0.143	0.116
Imperial Valley	1979	6.5	El Centro Array #13	21.9	0.139	0.117
Imperial Valley	1979	6.5	Niland Fire Station	35.9	0.109	0.069
Imperial Valley	1979	6.5	Plaster City	23.6	0.057	0.042
Imperial Valley	1979	6.5	Westmorland Fire Station	15.1	0.11	0.074
Loma Prieta	1989	6.9	Agnews State Hospital	28.2	0.172	0.159
Loma Prieta	1989	6.9	Capitola	14.5	0.529	0.443
Loma Prieta	1989	6.9	Gilroy Aray #3	14.4	0.555	0.367
Loma Prieta	1989	6.9	Gilroy Aray #4	16.1	0.417	0.212
Loma Prieta	1989	6.9	Gilroy Aray #7	24.2	0.323	0.226
Loma Prieta	1989	6.9	Hollister City Hall	28.2	0.247	0.215
Loma Prieta	1989	6.9	Hollister Differential Array	25.8	0.279	0.269
Loma Prieta	1989	6.9	Halls Valley	31.6	0.134	0.103
Loma Prieta	1989	6.9	Salinas - John & Work	32.6	0.112	0.091
Loma Prieta	1989	6.9	Palo Alto - SLAC Lab.	36.6	0.278	0.194
Loma Prieta	1989	6.9	Sunnyvale - Colton Ave.	28.8	0.209	0.207
Northridge	1994	6.7	LA - Centinela St.	30.9	0.465	0.322
Northridge	1994	6.7	Canoga Park - Topanga Can.	15.8	0.42	0.356
Northridge	1994	6.7	LA - N Faring Rd.	23.9	0.273	0.242
Northridge	1994	6.7	LA - FlectherDr.	29.5	0.24	0.162
Northridge	1994	6.7	Glendale - Las Palmas	25.4	0.357	0.206
Northridge	1994	6.7	LA - Holywood Stor FF	25.5	0.358	0.231
Northridge	1994	6.7	Lake Highes #1	36.3	0.087	0.077
Northridge	1994	6.7	Leona Valley #2	37.7	0.091	0.063
Northridge	1994	6.7	Leona Valley #6	38.5	0.178	0.131
Northridge	1994	6.7	La Crescenta - Newyork	22.3	0.178	0.159
Northridge	1994	6.7	LA - Pico & Sentous	32.7	0.186	0.103
Northridge	1994	6.7	Northridge - 17645 Saticoy St.	13.3	0.477	0.368
Northridge	1994	6.7	LA - Saturn st	30	0.474	0.439
Northridge	1994	6.7	LA - E Vernon Ave	39.3	0.153	0.12
San Fernando	1971	6.6	LA - Hollywood stor Lot	21.2	0.21	0.174
Superstition Hills	1987	6.7	Brawley	18.2	0.156	0.116
Superstition Hills	1987	6.7	El Cento Imp. Co. Cent	13.9	0.358	0.258
Superstition Hills	1987	6.7	Plaster City	21	0.186	0.121
Superstition Hills	1987	6.7	Westmorland Fire Station	13.3	0.211	0.172

Table 2.1 Site class D ground motion records

Event	Year	Moment Magnitude	Station	Closest distance (km)	PGA (g) Major Component	PGA (g) Minor Component
San Fernando	1971	6.6	Lake Hughes #4	19.6	0.192	0.153
San Fernando	1971	6.6	Lake Hughes #9	23.5	0.157	0.134
Morgan Hill	1984	6.2	Gilroy Array #1	16.2	0.098	0.069
Coyote Lake	1979	5.7	Gilroy Array #1	9.3	0.132	0.103
N. Palm Springs	1986	6	Silent Valley - Poppet Flat	25.8	0.139	0.113
N. Palm Springs	1986	6	Winchester, Bergman Ranch	57.6	0.093	0.07
N. Palm Springs	1986	6	Murrieta Hot Springs, Collings	63.3	0.053	0.049
N. Palm Springs	1986	6	Anza Fire Station	46.7	0.099	0.067
Whittier Narrows	1987	6	San Gabriel-E Grand Av	9	0.304	0.199
Loma Prieta	1989	6.9	Gilroy Array #1	11.2	0.473	0.411
Loma Prieta	1989	6.9	SAGO South - surface	34.7	0.073	0.067
Loma Prieta	1989	6.9	Monterey, City Hall	44.8	0.073	0.063
Loma Prieta	1989	6.9	South San Francisco, Sierra F	68.2	0.105	0.056
Loma Prieta	1989	6.9	San Francisco, Diamond Heig	77	0.113	0.098
Loma Prieta	1989	6.9	Piedmont, Piedmont Jr. High (	78.3	0.084	0.071
Loma Prieta	1989	6.9	San Francisco, Rincon Hill	79.7	0.092	0.078
Loma Prieta	1989	6.9	San Francisco, Pacific Height:	81.6	0.061	0.047
Loma Prieta	1989	6.9	San Francisco, Cliff House	84.4	0.108	0.075
Loma Prieta	1989	6.9	San Francisco, Telegraph Hill	82	0.077	0.036
Loma Prieta	1989	6.9	Point Bonita	88.6	0.072	0.071
Landers	1992	7.3	Twentynine Palms Park Maint	42.2	0.08	0.06
Landers	1992	7.3	Silent Valley, Poppet Flat	51.7	0.05	0.04
Landers	1992	7.3	Amboy	69.2	0.146	0.115
Northridge	1994	6.7	Vasquez Rocks Park	24.2	0.151	0.139
Northridge	1994	6.7	Lake Hughes #9	26.8	0.217	0.165
Northridge	1994	6.7	Los Angeles, Temple & Hope	32.3	0.184	0.126
Northridge	1994	6.7	Lake Hughes Array#4-Camp M	32.3	0.084	0.057
Northridge	1994	6.7	Mt Wilson, CIT Seismic Static	36.1	0.234	0.134
Northridge	1994	6.7	Los Angeles, City Terrace	37	0.316	0.263
Northridge	1994	6.7	Antelope Buttes	47.3	0.068	0.046
Northridge	1994	6.7	Leona Valley #3	37.8	0.106	0.084
Northridge	1994	6.7	L.A.- Wonderland Ave.	22.7	0.172	0.112
Northridge	1994	6.7	Mt. Baldy-Elementary School	71.5	0.08	0.07
Northridge	1994	6.7	San Gabriel-E. Grand Ave.	41.7	0.256	0.141
Northridge	1994	6.7	Sandberg-Bald Mtn.	43.4	0.098	0.091
Northridge	1994	6.7	Rancho Cucamonga-Deer Car	80	0.071	0.051
Northridge	1994	6.7	Littlerock-Brainard Can	46.9	0.072	0.06

Table 2.2 Site class AB ground motion records

Event	Year	Moment Magnitude	Station	Closest distance (km)
Imperial Valley	1940	7.0	El Centro Array #9	8.3
Park Field	1966	6.1	Cholame #5	5.3
Park Field	1966	6.1	Cholame #8	9.2
Imperial Valley	1979	6.5	Aeropuerto Mexicali	8.5
Imperial Valley	1979	6.5	Agrarias	12.9
Imperial Valley	1979	6.5	Bonds Corner	2.5
Imperial Valley	1979	6.5	Brawley Airport	8.5
Imperial Valley	1979	6.5	Calexico Fire Station	10.6
Imperial Valley	1979	6.5	EC County Center FF	7.6
Imperial Valley	1979	6.5	EC Meloland Overpass FF	0.5
Imperial Valley	1979	6.5	EL Centro Array #1	15.5
Imperial Valley	1979	6.5	EL Centro Array #4	4.2
Imperial Valley	1979	6.5	EL Centro Array #5	1
Imperial Valley	1979	6.5	EL Centro Array #6	1
Imperial Valley	1979	6.5	EL Centro Array #7	0.6
Imperial Valley	1979	6.5	EL Centro Array #8	3.8
Imperial Valley	1979	6.5	EL Centro Array #10	8.6
Imperial Valley	1979	6.5	EL Centro Array #11	12.6
Imperial Valley	1979	6.5	El Centro Differential Array	5.3
Imperial Valley	1979	6.5	Holtville Post Office	7.5
Imperial Valley	1979	6.5	SAHOP Casa Flores	11.1
Imperial Valley	1979	6.5	Westmorland Dire Sta	15.1
Coalinga	1983	6.4	Pleasant Valley P.P. - bldg	8.5
Coalinga	1983	6.4	Pleasant Valley P.P. - yard	8.5
Morgan Hill	1984	6.2	Golroy Array #2	15.1
Morgan Hill	1984	6.2	Golroy Array #3	14.6
Morgan Hill	1984	6.2	Golroy Array #4	12.8
Morgan Hill	1984	6.2	Golroy Array #7	14.0
Morgan Hill	1984	6.2	Halls Valey	3.4
Whittier Narrows	1987	6.0	Bell Gardens - Jaboneria	9.8
Whittier Narrows	1987	6.0	LA - E Vernon Ave #	10.8
Whittier Narrows	1987	6.0	La Habra - Briarcliff #	13.5
Whittier Narrows	1987	6.0	West Covina - S Orange #	10.5
Superstition	1987	6.7	EL Centro Imp. Co. Cent	13.9
Superstition	1987	6.7	Westmorland Fire Sta	13.3
Loma Prieta	1989	6.9	Capitola	14.5
Loma Prieta	1989	6.9	Gilroy - Historic Bldg	12.7
Loma Prieta	1989	6.9	Gilroy Array #2	12.7
Loma Prieta	1989	6.9	Gilroy Array #3	14.4
Erzikan	1992	6.9	Erzincan	2.0
Northridge	1994	6.7	Canoga Park - Tapanga Can	15.8
Northridge	1994	6.7	Canyon County - W Lost Cany	13.0
Northridge	1994	6.7	Jensen Filter Plant #	6.2
Northridge	1994	6.7	Newhall - Fire Sta #	7.1
Northridge	1994	6.7	Northridge - 17645 Saticoy St	13.3
Northridge	1994	6.7	Rinaldi Receiving Station	7.1
Northridge	1994	6.7	Sepulveda VA #	8.9
Northridge	1994	6.7	Sun Valley - Roscoe Blvd	12.3
Northridge	1994	6.7	Sylmar - Converter Sta #	6.2
Northridge	1994	6.7	Sylmar - Converter Sta East #	6.1
Northridge	1994	6.7	Sylmar - Olive View Med FF#	6.4
Park Field	1966	6.1	Cholane #12	14.7

Table 2.3 Near-fault ground motions

Event	Year	Moment Magnitude	Station	Closest distance (km)
Park Field	1966	6.1	Temblor pre-1969	9.9
Santa Barbara	1978	6.0	Santa Barbara Courthouse	14.0 *
Imperial Valley	1979	6.5	Parachute Test Site	14.2
Morgan Hill	1984	6.2	Anderson Dam (Downstream)	2.6
Morgan Hill	1984	6.2	Gilroy Array #6	11.8
Palm Springs	1986	6.0	Fun Valley	15.8
Palm Springs	1986	6.0	Morongo Valley	10.1
Palm Springs	1986	6.0	North Palm Springs	8.2
Whittier Narrows	1987	6.0	Garvey Res. - Control Bldg	12.1
Superstition	1987	6.7	Parachute Test Site	0.7
Loma Prieta	1989	6.9	Corralitos	5.1
Loma Prieta	1989	6.9	Gilroy - Gavillan Coll.	11.6
Loma Prieta	1989	6.9	Saratoga - Aloha Ave	13.0
Loma Prieta	1989	6.9	Saratoga - W Valley Coll.	13.7
Landers	1992	7.3	Josua Tree #	11.6
Northridge	1994	6.7	Arleta - Nordhoff Fire Sta #	9.2
Northridge	1994	6.7	LA- UCLA Grounds	14.9
Northridge	1994	6.7	N. Hollywood-Coldwater Can	14.6
Northridge	1994	6.7	Newhall- W. Pico Canyon Rd.	7.1
Northridge	1994	6.7	Pacoima Dam (downstr) #	8
Northridge	1994	6.7	Pacoima Kagel Canyon #	8.2
Kobe	1995	6.9	KJMA	0.6
Tabas	1978	7.4	Tabas	3.0*

* Hypocentral Distance

Table 2.3 Near-fault ground motions continued

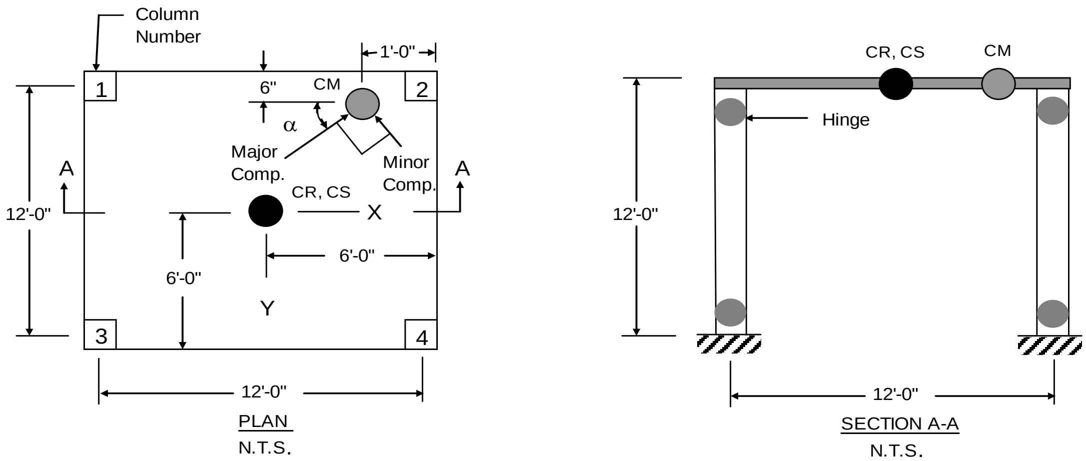

Figure 2.1 Schematic of the base case model TUB1 and TUB1*

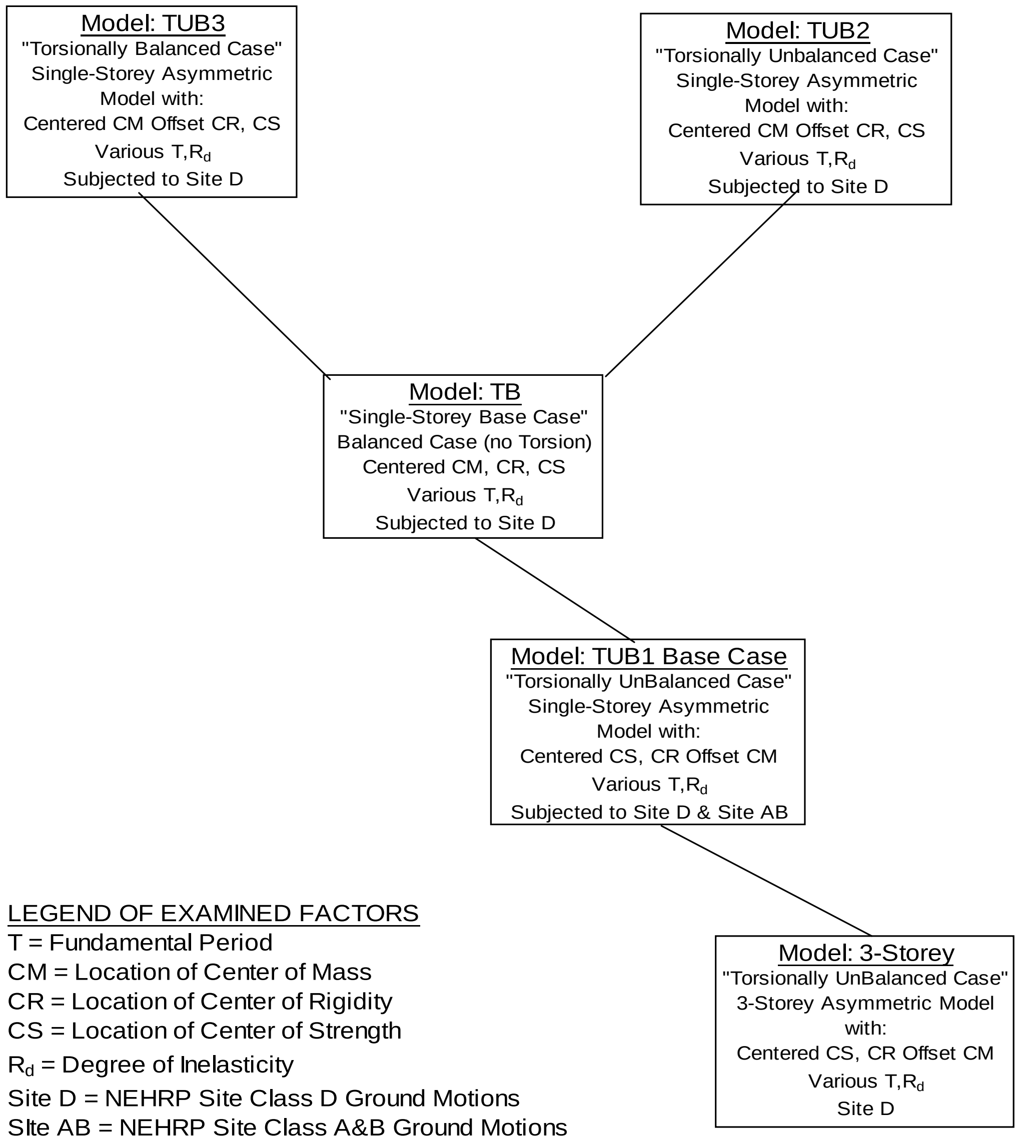

Figure 2.2 Relationship of base case model to other models examined.

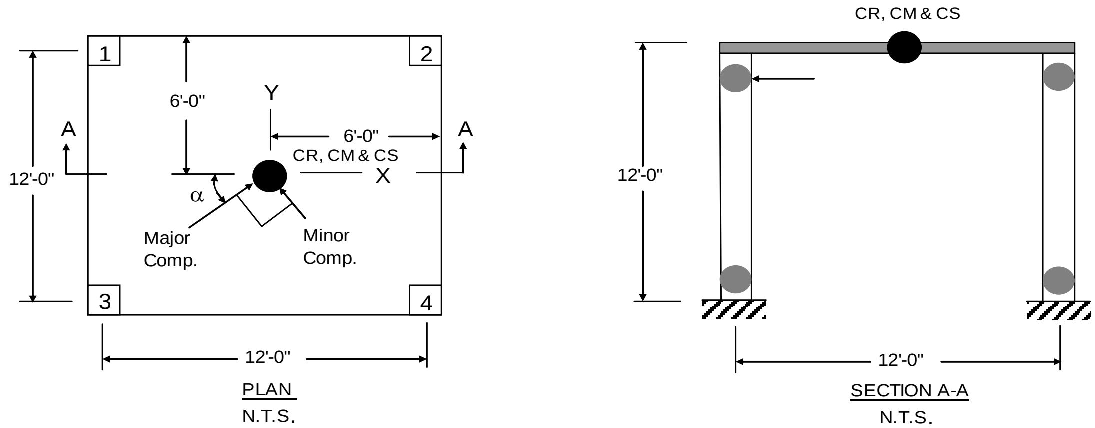

Figure 2.3 Schematic of model TB

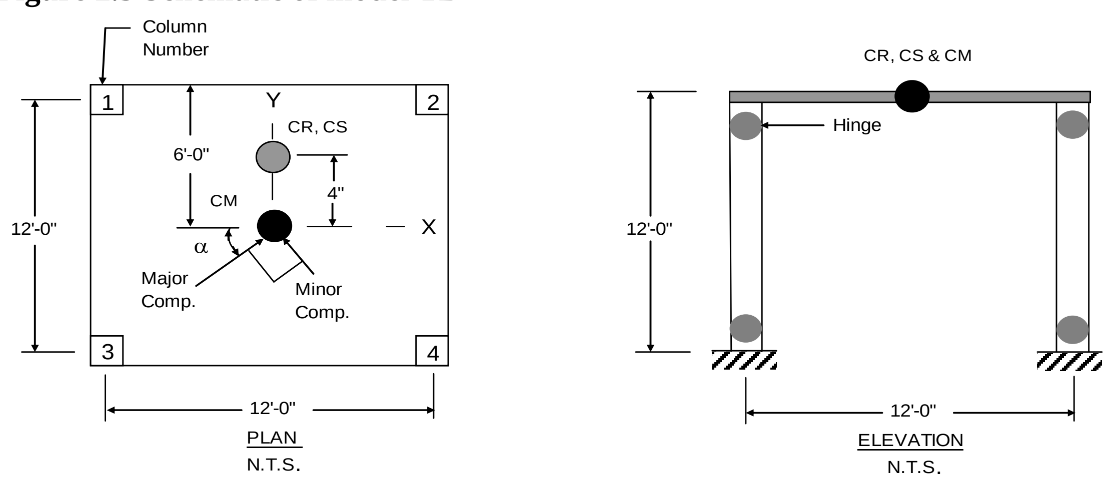

Figure 2.4 Schematic of model TUB2

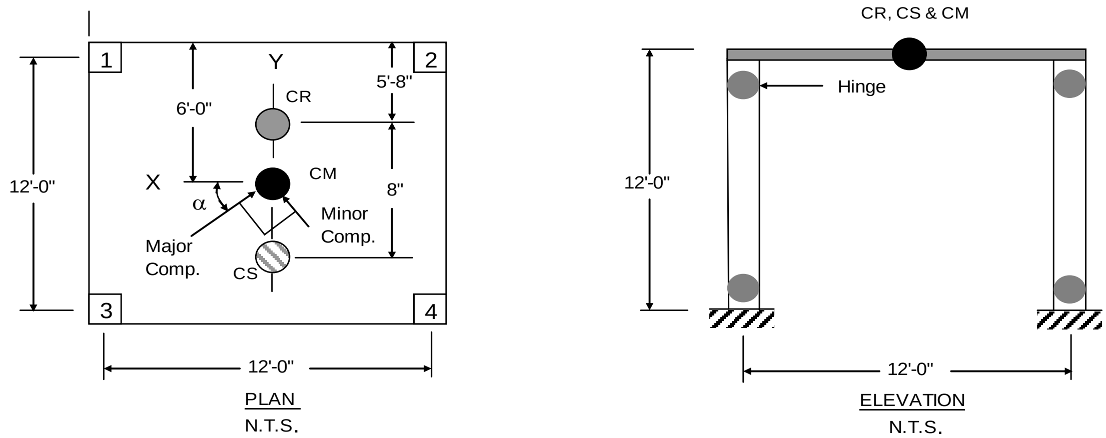

Figure 2.5 Schematic of model TUB3

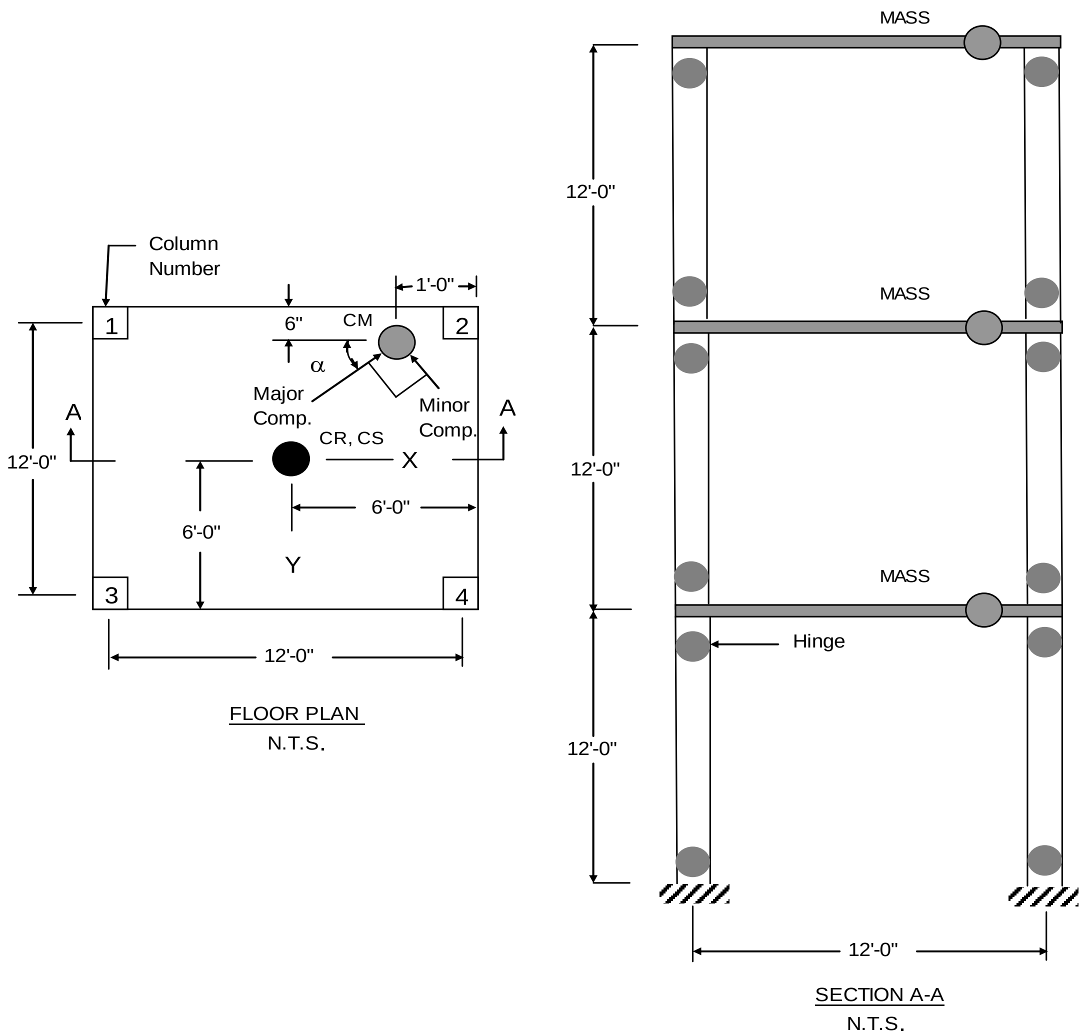

Figure 2.6 Schematic of the 3-storey structure

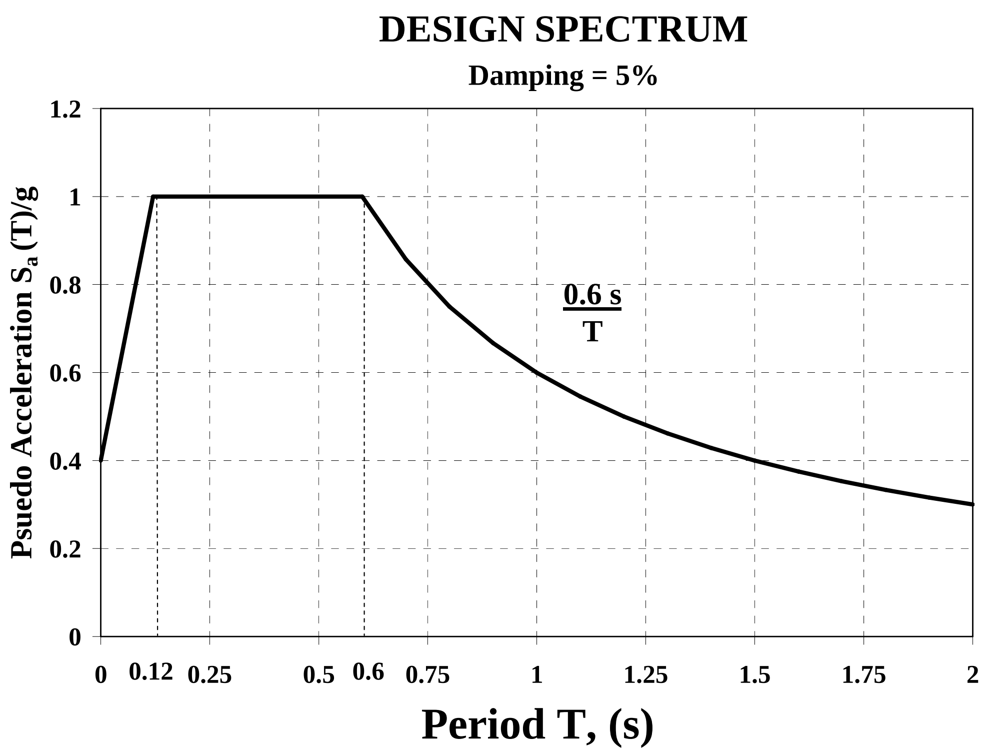

Figure 2.7 Design spectrum for a costal site in California

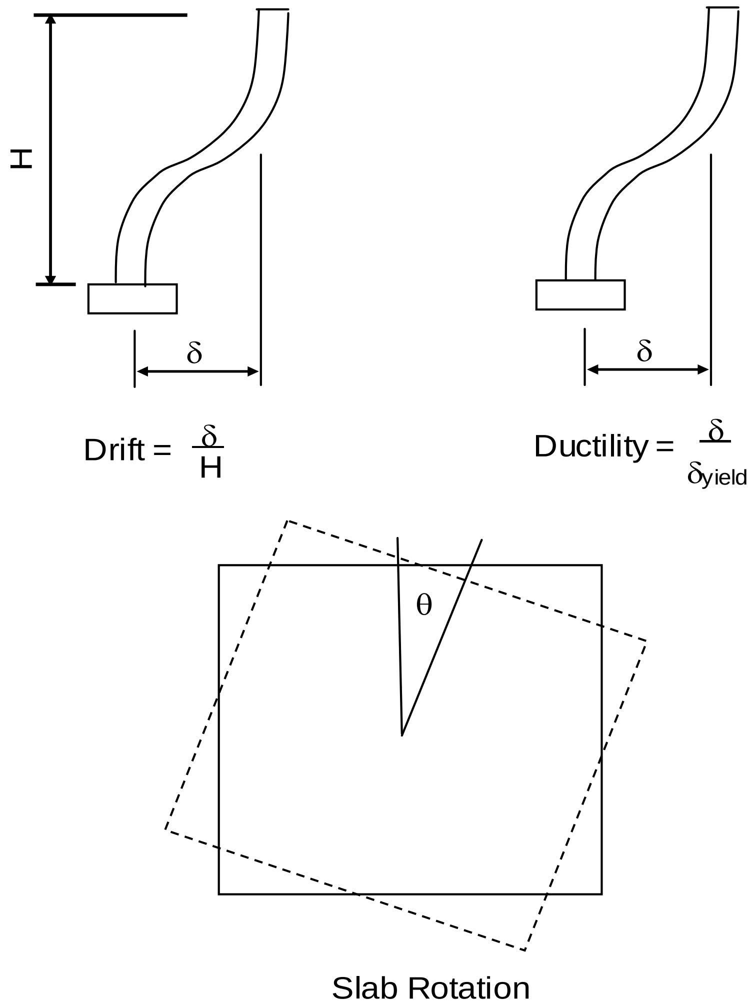

Figure 2.8 Graphical representations of engineering demand parameters (EDPs) used in this study.

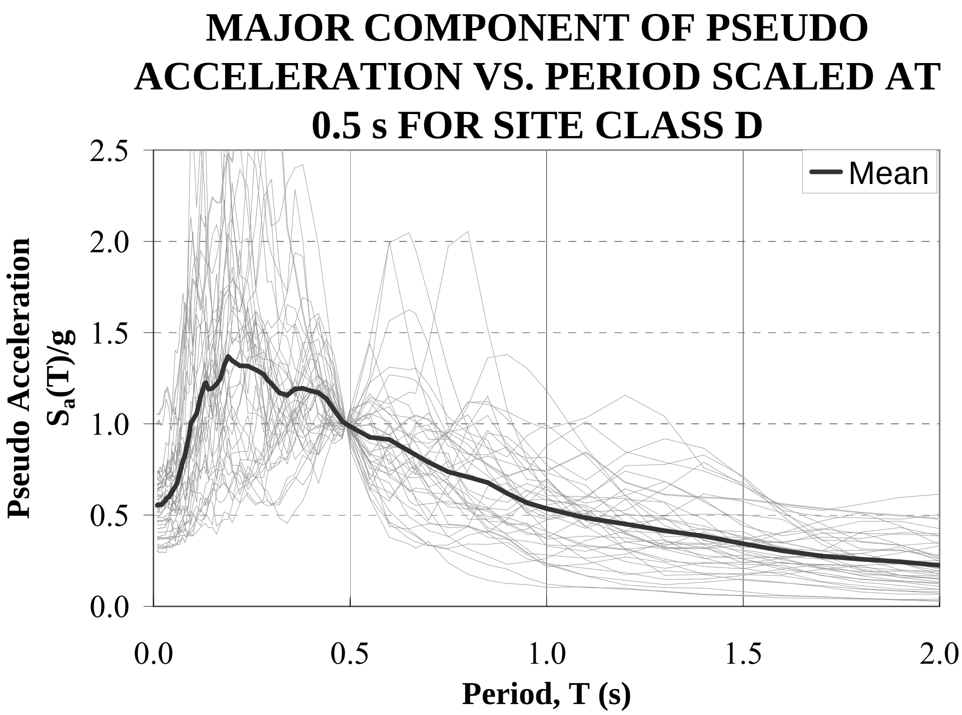

Figure 2.9 Scaled response spectra of major component at 0.5 s

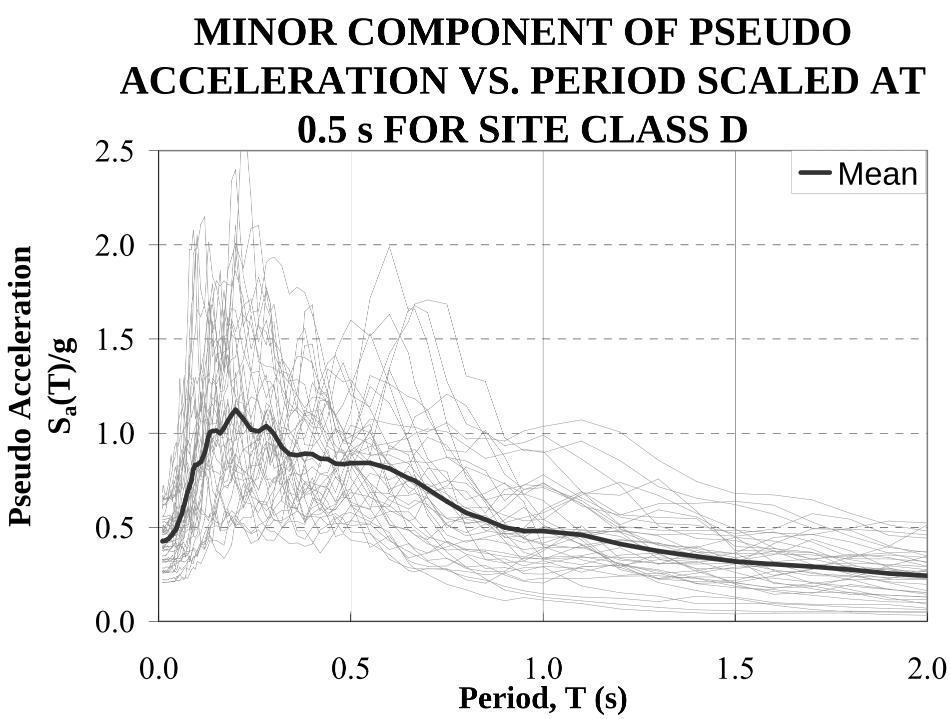

Figure 2.10 Scaled response spectra of minor component at 0.5 s

Chapter 3 Critical Response and its Dependence on Angle of Incidence, Torsion, and Ground Motion Frequency Content

INTRODUCTION

This chapter is the first of several that provided results regarding critical angle. Critical angle of response was examined for models TUB1 and TB that were subjected to site class D ground motions. Any trends regarding the angle of incidence that could say, minimize of the response of all EDPs were examined, or that certain angles of incidence produced larger critical responses more often than others were sought. How critical angle varied for an individual ground motion with degree of inelasticity was also examined. The difference of ductility magnitudes of the individual responses at other angles of incidence with respect to the principal building orientation was examined. The impact that factors such as fundamental period and relative design intensity had on this difference was examined. A brief look at the effect that critical angle had on the quantification of fragility functions for structural systems exposed to bi-directional ground motions was also illustrated. Ratios of inelastic to elastic slab rotations for model TUB1 are plotted versus increasing period and degree of inelasticity in an effort to determine if any appreciable trends could be noted. The effect that frequency content had on critical angle via model TUB1 subjected to ground motion sets other than site class D were also examined and the results found were compared to site class D ground motions. A majority of the results that pertain to models TUB1 and TB subjected to site D ground motions contained in this chapter can be found in the work done by Rigato and Medina (Rigato and Medina 2005)

CRITICAL ANGLE AND SITE D GROUND MOTIONS FOR MODEL TUB1

Location of Critical Angle for Ductility and Drift Demands for Model TUB1

For individual ground motions, both ductility and drift demands were sensitive to the angle of incidence of the ground motion input. This is illustrated in Figure 3.1 where the grey lines correspond to ductility ratios in the X-direction for individual ground motion pairs and the black line represents the average of the ductility ratios in the X-direction for a given angle of incidence. In this example, Column 1 of model TUB1 with a fundamental period of 0.5 s and R_d = 6 was utilized. From this figure it was evident that certain individual responses appeared to be more sensitive to angle of incidence than others. In addition, for a given level of inelastic behavior, ductility demands were found to be a function of the angle of incidence; however, the angle of incidence did not affect average ductility by a significant amount. Here, the average ductility of all columns was defined as the sum of the individual column ductility ratios in one direction divided by four. In addition, column ductility ratios did not exhibit a maximum at 0^o or at 90^o for the majority of R_d values studied. These trends can be seen in Figure 3.2 which displays for a given R_d, the mean of the average ductility of all columns, and the upper bound of maximum ductility (Figure 3.3) of all columns in the X-direction, μ_x (X-ductility) for the 0.5 s TUB1 model as a function of angle of incidence.

An alternative way of illustrating the angle at which critical response was achieved by an individual record was by examining histograms of upper bound maximum ductility demands in both the X- and Y-directions, which are shown in Figure 3.4 and 3.5 for the TUB1 model with a period of 1.0 s. As illustrated in these figures, maximums occured at any angle. While histograms of critical angles quantified how many maximum responses occurred for a given angle, they did little to describe how the critical angle of an individual record varied with relative design intensity. Such a graph that depicted the change in critical angle relative to $R_d = 1$ for individual record is illustrated in Figures 3.6 and 3.7 for fundamental periods of 0.2 s and 1.0 s respectively. Specifically, Figures 3.6 and 3.7 plotted the difference in critical angle for ductility in Column 1 as a function of R_d, relative to the angle at which the maximum occurred for that record for $R_d = 1$. The plots also provide a standard deviation of these angles for each R_d value. The graphs indicated that an individual response may initially achieve a maximum value at say 45^o for $R_d = 1$, but then achieved a maximum at 70^o for $R_d = 2$ (denoted as a + 25^o increment on the chart), only to have a maximum at $R_d = 4$ at a value of 10^o (a value of - 35^o on the chart) and so on. The individual values varied greatly with no discernable trend, despite the average of these individual records having approached values near 0^o. Plots are bounded by + 90^o and - 90^o due to the symmetry of the problem.

With regards to ductility magnitude, as R_d increased so did the average ductility as expected. Similar observations were made for the column ductility in the Y-direction, μ_y (Y-ductility, Figures 3.8 and 3.9); however, these latter results differed from those in the X-direction in that the magnitudes of the ductility ratios were slightly smaller and peaked at different angles for a given R_d. The behavioral pattern illustrated in Figures 3.2, 3.3, 3.8 and 3.9 was typical of what was found for all TUB1 models at all fundamental periods evaluated.

Graphs of the mean of the average drift and upper bound of maximum drift (Figure 3.10) produced very similar trends to those of ductility. The angle of incidence did not affect the average response by a significant amount, and drift did not exhibit a maximum at 0^o or at 90^o for the majority of R_d values studied. In addition, peak inelastic drift normalized by peak elastic drift values for two separate lines of columns indicated that on average, inelastic displacements relative to elastic ones did not peak at angles 0^o and 90^o as shown in Figure 3.11 and 3.12. Similar results were obtained in the Y-direction (Figure 3.13 and 3.14). Therefore, on average, inelastic drift demands occur at angles other than those based on the principal building orientation.

Location of Critical Angle for Slab Rotations and Model TUB1

Slab rotation demands for model TUB1 in general exhibited characteristics similar to those of drift and ductility demands in that their average response appeared to be rather unaffected by the angle of incidence as shown in Figure 3.15 for a fundamental period of 0.3 s, and their individual values varied greatly with angle of incidence (Figure 3.16). Like ductility and drift demands, critical angles of slab rotation varied for a given record with specified fundamental period and R_d value.

While the average slab rotations appeared to be weakly dependent on angle of incidence, the amount of torsion-induced damage and torsion itself may be reduced by allowing the building to experience higher levels of inelastic behavior. This phenomenon is illustrated in Figure 3.17 where ratios of inelastic slab rotations to elastic slab rotations are compared. This observation presupposes that slab rotations are a good indication of torsion. In particular, Figure 3.15 shows average slab rotations as a function of angle of incidence and degree of inelasticity for the 0.3 s TUB1 model, while Figure 3.17 depicts the ratio of inelastic to elastic slab rotations for angles 0^o and 90^o for all TUB1 models. Other studies such as those by Perus and Fajfar (Perus and Fajfar 2005) found that elastic slab rotations were greater than inelastic slab rotations for two building periods (0.4 s and 0.8 s). Studies by De-La-Colina (De-La-Colina 1999) also found slab rotations to decrease with increasing strength-reduction factor (R), i.e., with increased levels of inelastic behavior. Since the model characteristics in both references (such as mass and stiffness) are different than in this work, this phenomenon appears to be dependant on the fundamental period and strength-reduction factor (i.e., level of inelastic behavior).

DECREASE IN THE RATIO OF INELASTIC TO ELASTIC SLAB ROTATIONS WITH PERIOD

In the previous sections it was noted that on average, ratios of inelastic to elastic slab rotations decreased with increasing period and degree of inelasticity. This implies that a designer who wishes to minimize slab rotations need only increase the degree of inelasticity. This behavior also manifested itself for the other ground motion sets investigated and will now be explained. To better understand this behavior, individual responses are used to give a reasonable explanation as to why the ratio of inelastic to elastic slab rotation decreased with period. The hypothesis was that as a single line of columns has just started to yield in the TUB1 model for a given direction, its center of rigidity shifted from the geometric center increasing the lever arm that generates twist prior to yielding of the remaining columns. If the pseudo acceleration $S_a(T_1)$ response spectrum remained level or increased with fundamental period beyond the initial period of the structure (the region where the period of the structure is expected to elongate as it yields), larger twisting should occur with increasing R_d due to higher values of $S_a(T_1)$ and a larger moment arm. With regards to the moment arm, the columns in model TUB1 yielded in pairs whether in the X-direction or Y-direction, and were typically were a pair closest to the offset mass. When a column pair yielded, the center of rigidity shifted from the geometric center to either location 1 or 2 in Figure 3.18 depending on the column pair. The distance from the center of mass for the new location of the center of rigidity in either case was almost the same and can be calculated given that the post yield stiffness is 3% of the original stiffness. Figure 3.19 highlighted the major component $S_a(T_1)$ response spectra along with the individual responses and their mean (solid black line) from 0.2 s to 0.5 s for site class D. Here, record 98 (dotted black line) decreased greatly as compared to the mean in this region, while record 79 (dashed black line) increased greatly in this region. Inelastic behavior for record 98 should prompt smaller inelastic slab rotations as compared to elastic slab rotations since $S_a(T_1)$ decreases greatly despite the increased moment arm which according to Table 3.1 indeed did. Like wise, record 79 should have had inelastic slab rotations that tended to increase with R_d, which did as observed in Table 3.2. The response spectra of the major component in Figure 3.20 displays an additional record, record 111 from site AB that is similar to record 98 in behavior, plus a generated record that displays similar behavior labeled TS with similar behavior as record 79 at a period of 2.0 s along with the individual responses and mean of those responses. Slab rotations should decrease with inelasticity for record 111 according to the logic presented thus far which they do as illustrated in Table 3.3.

The TS function was a sine function that had the behavior shown in Figure 3.20, which was developed because no one record of the ground motion suites examined was able to display an increasing response spectrum behavior at this period range. Although the TS record does not increase as sharply as record 98 does at the 0.2 s range, the TUB1 model subjected to this function exhibits slab rotations that do increase with R_d as seen in Table 3.4.

CRITICAL ANGLE AND SITE D GROUND MOTIONS FOR MODEL TB

Critical Angles of Ductility and Drift Demands for Model TB

Much like model TUB1, model TB was sensitive to the angle of incidence of the ground motion input. The grey lines indicating individual X-ductility values relative to the average of these values (the solid black line) is illustrated in Figure 3.21 much like Figure 3.1 displayed for the TUB1 model. Column 1 of model TB with a fundamental period of 0.5 s and R_d = 6 in particular was displayed. The angle of incidence did little to affect mean of average ductility (Figure 3.22) by a significant amount despite individual values being quite sensitive to angle of incidence. Like the previous model, Model TB mimicked its trends with regards to column ductility ratios as they did not exhibit a maximum at 0^o or at 90^o for the majority of R_d values studied. These trends are seen in Figure 3.22-3.23, which displayed for a given R_d, the mean of the average ductility of all columns and the upper bound of maximum ductility values of all columns in the X-direction, μ_x, for the 0.5 s TB model as a function of angle of incidence.

Here too, histograms of upper bound maximum ductility demands in both the X- and Y-directions showed that critical angle of maximum ductility can manifest itself at a variety of angles as they did for the TUB1 model. Figure 3.24 and 3.25 for the TB model were the counterparts to Figures 3.4 and 3.5 at fundamental periods of 0.5 s. Critical angle values for individual responses experienced by the TB model varied greatly with relative design intensity. The change in critical angle relative to $R_d = 1$ for Column 1 with increasing R_d value, is shown in Figures 3.26 and 3.27, the counterparts to Figures 3.6 and 3.7 for model TUB1.

With regards to ductility magnitudes, a difference between the mean average and upper bound of maximum values for the base case model and the TB model was quite visible. At 0.5 s, TB models (Figure 3.28 and 3.29) experience larger ductility demands compared to the TUB1 counter parts (Figure 3.2 and 3.3) at the same fundamental period. While the TUB1 model may experience smaller ductility demands, their columns were also stiffer than those of the TB model and had larger plastic moment values assigned to the hinges. This occurred due to the seismic loads being resisted in both the X and Y-directions for a given component for model TUB1, while the response for model TB was uncoupled in this respect. The work by Humar and Kumar (Humar and Kumar 1999) also resulted in higher ductility demands in TB models for a given period; however, the center of rigidity rather than mass was offset in order to induce torsion. This difference also reflects the sensitivity of response of models TUB1 and model TB to the location of mass in the model, in that while the amount of mass in both models was the same, the response magnitudes are quite different. While Figures 3.28 and 3.29 concerned themselves with ductility in the X-direction, similar observations were made for the column ductility in the Y-direction (μ_y) (Figures 3.30 and 3.31). However, these latter results differed from those in the X-direction in that they peaked at different angles for a given R_d similarly to the TUB1 model. Figures 3.28, 3.29, 3.30 and 3.31 were typical of what was found for all TB models. Given that TB models tended to have larger ductility demands and therefore could be expected to have greater amounts of damage, a designer may wish to pay just as much attention if not more to their sensitivity to the application of seismic loads.

Concerning drift, TB models had mean of average responses that did not show a great sensitivity to angle of incidence like TUB models, and drift did not exhibit a maximum at 0^o or at 90^o for the majority of R_d values studied as shown for the TB model with the fundamental period. Examples of these phenomena are displayed in Figure 3.32 and 3.33.

Regardless of whether or not torsional effects were significant, both maximum and average ductility demands occurred at different angles for a given R_d for both TUB1 and TB models. Therefore, damage assessment based on either maximum or average story ductility ratios will be dependent on the angle of incidence of the ground motion input. This observation was found to be the case for all models regardless of ground motion set to which it was subjected too.

CRITICAL RESPONSE VS. RESPONSE AT PRINCIPAL BUILDING ORIENTATIONS

Having examined the seismic responses of the TUB1 model and the TB model as a function of angle of incidence, it was apparent that maxima did not always occur when the major component of ground motion was applied at $\alpha = 0^o$ or at 90^o. Given this behavior, it becomes important to develop simplified design procedures to quantify seismic demands as a function of the angle of incidence. Results thus far, have not show consistent, stable trends that will allow the robust quantification of such demands. However, on average, the ratio of the maximum ductility demand of all columns at any angle of incidence to the maximum ductility demand at any column at 0^o (for ductility in the X-direction) $Max\ \mu_x/Max\ \mu_{x0}$, and at 90^o (for ductility in the Y-direction) $Max\ \mu_y/Max\ \mu_{y90}$ varied between 1.1 and 1.7 for these two structures. This variation exhibited trends that indicate a dependence with respect to period and a weak dependence with respect to R_d (as shown in Figure 3.34 and 3.35). Figure 3.34 illustrated this behavior for $Max\ \mu_x/Max\ \mu_{x0}$. Figure 3.35 was similar with the exception that $Max\ \mu_y/Max\ \mu_{y90}$ is examined. Due to the symmetry of the model, the results for the TB model were identical in both figures. An evaluation of the mean of the ratio of the peak average ductility in the X-direction at any angle of incidence to the average ductility demand at 0^o and the ratio of the maximum ductility demand at any angle of incidence to the maximum ductility demand at 0^o produced very similar results. Although these graphs were for ductility, they can be interchanged for drift values because the properties of each column in any given model (i.e., stiffness and yield rotation) were the same. These results reinforced the notion that design and performance assessment procedures based on ground motions applied at the principal orientations of the building will tend to underestimate peak inelastic seismic demands as compared to other orientations of the building, especially at longer periods (greater than 0.5 seconds).

IMPLICATIONS FOR PERFORMANCE-BASED DESIGN

Thus far, the results for models such as TB and TUB1 models presented in previous sections demonstrated that seismic demands on inelastic buildings exposed to bi-directional ground motions can be underestimated if the pair of ground motion records is only applied at the principal orientations of the building. The implication is that inaccurate estimates of damage assessment, and hence, direct dollar losses could be obtained from performance evaluation conducted with bi-directional ground motions applied at 0^o and 90^o. This is illustrated with the ductility demand fragility curves shown in Figure 3.36 and 3.37 for model TUB1. A fragility function is a cumulative density function of the form:

$$P(X \leq x_0) = \int_{-\infty}^{x_0} f_x(x)dx \qquad 3.1$$

Which is bound between the values of 0 and 1 and never decreases with increasing x_0 The value obtained from equation 3.1 ($P(X \leq x_0)$) is the probability that the random variable X is contained within the interval ($-\infty$,x_0) (Note that Figures 3.36 and 3.37 plot 1-($P(X \leq x_0)$). Here, that random variable was ductility demands and was used to quantify the likelihood of a given quantity (ductility in this case) to exceed a certain threshold as say another variable (S_a/g in this case) was increased, graphically. Their use with regards to performance based assessment and design in this case shows how certain angles observe more ductility demands than others. From figures 3.36 and 3.37, it was observed that certain angles were more likely to have had greater ductility demands than others. Here, the probability that a given $\mu_0 = 2.0$ will be exceeded was plotted versus $S_a(T_1)/g$ which was determined by back calculating from a given R_d with Eq. 3.1 assuming that the normalized base shear strength of the structure γ, was equal to 0.25. These figures indicate that for most $S_a(T_1)/g$ values, results at different angles such as $\alpha = 45^o$ (Figure 3.36) and 90^o for the 2.0 s TUB1 model had a greater likelihood of exceeding a ductility value of 2.0 as compared to the results at 0^o. The exception was the range corresponding to $S_a(T_1)/g > 0.75$ in which differences between fragilities for 90^o and 0^o exhibit opposite trends. These observations imply that damage estimates based on fragilities for ground motions applied at principal orientations can be grossly inadequate.

EFFECT OF GROUND MOTION FREQUENCY CONTENT ON CRITICAL ANGLE

Differences in Drift, Slab Rotation and Ductility Demands for Site AB Ground Motions

The magnitudes of drift, ductility and slab rotation demands of the TUB1 model exposed to ground motions that corresponded to NEHRP site classes A and B were different than those obtained using ground motions recorded in stiff soil sites (see Figures 3.38 - 3.40). These differences in magnitudes are explained by the differences in the scaled response spectra of site AB (Figures 3.41 and 3.42) and site D (Figures 3.43 and 3.44) where site AB's minor component tended to have a smaller average S_a at longer periods than site D, explaining the somewhat smaller response magnitudes observed for inelastic behavior. Figures 3.38 and 3.39 indicate that average and maximum responses typically did not occur at 0^o and 90^o, and that the critical angle of response can occur at virtually any angle much like the TUB1 model exposed to site D ground motions, as shown by the individual responses displayed in Figure 3.40. With respect to the ratio of $Max\ \mu_x/Max\ \mu_{x0}$, Figure 3.45 displays a different trend than that of Figure 3.34, in that the ratio was higher at 1.0 s and smaller at 2.0 s than that of site D. This discrepancy was found to be due primarily to the scaling of the ground motions at a given period and will be discussed in further detail in Chapter 5 where additional statistics were employed. Inelastic to elastic slab rotations were also found to decrease with increasing fundamental period and degree of inelasticity as seen in Figure 3.46.

Effect of Bi-Directional Near Fault Ground Motions

The general trends observed in the variability of the individual responses of model TUB1 exposed to far-field ground motions (site class D) were consistent with those observed with the near-fault ground motion set. Figure 3.47 illustrates this for the TUB1 model with a fundamental period of 0.5 s with regard to slab rotations. Here, the individual responses vary quite a bit while the average value for $R_d = 1$ appears to be weakly dependent on angle of incidence. Figure 3.48 shows that the average slab rotations also decrease with increasing R_d, just like the slab rotations based on site D ground motion set.

SUMMARY AND CONCLUSIONS

In this chapter, critical angle was examined for models TUB1 and TB which were subjected to site class D ground motions, site class AB ground motions and near-fault ground motions. An examination of individual responses and their average values was made. Histograms indicating where the critical angle of response occurred for a given ground motion and a given degree of inelasticity were also illustrated. While histograms indicated at which angles the response was critical, figures illustrating how the critical angle changed with respect to degree of inelasticity for a given individual response with degree of inelasticity were also displayed. Ratios of maximum ductility for any angle over the ductility that occurred at principal building orientations were calculated and displayed as a function of fundamental period and degree of inelasticity. Fragility curves compared the response at angles other than those based on the principal building orientation in a performance based reference frame. Inelastic slab rotations relative to elastic slab rotations were found to decrease with fundamental period and degree of inelasticity for both ground motion sets, and a more in-depth investigation of this phenomenon was conducted.

From the two models examined, models TUB1 and TB, it was found that critical angle occurred at just about any angle of incidence. This was seen from plots of ductility for individual responses. Histograms of critical angle confirmed this phenomenon for all degrees of inelasticity. That is, the majority of records had critical angles that occurred at angles other those of the principal building orientation.

The critical angle of a given ground motion varied greatly with degree of inelasticity and was difficult to predict. While individual responses were found to be strongly dependent on angle of incidence, their average was not as sensitive to the angle of incidence. The ratio of ductility demands at these critical angles relative to the ductility demand at the principal building orientation were plotted versus fundamental period and degree of inelasticity and showed that the response can be as much as 15%-70% greater than the response that occurred when ground motions were applied at the principal building orientation. Casting this last result in a performance based design point of view, certain angles were found to be more susceptible to larger ductility demands than others, indicating that for assessment purposes, estimates that are based on the principal building orientation alone can lead to underestimation of damage.

With regards to frequency content, site class AB and near fault ground motions produced trends that were similar to those based on ground motion site class D. That is, maximum responses often occurred when ground motions were applied at angles other than those based on the principal building orientation regardless of the ground motion set. Slab rotations for model TUB1 were found to decrease with increasing period and degree of inelasticity on average, for ground motions based on site class D, AB and preliminary work with near-fault ground motions. An investigation of this behavior indicated that was a function of the ground motion spectra and the manner in which the columns of the structure yielded. The following chapter, chapter 4, looked specifically at critical angle and its sensitivity to the structural configuration and properties of the models.

Record 98 (Site D) TUB1 0.2 s	
R_d	Slab Rotation (radians)
Elastic	0.004417
1	0.004136
2	0.002314
4	0.001196
6	0.000815

Table 3.1 Decreasing slab rotations with R_d, record 98 (site D)

Record 79 (Site D) TUB1 0.2 s	
R_d	Slab Rotation (radians)
Elastic	0.002006
1	0.002006
2	0.006532
4	0.008373
6	0.007109

Table 3.2 Increasing slab rotations with R_d, record 79 (site D)

Record 111 (Site AB) TUB1 2.0 s	
R_d	Slab Rotation (radians)
Elastic	0.002516
1	0.002516
2	0.002296
4	0.001213
6	0.000846

Table 3.3 Decreasing slab rotations with R_d, record 111 (site AB)

Record TS TUB1 2.0 s

R_d	Slab Rotation (radians)
Elastic	0.002262
1	0.002262
2	0.00255
4	0.002724
6	0.002767

Table 3.4 Increasing slab rotations with R_d, TS function

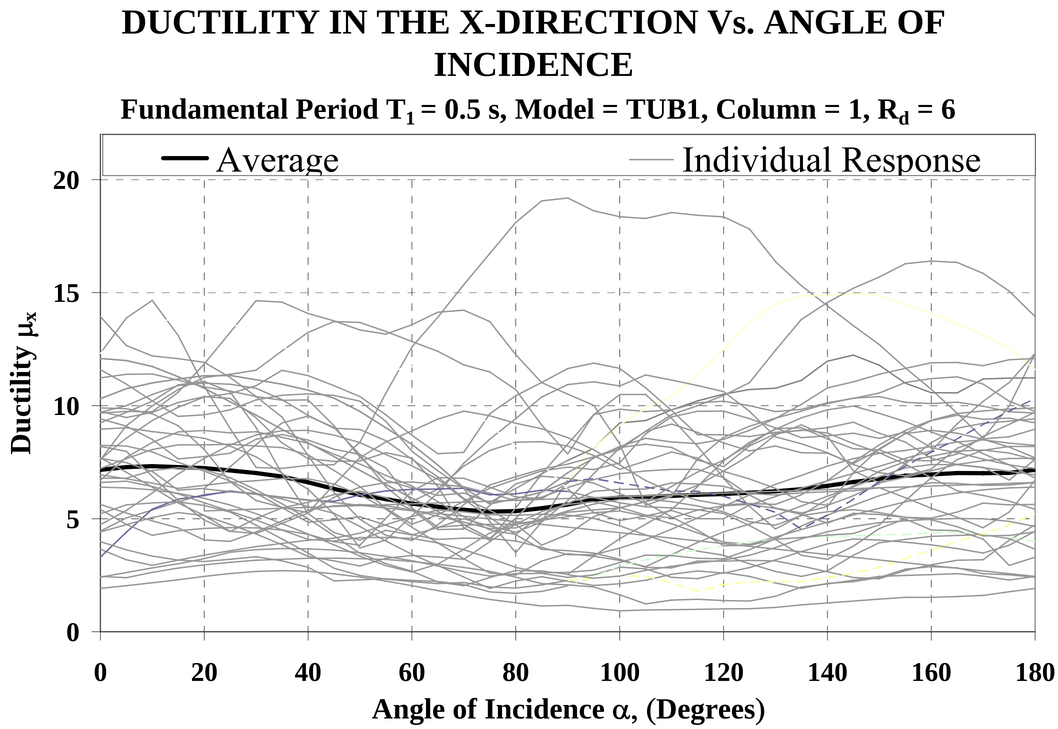

Figure 3.1 Dependence of ductility demands in the X-direction on angle of incidence at a fundamental period of 0.5 s for model TUB1

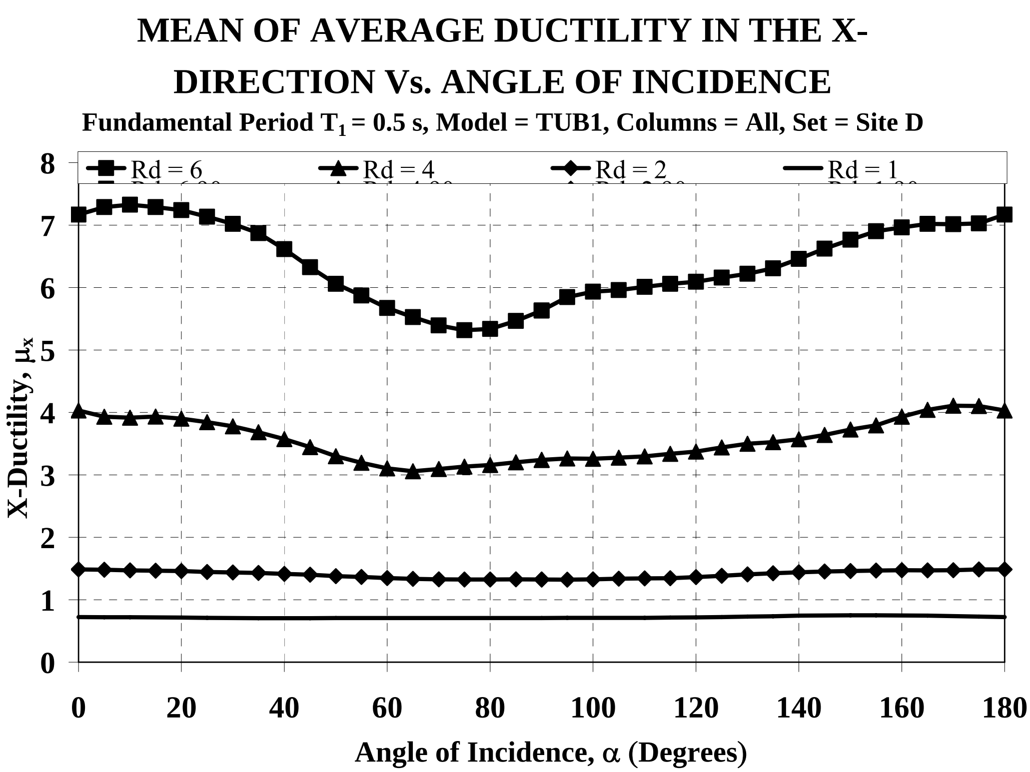

Figure 3.2 Influence of angle of incidence on average ductilities in the X-direction at a fundamental period of 0.5 s for model TUB1

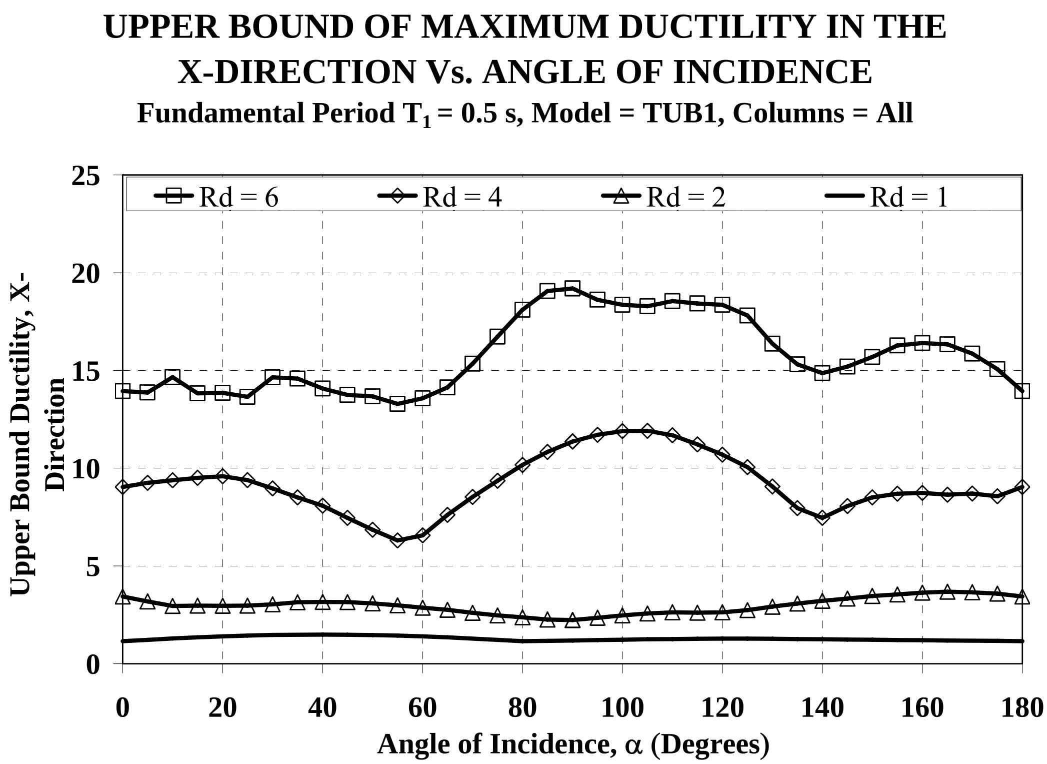

Figure 3.3 Influence of angle of incidence on upper bound of maximum ductilities in the X-direction at a fundamental period of 0.5 for the TUB1 model

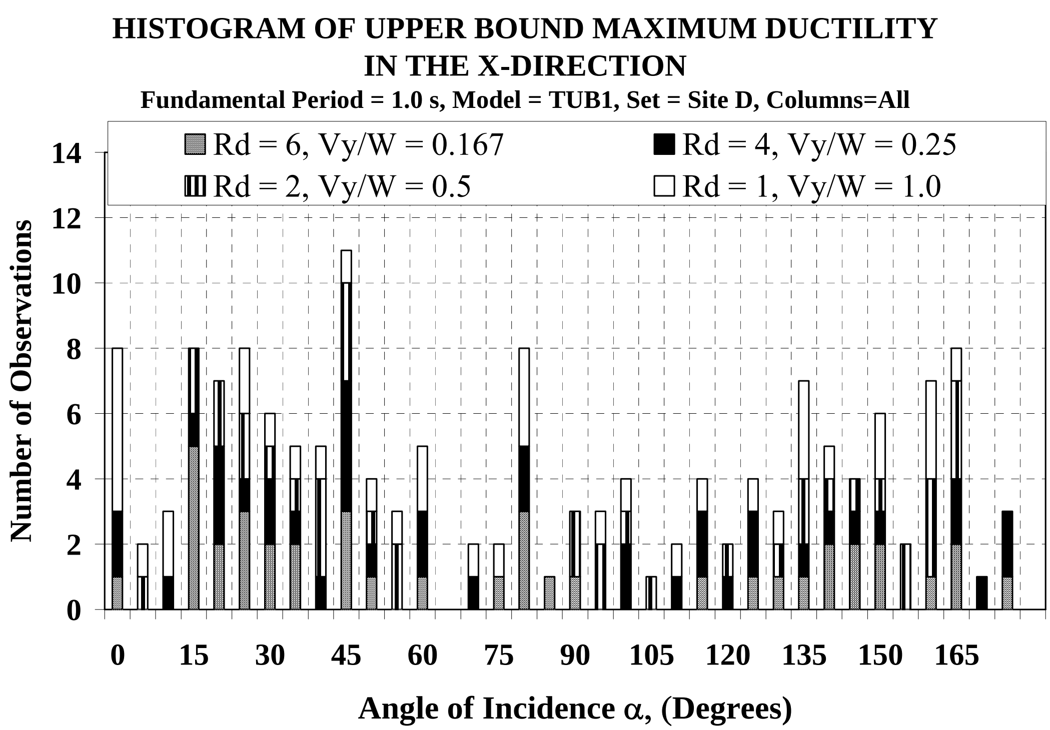

Figure 3.4 Angles of incidence at which upper bound of maximum ductility achieved a maximum in the X-direction at a fundamental period of 1.0 s for the TUB1 model

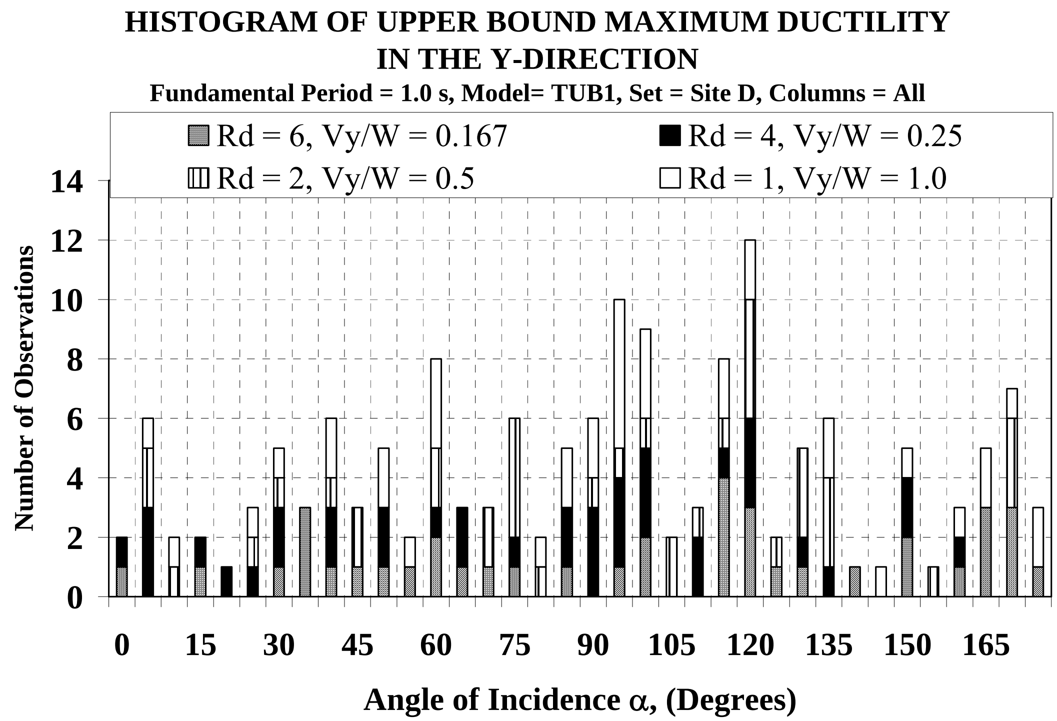

Figure 3.5 Angles of incidence at which upper bound of maximum ductility achieved a maximum in the Y-direction at 1.0 s for the TUB1 model

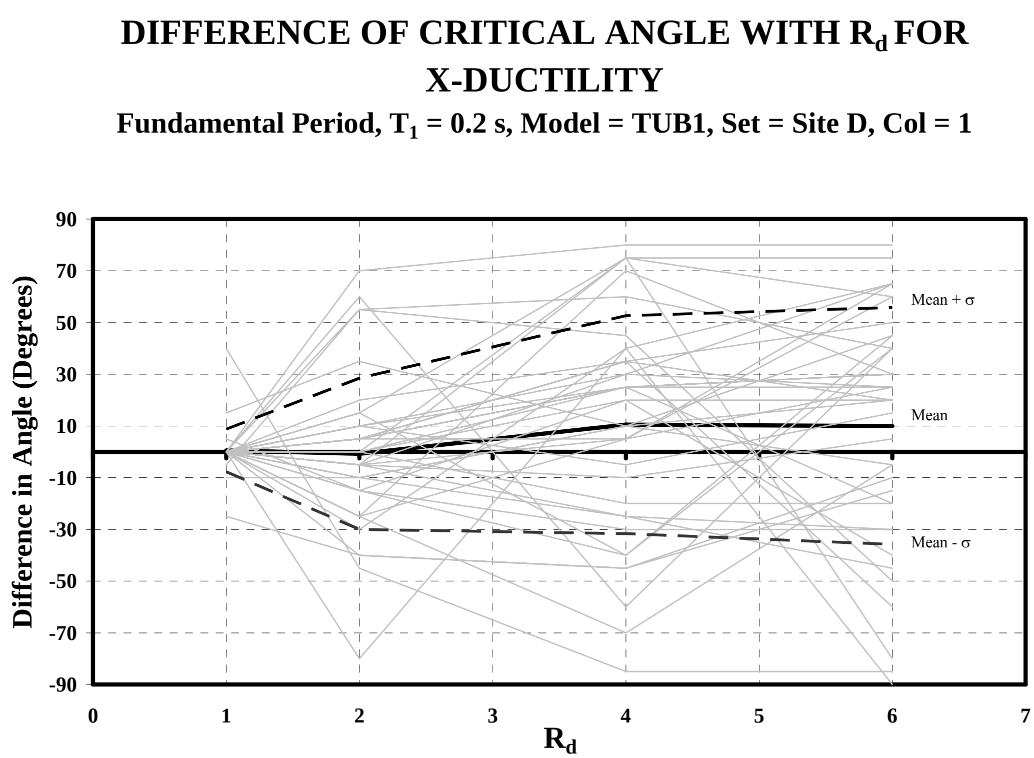

Figure 3.6 Difference of critical angle with respect to R_d = 1 at a fundamental period of 0.2 s for the TUB1 model

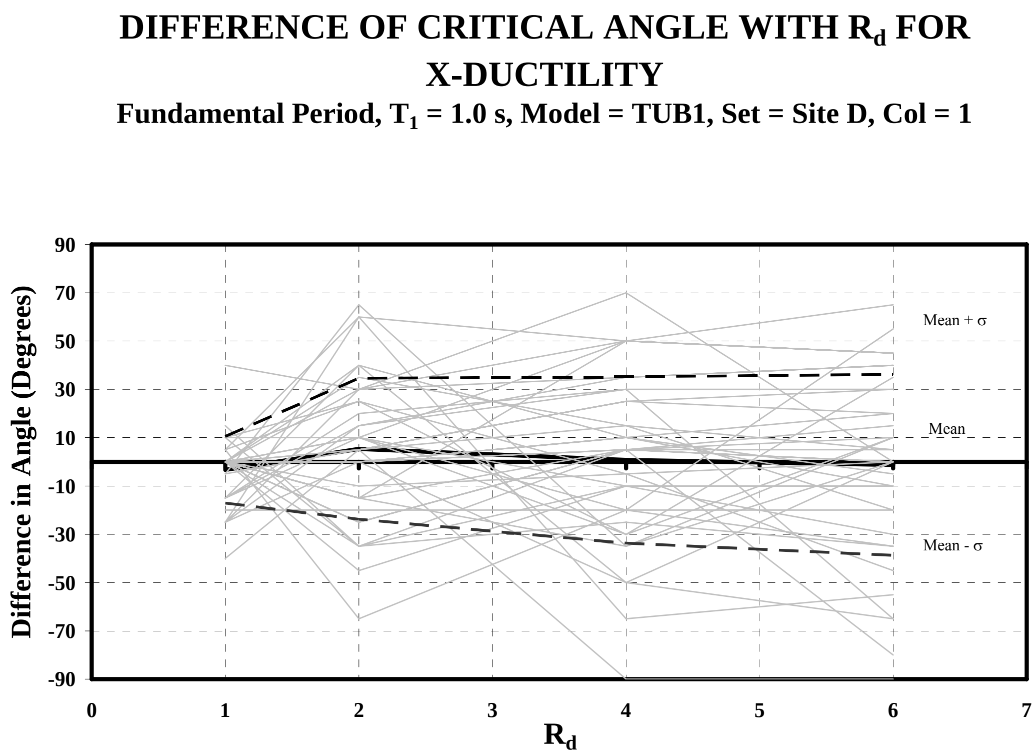

Figure 3.7 Difference of critical angle with respect to R_d = 1 at a fundamental period of 1.0 s for the TUB1 model

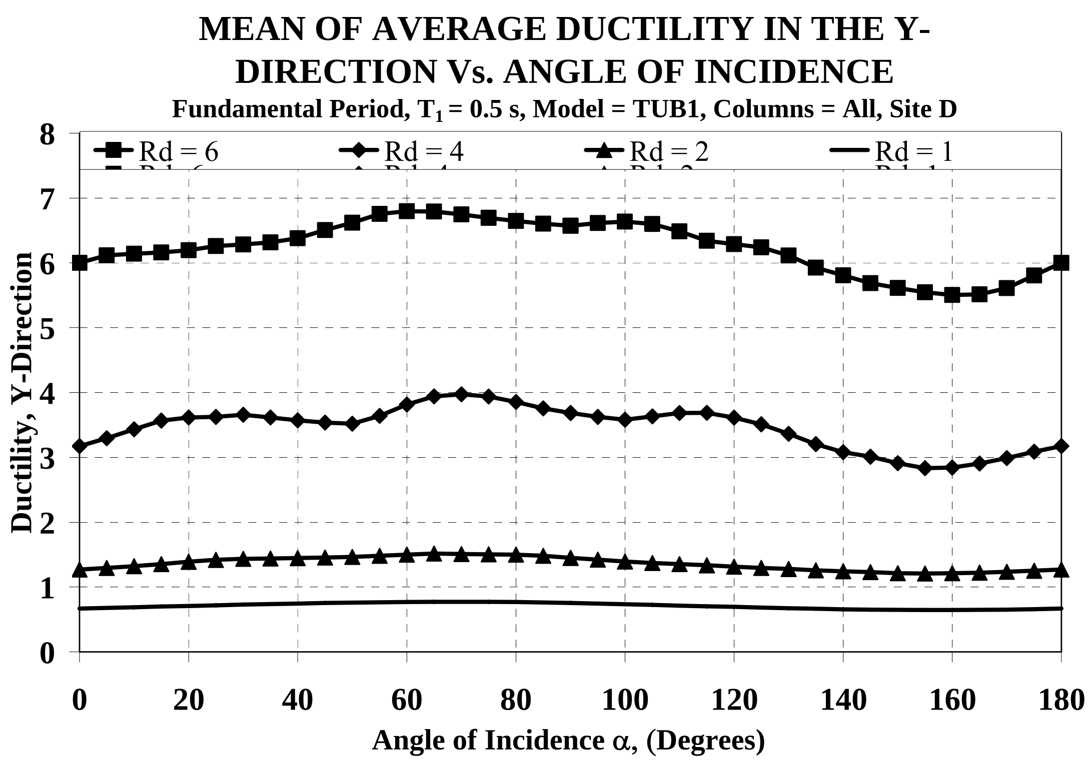

Figure 3.8 Influence of angle of incidence on average ductilities in the Y-direction at a fundamental period of 0.5 s for model TUB1

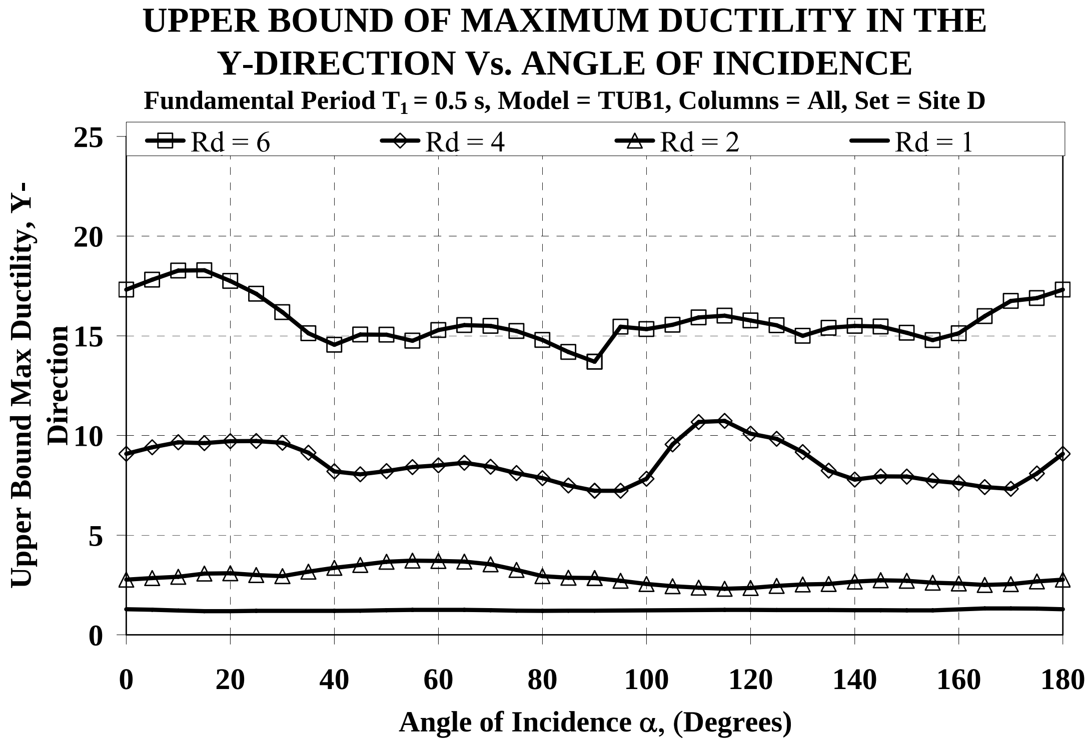

Figure 3.9 Influence of angle of incidence on upper bound of maximum ductilities in the Y-direction at a fundamental period of 0.5 s for model TUB1

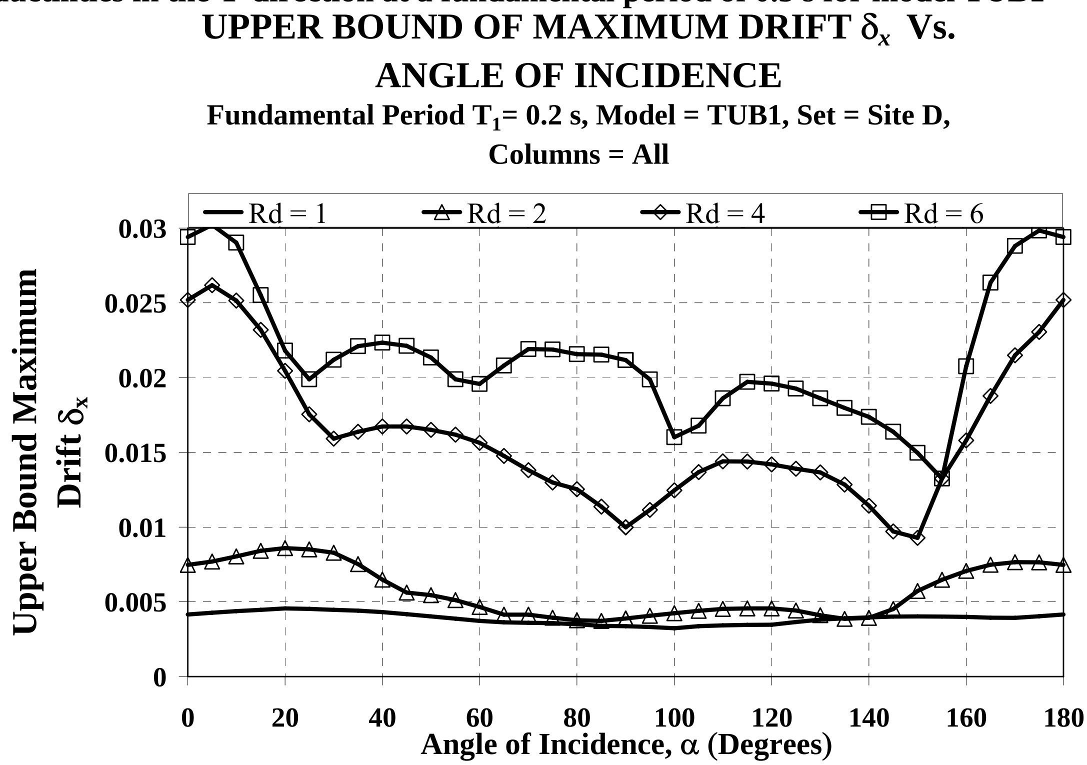

Figure 3.10 Dependence of upper bound of maximum drift values in the X-direction with angle of incidence at a fundamental period of 0.2 s for model TUB1

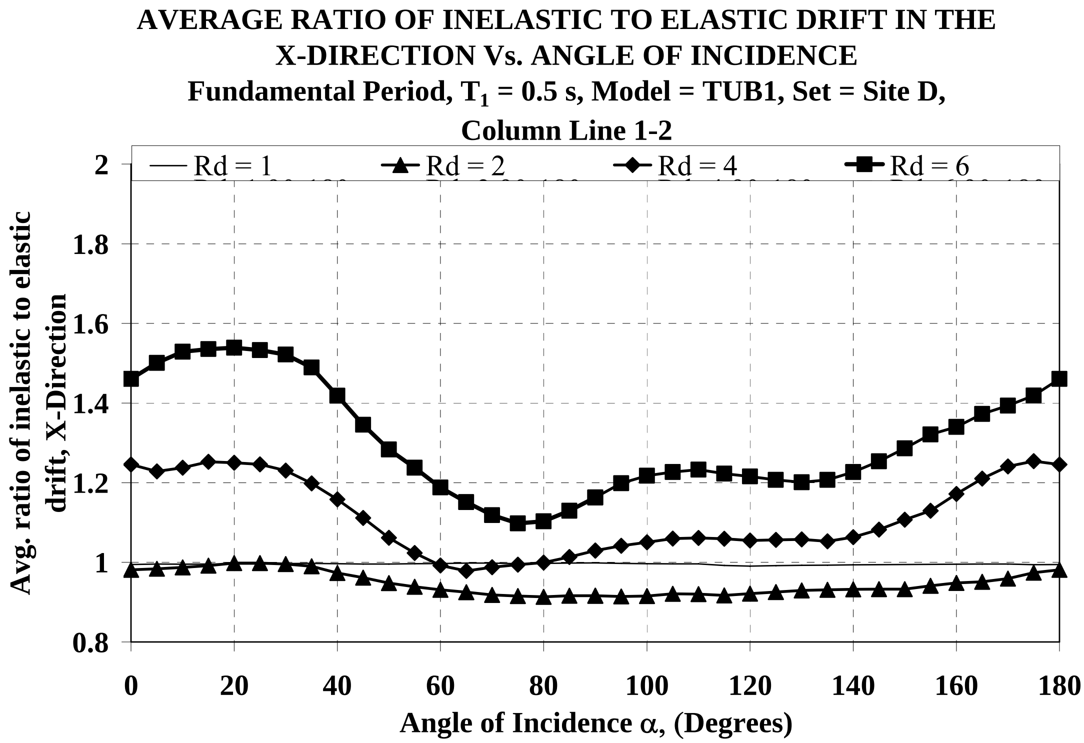

Figure 3.11 Variation of the ratio of inelastic to elastic drifts in the X-direction with angle of incidence, column line 1-2 at a fundamental period of 0.5 s for model TUB1

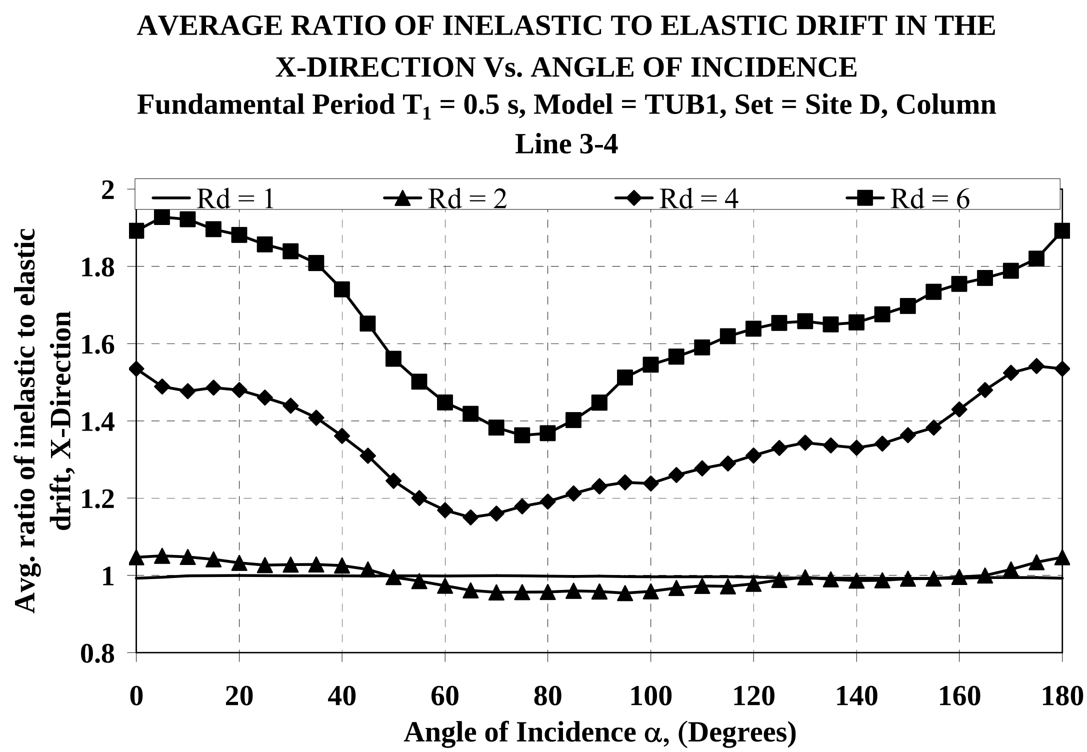

Figure 3.12 Variation of the ratio of inelastic to elastic drifts in the X-direction with angle of incidence, column line 3-4 at a fundamental period of 0.5 s for model TUB1

AVERAGE RATIO OF INELASTIC TO ELASTIC DRIFT IN THE Y-DIRECTION Vs. ANGLE OF INCIDENCE
Fundamental Period T_1 = 0.5 s, Model = TUB1, Set = Site D, Column Line 1-3

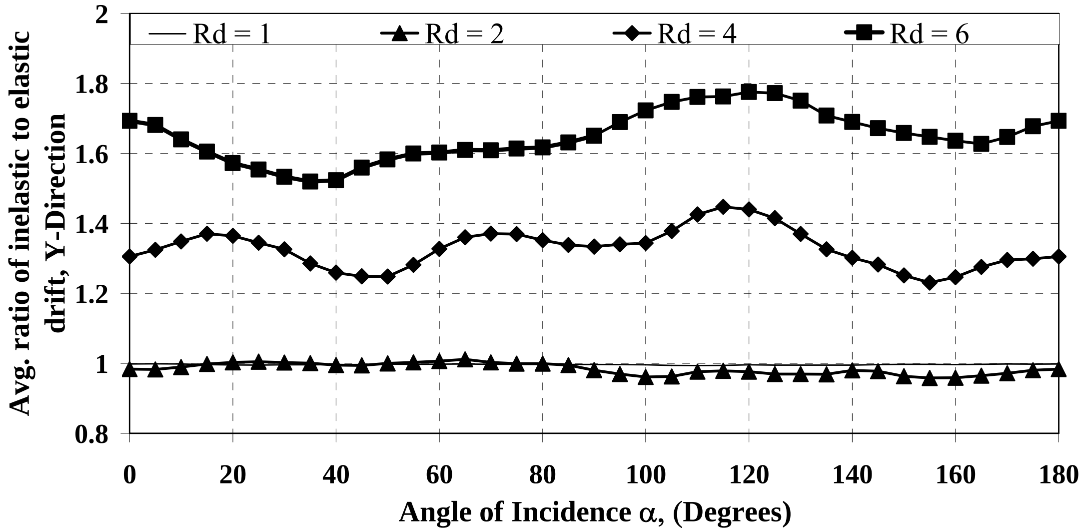

Figure 3.13 Variation of the average ratio of inelastic to elastic drifts in the Y-direction with angle of incidence, column line 1-3

AVERAGE RATIO OF INELASTIC TO ELASTIC DRIFT IN THE Y-DIRECTION Vs. ANGLE OF INCIDENCE
Fundamental Period T_1 = 0.5 s, Model = TUB1, Set = Site D, Column Line 2-4

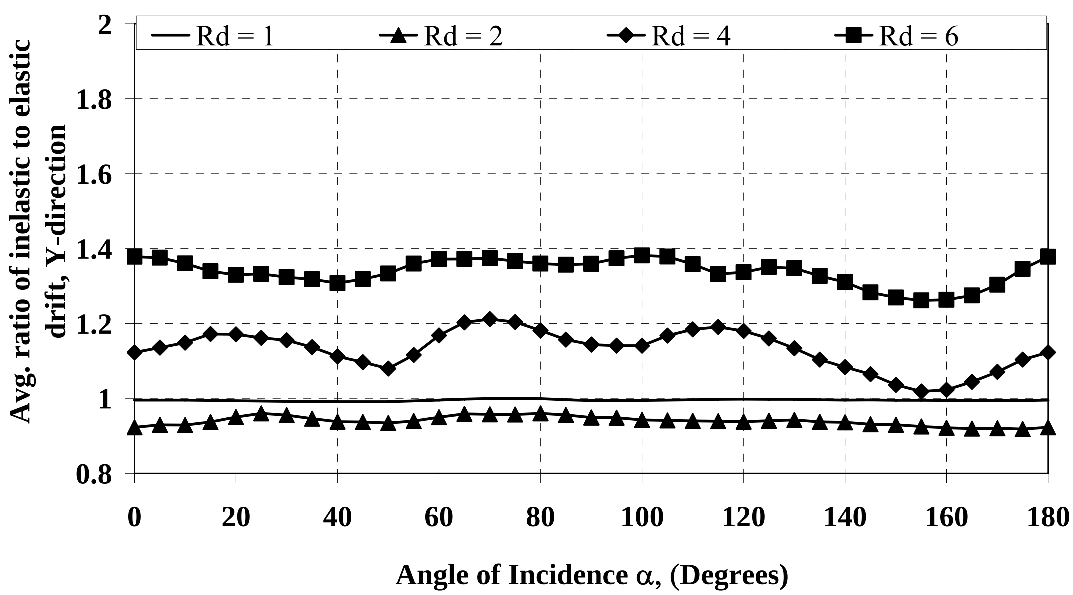

Figure 3.14 Variation of the average ratio of inelastic to elastic drifts in the Y-direction with angle of incidence, column lines 2-4.

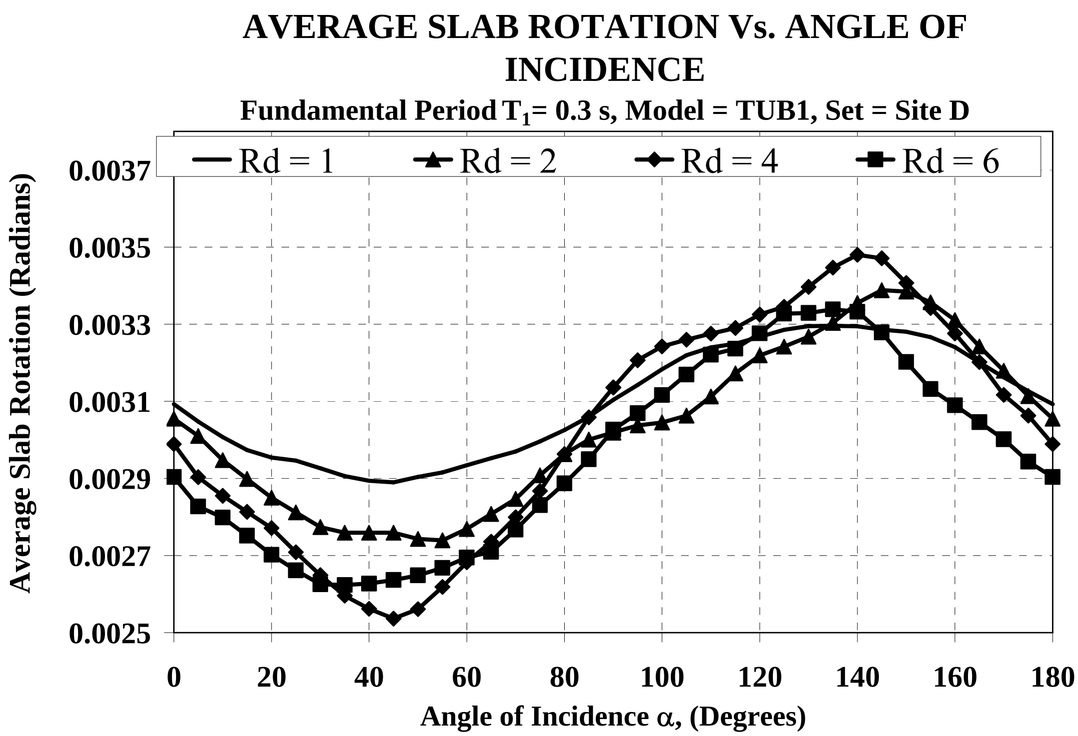

Figure 3.15 Relatively stable variation of average slab rotations with angle of incidence at a fundamental period of 0.3 s for model TUB1

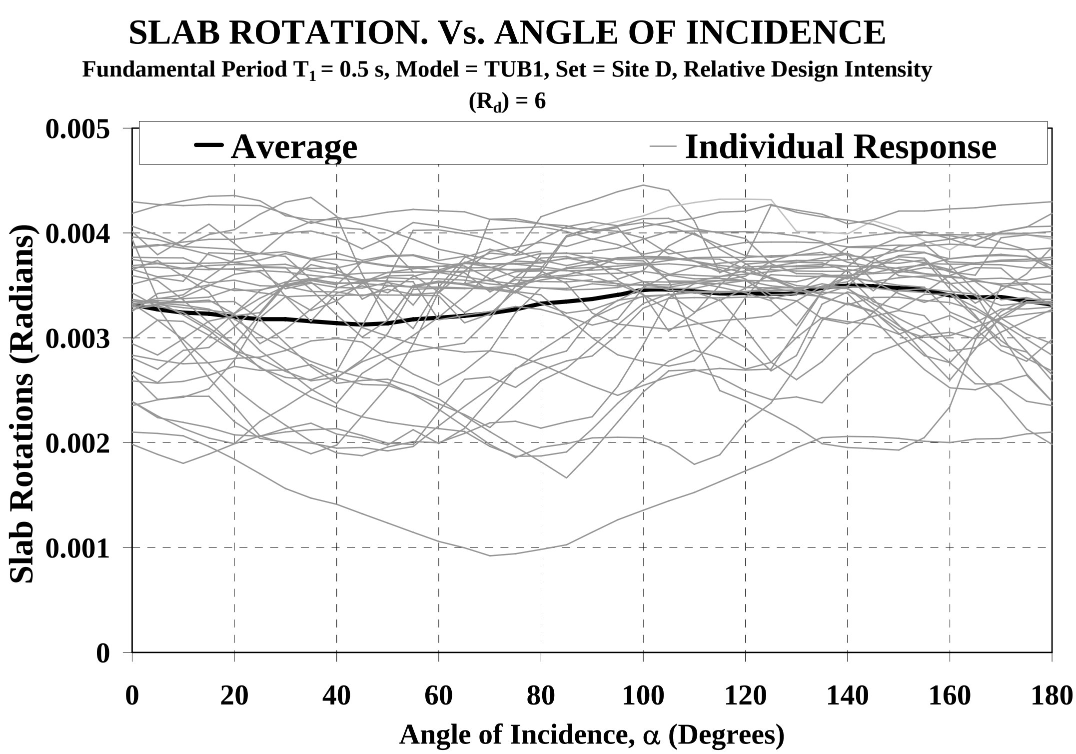

Figure 3.16 Individual response sensitivity with angle as compared to their average value for R_d = 6, at a fundamental period of 0.5 s for model TUB1

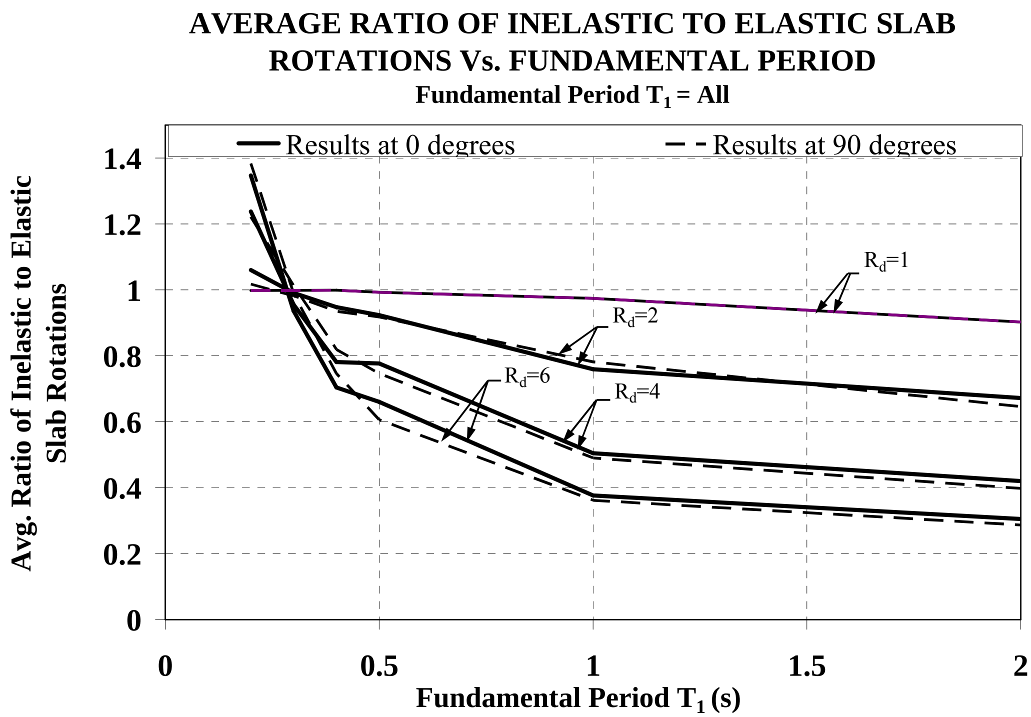

Figure 3.17 Dependence of the average ratio of inelastic to elastic slab rotation on fundamental period at 0° and 90° for all TUB1 models subjected to site D ground motions

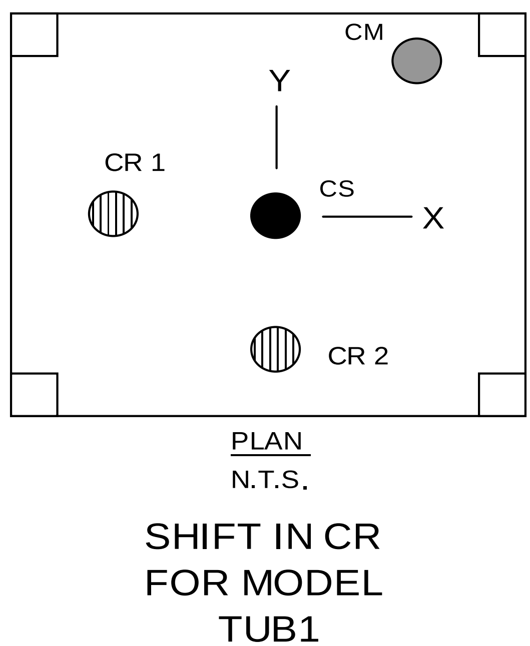

Figure 3.18 Center of rigidity shift for model TUB1

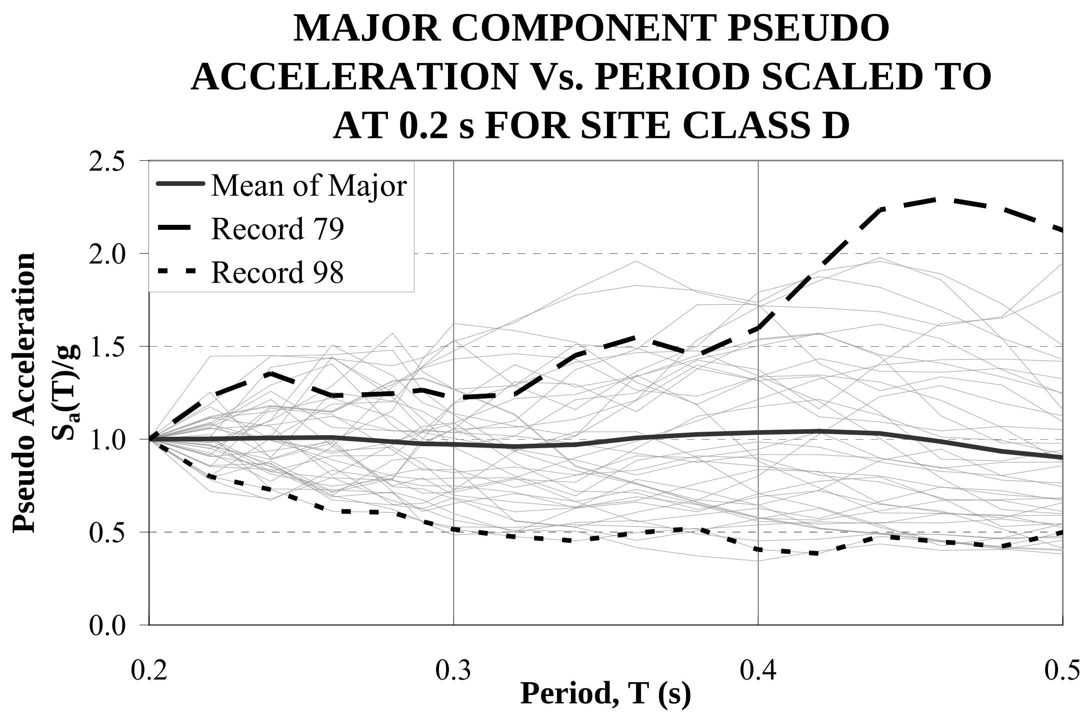

Figure 3.19 Scaled major component spectra with records 79 and 98 beyond 0.2 s showcased for site D

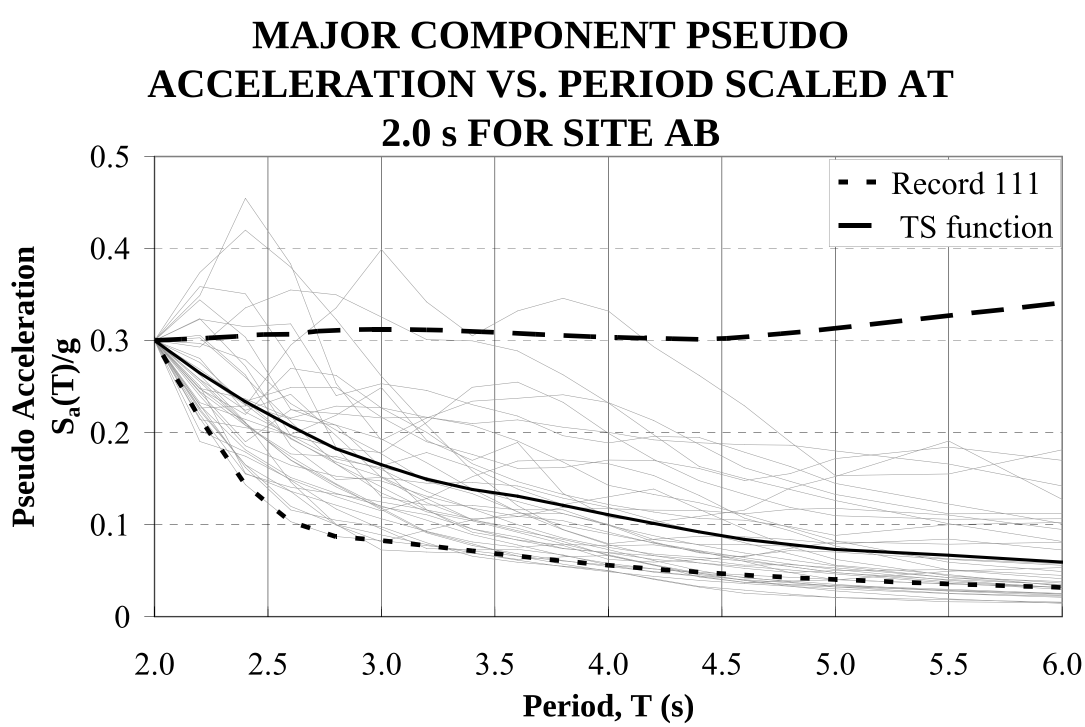

Figure 3.20 Major component spectra with records 111 and TS function beyond 2.0 s showcased for site AB

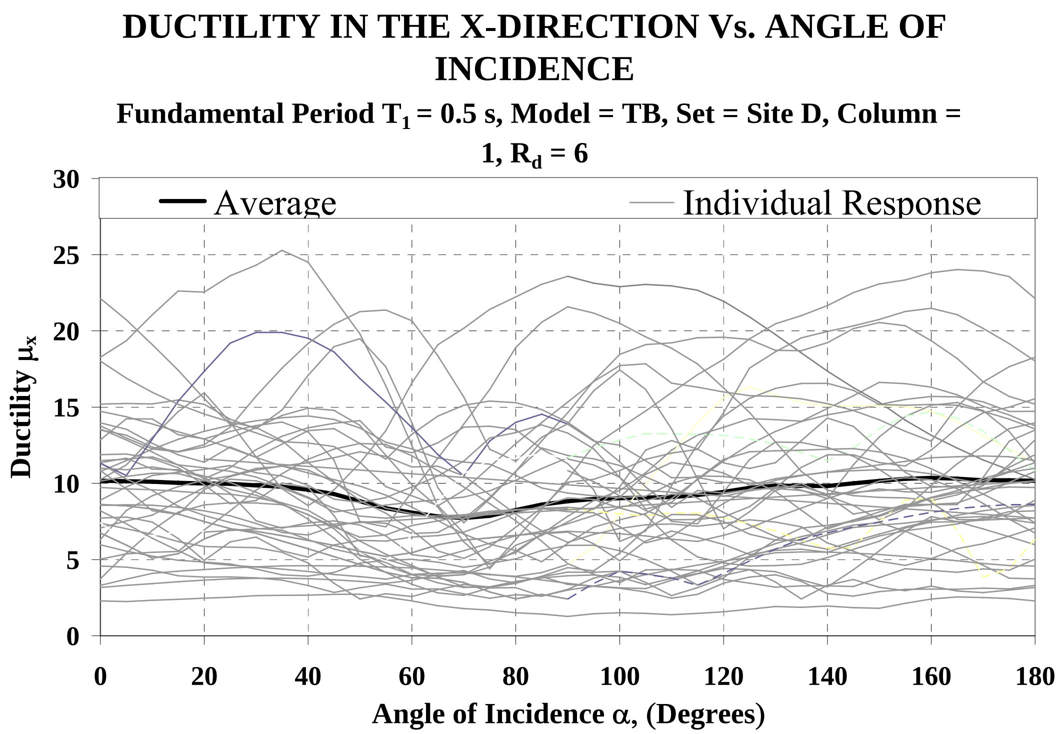

Figure 3.21 Dependence of ductility demands in the X-direction on angle of incidence at a fundamental period of 0.5 s for model TB, $R_d = 6$

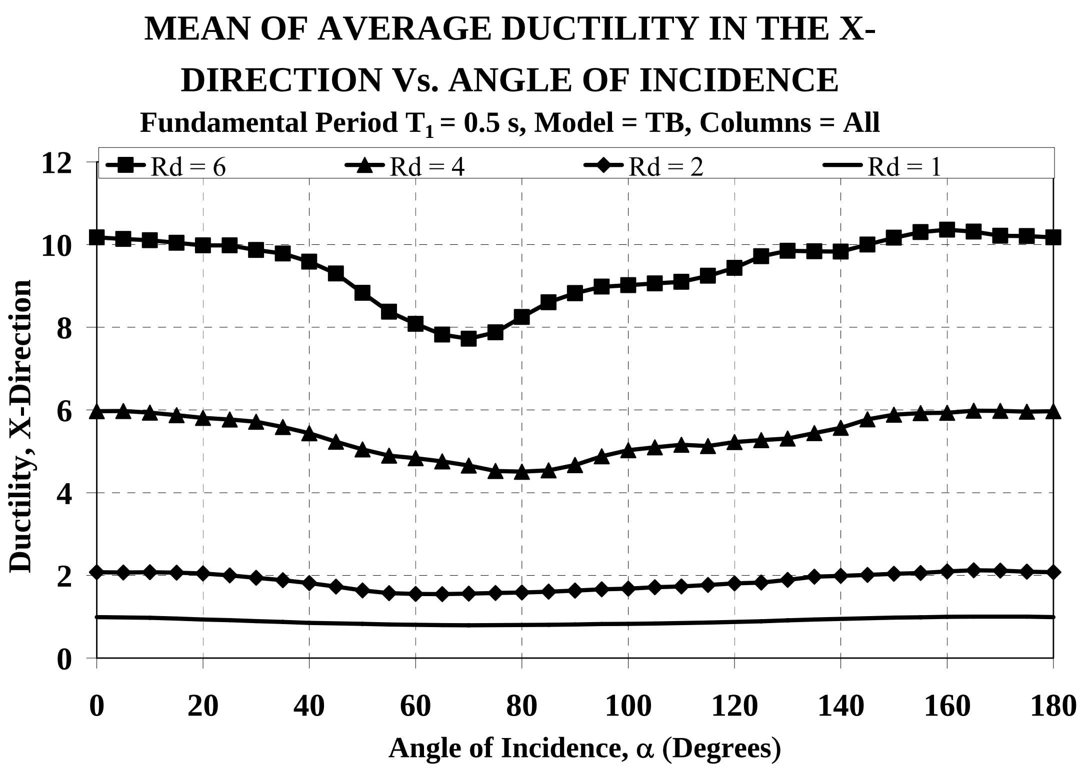

Figure 3.22 Influence of angle of incidence on average ductilities in the X-direction at a fundamental period of 0.5 s for model TB

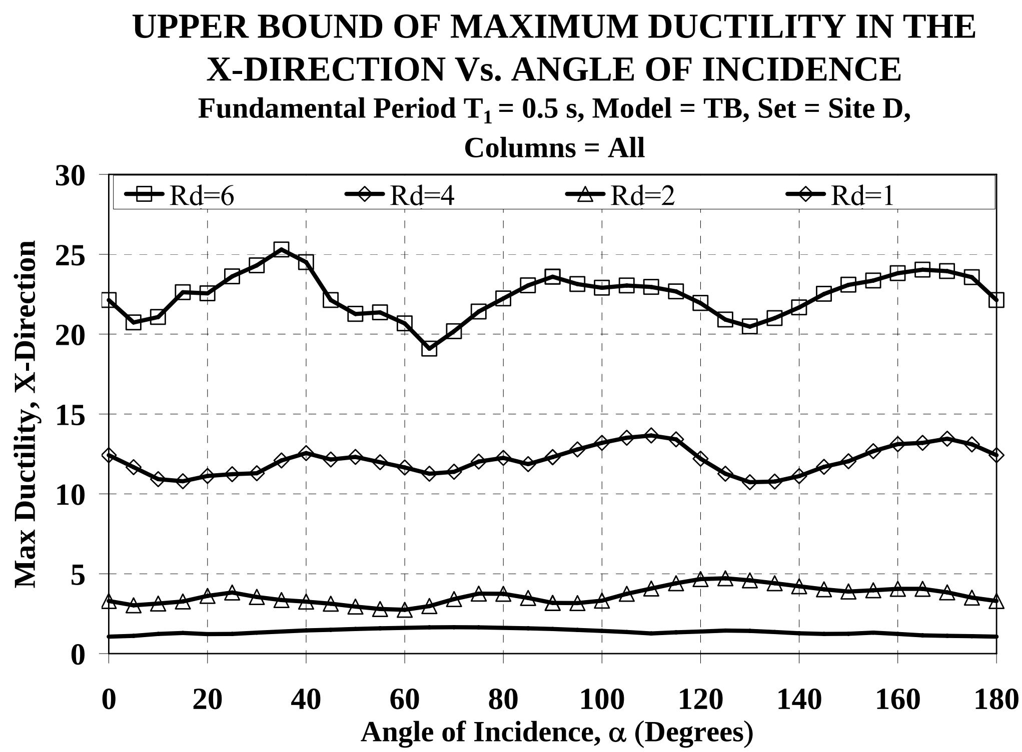

Figure 3.23 Influence of angle of incidence on upper bound of maximum ductilities in the X-direction at a fundamental period of 0.5 s for model TB

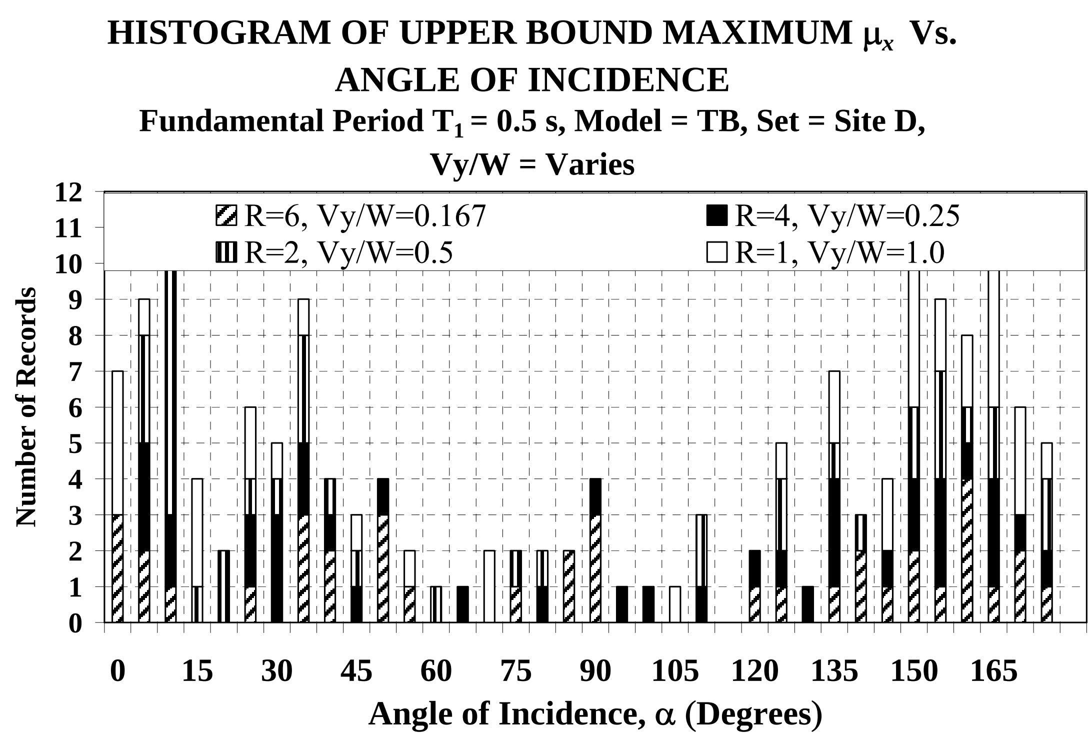

Figure 3.24 Angles of Incidence at which X-ductility achieved a upper bound of maximum ductility at a fundamental period of 0.5 s for the TB model

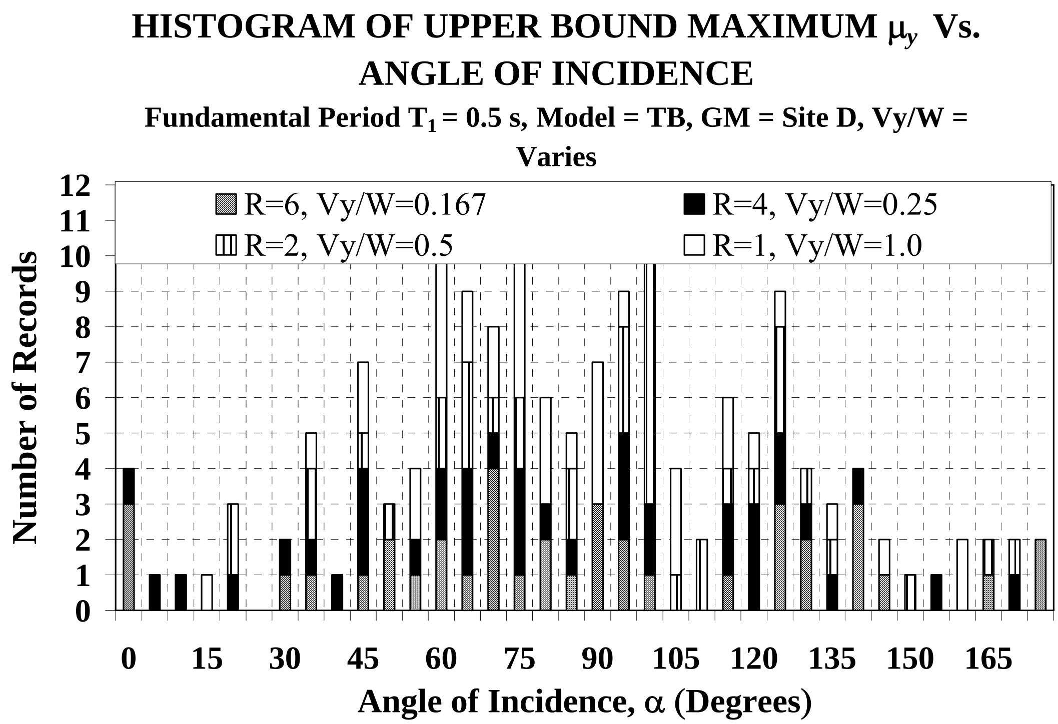

Figure 3.25 Angles of incidence at which Y-ductility achieved a upper bound of maximum ductility in the Y-direction at a fundamental period of 0.5 s for model TB

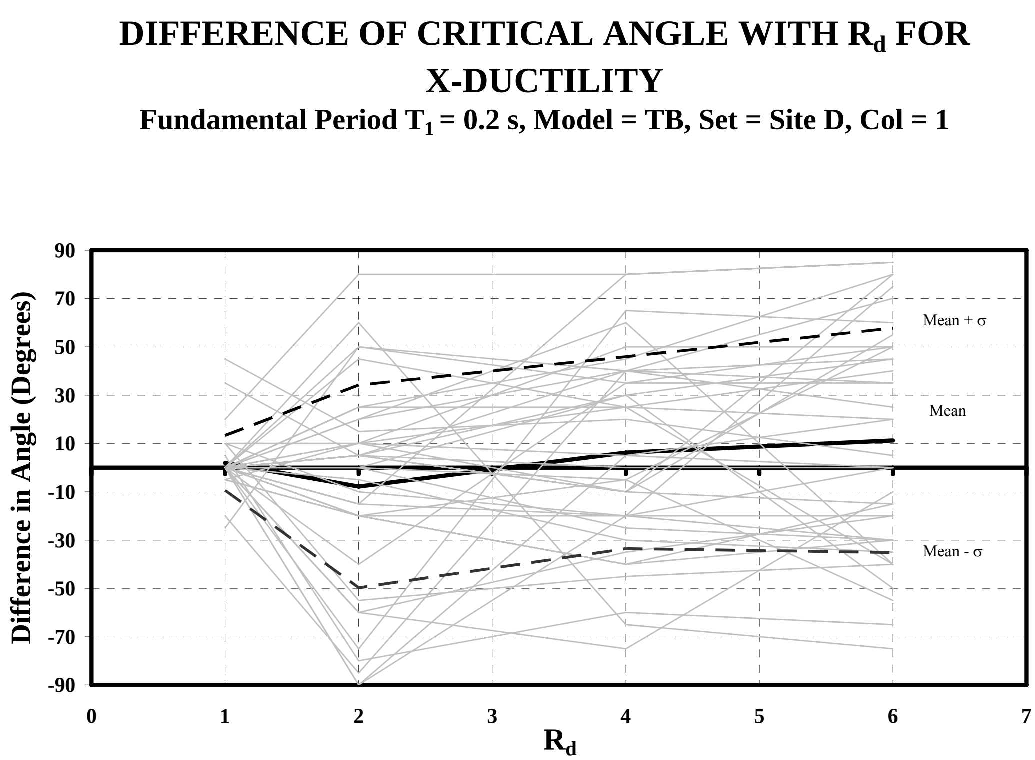

Figure 3.26 Difference of critical angle with respect to R_d = 1 at fundamental period of 0.2 s for the TB model.

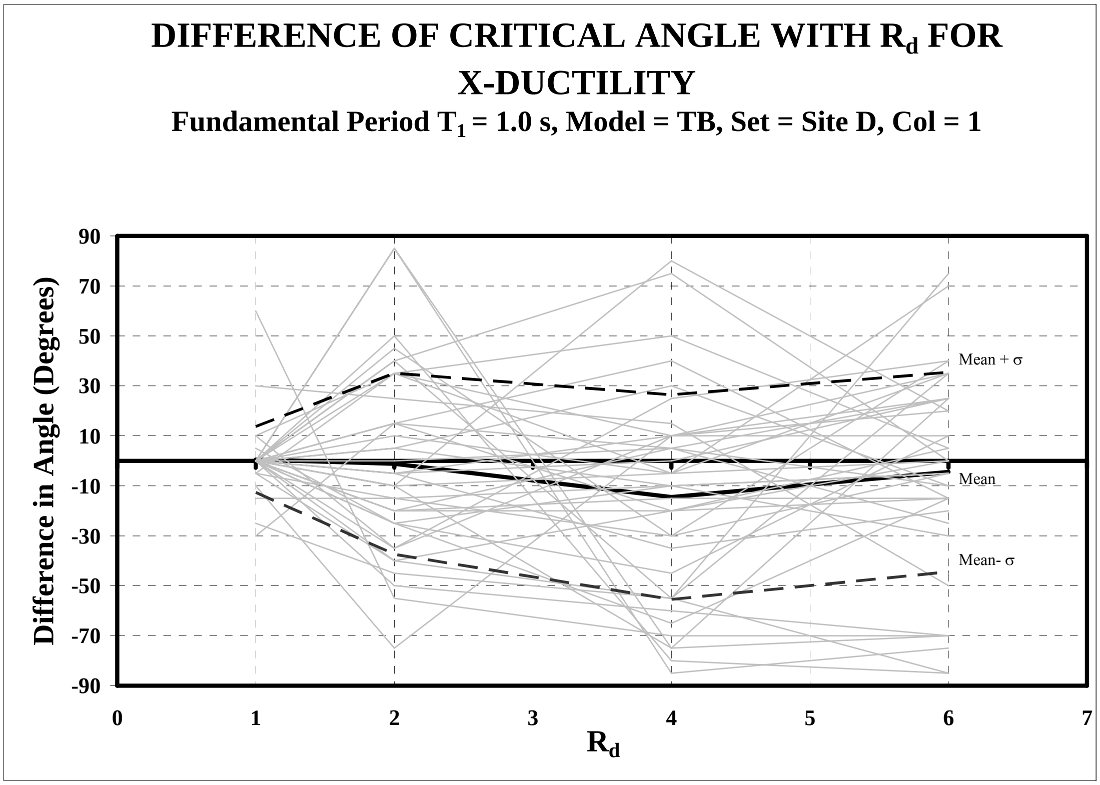

Figure 3.27 Difference of critical angle with respect to the R_d =1 at fundamental period of 1.0 s for the TB model.

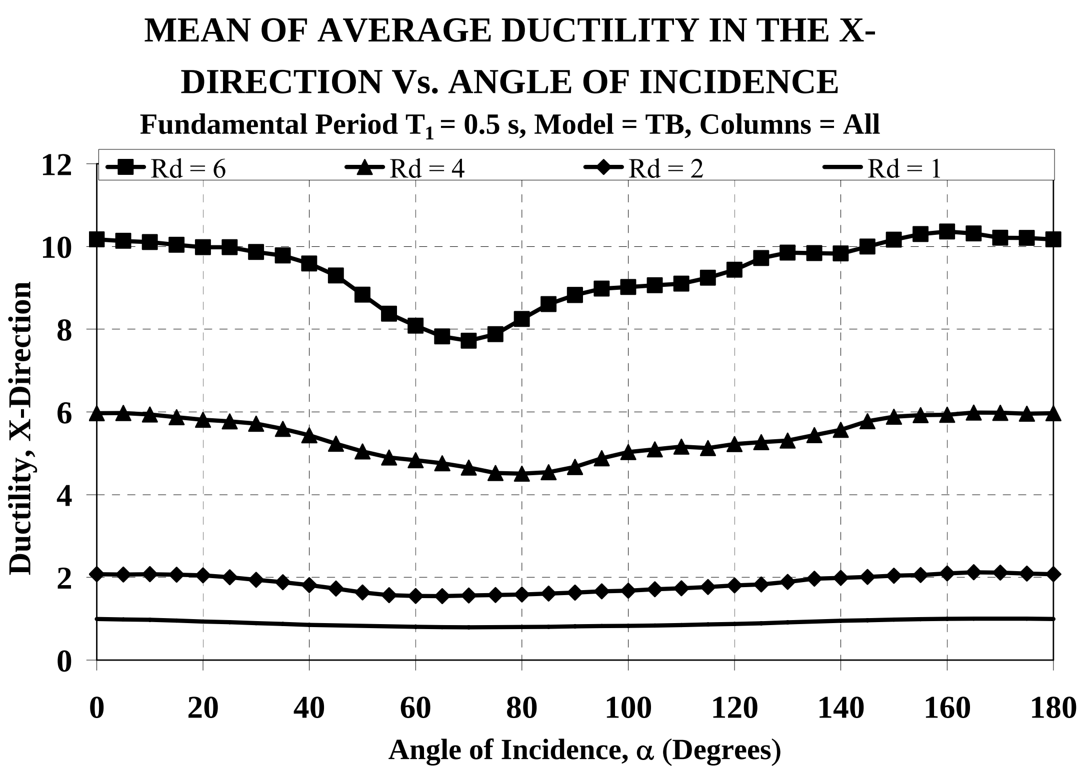

Figure 3.28 Dependence of average ductilities in the X-direction with angle of incidence at a fundamental period of 0.5 s for model TB

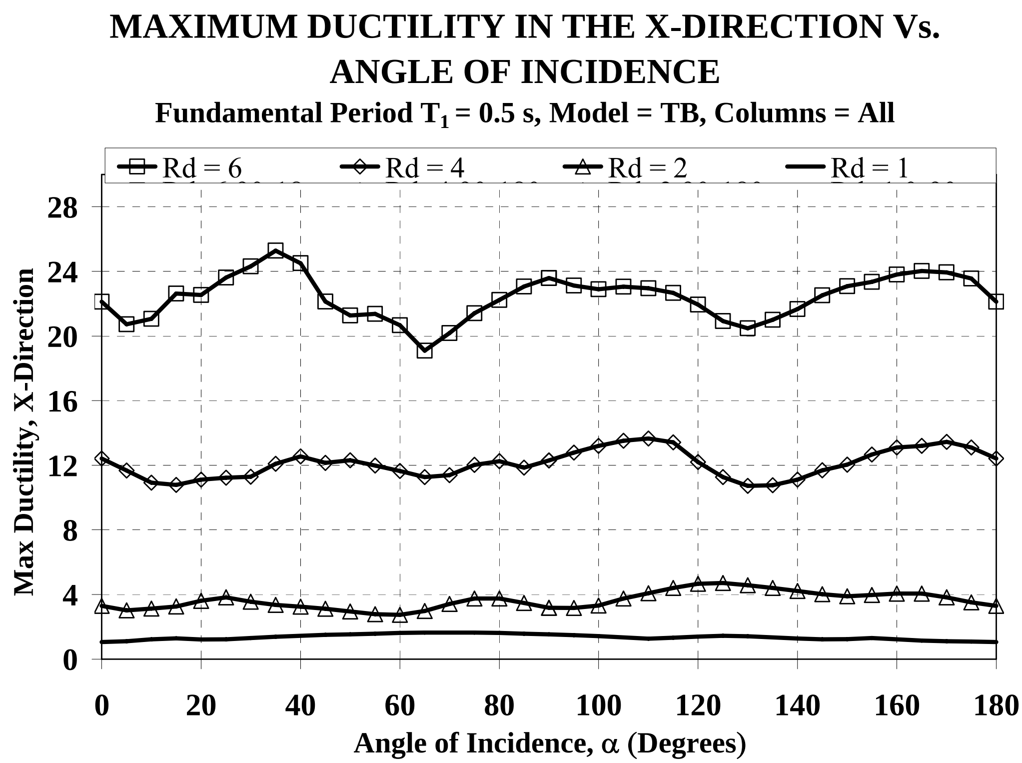

Figure 3.29 Dependence of upper bound maximum ductilities in the X-direction with angle of incidence at a fundamental period of 0.5 s for model TB

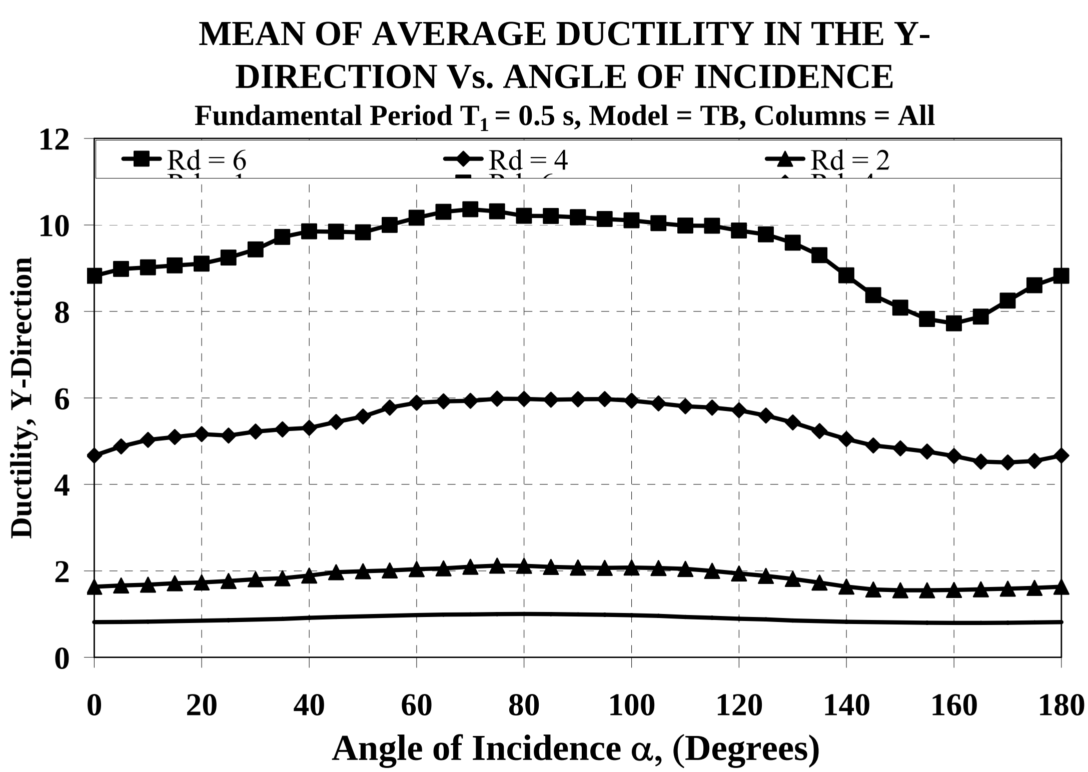

Figure 3.30 Dependence of average ductilities in the Y-direction with angle of incidence at a fundamental period of 0.5 s for model TB

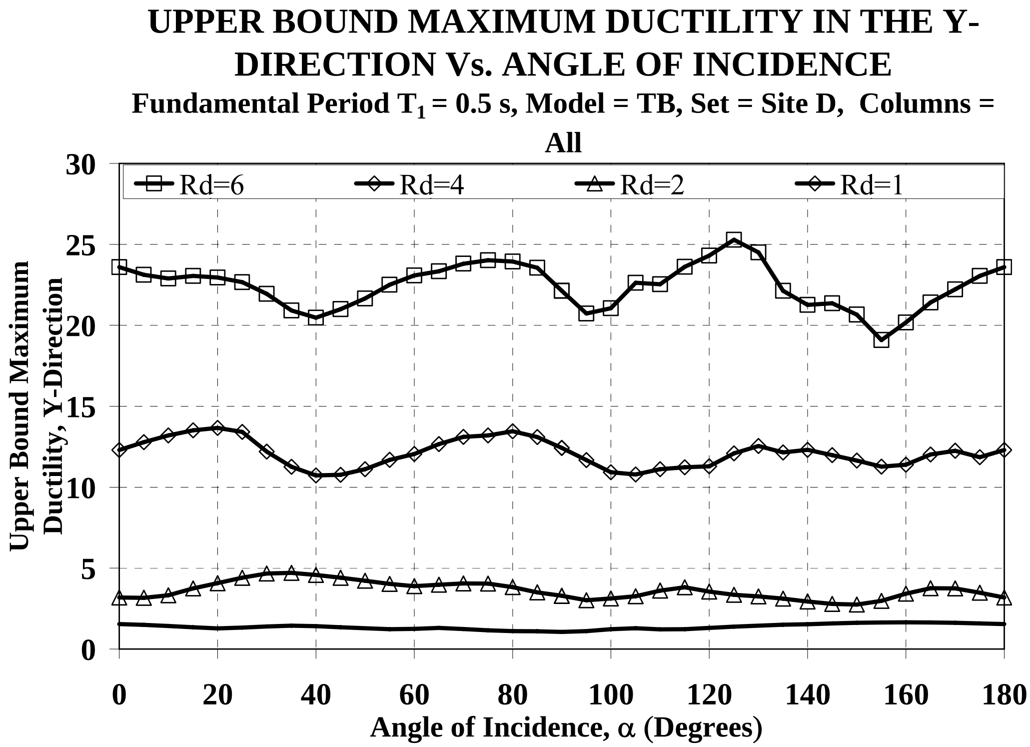

Figure 3.31 Dependence of upper bound of maximum ductilities in the Y-direction with angle of incidence at a fundamental period of 0.5 s for model TB

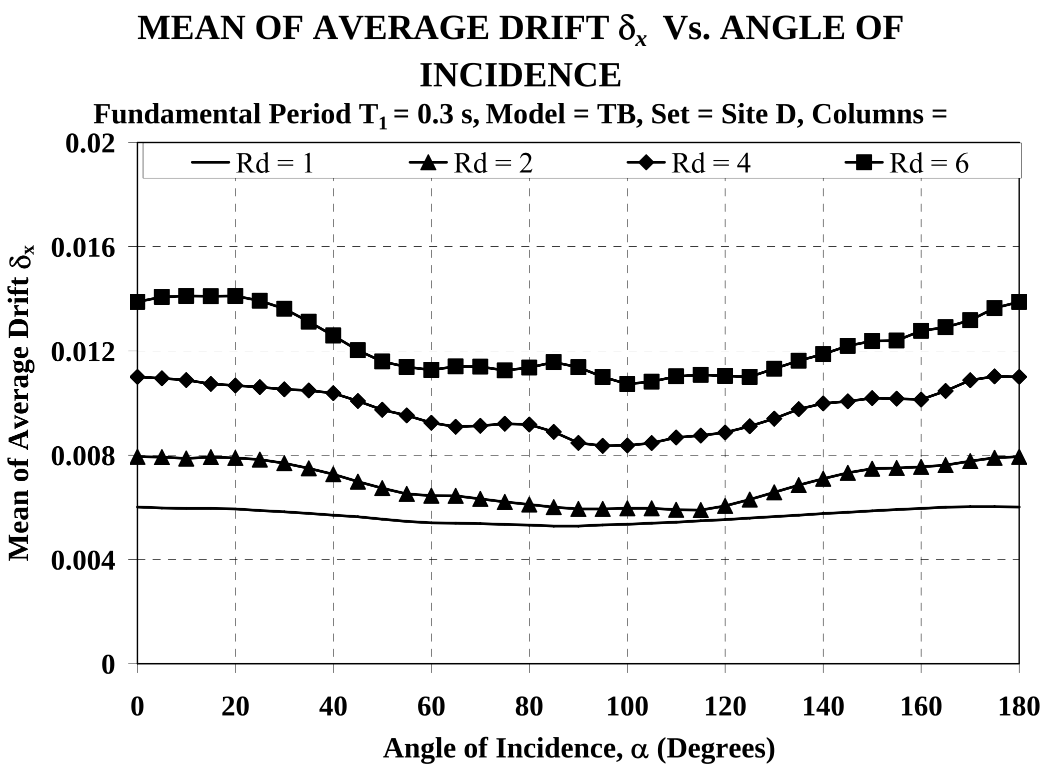

Figure 3.32 Dependence of mean of average drift in the X-direction with angle of incidence at a fundamental period of 0.3 s for model TB

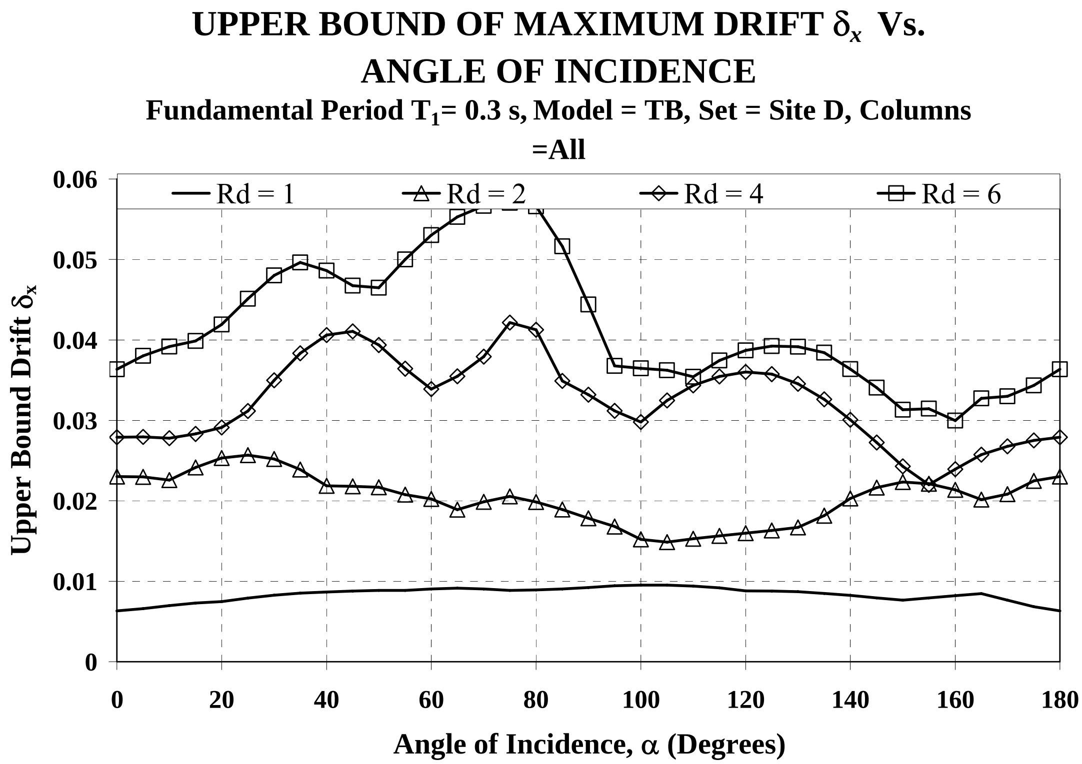

Figure 3.33 Dependence of upper bound of maximum drift in the X-direction with angle of incidence at a fundamental period of 0.3 s for model TB

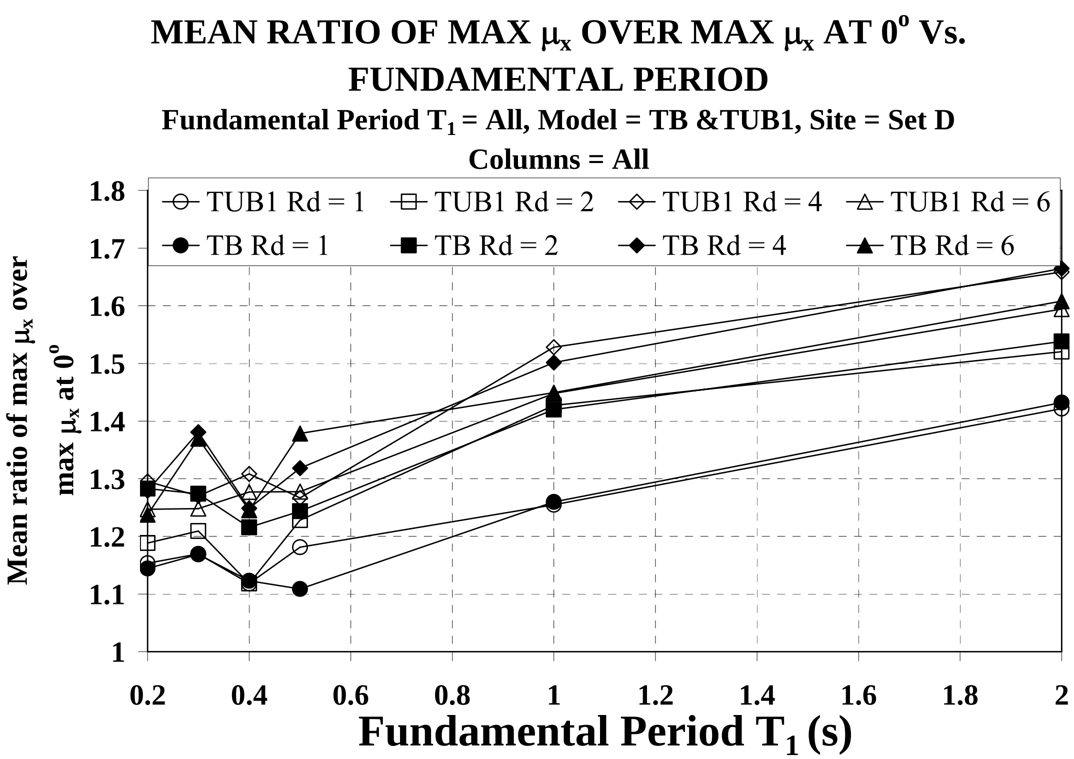

Figure 3.34 Behavior of *Max* μ_x*/Max* μ_{x0} for a given relative design intensity as a function of fundamental period

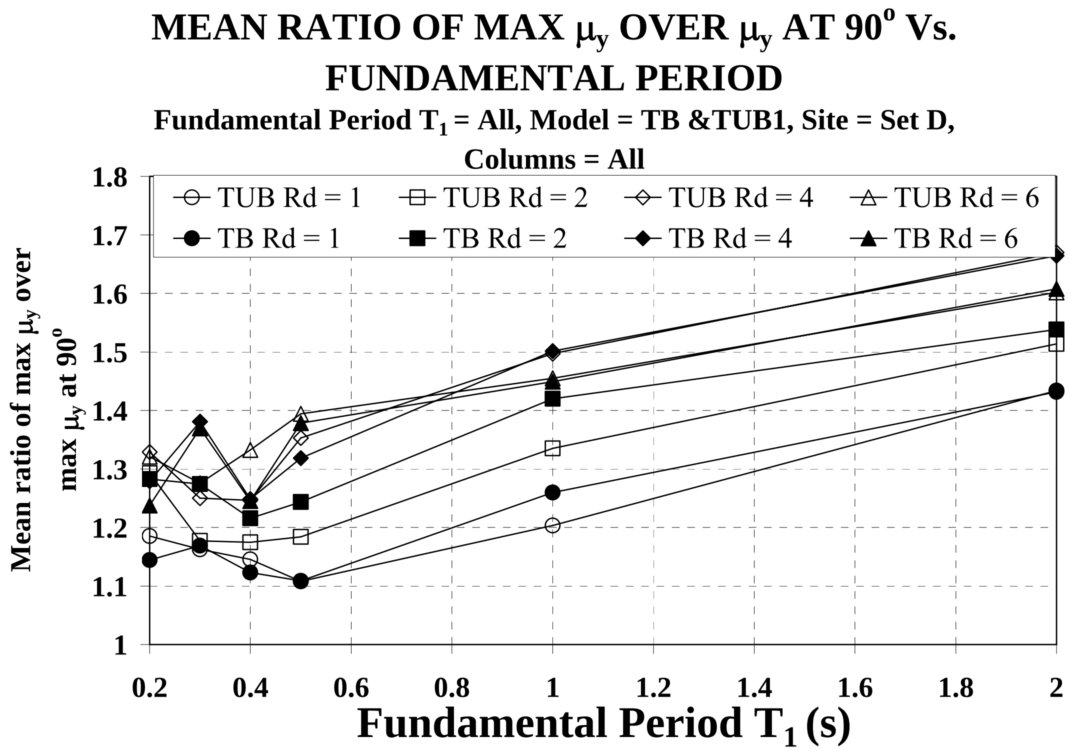

Figure 3.35 Behavior of *Max* μ_y*/Max* μ_{y90} for a given relative design intensity as a function of fundamental period

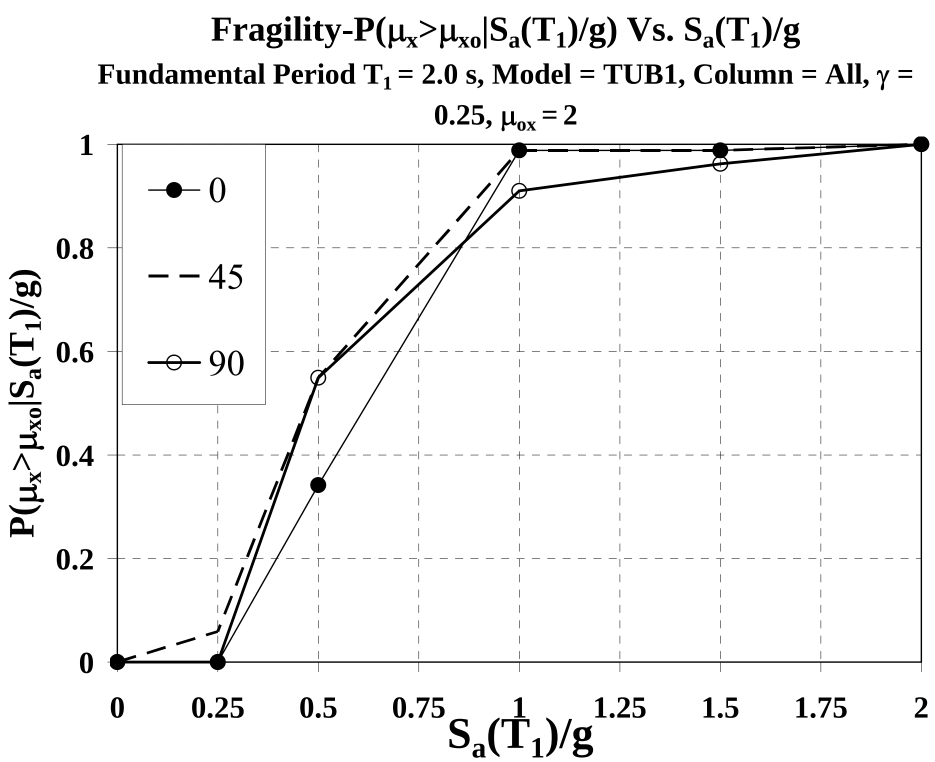

Figure 3.36 Fragility curves for ductility demands in the X-direction as a function of angle of incidence, at a fundamental period of 2.0 s for model TUB1

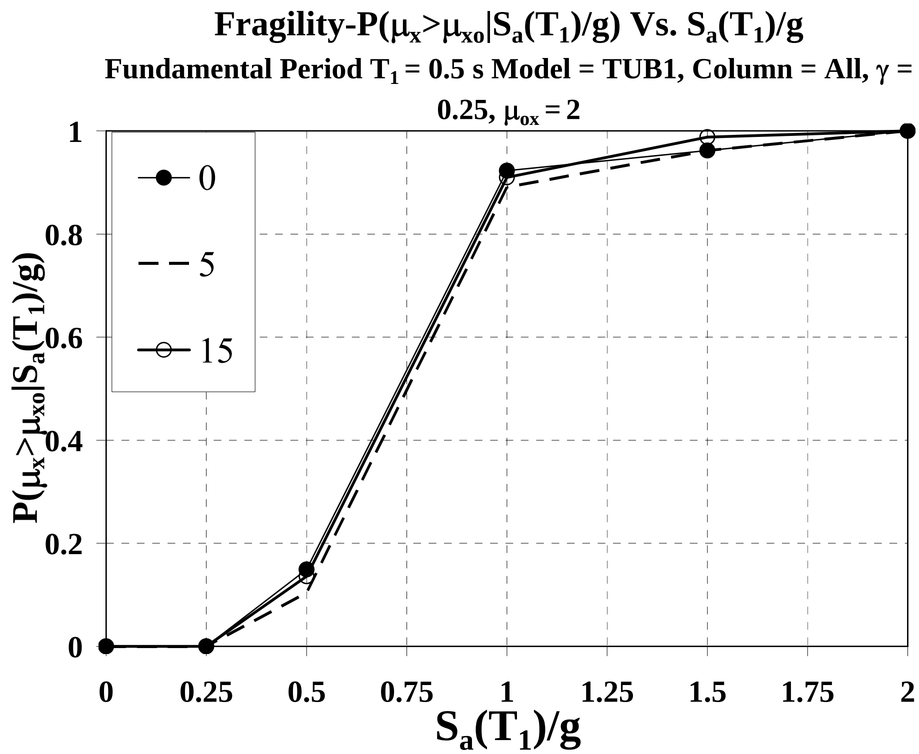

Figure 3.37 Fragility curves for ductility demands in the X-direction as a function of angle of incidence at a fundamental period of 0.5 s for model TUB1

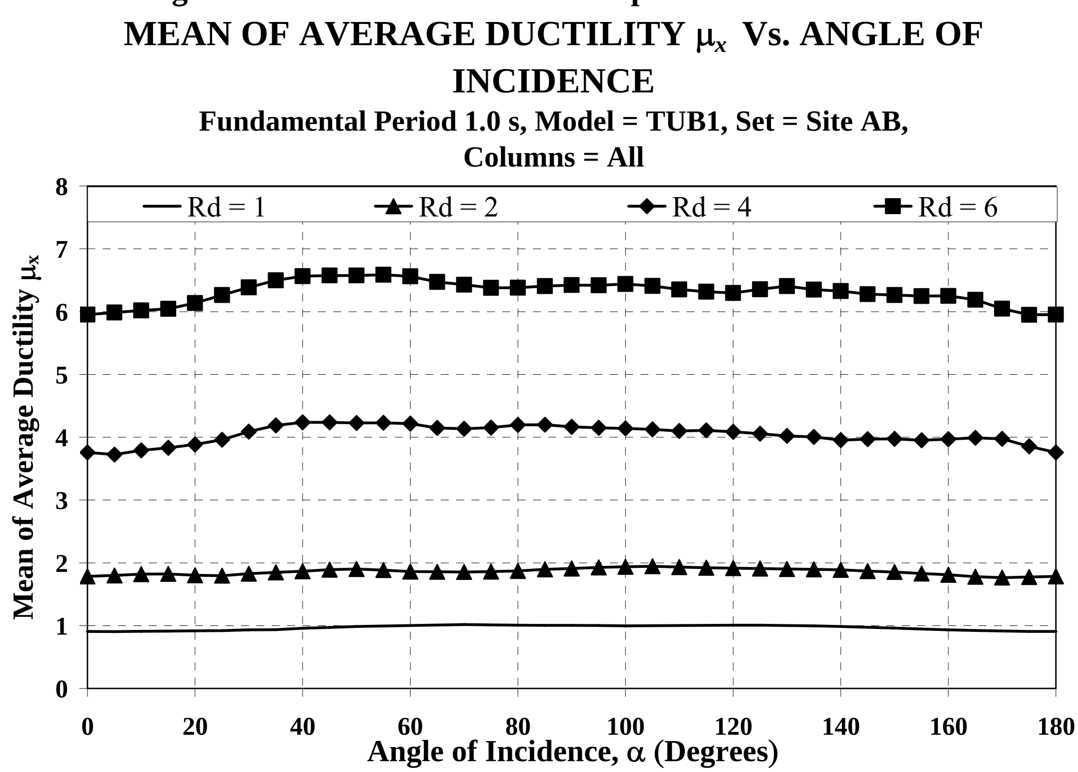

Figure 3.38 Dependence of average X-ductility on angle of incidence at a fundamental period of 1.0 s for the TUB1 model subjected to site class AB records

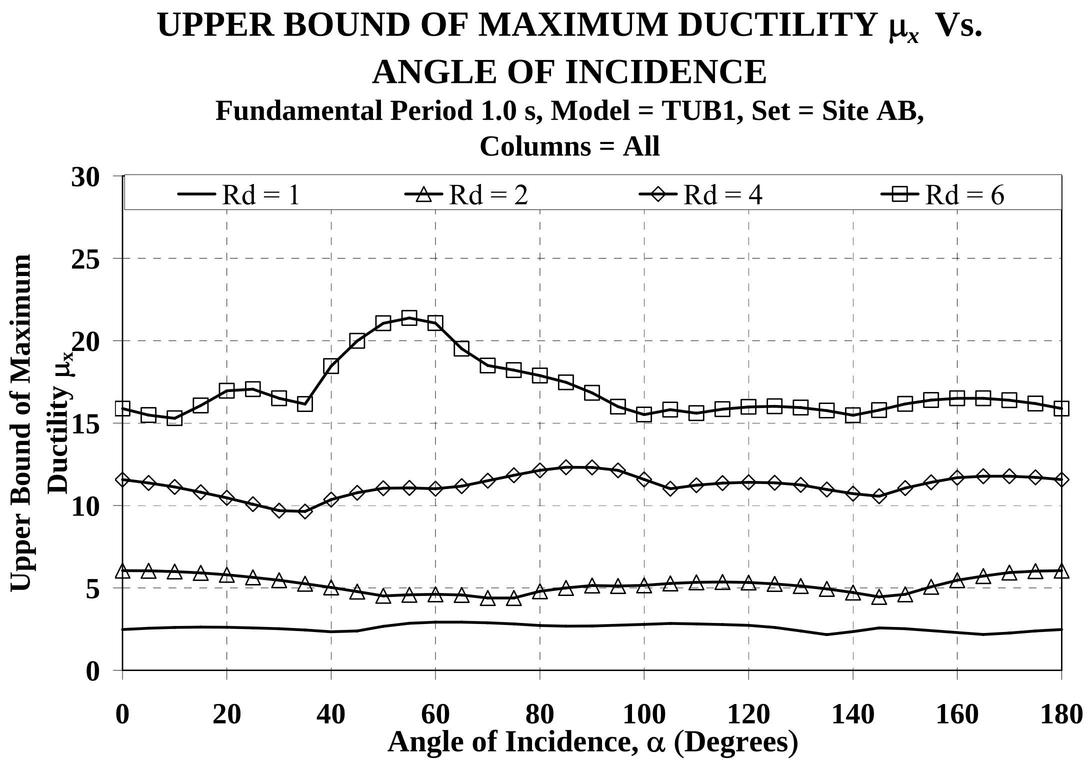

Figure 3.39 Dependence of upper bound of maximum X-ductility on angle of incidence for TUB1 model subjected to site class AB records at a fundamental period of 1.0 s for model TUB1

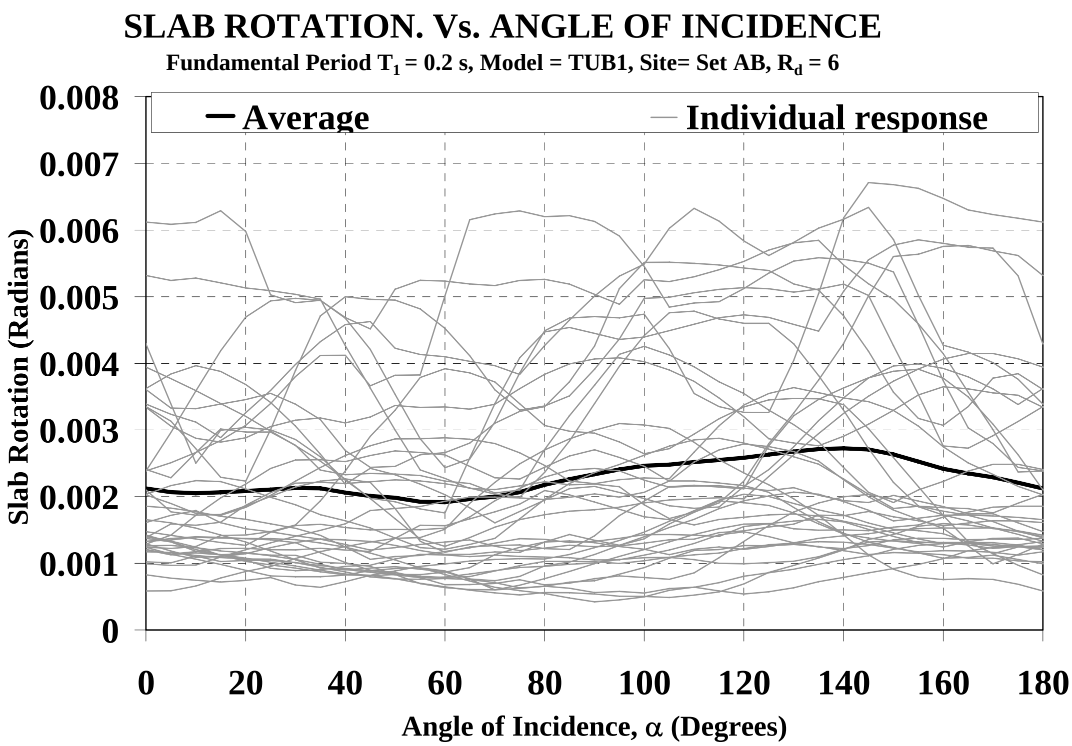

Figure 3.40 Dependence of slab rotations with angle of incidence for site AB at a fundamental period of 0.2 s for the TUB1 model

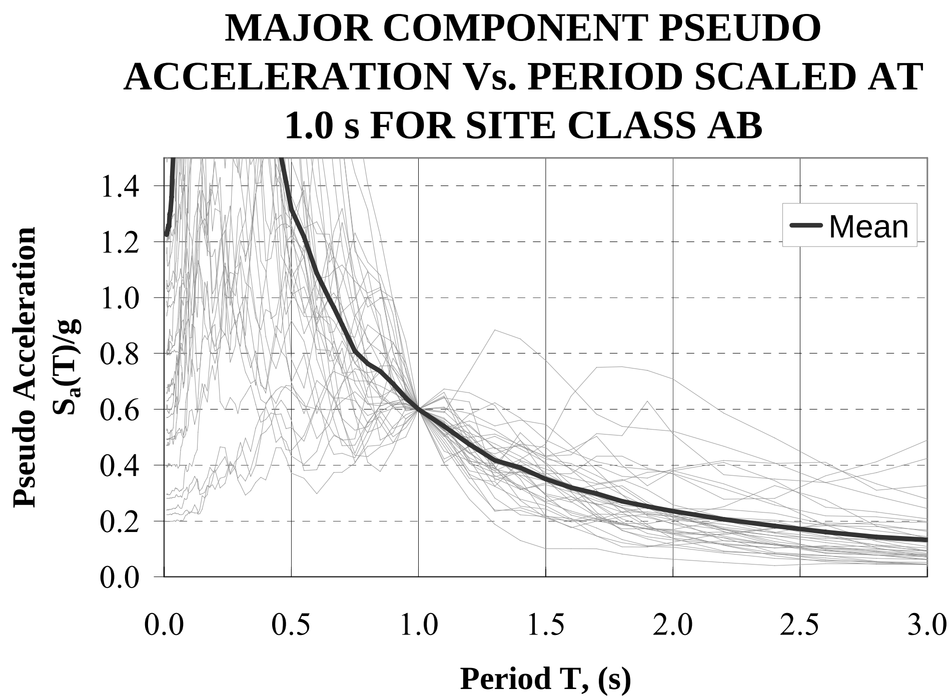

Figure 3.41 Scaled response spectra of major component at 1.0 s, site class AB

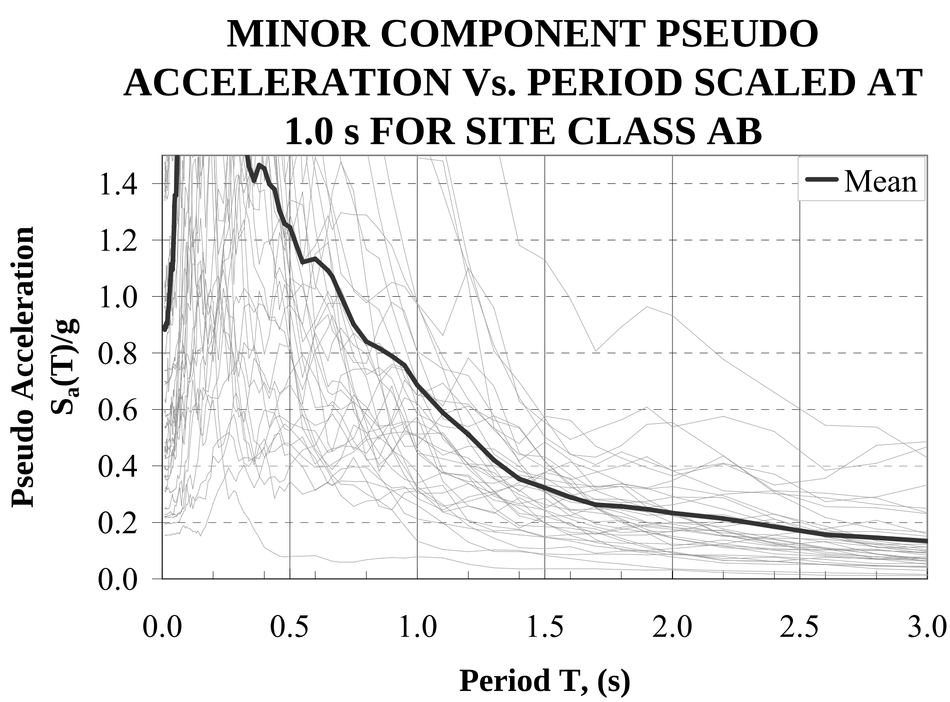

Figure 3.42 Scaled response spectra of minor component at 1.0 s, site class AB

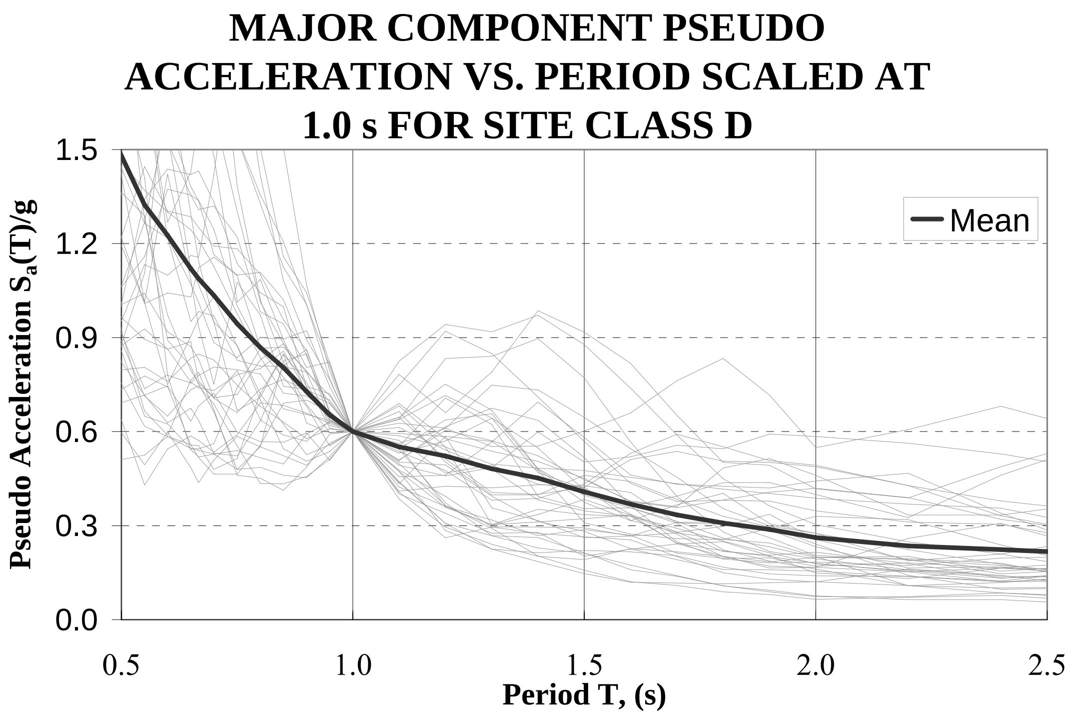

Figure 3.43 Scaled response spectra of major component at 1.0 s, site class D

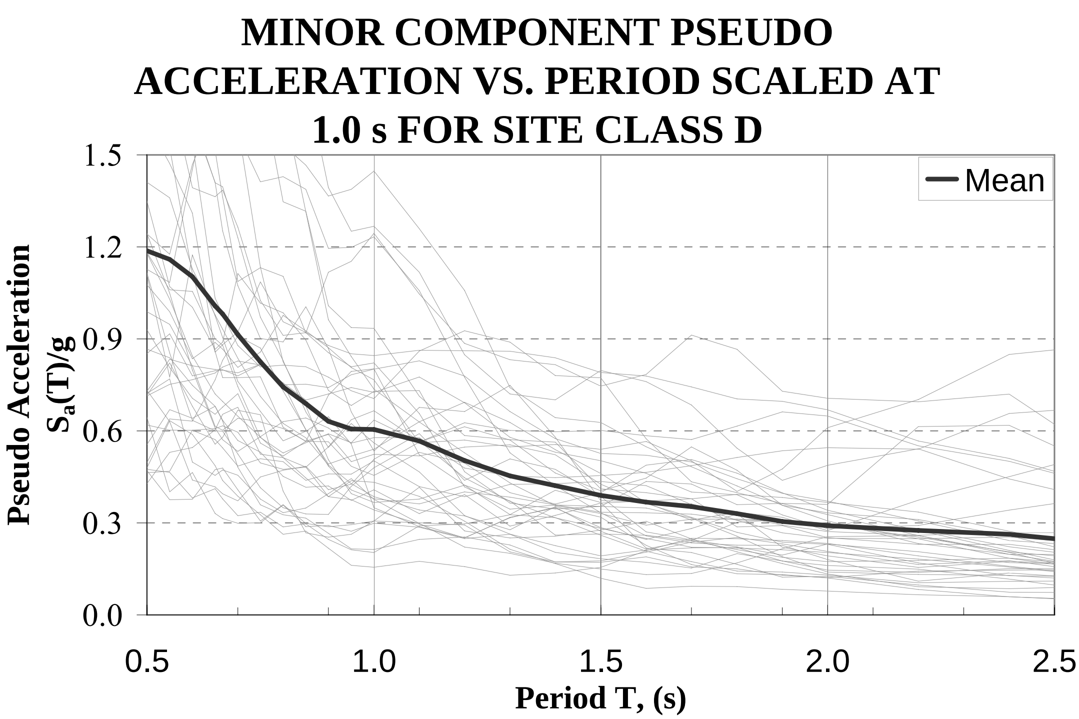

Figure 3.44 Scaled response spectra of minor component at 1.0 s, site class D

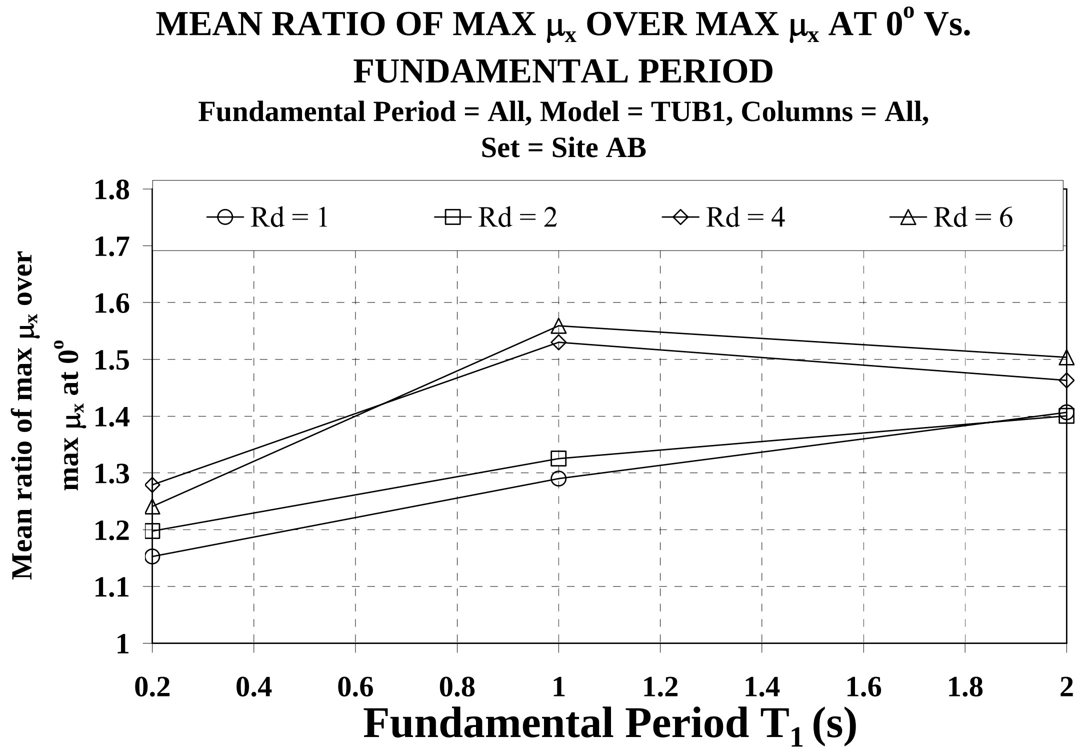

Figure 3.45 Behavior of *Max μ_x/Max μ_{x0}* for a given relative design intensity as a function of fundamental period, site AB

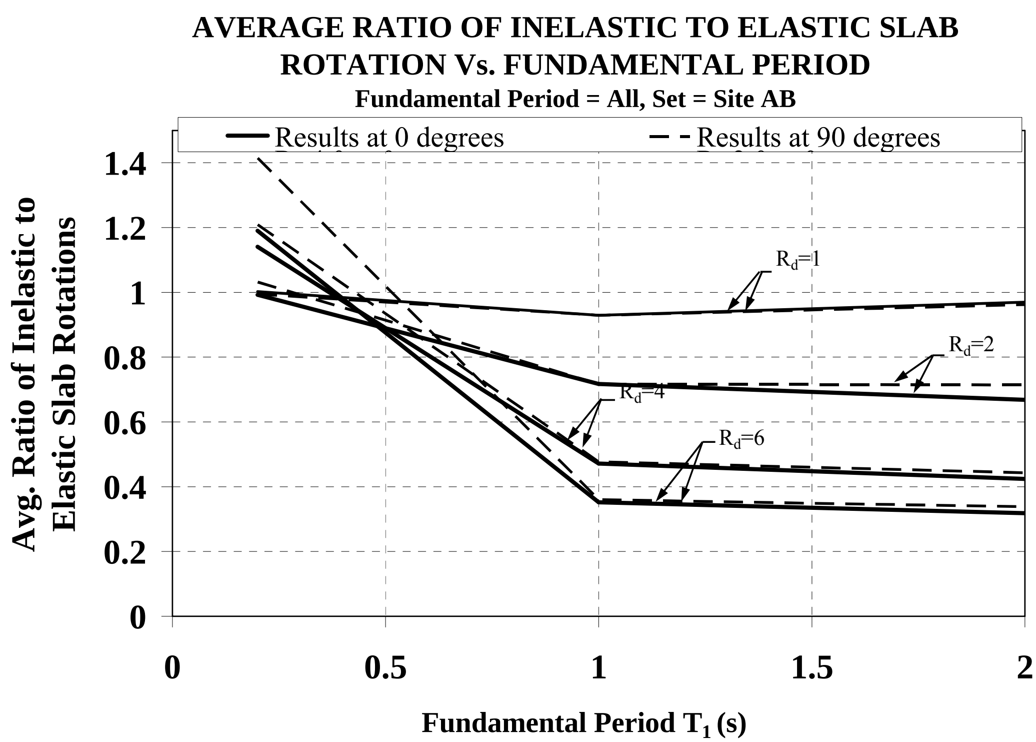

Figure 3.46 Decrease of inelastic to elastic slab rotations with period, site AB

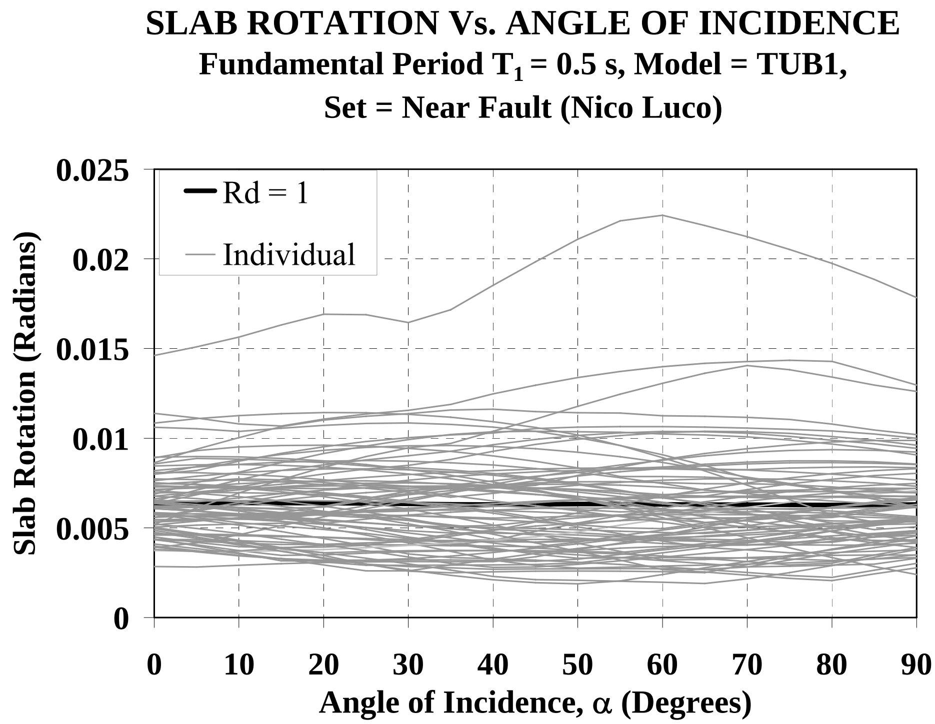

Figure 3.47 Dependence of slab rotation to angle of incidence for near-fault records at a fundamental period of 0.5 s for model TUB1

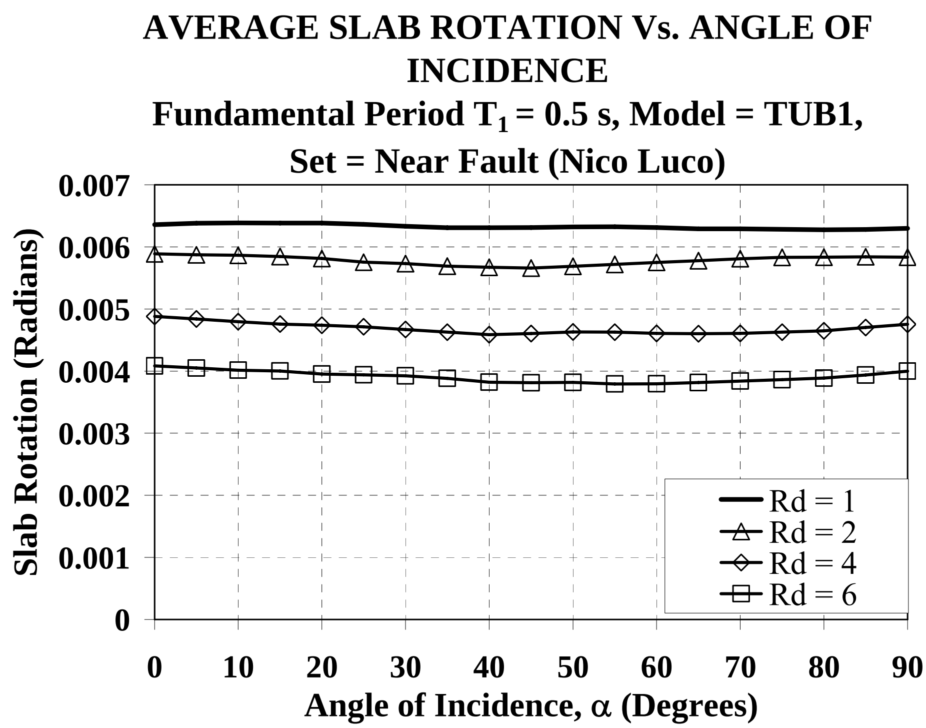

Figure 3.48 Dependence of average slab rotations on angle of incidence for near-fault records at a fundamental period of 0.5 s for model TUB1

Chapter 4 Dependence of Critical Angle on Structural Configuration

Where the last chapter was primarily focused on the base case model and the influence that frequency content had on the critical response, this chapter deals primarily with the influence that the structural configuration had on critical response. To this end, a modified TUB1 model, model TUB1* which had a considerably larger amount of mass than that of model TUB1 was examined to determine what influence mass had on the critical response. This was followed by the examination of models TUB2 and TUB3 which had different configurations of strength, rigidity and mass, which not only examined the critical response of systems with torsional effects induced via similar moment arms, but also examined the so called "balanced condition" and its ability to minimize torsional response. Models TUB1*, TUB2, TUB3 and the 3-storey structure examined in this section were subjected to only ground motion based on site class D. While the magnitudes of EDPs such as slab rotation and ductility varied, their trends were found to not be all that dissimilar to what has been found previously. The ability of the balanced condition to reduce torsional demands versus a system with a similar moment arm was found to be questionable.

THE EFFECT OF MASS ON CRITICAL RESPONSE

While several parameters have been examined in this study such as fundamental period and degree of inelasticity and their direct influence on critical angle, nothing has been said with respect to the variation of mass of the structure. So far it has been implicitly assumed that it would have had little impact on the trends seen thus far, regarding individual critical response and the average of these responses even if the magnitude of these EDPs are different. Moreover, this study focused more on general trends regarding critical angle and the quantification of the maximum demand relative to the principal axes of the structure rather than the magnitudes of the response themselves. Nevertheless, it was of interest to know what effect mass may have had on critical angles and the EDPs examined.

The results of slab rotation for the TUB1* model indicated that the average response of individual values tend to be less dependent on the angle of incidence than their individual counterparts much like that of TUB1 as illustrated in Figure 4.1. While the magnitudes of the average slab rotation are indeed much larger than those observed in TUB1 model (Figure 4.2) with a fundamental period of 1.0 s, this was not necessarily due to a larger mass attracting more force and therefore larger torsion. This behavior was primarily attributed to differences in the ratio of torsional stiffness to mass, which are not the same for both models, at a given fundamental period. That is, Model TUB1* was more flexible with regards to twisting as the third mode which corresponds to pure rotation was three times as large as the TUB1 model at this period. Also of note, was the fact that average inelastic response values decreased with degree of inelasticity, similarly to the TUB1 model at this period. With respect to ductility, the magnitude disparity between TUB1* and TUB1 was much less; however, altogether different in that the average critical angle and upper bound maximum values occur at different angles. The magnitudes with respect to ductility

(Figure 4.3-4.4) are similar to the TUB1 model at 1.0 s since the plastic moments assigned to the hinges are calculated relative to the mass of the structure, and both the first and second modes of the structure are similar. Drift magnitudes were also found to be similar to those of model TUB1.

Given that individual responses and their average for the TUB1* model exhibited similar trends to the TUB1 model, it can be concluded that the amount of mass used for the TUB1 model was adequate with respect to the study of those trends. Had the trends for the TUB1* suggested that say, individual values all obtained maximum responses around the same angle of incidence, or that the degree of R_d had no effect on the location of the critical angle, it would be clear that the amount of mass used thus far for the TUB1 models merits additional justification and/or investigation. This does not mean that mass does not affect the critical angle, or the magnitude, as Figure 4.1, 4.3 and 4.4 vs. those of TUB1 at this period (Figures 4.5 - 4.6) certainly show that they do, but the ability to predict their trend was no more apparent.

CRITICAL RESPONSE FOR STRUCTURES WITH OFFSET RIGIDITY AND STRENGTH

Drift, Ductility and Slab Rotation Demands for Models TUB2 and TUB3

With regards to critical angle, the only structures that have been examined thus far with torsion induced effects have been those due to off-set mass. Since torsion can be induced in structures that do not have offset mass it was important to look at structures that had torsion induced effects via offset rigidity and strength.

This section outlines two, single-storey structures that had torsional effects via the aforementioned configurations.

Ductility and drift demands for models TUB2 and TUB3 subjected to site D ground motions were found to be similar to that of the TB model for all fundamental periods given their small moment arms that generate torsion, as shown by average ductility demands at a fundamental period of 0.2 s, where Figure 4.7 illustrates average ductility demands for the TB model at this period, and Figures 4.8 and 4.9 are the ductilities of models TUB2 and TUB3 respectively. The individual responses are quite sensitive to angle of incidence as Figure 4.10 and 4.11 illustrate for the TUB2 and TUB3 models for slab rotations at a fundamental period of 0.2 s, while their average values are not so sensitive to angle of incidence. The ratio of maximum ductility demand in the X-direction at any angle of incidence to the maximum ductility demand in the X-direction at 0^o are also very similar to those observed for the TB model, as illustrated in Figures 4.12 for models TUB2 and TUB3. The ratio of the maximum ductility demand in the X-direction at any angle of incidence to the maximum ductility demand in the X-direction at 0^o showed that on average maximum values tended to occur when ground motions are applied at angles other than the principal orientation of the structure. This implied that structures with torsion induced via offset strength and rigidity can have demands that are typically underestimated when those demands are based on the principal building orientations.

The Balanced Condition

While drift and ductility demands were comparable for both the TUB2 and TUB3 models, and similar to those of the TB model, slab rotations; however, were a different matter. Both TUB2 and TUB3 models had slab rotation magnitudes that were typically smaller than those of the TUB1 model for all fundamental periods examined, as shown in Figures 4.13 and 4.14 vs. the TUB1 model (Figure 4.15) at a fundamental period of 0.2 s, however, the emphasis here was on the relative magnitude of slab rotations for the TUB2 model vs. those of the TUB3 model. From Figures 4.13 and 4.14 at a fundamental period of 0.2 s, it was clear that the model that exhibited the "balanced condition" (model TUB3) on average had larger slab rotation demands for most degrees of inelasticity and angles of incidence examined.

However, the slab rotation demands observed for models TUB2 and TUB3 contradict the findings of Myslimaj and Tso (Myslimaj and Tso 2005) and was found to be the case for all fundamental periods examined. The contradiction in the findings could be due to the way in which the parametric study conducted by Myslimaj and Tso for a numerical example was done, in which a single set of orthogonal ground motion components were applied at only the principal building orientations. The component directed along the X-axis of their structure (angle of incidence of 0^{o} in this work), which was a principal building orientation in their work, was scaled to 0.3g while the second component directed along the Y-axis (angle of incidence equal to 90^{o} in this work) was scaled proportionally to it. In their numerical example, strength and rigidity configurations were adjusted relative to the center of mass that stayed at the geometric center of their one-storey structure. While the centers of strength and rigidity maintained the same relative distance from each other while the distance of the pair from the center of mass varied, less attention was paid to the lever arm that induced torsion via offset strength and rigidity (Figure 4.16). The potential deficiency was that the configurations of strength and rigidity that appeared to have greater slab rotations than that of the balanced condition, did in part due to their having larger lever arms in the first place, relative to the balanced condition. In contrast, the TUB2 and TUB3 models had torsion induced by lever arms that are comparable to each other.

It was important to note that while it was possible for the "balanced condition" to produce smaller torsional demands for an individual ground motion for a given angle of incidence, this work found that on average this was not the case for the models developed. Ratios of inelastic to elastic slab rotations tended to decrease with increasing degree of inelasticity and increasing fundamental period, much like model TUB1.

CRITICAL RESPONSE FOR A 3-STOREY STRUCTURE

In general, the 3-storey structure subjected to site D ground motions exhibited behavior that has been found for one-storey structures. Individual responses tended to be sensitive to angle of incidence but the mean of average ductilities tended to show little dependence on the angle of incidence as exhibited in Figures 4.17 and 4.18 at a fundamental period of 1.0 s and 2.0 s at the 3rd floor respectively while upper bound maximums showed slightly more sensitivity. This was typical of what was observed for drift and slab rotations at both fundamental periods for all floors. Maximum ductility demand in the X-direction at any angle of incidence to the maximum ductility demand in the X-direction at 0^{o} depended on the floor examined as shown in figures 4.19-4.21 but typically increased with fundamental period and were bound between values of 1.15 and 1.85 similarly to the maximum ductility demand in the X-direction at any angle of incidence to the maximum ductility demand in the X-direction at 0^{o} for the TUB1 model. Similar to the single-storey structures examined, ductility ratios for the 3-storey structure showed that on average maximum values tended to occur when ground motions were applied at angles other than the principal orientation of the structure, and implied that the phenomenon that occurred for single-storey structures also manifests itself in multistory structures without vertical irregularities. Demands found in this 3-storey structure typically were also underestimated when compared to demands based on principal building orientations alone. The behavior that was observed for models TUB1, TUB1*, TUB2 and TUB3 with regards to decreasing ratios of inelastic to elastic slab rotations was also noted for this multi-storey structure as seen in Figure 4.22, which depicts slab rotations for Floor 1 at a fundamental period of 1.0 s.

Response of a "Realistic" Multi-Storey Structure

All the models in this work consisted of either idealized one-storey structures or a 3-storey structure. While such models can be useful in drawing conclusions for general behavior noted thus far, it was still useful to verify that similar behavior can occur in more "realistic structures". So far, it has been noted that individual responses of the EDPs defined in this work can vary quite a bit with angle of incidence. Figure 4.23 (reproduced from Athanatopoulou 2005) illustrated this behavior for axial force at column C3 of an asymmetric 5-storey reinforced concrete structure (Figure 4.24) which had 5% damping for all modes where the ratio of maximum axial force at any angle of incidence to axial force in the X-direction at 0^o for column 3 reached a ratio of approximately 1.45 along the Y-axis of Figure 4.23 for the angle of incidences examined. Other quantities such as bending moment, shear force and displacement approach ratios as high as 1.8 with respect to the response that occurs at an angle of incidence of 0^o (Figures 4.25-4.27). The first floor of this structure had a height of 14'-9" while the remaining floors had a height of 9'-10". Three time histories for El Centro, Loma Prieta and Kobe were conducted for this structure each of which were composed of three components (two lateral and one vertical). The first floor of this structure had a mass of about 247 kips worth of weight while floors 2-4 had mass equal to 233 kips and the remaining floor had a weight of 175 kips.

Another example of where a more "realistic structure" exhibited some of the general behavior noted in this work can be found in the work done by Franklin and Volker (Franklin and Volker 1982). In their work, an auxiliary reinforced concrete diesel power building modeled as a 3D structure was subjected to El Centro ground motion with 2 lateral components at 3 angles of incidence (0^o, 90^o, and 45^o). This 4 storey, shear wall structure had overall dimensions of 74' wide x 75'long x 76' tall and was modeled as having 4% damping which represented concrete sections that had significant cracks. From the nonlinear time history analysis performed, it was observed that slab rotations were greater at an angle of incidence of 45^o than at the principal building orientations (0^o, 90^o). Ductility factors defined in their work were a function of yield, and post yield rotations which for individual wall members at angles of incidence of 45^o were larger than the results at 90^o but not greater than at 0^o for certain members. Their work shows that angles of incidence other than those based on principal orientations can produce demands which are larger, and at the same time, show that EDPs of interest can not be necessarily minimized by one given angle of incidence.

SUMMARY AND CONCLUSIONS

This chapter shifted focus from frequency-content-based effects with regards to critical angle to structural-configuration effects. Specifically, with regards to single-storey structures subjected to NEHRP site D ground motions, the sensitivity of critical angle with respect to the amount of mass, placement of center of strength and center of rigidity was examined for the following EDPs: ductility, drift and slab rotation. The results of the so called “balanced condition” was investigated, while the effect that additional stories had on critical angle was examined via the 3-storey structure subjected to site class D ground motions. Finally, a more “realistic structure” from Athanatopoulou 2005 showcased several phenomena that have been observed for both single and multi-storey structures of this work.

While additional mass in model TUB1* as compared to model TUB1 tended to change the magnitudes of slab rotations, and to a smaller extent drift and ductility, the trends exhibited by this model were very similar to those of model TUB1, in that individual responses were sensitive to angle of incidence with no discernable pattern while the average of those individual responses appeared to be weakly dependent on angle of incidence. Since trends for model TUB1* were no different than those of model TUB1, it was concluded that the amount of mass in the models examined in this work were sufficient to study critical responses. The ratio of the maximum ductility demand in the X-direction at any angle of incidence to the maximum ductility demand in the X-direction at 0^o for this model was very similar to that of model TUB1, indicating that the angle of incidence tended to occur at angles other than the principal orientation. Therefore, demands tended to be underestimated as compared to the demands at the principal orientation.

With regards to drift and ductility for models TUB2 and TUB3, the critical response exhibited several familiar phenomena in that the individual responses were sensitive to the angle of incidence while the average of these individual responses appeared to be less sensitive to angle of incidence. The ratio of the maximum ductility demand in the X-direction at any angle of incidence to the maximum ductility demand in the X-direction at 0^o was very similar to model TB. With regards to slab rotation however, the difference was quite clear: The balanced condition (model TUB3) does not necessarily produce smaller torsional demands at most angles. While larger responses can occur for a given ground motion for model TUB2, they on average do not occur for all degrees of inelasticity. Ratios of inelastic to elastic slab rotations tended to decrease with increasing fundamental period and increasing degree of inelasticity, similar to model TUB1.

Finally, the behavior that has been found for all single-storey structures also manifested itself in the 3-storey structure. In particular, individual responses of drift, ductility and slab rotation were sensitive to the angle of incidence, but their average appeared to be less sensitive to angle of incidence. The ratio of the maximum ductility demand in the X-direction at any angle of incidence to the maximum ductility demand in the X-direction at 0^o tended to increase with fundamental period for each floor examined although at different rates, but paralleled the results of other models subjected to site D ground motions. Slab rotations also decreased with increasing period and degree of inelasticity. As an example of a "real" structure, a 5-storey structure from prior work by Athanatopoulou (Athanatopoulou 2005) was called to attention and provided results that were similar to those of this work. In this regard, with respect to maximum response of this more realistic structure subjected to three ground motions, the work by Athanatopoulou illustrated that displacement, maximum moment, shear force and column axial force typically did not have maximums at principal building orientations.

The conclusion that can be drawn from those results and of this chapter are that the critical response does not occur at principal orientations even for structures with significantly different configurations of center of strength, center of rigidity, center of mass, and number of stories (up to three or so). Given the difficulty of determining any discernable pattern in the critical angle, the following chapter focused primarily upon statistical quantities of the ratio of the maximum ductility demand in the X-direction at any angle of incidence to the maximum ductility demand in the X-direction at 0^o to other parameters in an attempt to better understand the critical response.

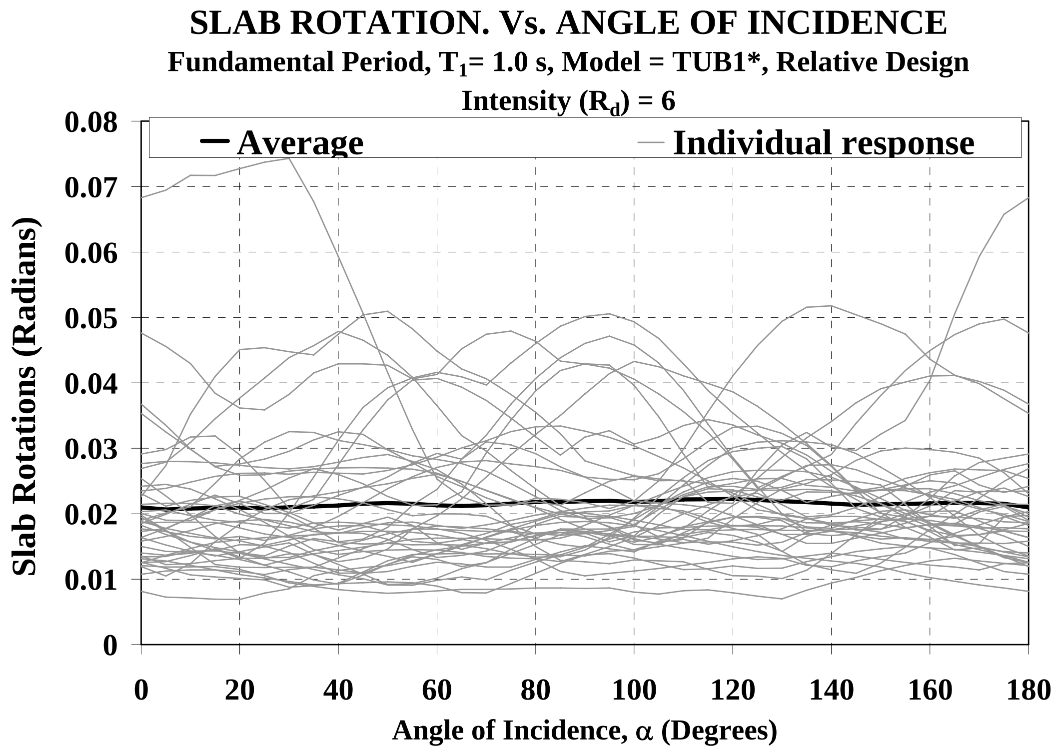

Figure 4.1 Dependence of slab rotations with angle of incidence for the model TUB1* and for R_d = 6

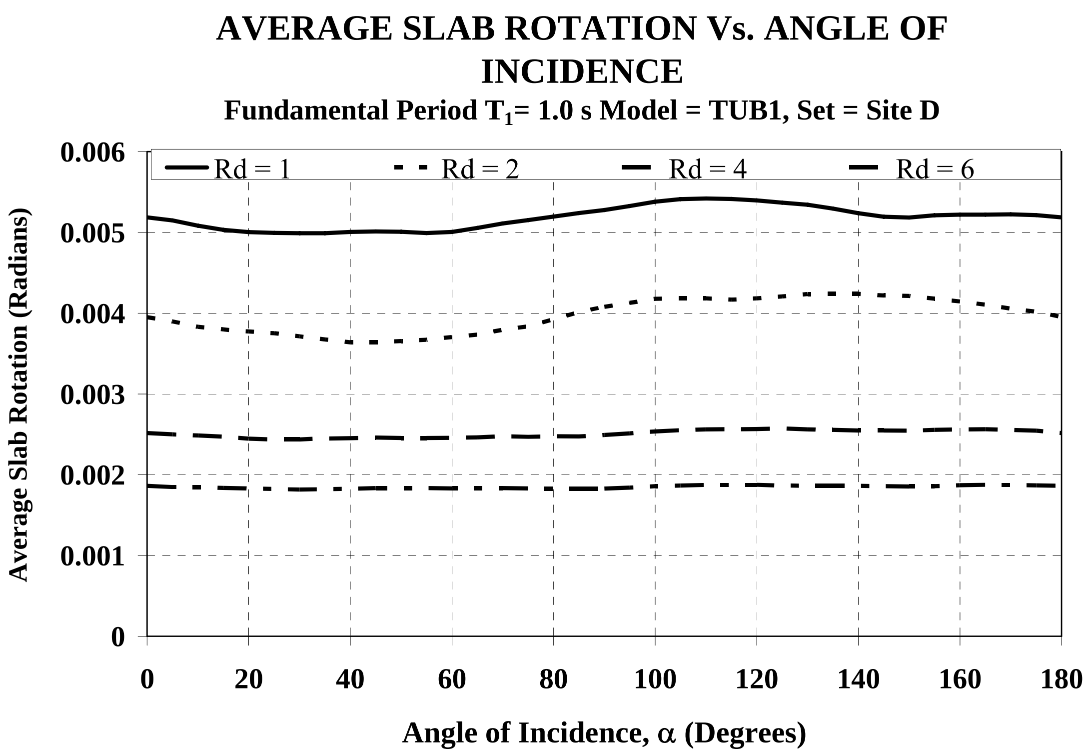

Figure 4.2 Dependence of average slab rotations with angle of incidence for TUB1 and fundamental period of 1.0 s.

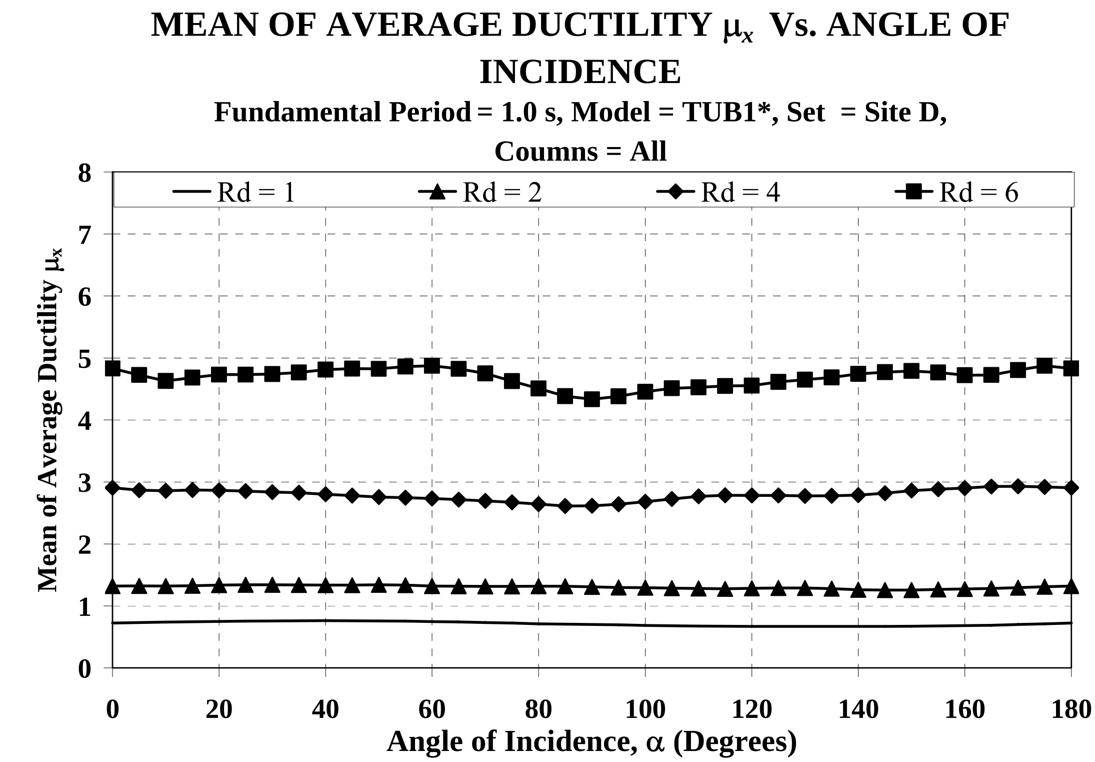

Figure 4.3 Dependence of average ductilities in the x-direction with angle of incidence for TUB1* and fundamental period of 1.0 s.

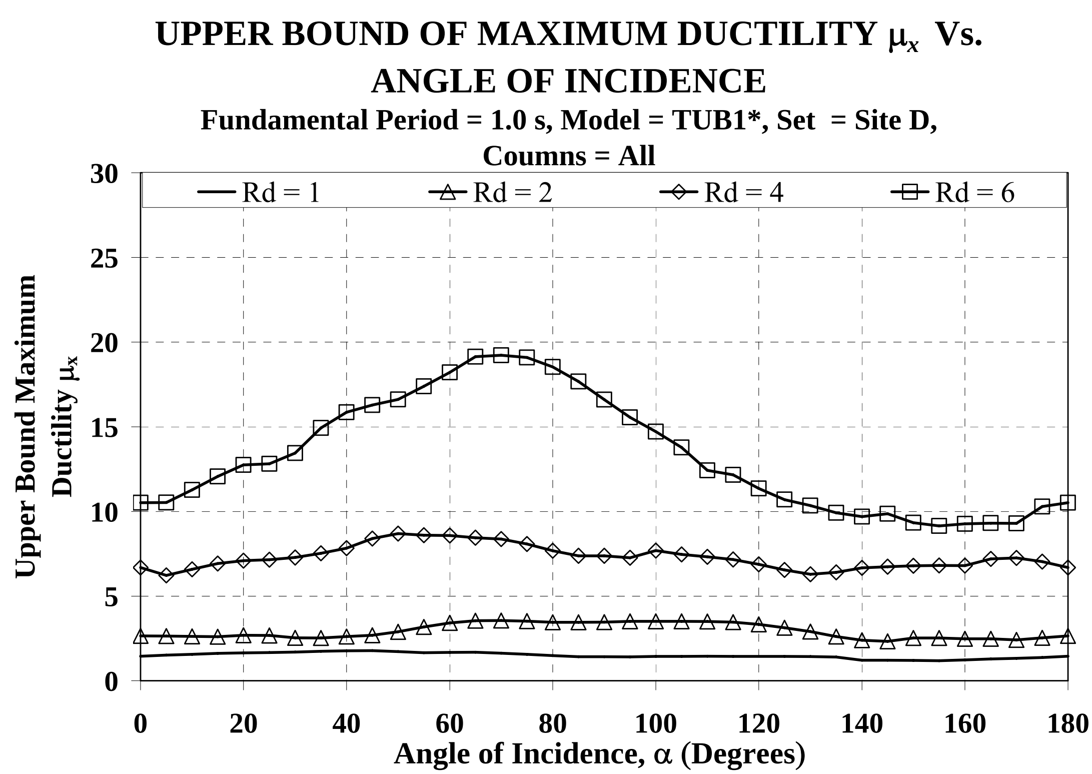

Figure 4.4 Dependence of upper bound of maximum ductilities with angle of incidence for TUB1* and fundamental period of 1.0 s.

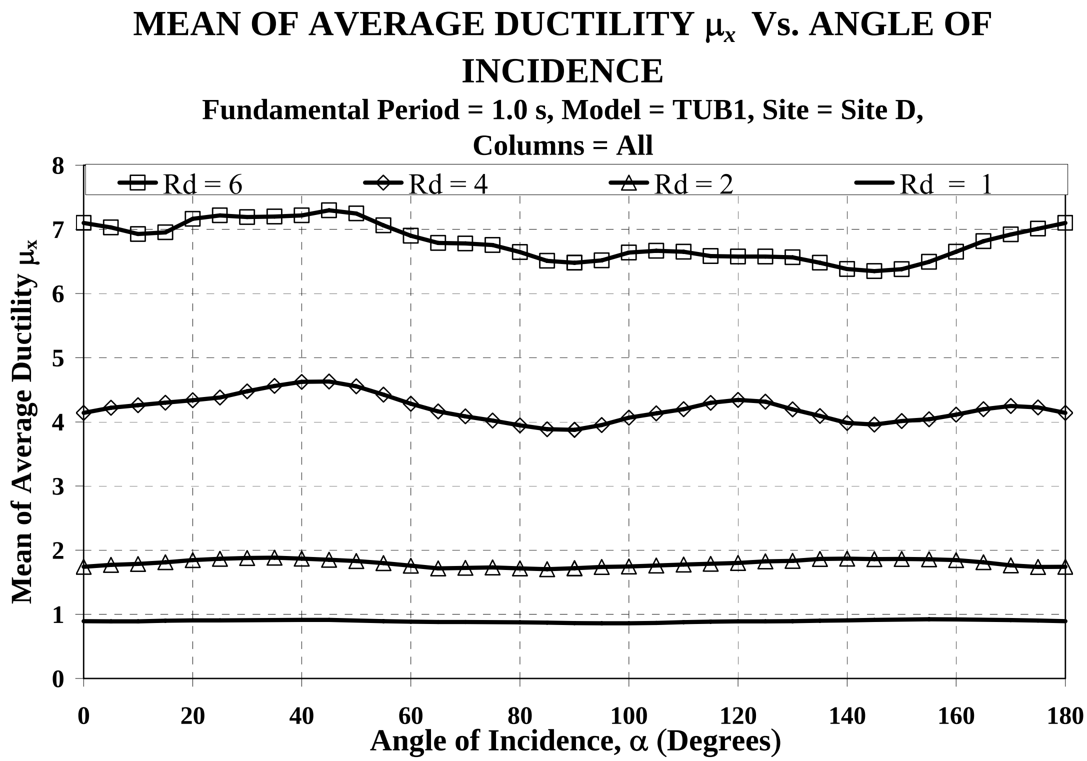

Figure 4.5 Dependence of average ductilities with angle of incidence for model TUB1 with fundamental period of 1.0 s.

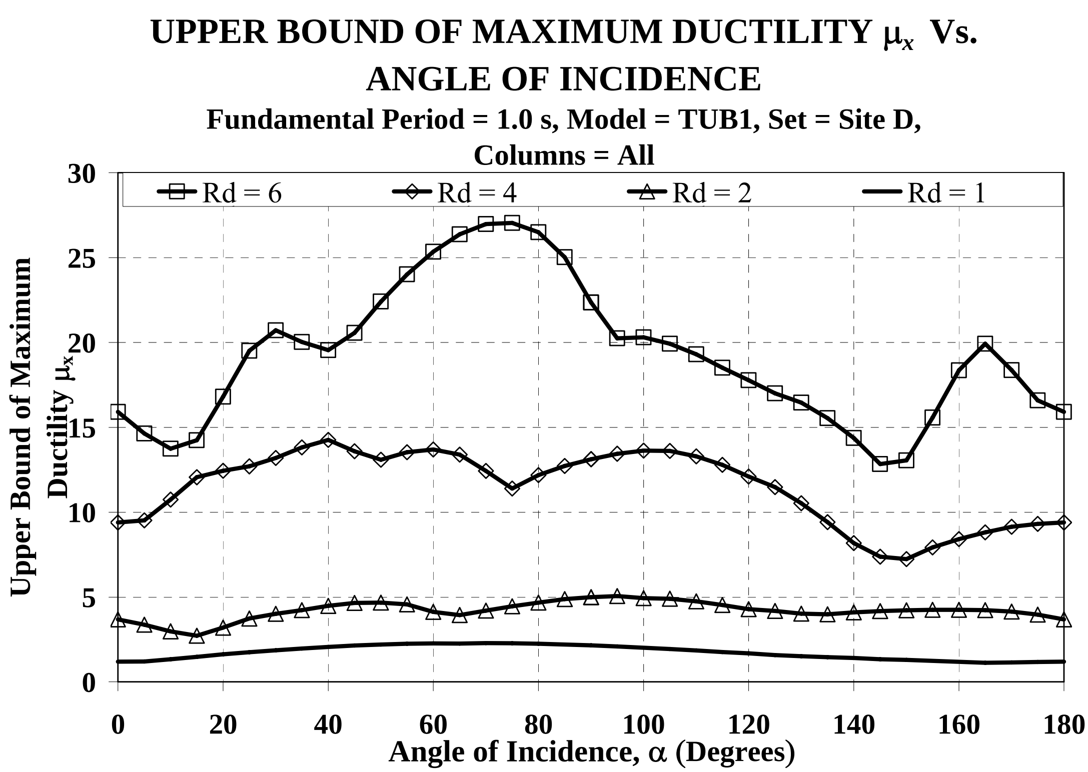

Figure 4.6 Dependence of upper bound of maximum ductilities in the x-direction with angle of incidence for model TUB1 with fundamental period of 1.0 s.

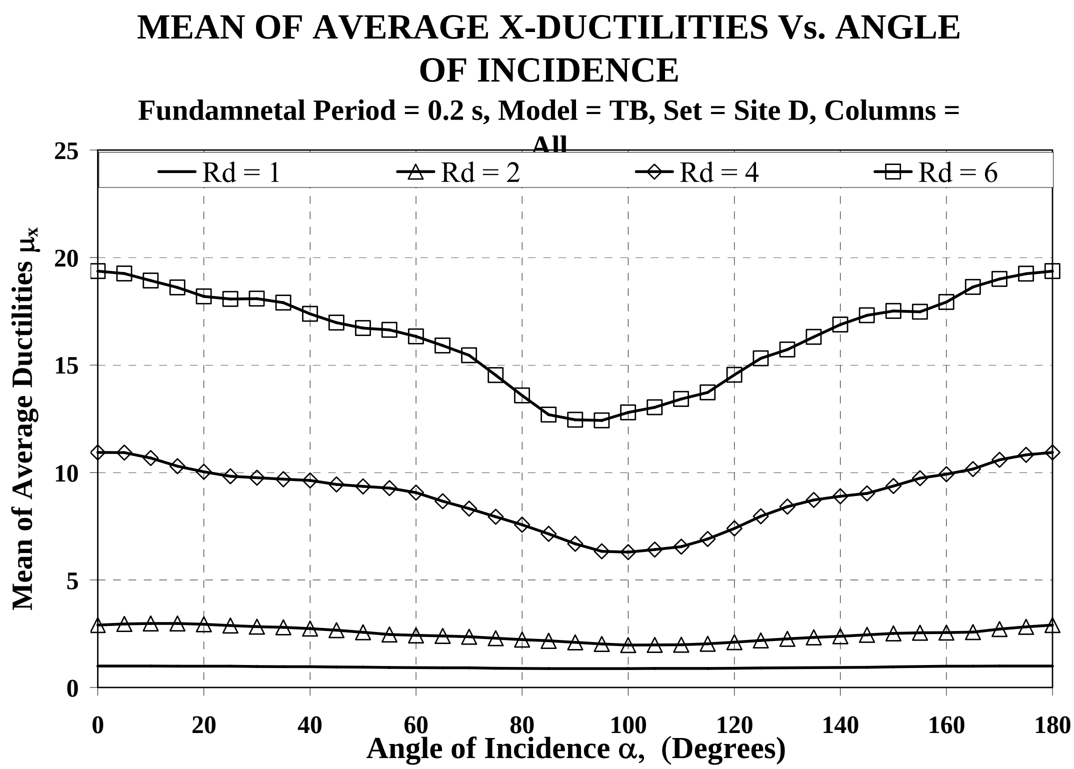

Figure 4.7 Average ductilities in the X-direction and their dependence on angle of incidence, model TB, fundamental period of 0.2 s

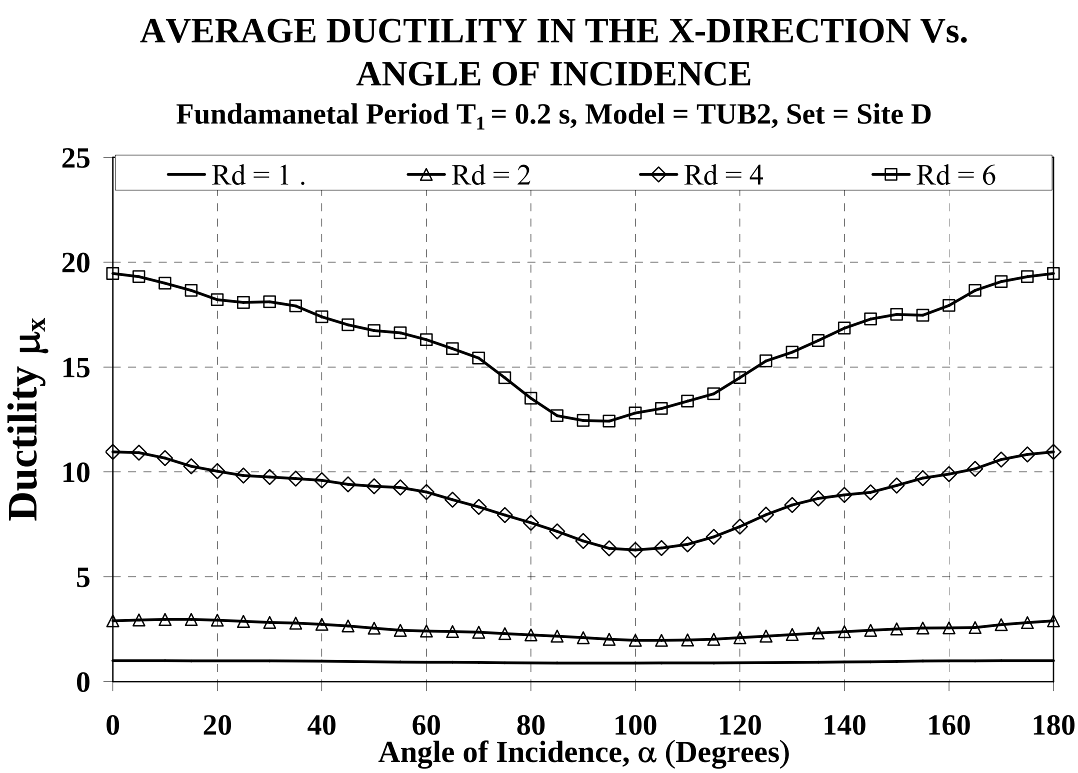

Figure 4.8 Average ductilities in the X-direction and their dependence on angle of incidence, model TUB2, fundamental period of 0.2 s

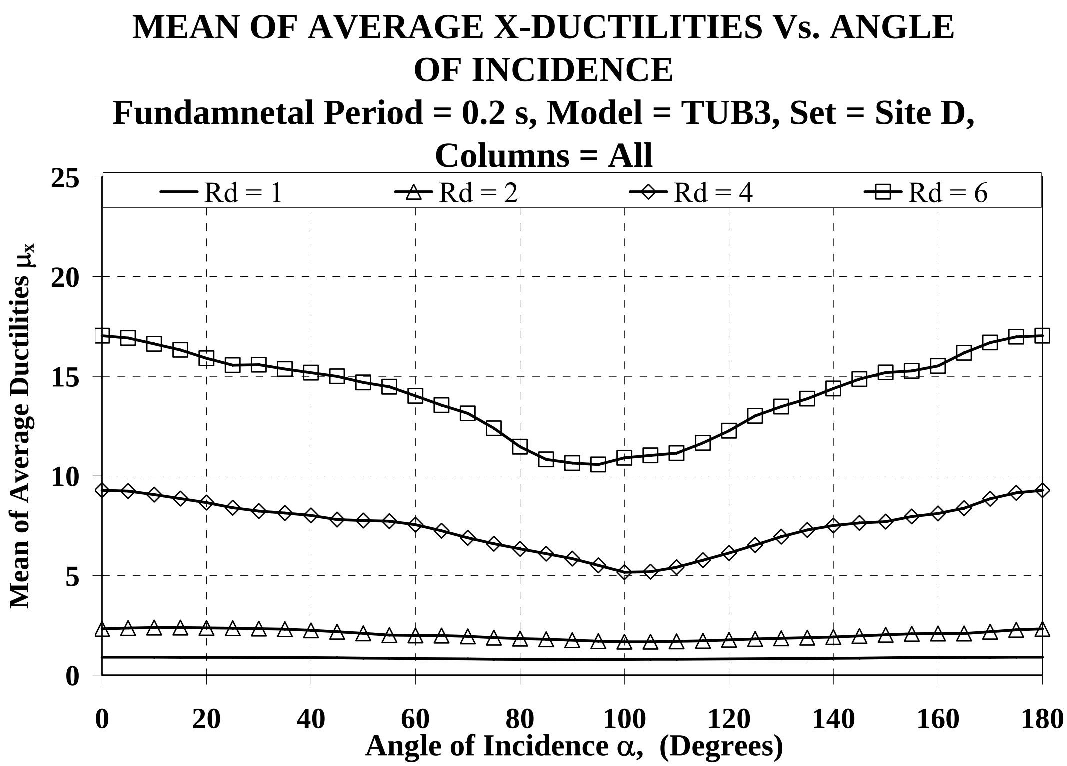

Figure 4.9 Average ductilities in the X-direction and their dependence on angle of incidence, model TUB3, fundamental period of 0.2 s

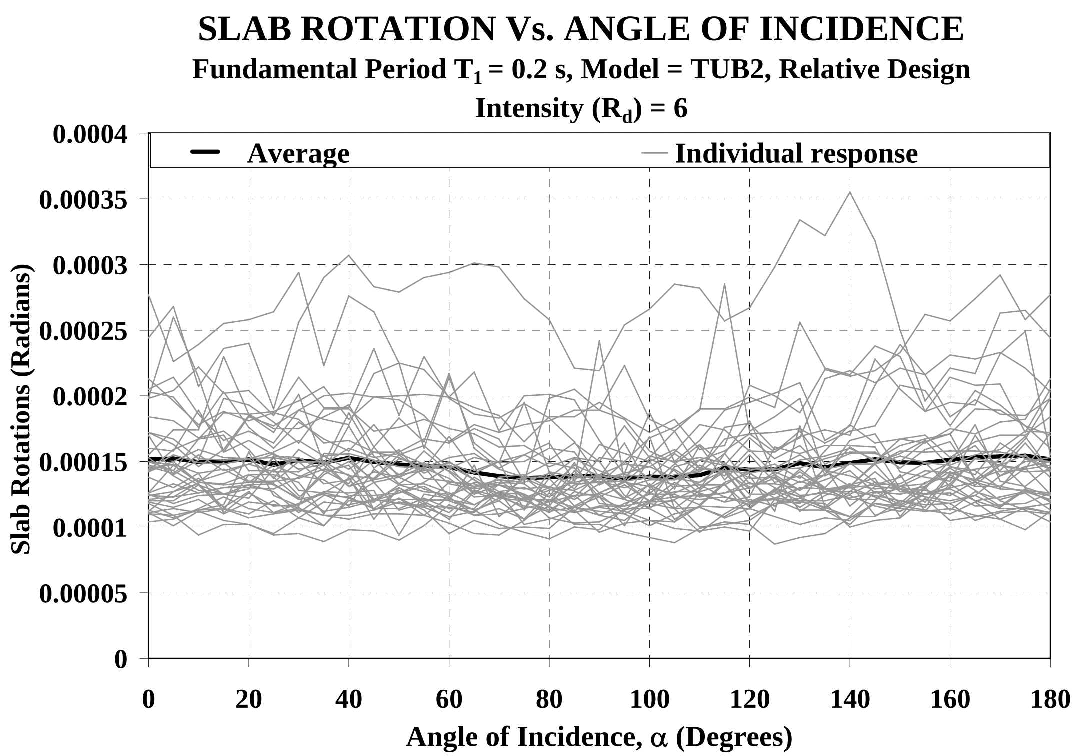

Figure 4.10 Dependence of slab rotations with angle of incidence at a fundamental period of 0.2 s for the TUB2 model for R_d = 6

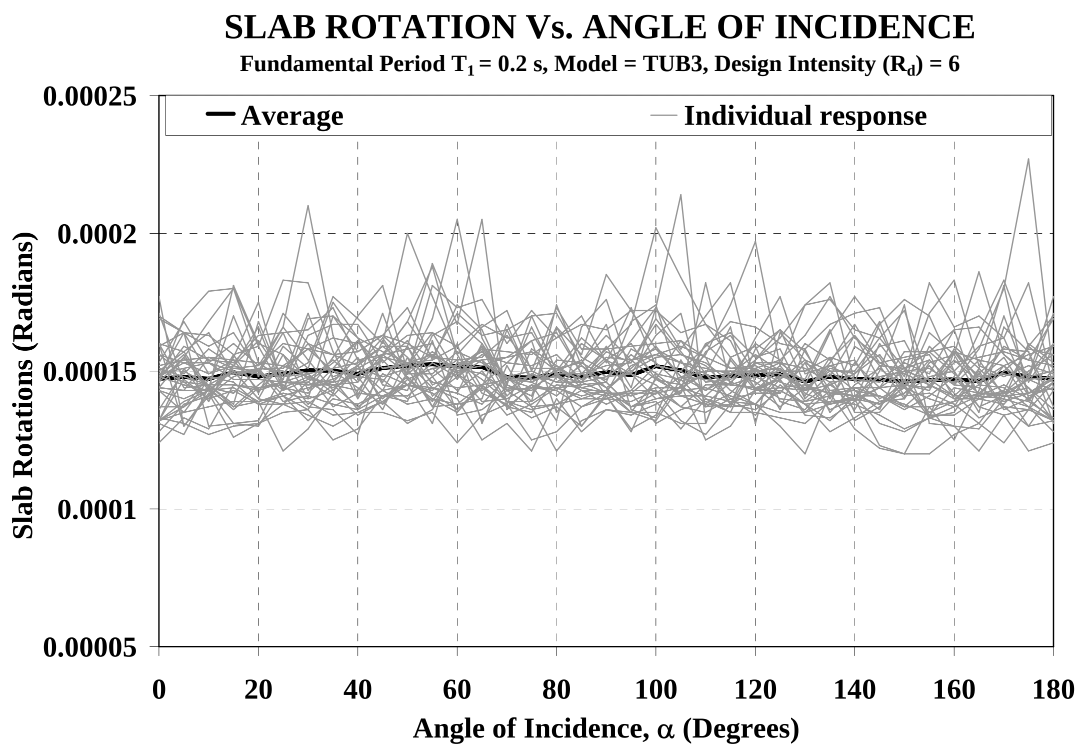

Figure 4.11 Dependence of slab rotations with angle of incidence for the TUB3 model for R_d = 6

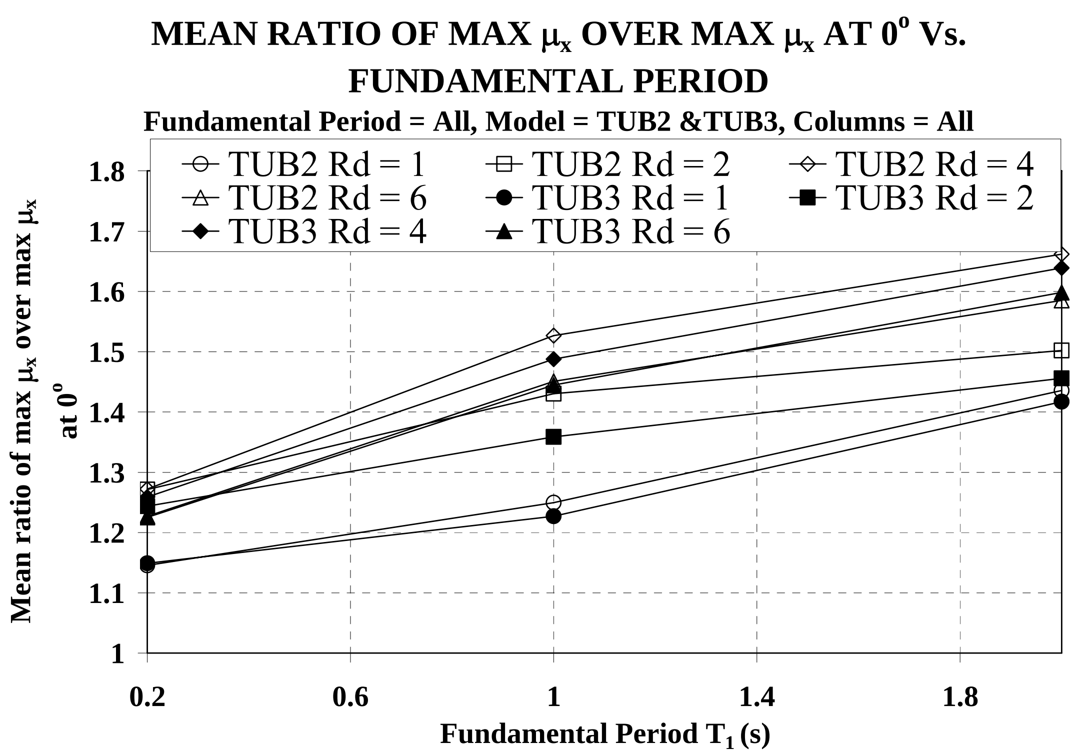

Figure 4.12 of *Max μ_x/Max μ_{x0}* for a given relative design intensity as a function of fundamental period, site D for models TUB2&TUB3

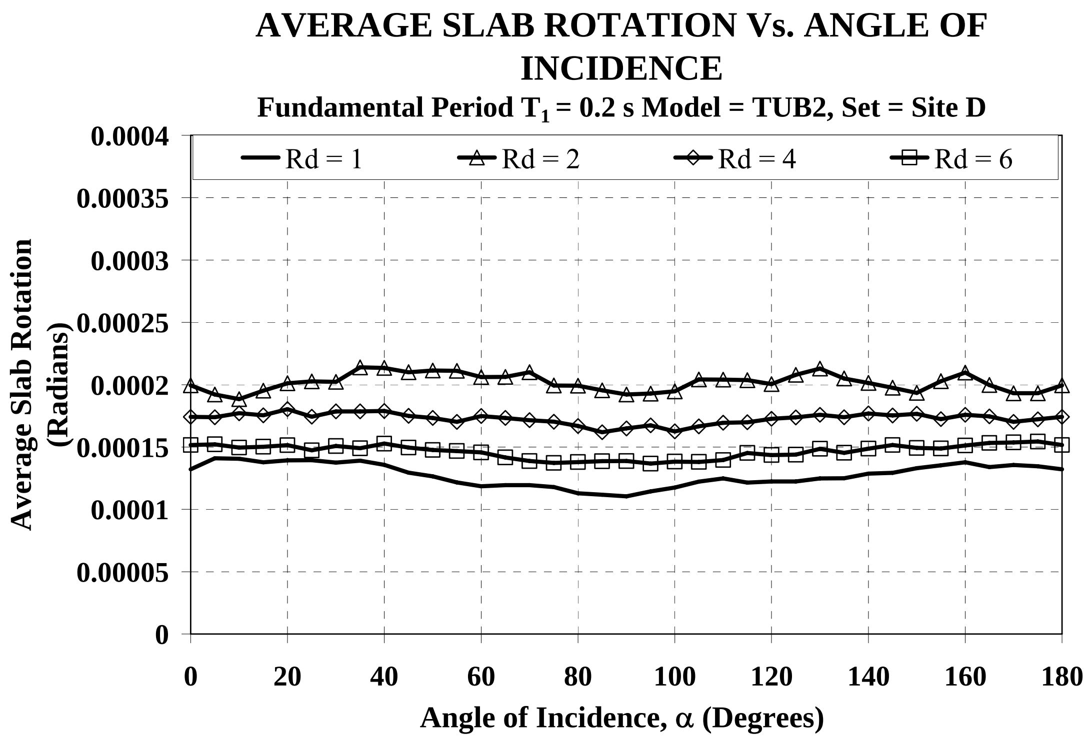

Figure 4.13 Dependence of average slab rotations to angle of incidence for model TUB2 at a fundamental period of 0.2 s

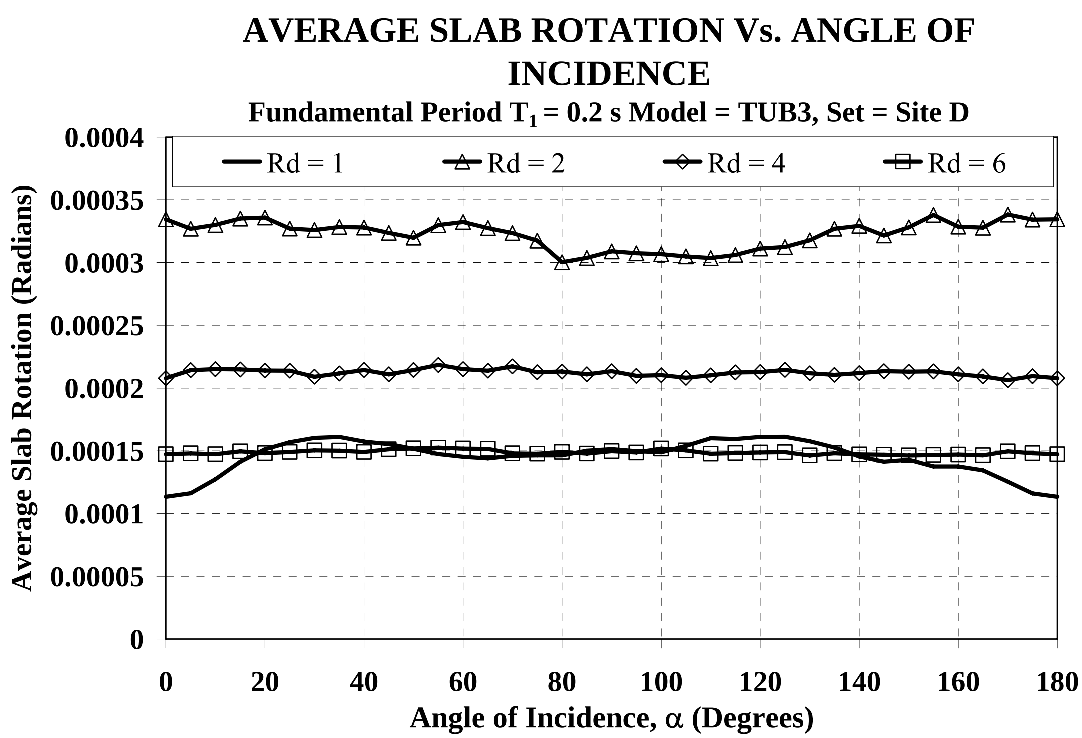

Figure 4.14 Dependence of average slab rotations to angle of incidence for model TUB3 at a fundamental period of 0.2 s

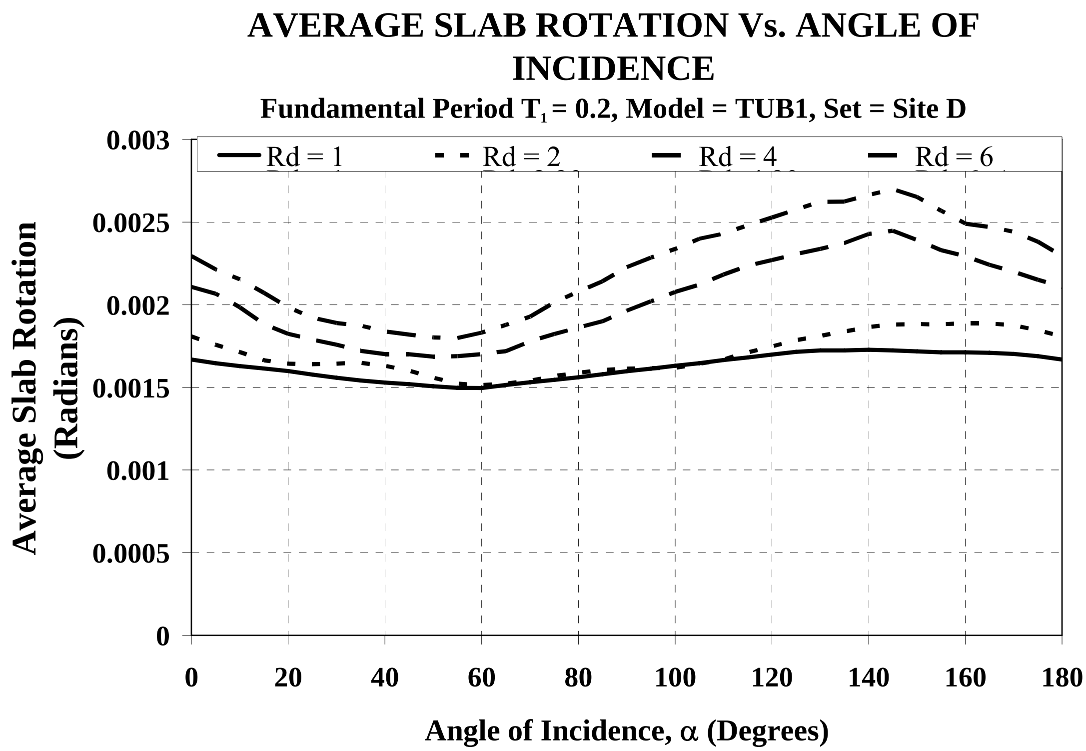

Figure 4.15 Dependence of average slab rotations on angle of incidence for model TUB1 at a fundamental period of 0.2 s

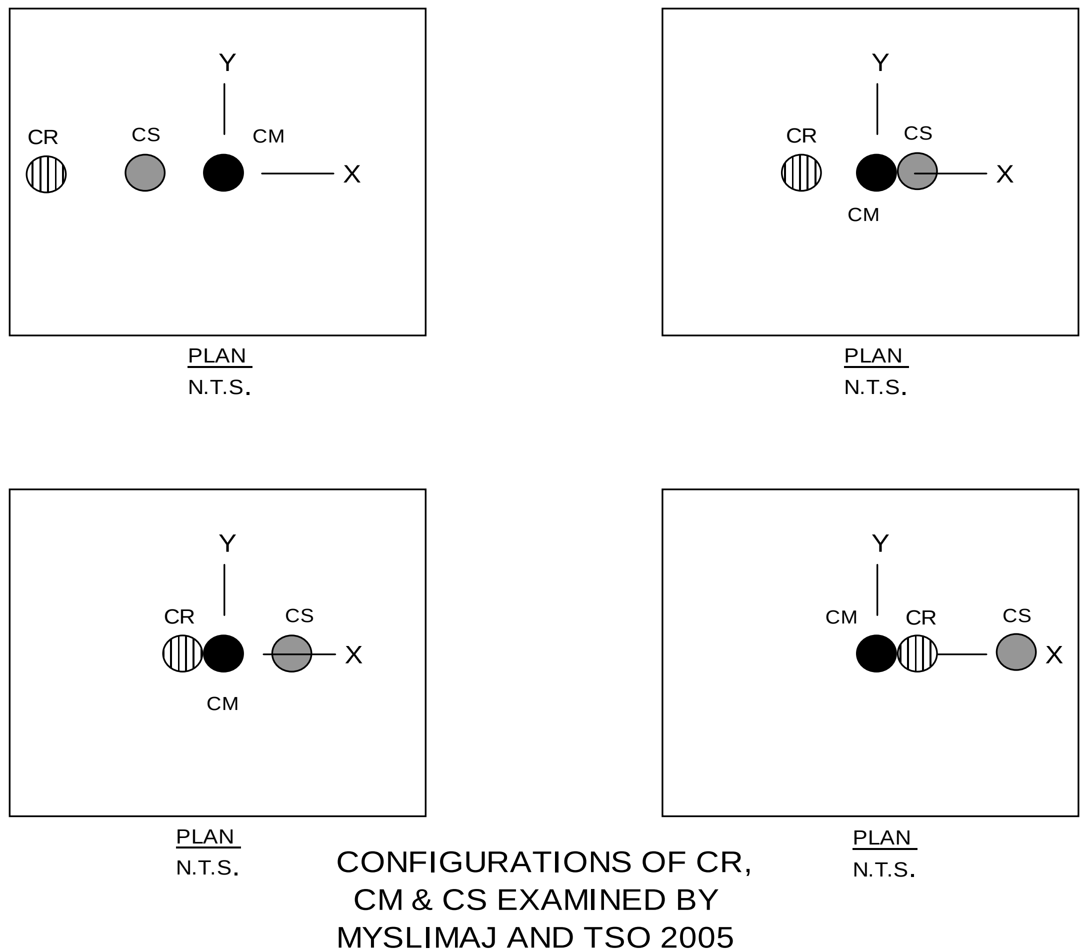

Figure 4.16 Schematic configuration of centers of strength, mass and rigidity examined for an asymmetric structure used by Myslimaj and Tso (2005)

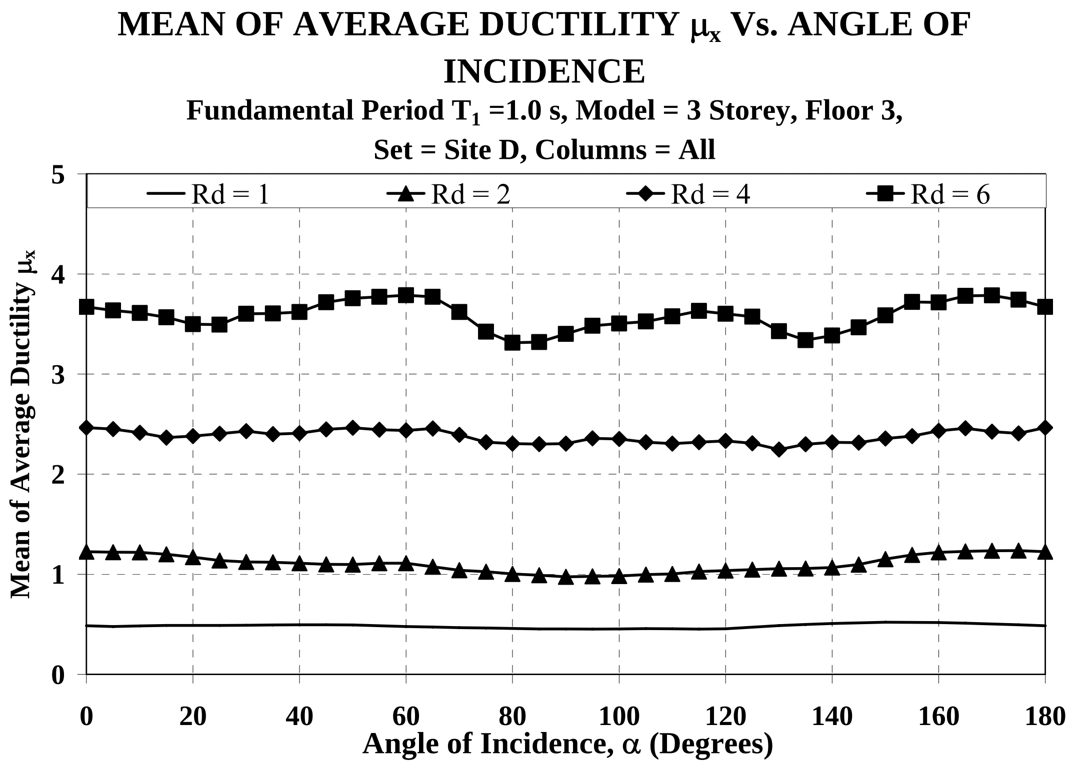

Figure 4.17 Mean of average ductilities in the X-direction and their dependence on angle of incidence, 3-storey model, 3rd floor, fundamental period of 1.0 s

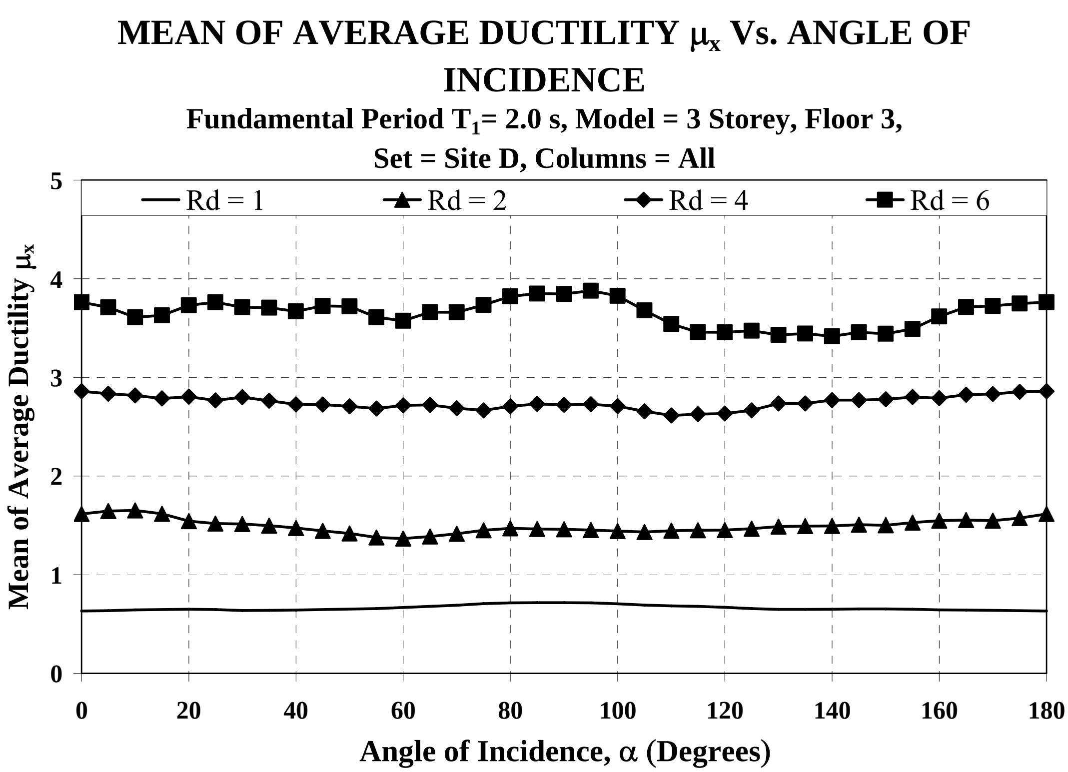

Figure 4.18 Mean of average ductilities in the X-direction and their dependence on angle of incidence, 3-storey model, 3rd floor, fundamental period of 2.0 s

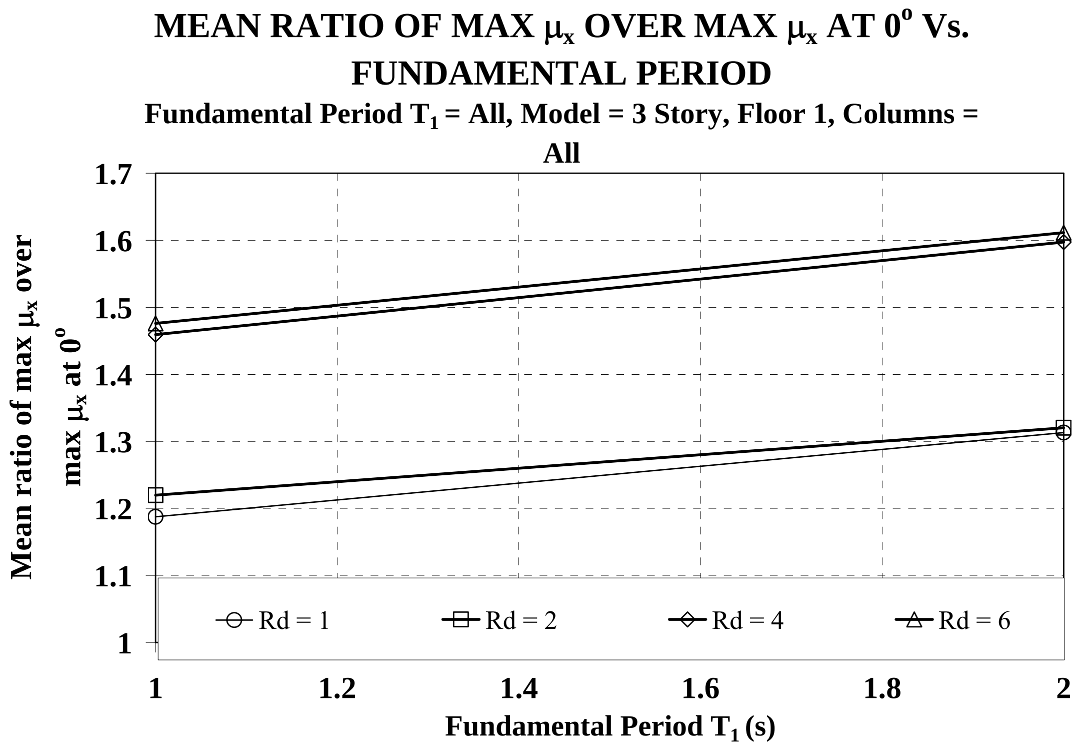

Figure 4.19 Mean of *Max μ_x/Max μ_{x0}* and their dependence on fundamental period, 3-storey model, 1st floor

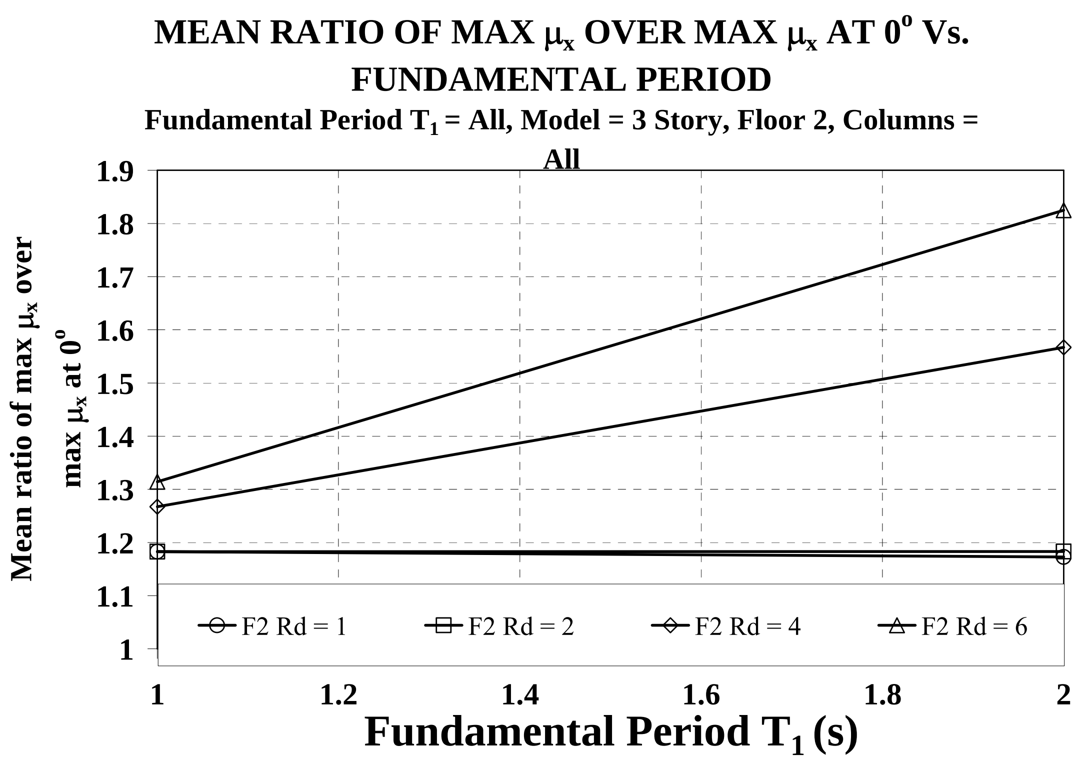

Figure 4.20 Mean of *Max μ_x/Max μ_{x0}* and their dependence on fundamental period, 3-storey model, 2nd floor

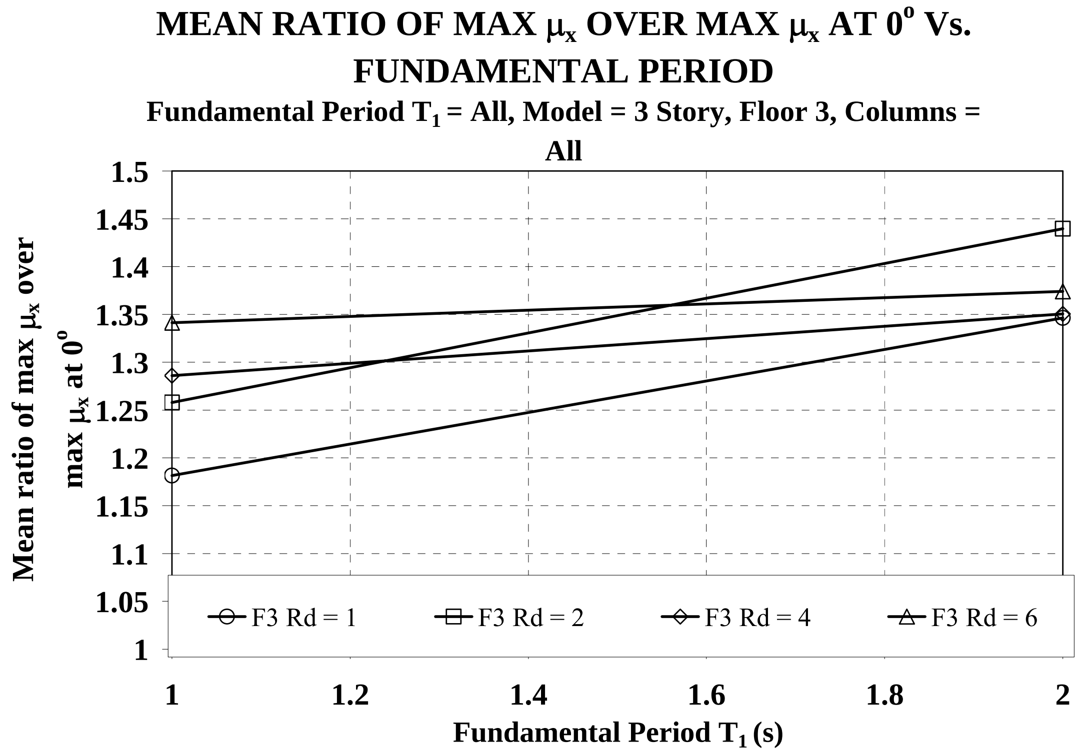

Figure 4.21 Mean of *Max μ_x/Max μ_{x0}* and their dependence on fundamental period, 3-storey model, 3rd floor

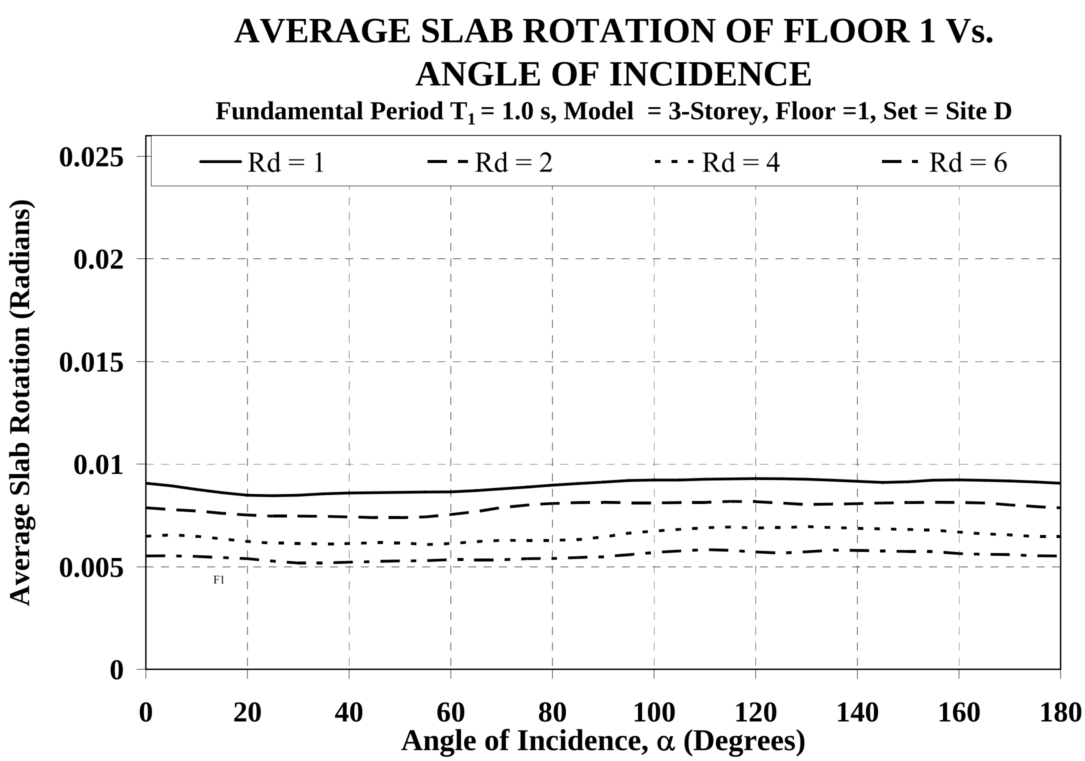

Figure 4.22 Dependence of average slab rotations on angle of incidence for the 3-storey model at a fundamental period of 1.0 s for floor 1

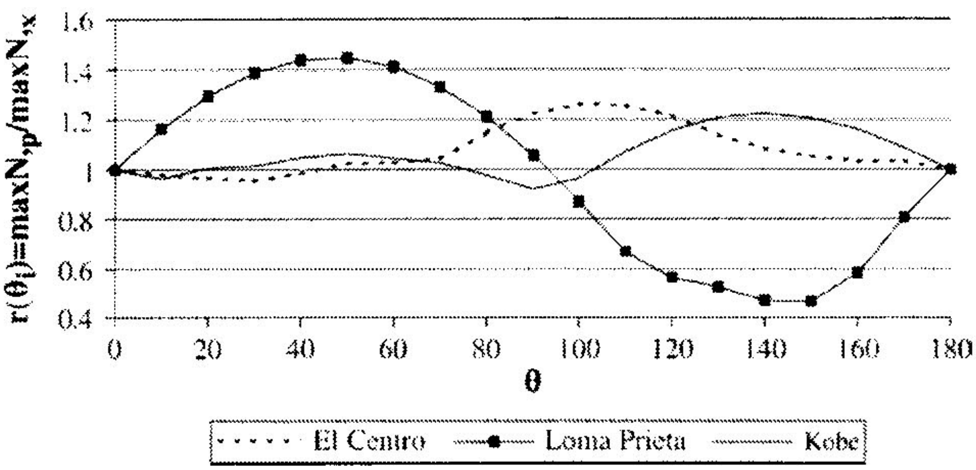

Fig. 20. Variation of the orientation effect ratio of the axial force *N* in column C3.

Figure 4.23 Dependence of the ratio of axial force w/r to axial force at 0^o as a function of angle of incidence at column C3 (reproduced from Athanatopoulou 2005)

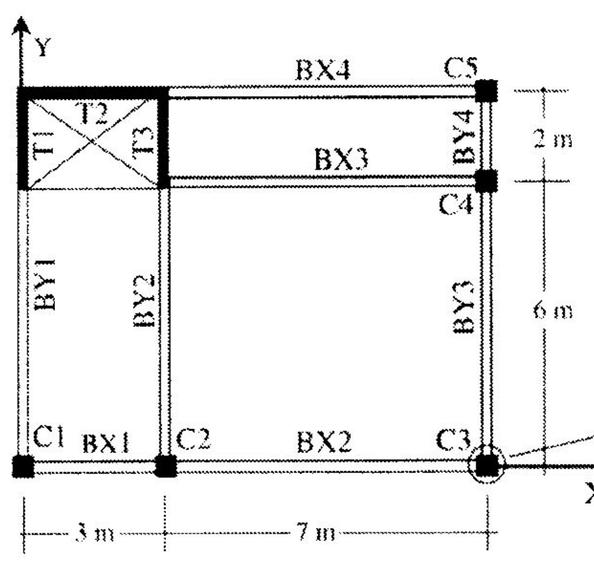

Columns	50/50 (cm)
Beams	25/60 (cm)
Shear walls T1,T3	25/200 (cm)
Shear wall T2	25/300 (cm)
E	2,9*10^{7}kN/m^2

Fig. 8. Five-story asymmetric building. Plan view and geometrical properties.

Figure 4.24 Schematic of a “realistic” 5-storey structure (reproduced from Athanatopoulou 2005)

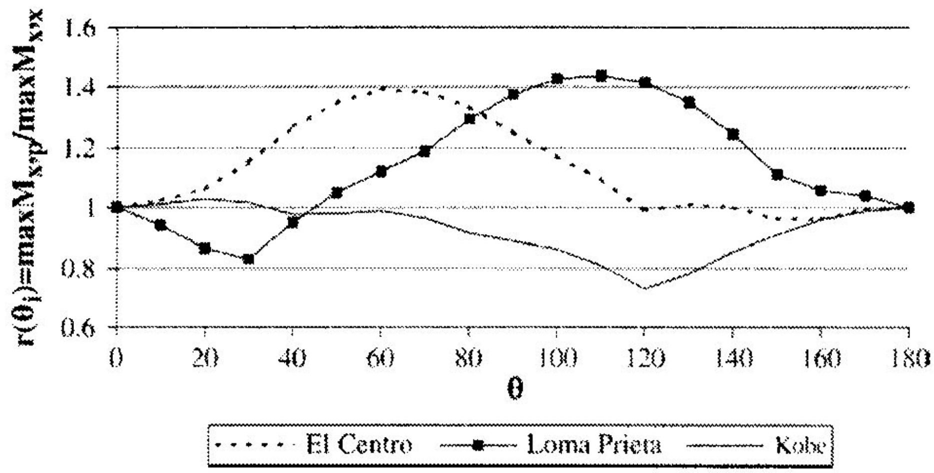

Fig. 21. Variation of the orientation effect ratio of the bending moment M_x in column C3.

Figure 4.25 Dependence of the ratio of moment M_x w/r to moment at 0^o as a function of angle of incidence column C3 (reproduced from Athanatopoulou 2005)

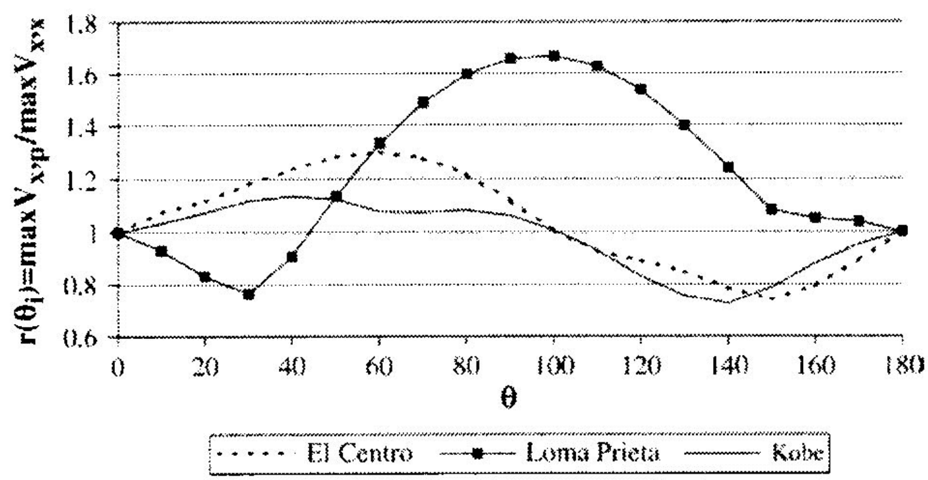

Fig. 22. Variation of the orientation effect ratio of the shear force V_x in column C3.

Figure 4.26 Dependence of the ratio of shear V_x w/r to V_x at 0^o as a function of angle of incidence at column C3 (reproduced from Athanatopoulou 2005)

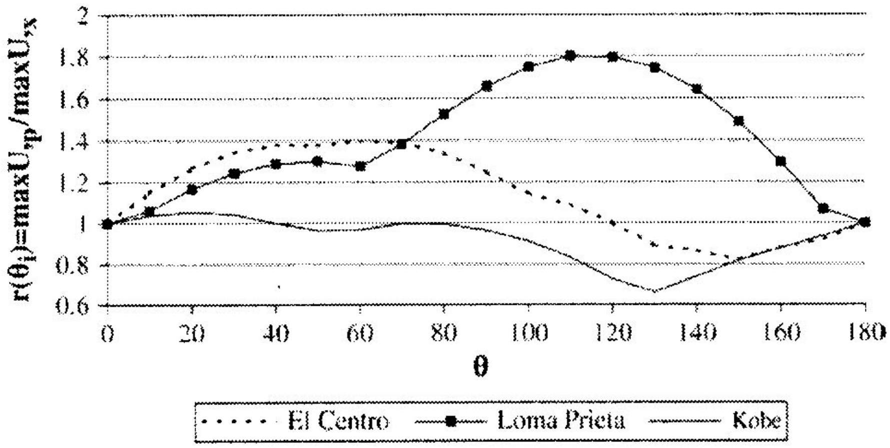

Fig. 23. Variation of the orientation effect ratio of the resultant displacement u of joint J77.

Figure 4.27 Dependence of the ratio of resultant displacement w/r to resultant displacement at 0^o in the X-direction as a function of angle of incidence at column C3 (reproduced from Athanatopoulou 2005)

Chapter 5 Statistical Evaluation of the Dependence of Ductility Ratios on Ground Motion Characteristics and Structural Properties.

INTRODUCTION

In an effort to understand and quantify any discernable trends with respect to critical angle, the majority of this work has characterized critical angle via an examination of individual responses, the average of the all responses, and upper bound of maximum values. Because of the limitations involved in the explicit quantification of critical angle for a given structure and ground motion pair, the focus of this chapter was on the quantification of the scatter present in engineering demand parameters when structures examined were exposed to bi-directional ground motions. In addition, statistical studies were conducted to identify those parameters that are most relevant for the estimation of peak seismic demands of systems exposed to ground motion pairs applied at different building orientations. More specifically, these studies included the calculation of statistical correlations between parameters, e.g., moment magnitude and the ratio of $Max\ \mu_x/Max\ \mu_{x0}$, as well as hypothesis testing.

Record-to-Record Variability of Ductility Demands as a Function of Ground Motion Frequency Content

A typical representation of the record-to-record variability of ductility demands is presented in Figures 5.1-5.3 for model TUB1 while Figures 5.4-5.5 are typical of model TB. The results in these figures correspond to the standard deviation of ductility in the X-direction conditioned on the angle of incidence. When comparing standard deviations of models TB and TUB1 for higher degrees of inelasticity, the trends observed for model TB (Figure 5.4-5.5) looked very much like those of TUB1 (Figures 5.1-5.3) for all fundamental periods.

For smaller degrees of inelasticity, the standard deviations at short fundamental periods are weakly dependent on angle of incidence for model TUB1 (Figure 5.1). As the fundamental period increases, the standard deviations at these small degrees of inelasticity tend to be more shaped like a bow string, in that at angles 0^o and 180^o, the standard deviations are small. For the TB case and smaller degrees of inelasticity, the standard deviations resemble that of a bow string shape regardless of fundamental period as seen in Figures 5.4-5.5. For relatively smaller degrees of inelasticity, torsion from model TUB1 tends to "even out" the standard deviations at all angles of incidence for smaller fundamental periods as seen in Figure 5.1. The bowstring behavior seen in model TB was attributed to the fact that the minor component does not contribute to the X-ductilities when the major component which was scaled to the same $S_a(T_1)$ value was aligned with the X-axis at 0^o. The reverse becomes true for the standard deviations at 90^o since the minor component, which was not scaled to the same value of S_a, was aligned along the X-axis. As an example, Figure 5.6 shows the scatter of the scaled minor component at 2.0 s. Theoretically, standard deviations values of ductilities in the X-direction at angles of incidence equal to 0^o should be zero. This was not the case in this instance given that the tuning of the column stiffness introduced small, round-off errors that led to fundamental periods that were slightly off, and not all significant figures were kept with regard to the scaling of $S_a(T_1)$ for all analyses.

Figures 5.7-5.8 illustrate the standard deviation of the major and minor component as a function of the fundamental period of interest for ground motions recorded on stiff soils (site D). For a given fundamental period, the standard deviations of the scaled major component had null values at the fundamental period of interest since all records were scaled to the same value at this period.

With regards to models TUB2 and TUB3, the standard deviation of the ductility demand in the X-direction at any angle of incidence (Figure 5.9) were very similar to those observed for the TB model indicating that torsional demands are negligible. The standard deviations of ductility for the 3-storey structure generally exhibited the same trends as the TUB1 model for equivalent fundamental periods (Figure 5.10).

The magnitude of the standard deviations of ductility for model TUB1 exposed to ground motion pairs recorded on rock sites (site AB) differed from those based on site D in magnitude, but only slightly. Specifically those based on site AB tended to be marginally smaller in general than those based on site D, but showed similar trends as exhibited in Figures 5.11 and 5.12.

The magnitude of the standard deviations of ductility tended to be larger at smaller fundamental periods and decreased with increasing fundamental period. This can be explained by the inherent record-to-record variability of the ground motion components themselves, which generally had larger amounts of scatter just beyond the fundamental period such as for a given fundamental period of say, 0.2 s (Figure

5.13) as compared to the scatter beyond 2.0 s (Figure 5.14). The counterparts to Figures 5.7-5.8, Figures 5.15-5.16, summarize the standard deviation of the scaled major and minor component as a function of fundamental period of interest for ground motions recorded on rock sites.

The above implies that while standard deviation magnitudes may be different with respect to ground motion frequency content, the trends of those standard deviations are not very dependant on local site conditions. In addition, similar trends can be expected at higher degrees of inelasticity, regardless of fundamental period. It was important to note that the dependence on frequency content addressed in this section did not include soft-soil or near-fault conditions, which were not the subject of this study.

Record-to-Record Variability of $Max\ \mu_x/Max\ \mu_{x0}$ as a Function of Structural Configuration

The standard deviation of the ratio of the $Max\ \mu_x/Max\ \mu_{x0}$ for models TUB1 and TB are presented in Figure 5.17-5.18. It can be observed that both models had similar standard deviation shapes that generally increased with fundamental period. The standard deviation of the ratio of $Max\ \mu_x/Max\ \mu_{x0}$ for models TUB2 and TUB3 are also very similar to those observed for the TB model, as illustrated in Figures 5.19 and 5.20. Standard deviations of these ductility ratios were similar for the 3-storey structure, and generally exhibited the same trends as the TUB1 model for equivalent fundamental periods, while models subjected to ground motion set AB showed trends similar to the ratios themselves with increasing fundamental period. Regardless of the structural configuration examined for a given ground motion set, the standard deviation of the ratio of the $Max\ \mu_x/Max\ \mu_{x0}$ generally exhibited similar trends with increasing fundamental period.

Record-to-Record Variability of Slab Rotation and Drift Demands as a Function of Ground Motion Frequency Content and Structural Configuration

Standard deviations of slab rotations for all models in general were small (coefficient of variation typically less than 0.1), and in general tended to increase or decrease with degree of inelasticity much like the slab rotations themselves. This is illustrated in Figure 5.21 for model TUB1 with a fundamental period of 0.2 s subjected to site class D ground motions. Standard deviations tended to be most sensitive to angle of incidence for smaller degrees of inelasticity, and "evened out" at larger degrees of inelasticity. Models TUB2 and TUB3 exhibited very small standard deviations for the fundamental periods examined and the difference between both models was also small for most degrees of inelasticity. Standard deviations of slab rotation for the 3-storey model exhibited similar trends as the model TUB1 with the same corresponding fundamental period as shown in Figure 5.22-5.23.

When subjected to site AB ground motion pairs, standard deviations of slab rotation for model TUB1 exhibited similar behavior to those based on site D. With regards to drift, trends similar to ductility were exhibited in practically all cases. Trends seen in Figure 5.1 with regards to ductility in the X-direction can also be seen in Figure 5.24 for drift in the X-direction. Although model TUB1 was subjected to different ground motion sets, the behavioral trends observed with regards to standard deviations of drift and slab rotation did not differ significantly, implying that these trends were not very site dependant.

So far, the emphasis of the preceding sections has been on the record-to-record variability of the EDPs examined. The next section evaluates why certain individual records are more sensitivity to angle of incidence than others. This can also be found in the work done by Rigato and Medina (Rigato and Medina 2007).

Sensitivity of Ductility "Variation" to Lateral Ground Motion Components

It has been observed that some ground motion records are more sensitive to angle of incidence than others. It would be quite useful to know *a priori* which records seem to be more sensitive to angle of incidence than another. Therefore, in an effort to better understand why an individual record may produce significant variations for a given EDP with respect to angle while another may not, the variation of ductility demands with respect to the ratio of $S_a(T_1)/g$ (major component)/ $S_a(T_1)/g$ (minor component) of a ground motion was investigated. For a given model and direction (i.e., X- or Y-direction), *variation* was defined as the ratio of the maximum value of ductility observed for a given pair of records at any angle divided by the minimum value for the same pair of records (Figure 5.25). The dependence of the ductility variation with the ratio $S_a(T_1)/g$ (major component)/ $S_a(T_1)/g$ (minor component) at various periods was investigated. The ratios were calculated at the fundamental period of vibration of the structures and at periods up to two times the fundamental period. These results failed to illustrate a significant correlation of the ratio $S_a(T_1)/g$ (major component)/ $S_a(T_1)/g$ (minor component) with ductility variation, as illustrated in the representative case shown in Figure 5.26 for column 1 of the TUB1 structure with a fundamental period of 0.5 s. This indicates that the relationship between ductility demand variation and angle of incidence was not strongly dependent on these ground motion spectral ratios. For example, in Figure 5.26, the correlation coefficient between ductility variation and the ratio $S_a(T_1)/g$ (major component)/ $S_a(T_1)/g$ (minor component) was equal to 0.33. The linear model fitted to this data is also shown in Figure 5.26. Based on this information, the observed differences in the magnitude of ductility demands as a function of angle of incidence of ground motion input were attributed to differences in the frequency-content characteristics of the ground motion records.

CORRELATION OF $Max\ \mu_x/Max\ \mu_{x0}$ TO VARIOUS PARAMETERS

Dependency of $Max\ \mu_x/Max\ \mu_{x0}$ on Lateral Ground Motion Components

The mean ratio of $Max\ \mu_x/Max\ \mu_{x0}$ has been used to quantify maximum responses relative to the responses obtained at the principal building orientation. It has been used for all building configurations and all ground motion suites. Previous figures in chapter 3 indicated that these ratios depend to some extent on fundamental period, R_d, and ground motion suite, i.e., frequency content. The aim of this section was to look at the correlation (if any) of $Max\ \mu_x/Max\ \mu_{x0}$ with parameters such as fundamental period and R_d. Tables indicating the degree of correlation of the $Max\ \mu_x/Max\ \mu_{x0}$ to $S_a(T_1)/g$ (minor)/ $S_a(T_1)/g$ (major) for *all* fundamental periods for a given model, site, and for a particular R_d value rather than for *a specific* fundamental period, for a given model, site, degree of inelasticity are tabulated in Tables 5.2-5.4.

These tables also document the improvement that nonlinear functions determined to have the “best fit” had on the correlation coefficient (column 9), which was typically based on a higher order polynomial that varied from a 5th to 19th order (detailed in column 10). Figure 5.27 is an example of a linear model and the best fitting model (a 14th order polynomial) associated to the relation of $Max\ \mu_x/Max\ \mu_{x0}$ to $S_a\ (T_1)/g$ (minor)/ $S_a\ (T_1)/g$ (major). This was done in an effort to determine how much improvement in correlation was obtainable by using a nonlinear function. The standard error (S_e) over standard deviation (stdev, $S_{deviation}$), which indicates how well a regression equation fits the data (where smaller ratios indicate a better fit), marginally improved with increasing complexity of regressed function form (columns 5 and 8). Column 3 indicates that the correlation between $Max\ \mu_x/Max\ \mu_{x0}$ and $S_a\ (T_1)/g$ (minor)/ $S_a\ (T_1)/g$ (major) degrades with increasing degree of inelasticity which was not surprising given that S_a (minor)/ S_a (major) was based on spectral values at the initial fundamental period of the system. The stronger correlation for the TB model without torsion can be interpreted as weakening once torsion has been introduced. The interaction of the modes for the TUB1 model reduced the correlation of ductility demands ratios to $S_a\ (T_1)/g$ (minor)/ $S_a\ (T_1)/g$ (major) despite having exhibited similar trends as the TB model. Use of a nonlinear model rather than a linear one tended to improve the correlation coefficient (column 6) as indicated in Table 5.2-5.4, but not by a significant amount. Regardless of fundamental period, model type and ground motion frequency content, $Max\ \mu_x/Max\ \mu_{x0}$ can be estimated by $S_a\ (T_1)/g$ (minor)/ $S_a\ (T_1)/g$ (major) for small degrees of inelasticity.

Dependency of *Max* μ_x/*Max* μ_{x0} on Fundamental Period

Regression studies focusing on fundamental period rather than $S_a(T_1)/g$ (minor)/ $S_a(T_1)/g$ (major) indicated a rather weak dependence on period for models TB and TUB1 subjected to ground motion sets for sites D and AB for a given R_d. Correlation coefficient values were typically less than 0.4 for these linear regressions and are summarized in Tables 5.5-5.7

Ratios of the standard error based on these linear regressions to the standard deviation of the *Max* μ_x/*Max* μ_{x0} were poor. More complex models fitted to the data provided only a small improvement of the correlation coefficient as indicated in column 6. Figure 5.28 illustrates a typical plot of individual *Max* μ_x/*Max* μ_{x0} vs. fundamental period for the TB model with $R_d = 2$. The scatter in this plot illustrates the rather poor correlation of *Max* μ_x/*Max* μ_{x0} to fundamental period graphically.

Given the small correlation coefficient in the preceding sections with regards to the dependence of *Max* μ_x/*Max* μ_{x0} to fundamental period, hypothesis testing was conducted on the slope coefficient (b) of the aforementioned linear regressions to quantify more accurately the dependence on fundamental period of vibration of the structure. Similar hypothesis testing was not conducted for $S_a(T_1)/g$ (minor)/ $S_a(T_1)/g$ (major) rather than fundamental period since it was clear at least for smaller degrees of inelasticity, that there was a significant relationship between *Max* μ_x/*Max* μ_{x0} to $S_a(T_1)/g$ (minor)/ $S_a(T_1)/g$ (major). From Tables 5.8-5.10, and for a given level of significance α (columns 3 and 4), the null hypothesis (slope coefficient $b = 0$ i.e. there was no dependency on fundamental period) was rejected for both levels of significance. Or in other words, we can not say with either 99% or 95% confidence that $Max\ \mu_x/Max\ \mu_{x0}$ was independent of fundamental period. A relation most likely exists, albeit a rather weak one.

Dependency of $Max\ \mu_x/Max\ \mu_{x0}$ to Degree of Inelasticity, R_d

Similar regression studies of $Max\ \mu_x/Max\ \mu_{x0}$ for all R_d for a given fundamental period indicated that a poor correlation exists between $Max\ \mu_x/Max\ \mu_{x0}$ and R_d . Nonlinear models again did little to improve the ratio of the standard error to standard deviation as displayed in Tables 5.11-5.13. The majority of the correlation coefficients for the linear regression were often around 0.2.

Hypothesis testing on the slope coefficient for the null hypothesis b = 0, for the linear regressions gave mixed results regarding the dependence of $Max\ \mu_x/Max\ \mu_{x0}$ on R_d. From Tables 5.14-16 it was not clear that a dependence of maximum ductility over maximum ductility at 0^o on R_d exists, given that not all hypothesis testing can be rejected at the 95% and 99% confidence level. That is, for the stated level of significance α in columns 3 and 4, the null hypothesis that the slope coefficient b = 0 was rejected at a significance level of α = 1% in all cases, but was accepted in some instances for significance level of α = 5%. Figure 5.29 illustrates the dependence of $Max\ \mu_x/Max\ \mu_{x0}$ on R_d for the TUB1 model subjected to site D ground motions for a fundamental period equal to 1.0 s. The large scatter in this figure supports the poor correlations observed in Tables 5.14-5.16.

Dependency of Standard Deviation of $Max\ \mu_x/Max\ \mu_{x0}$ to Lateral Ground Motion Components

While the correlation between $S_a(T_1)/g$ (minor)/ $S_a(T_1)/g$ (major) and $Max\ \mu_x/Max\ \mu_{x0}$ tended to deteriorate with increasing R_d values, the standard deviations of maximum ductility over maximum ductility at 0^o tended to correlate very well with the standard deviation of $S_a(T_1)/g$ (minor)/ $S_a(T_1)/g$ (major) for most R_d values. Figure 5.30 depicts the standard deviation of $S_a(T_1)/g$ (minor)/ $S_a(T_1)/g$ (major) vs. fundamental period. Any scatter in the ratio of the lateral components of the ground motion input should manifest itself as scatter in the $Max\ \mu_x/Max\ \mu_{x0}$. Tables 5.17-5.19 summarize the correlation coefficients produced from linear regressions performed on the data. These results are most useful given that $Max\ \mu_x/Max\ \mu_{x0}$ and its standard deviations are relatively stable, allowing estimates of these two quantities to be made based on $S_a(T_1)/g$ (minor)/ $S_a(T_1)/g$ (major) and its standard deviations respectively. As a rule of thumb, with respect to average $Max\ \mu_x/Max\ \mu_{x0}$, suggested envelope values from 1.5 to 1.85 are characterized by the equation:

$$Max\mu_x / Max\mu_{xo} = 0.175 \cdot T_1 + 1.5 \tag{5.1}$$

And are shown in Figure 5.31 regardless of the model, R_d and site classification (rock or stiff soil). An equation for the envelope values for the average plus a standard deviation vary from 2.25 to 2.5 and is as follows:

$$Max\mu_x / Max\mu_{xo} = 0.125 \cdot T_1 + 2.25 \tag{5.2}$$

Which is also illustrated in Figure 5.31.

Dependence of $Max\ \mu_x/Max\ \mu_{x0}$ to Fault Rupture Distance[1] and Moment Magnitude

In order to allow general statements to be made about the $Max\ \mu_x/Max\ \mu_{x0}$, in context to engineering relationships that depend on other ground motion parameters not investigated thus far such as moment magnitude and fault rupture distance, the relationship of these parameters to $Max\ \mu_x/Max\ \mu_{x0}$ must be investigated. Generally, correlation coefficients of linear regressions indicated a very poor relationship between these two parameters and $Max\ \mu_x/Max\ \mu_{x0}$. Summarized in Tables 5.20-5.25, correlation coefficients were often less than 0.1 with respect to moment magnitude and distance to the fault rupture zone for a given R_d value. Higher order functions did little to improve the correlation and are not shown.

Hypothesis testing on the slope of the linear regression expressions indicated that statistically, there was no dependence on $Max\ \mu_x/Max\ \mu_{x0}$ on distance to the fault rupture zone with 99% confidence for a given R_d value in almost all cases. Dependence on moment magnitude can also be ruled out for the majority of cases examined. Tables 5.26-5.31 summarize these results while Figures 5.32-5.33 display the typical dependence of moment magnitude to $Max\ \mu_x/Max\ \mu_{x0}$, and the dependence of distance to the fault rupture zone and $Max\ \mu_x/Max\ \mu_{x0}$ respectively for the TB model subjected to ground motion site D for all fundamental periods and for $R_d = 4$. This implies that $Max\ \mu_x/Max\ \mu_{x0}$ was weakly dependent on fault rupture distance and moment magnitude, which will have the potential to facilitate the analyses, as well as

[1] Closest distance to fault rupture zone.

the record selection process as part of probabilistic seismic demand evaluation studies based on this ratio.

SUMMARY AND CONCLUSIONS

The purpose of the statistical studies presented in this chapter was to quantify and evaluate the dependence of seismic demands for structures exposed to bi-directional ground motions as a function of ground motion frequency content; to quantify the scatter of the results, and to identify which structural and ground motion parameters had the greatest influence on the ratios of $Max\ \mu_x/Max\ \mu_{x0}$.

Magnitudes of standard deviations varied with model type. Their shapes which were found to be dependant on the model type for low fundamental periods gradually became similar with increasing period. Similar shapes however were observed among all model types for higher degrees of inelasticity particularly at longer periods. With respect to frequency content, the magnitudes of the standard deviations varied, but exhibited similar shapes and behavior.

The variation of ductility as defined in this chapter, was found to correlate well with $S_a\,(T_1)/g$ (major)/ $S_a\,(T_1)/g$ (minor) for model TB and small degrees of inelasticity. At higher degrees of inelasticity however, the correlation degenerated. Due to the interaction of the modes in the TUB1, the correlation was typically poorer than those of the corresponding TB models.

The ratio of $Max\ \mu_x/Max\ \mu_{x0}$ was found to correlate best to the following parameters in order of decreasing correlation: $S_a\,(T_1)/g$ (minor)/ $S_a\,(T_1)/g$ (major), fundamental period and degree of inelasticity, moment magnitude and distance to the fault rupture zone. Since $S_a\,(T_1)/g$ (minor)/ $S_a\,(T_1)/g$ (major) correlated best to this ratio, especially for smaller degrees of inelasticity, it was not subjected to hypothesis testing. Of these parameters, it was found that the distance to fault rupture zone could be considered to have had no influence on *Max* μ_x/*Max* μ_{x0} with a 99% degree of confidence for almost all TUB1 and TB models subjected to both site D and site AB ground motion sets. The same was true for moment magnitude in most cases. Such confidence could not be obtained with respect to fundamental period or degree of inelasticity, however.

What can be concluded from this chapter was that the ratio of *Max* μ_x/*Max* μ_{x0} was most dependant on $S_a\,(T_1)$/g (minor)/ $S_a\,(T_1)$/g (major) followed by fundamental period and degree of inelasticity. In addition, the trends observed for standard deviations for models with different structural configurations subjected to the same ground motion set suggest that those trends are independent of structural configuration at longer fundamental periods, or for higher degrees of inelasticity at all fundamental periods. The standard deviations of *Max* μ_x/*Max* μ_{x0} correlated very well to the standard deviations of on $S_a\,(T_1)$/g (minor)/ $S_a\,(T_1)$/g (major) allowing estimates of the standard deviations of *Max* μ_x/*Max* μ_{x0} to be made based on the standard deviations of $S_a\,(T_1)$/g (minor)/ $S_a\,(T_1)$/g (major). Suggested envelope values for average *Max* μ_x/*Max* μ_{x0} ratios varied from 1.5 to 1.85, while average values plus a standard deviation varied from 2.25 to 2.5.

Table of nonlinear models used for regression analysis	
column	
(1)	(2)
f(x)	Non Linear Model
L	Linear function of the Form y=a+bx
3	3rd degree Polynomial Fit: y=a+bx+cx^2+dx^3...
4	4th Degree Polynomial Fit: y=a+bx+cx^2+dx^3...
5	5th Degree Polynomial: y=a+bx+cx^2+dx^3...
8	8th Degree Polynomial : y=a+bx+cx^2+dx^3...
10	10th Degree Polynomial : y=a+bx+cx^2+dx^3...
14	14th Degree Polynomial: y=a+bx+cx^2+dx^3...
15	15th Degree Polynomial: y=a+bx+cx^2+dx^3...
16	16th Degree Polynomial: y=a+bx+cx^2+dx^3...
17	17th Degree Polynomial : y=a+bx+cx^2+dx^3...
19	19th Degree Polynomial : y=a+bx+cx^2+dx^3...
R	Rational Function: y=(a+bx)/(1+cx+dx^2)
G	Gaussian Model: y=a*exp((-(b-x)^2)/(2*c^2))
RC	Reciprocal Logarithm Fit: y=1/(a+b*ln(x))
E	Exponential Association: y=a(1-exp(-bx)
R	Reciprocal Quadratic: y=1/(a+bx+cx^2)
M	MMF Model: y=(a*b+c*x^d)/(b+x^d)
S	Sinusoidal Fit: y=a+b*cos(cx+d)

Table 5.1 Legend of nonlinear models

Model TUB1 Site D									
column									
(1)	(2)	(3)	(4)	(5)	(6)	(7)	(8)	(9)	(10)
Data Parameters		Regression based on a Linear function*				Regression based on "best fit" nonlinear function *			
R_d	Stdev	Corr. Coef.	f(x)	S_e	$S_e/S_{deviation}$	Corr Coeff	S_e	$S_e/S_{deviation}$	Corr. Increase	f(x)
1	0.31	0.69	L	0.21	0.67	0.73	0.20	0.64	5%	5
2	0.40	0.62	L	0.25	0.62	0.71	0.23	0.58	15%	16
4	0.57	0.48	L	0.45	0.79	0.55	0.55	0.96	13%	14
6	0.49	0.22	L	0.40	0.83	0.56	0.35	0.73	152%	15

* See Table 5.1 for definition of functions used

Table 5.2 Regression data illustrating dependency of $Max\ \mu_x/Max\ \mu_{x0}$ for all fundamental periods and a specific R_d value on $S_a\,(T_1)/g$ (minor)/ $S_a\,(T_1)/g$ (major) for model TUB1, site D

Model TB Site D									
column									
(1)	(2)	(3)	(4)	(5)	(6)	(7)	(8)	(9)	(10)
Data Parameters		Regression based on a Linear function				Regression based on "best fit" nonlinear function			
R_d	Stdev	Corr. Coef.	f(x)	S_e	$S_e/S_{deviation}$	Corr Coeff	S_e	$S_e/S_{deviation}$	Corr. Increase	f(x)
1	0.28	0.86	L	0.14	0.51	0.88	0.14	0.48	2%	8
2	0.38	0.61	L	0.31	0.81	0.71	0.28	0.73	16%	10
4	0.48	0.60	L	0.30	0.63	0.69	0.28	0.58	15%	10
6	0.47	0.36	L	0.44	0.94	0.43	0.44	0.94	20%	17

* See Table 5.1 for definition of functions used

Table 5.3 Regression data illustrating dependency of *Max* μ_x/*Max* μ_{x0} for all fundamental periods and a specific R_d value on $S_a\,(T_1)/g$ (minor)/ $S_a\,(T_1)/g$ (major) for model TB, site D

Model TUB1 Site AB										
column										
(1)	(2)	(3)		(4)	(5)	(6)	(7)	(8)	(9)	(10)
Data Parameters		Regression based on a Linear function				Regression based on "best fit" nonlinear function				
R_d	Stdev	Corr. Coef.	f(x)	S_e	$S_e/S_{deviation}$	Corr Coeff	S_e	$S_e/S_{deviation}$	Corr. Increase	f(x)
1	0.29	0.49	L	0.27	0.95	0.76	0.21	0.74	55%	10
2	0.32	0.45	L	0.36	1.14	0.72	0.30	0.96	62%	19
4	0.52	0.31	L	0.54	1.05	0.52	0.51	0.99	66%	10
6	0.41	0.36	L	0.46	1.11	0.68	0.39	0.95	90%	19

* See Table 5.1 for definition of functions used

Table 5.4 Regression data illustrating dependency of *Max* μ_x/*Max* μ_{x0} on $S_a\,(T_1)/g$ (minor)/ $S_a\,(T_1)/g$ (major) for all fundamental periods and a specific R_d value for model TUB1, site AB

Model TUB1 Site D									
column									
(1)	(2)	(3)		(4)	(5)	(6)	(7)	(8)	(9)	(10)
Data Parameters		Regression based on a Linear function				Regression based on "best fit" nonlinear function				
R_d	Stdev	Corr. Coef.	f(x)	S_e	$S_e/S_{deviation}$	Corr Coeff	S_e	$S_e/S_{deviation}$	Corr. Increase	f(x)
1	0.29	0.34	L	0.27	0.94	0.35	0.27	0.95	3%	5
2	0.32	0.42	L	0.29	0.90	0.45	0.29	0.90	8%	5
4	0.52	0.28	L	0.50	0.96	0.29	0.50	0.96	5%	R
6	0.41	0.32	L	0.40	0.96	0.37	0.50	1.20	17%	6

* See Table 5.1 for definition of functions used

Table 5.5 Correlation of $Max\ \mu_x/Max\ \mu_{x0}$ to fundamental period for a specific R_d value, model TUB1, site D

Model TB Site D										
column										
(1)	(2)	(3)		(4)	(5)	(6)	(7)	(8)	(9)	(10)
Data Parameters		Regression based on a Linear function				Regression based on "best fit" nonlinear function				
R_d	Stdev	Corr. Coef.	f(x)	S_e	$S_e/S_{deviation}$	Corr Coeff	S_e	$S_e/S_{deviation}$	Corr. Increase	f(x)
1	0.28	0.38	L	0.26	0.92	0.40	0.26	0.92	3%	4
2	0.38	0.28	L	0.36	0.96	0.30	0.36	0.96	8%	3
4	0.48	0.28	L	0.46	0.96	0.30	0.46	0.96	5%	5
6	0.47	0.25	L	0.45	0.97	0.27	0.45	0.97	17%	5

* See Table 5.1 for definition of functions used

Table 5.6 Correlation of $Max\ \mu_x/Max\ \mu_{x0}$ to fundamental period for a specific R_d value, model TB, site D

Model TUB1 Site AB									
column									
(1)	(2)	(3)	(4)	(5)	(6)	(7)	(8)	(9)	(10)
Data Parameters		Regression based on a Linear function				Regression based on "best fit" nonlinear function			
R_d	Stdev	Corr. Coef.	f(x)	S_e	$S_e/S_{deviation}$	Corr Coeff	S_e	$S_e/S_{deviation}$	Corr. Increase	f(x)
1	0.31	0.12	L	0.31	1.00	0.19	0.31	0.99	3%	G
2	0.40	0.19	L	0.40	0.99	0.20	0.39	0.98	8%	RC
4	0.57	0.15	L	0.57	0.99	0.20	0.56	0.98	5%	E
6	0.49	0.15	L	0.48	0.99	0.27	0.47	0.97	17%	G

* See Table 5.1 for definition of functions used

Table 5.7 Correlation of *Max* μ_x/*Max* μ_{x0} to fundamental period for a specific R_d value, model TUB1, site AB

Model TUB1, Site D			
column			
(1)	(2)	(3)	(4)
Data Parameters		Hypothesis based on a Linear function	
R_d	b (slope)	α = 5%	α = 1%
1	0.16	Reject	Reject
2	0.21	Reject	Reject
4	0.23	Reject	Reject
6	0.22	Reject	Reject

Table 5.8 Dependency likelihood of *Max* μ_x/*Max* μ_{x0} to fundamental period for a specific R_d value for model TUB1, site D

Model TB, Site D			
column			
(1)	(2)	(3)	(4)
Data Parameters		Hypothesis based on a Linear function	
R_d	b (slope)	α = 5%	α = 1%
1	0.5341	Reject	Reject
2	0.5199	Reject	Reject
4	0.5033	Reject	Reject
6	0.368	Reject	Reject

Table 5.9 Dependency likelihood of $Max\ \mu_x/Max\ \mu_{x0}$ to fundamental period for a specific R_d value for model TB, site D

Model TUB1, Site AB			
column			
(1)	(2)	(3)	(4)
Data Parameters		Hypothesis based on a Linear function	
R_d	b (slope)	α = 5%	α = 1%
1	0.0497	Reject	Reject
2	0.1047	Reject	Reject
4	0.1189	Reject	Reject
6	0.0988	Reject	Reject

Table 5.10 Dependency likelihood of $Max\ \mu_x/Max\ \mu_{x0}$ to fundamental period for a specific R_d value for model TUB1, site AB

Model TUB1 Site D column									
(1)	(2)	(3)		(4)	(5)	(6)	(7)	(8)	(9)	(10)
Data Parameters		Regression based on a Linear function				Regression based on "best fit" nonlinear function				
Period	Stdev	Corr Coeff	f(x)	S_e	$S_e/S_{deviation}$	Corr Coeff	S_e	$S_e/S_{deviation}$	Corr. Increase	f(x)
0.2	0.23	0.17	L	0.23	0.99	0.23	0.23	0.99	34%	5
0.3	0.25	0.14	L	0.25	0.99	0.16	0.25	1.00	15%	S
0.4	0.26	0.24	L	0.23	0.88	0.21	0.23	0.88	-12%	R
0.5	0.22	0.20	L	0.23	1.06	0.22	0.23	1.06	5%	M
1	0.54	0.16	L	0.53	0.99	0.20	0.53	0.99	27%	4
2	0.53	0.13	L	0.54	1.01	0.16	0.54	1.01	20%	5

* See Table 5.1 for definition of functions used

Table 5.11 Correlation of $Max\ \mu_x/Max\ \mu_{x0}$ to all R_d for a specific fundamental period model TUB1, site D

Model TB Site D column										
(1)	(2)	(3)		(4)	(5)	(6)	(7)	(8)	(9)	(10)
Data Parameters		Regression based on a Linear function				Regression based on "best fit" nonlinear function				
Period	Stdev	Corr Coeff	f(x)	S_e	$S_e/S_{deviation}$	Corr Coeff	S_e	$S_e/S_{deviation}$	Corr. Increase	f(x)
0.2	0.3	0.14	L	0.28	0.92	0.22	0.28	0.91	56%	4
0.3	0.34	0.29	L	0.32	0.93	0.31	0.32	0.93	8%	M
0.4	0.26	0.24	L	0.22	0.83	0.27	0.21	0.83	14%	M
0.5	0.31	0.38	L	0.25	0.81	0.40	0.25	0.81	4%	4
1	0.53	0.17	L	0.53	1.00	0.20	0.53	1.00	20%	4
2	0.56	0.12	L	0.56	1.00	0.15	0.56	1.00	21%	3

* See Table 5.1 for definition of functions used

Table 5.12 Correlation of $Max\ \mu_x/Max\ \mu_{x0}$ to all R_d for a specific fundamental period model TB, site D

Model TUB1 Site AB									
column									
(1)	(2)	(3)	(4)	(5)	(6)	(7)	(8)	(9)	(10)
Data Parameters		Regression based on a Linear function				Regression based on "best fit" nonlinear function			
Period	Stdev	Corr Coeff	f(x)	S_e	$S_e/S_{deviation}$	Corr Coeff	S_e	$S_e/S_{deviation}$	Corr. Increase	f(x)
0.2	0.26	0.18	L	0.27	1.04	0.21	0.27	1.04	16%	3
1	0.51	0.23	L	0.50	0.98	0.24	0.50	0.98	5%	M
2	0.46	0.18	L	0.45	0.99	0.22	0.46	0.99	21%	4

* See Table 5.1 for definition of functions used

Table 5.13 Correlation of $Max\ \mu_x/Max\ \mu_{x0}$ to all R_d for a specific fundamental period model TUB1, site AB

Model TUB1 Site D			
column			
(1)	(2)	(3)	(4)
Data Parameters		Hypothesis based on a Linear function	
Period	b (slope)	α = 5%	α = 1%
0.2	0.01	Reject	Reject
0.3	0.02	Accept	Reject
0.4	0.02	Reject	Reject
0.5	0.02	Reject	Reject
1	0.04	Accept	Reject
2	0.0337	Accept	Reject

Table 5.14 Dependency likelihood of $Max\ \mu_x/Max\ \mu_{x0}$ to all R_d value for a specific fundamental period model TUB1, site D

Model TB, Site D			
column			
(1)	(2)	(3)	(4)
Data Parameters		Hypothesis based on a Linear function	
Period	b (slope)	α = 5%	α = 1%
0.2	0.02	Accept	Reject
0.3	0.04	Reject	Reject
0.4	0.02	Reject	Reject
0.5	0.05	Reject	Reject
1	0.04	Accept	Reject
2	0.0316	Accept	Reject

Table 5.15 Dependency likelihood of $Max\ \mu_x/Max\ \mu_{x0}$ to all R_d value for a specific fundamental period model TB, site D

Model TUB1, Site AB			
column			
(1)	(2)	(3)	(4)
Data Parameters		Hypothesis based on a Linear function	
Period	b (slope)	α = 5%	α = 1%
0.2	0.02	Reject	Reject
1.0	0.05	Reject	Reject
2.0	0.04	Reject	Reject

Table 5.16 Dependency likelihood of $Max\ \mu_x/Max\ \mu_{x0}$ to all R_d value for a specific fundamental period model TUB1, site AB

Model TUB1 Site D					
column					
(1)	(2)	(3)	(4)	(5)	(6)
Data Parameters		Linear Regression Parameters			
R_d	Stdev	Corr Coeff	S_e	$S_e/S_{deviation}$	f(X)
1	0.12	0.95	0.04	0.36	L
2	0.11	0.92	0.07	0.65	L
4	0.20	0.87	0.13	0.66	L
6	0.17	0.69	0.14	0.81	L

* See Table 5.1 for definition of functions used

Table 5.17 Correlation of $Max\ \mu_x/Max\ \mu_{x0}$ standard deviations to $S_a\,(T_1)/g$ (minor)/ $S_a\,(T_1)/g$ (major) standard deviations for all fundamental periods and a specific R_d value model TUB1, site D

Model TB Site D					
column					
(1)	(2)	(3)	(4)	(5)	(6)
Data Parameters		Linear Regression Parameters			
R_d	Stdev	Corr Coeff	S_e	Se/Sdeviation	f(X)
1	0.11	0.91	0.05	0.46	L
2	0.14	0.91	0.06	0.47	L
4	0.21	0.67	0.17	0.83	L
6	0.18	0.79	0.12	0.68	L

* See Table 5.1 for definition of functions used

Table 5.18 Correlation of $Max\ \mu_x/Max\ \mu_{x0}$ standard deviations to $S_a\,(T_1)/g$ (minor)/ $S_a\,(T_1)/g$ (major) standard deviations for all fundamental periods and a specific R_d value model TB, site D

Model TUB1 Site AB					
column					
(1)	(2)	(3)	(4)	(5)	(6)
Data Parameters		Linear Regression Parameters			
R_d	Stdev	Corr Coeff	S_e	$S_e/S_{deviation}$	f(X)
1	0.10	1.00	0.01	0.08	L
2	0.11	1.00	0.06	0.51	L
4	0.19	0.50	0.23	1.23	L
6	0.20	0.95	0.09	0.45	L

* See Table 5.1 for definition of functions used

Table 5.19 Correlation of *Max* μ_x/*Max* μ_{x0} standard deviations to S_a $(T_1)/g$ (minor)/ S_a $(T_1)/g$ (major) standard deviations for all fundamental periods and a specific R_d value model TUB1, site AB

Model TUB1 Site D					
column					
(1)	(2)	(3)	(4)	(5)	(6)
Data Parameters		Regression based on a Linear function			
R_d	Stdev	Corr Coeff	Se	Se/Sdeviation	f(x)
1	0.28	0.11	0.28	1.00	L
2	0.38	0.11	0.37	1.00	L
4	0.48	0.12	0.47	0.99	L
6	0.47	0.15	0.46	0.99	L

* See Table 5.1 for definition of functions used

Table 5.20 Correlation of *Max* μ_x/*Max* μ_{x0} for all fundamental periods and a specific R_d value on moment magnitude for model TUB1, site D

Model TB Site D					
column					
(1)	(2)	(3)	(4)	(5)	(6)
Data Parameters		Regression based on a Linear function			
R_d	Stdev	Corr Coeff	Se	Se/Sdeviation	f(x)
1	0.29	0.04	0.29	1.00	L
2	0.32	0.11	0.31	1.00	L
4	0.52	0.10	0.52	1.00	L
6	0.41	0.10	0.41	1.00	L

* See Table 5.1 for definition of functions used

Table 5.21 Correlation of $Max\ \mu_x/Max\ \mu_{x0}$ for all fundamental periods and a specific R_d value on moment magnitude for model TB, site D

Model TUB1 Site AB					
column					
(1)	(2)	(3)	(4)	(5)	(6)
Data Parameters		Regression based on a Linear function			
R_d	Stdev	Corr Coeff	S_e	$S_e/S_{deviation}$	f(x)
1	0.31	0.02	0.31	1.00	L
2	0.40	0.02	0.40	1.00	L
4	0.57	0.06	0.57	1.00	L
6	0.49	0.08	0.49	1.00	L

* See Table 5.1 for definition of functions used

Table 5.22 Correlation of $Max\ \mu_x/Max\ \mu_{x0}$ for all fundamental periods and a specific R_d value on moment magnitude for model TUB1, site AB

Model TUB1 Site D					
column					
(1)	(2)	(3)	(4)	(5)	(6)
Data Parameters		Regression based on a Linear function			
R_d	Stdev	Corr Coeff	Se	Se/Sdeviation	f(x)
1	0.29	0.02	0.29	1.00	L
2	0.32	0.01	0.32	1.00	L
4	0.52	0.08	0.52	1.00	L
6	0.41	0.09	0.41	1.00	L

* See Table 5.1 for definition of functions used

Table 5.23 Correlation of $Max\ \mu_x/Max\ \mu_{x0}$ for all fundamental periods and a specific R_d value on distance to fault rupture zone for model TUB1, site D

Model TB Site D					
column					
(1)	(2)	(3)	(4)	(5)	(6)
Data Parameters		Regression based on a Linear function			
R_d	Stdev	Corr Coeff	Se	Se/Sdeviation	f(x)
1	0.28	0.11	0.28	1.00	L
2	0.38	0.11	0.37	1.00	L
4	0.48	0.12	0.48	1.00	L
6	0.47	0.15	0.47	1.00	L

* See Table 5.1 for definition of functions used

Table 5.24 Correlation of $Max\ \mu_x/Max\ \mu_{x0}$ for all fundamental periods and a specific R_d value on distance to fault rupture zone for model TB, site D

Model TUB1 Site AB					
column					
(1)	(2)	(3)	(4)	(5)	(6)
Data Parameters		Regression based on a Linear function			
R_d	Stdev	Corr Coeff	S_e	$S_e/S_{deviation}$	f(x)
1	0.31	0.08	0.31	1.00	L
2	0.40	0.04	0.40	1.00	L
4	0.57	0.07	0.57	1.00	L
6	0.49	0.12	0.49	1.00	L

* See Table 5.1 for definition of functions used

Table 5.25 Correlation of $Max\ \mu_x/Max\ \mu_{x0}$ for all fundamental periods and a specific R_d value on distance to fault rupture zone for model TUB1, site AB

Model TUB1 Site D			
column			
(1)	(2)	(3)	(4)
Data Parameters		Hypothesis based on a Linear function	
R_d	b (slope)	Accept with 95% Confidence?	Accept with 99% Confidence?
1	0.07	Accept	Accept
2	0.25	Accept	Accept
4	0.36	Accept	Accept
6	0.29	Accept	Accept

Table 5.26 Likely hood of dependency of $Max\ \mu_x/Max\ \mu_{x0}$ for all fundamental periods and a specific R_d value on moment magnitude for model TUB1, site D

Model TB Site D			
column			
(1)	(2)	(3)	(4)
Data Parameters		Hypothesis based on a Linear function	
R_d	b (slope)	Accept with 95% Confidence?	Accept with 99% Confidence?
1	0.206381	Accept	Accept
2	0.297991	Accept	Accept
4	0.406414	Accept	Accept
6	0.479117	Accept	Reject

Table 5.27 Likely hood of dependency of *Max* μ_x/*Max* μ_{x0} for all fundamental periods and a specific R_d value on moment magnitude for model TB, site D

Model TUB1 Site AB			
column			
(1)	(2)	(3)	(4)
Data Parameters		Hypothesis based on a Linear function	
R_d	b (slope)	Accept with 95% Confidence?	Accept with 99% Confidence?
1	-0.015277	Accept	Accept
2	0.023509	Reject	Reject
4	0.111615	Reject	Reject
6	0.150889	Reject	Reject

Table 5.28 Likely hood of dependency of *Max* μ_x/*Max* μ_{x0} for all fundamental periods and a specific R_d value on moment magnitude for model TUB1, site AB

Model TUB1 Site D			
column			
(1)	(2)	(3)	(4)
Data Parameters		Hypothesis based on a Linear function	
R_d	b (slope)	Accept with 95% Confidence?	Accept with 99% Confidence?
1	0.001	Accept	Accept
2	0.005	Accept	Accept
4	-0.004	Accept	Accept
6	0.001	Accept	Accept

Table 5.29 Likely hood of dependency of *Max* μ_x/*Max* μ_{x0} for all fundamental periods and a specific R_d value on distance from the fault rupture zone for model TUB1, site D

Model TB site D			
column			
(1)	(2)	(3)	(4)
Data Parameters		Hypothesis based on a Linear function	
R_d	b (slope)	Accept with 95% Confidence?	Accept with 99% Confidence?
1	0.0006	Accept	Accept
2	0.0003	Accept	Accept
4	0.0052	Accept	Accept
6	0.0045	Accept	Accept

Table 5.30 Likely hood of dependency of *Max* μ_x/*Max* μ_{x0} for all fundamental periods and a specific R_d value on distance from the fault rupture zone for model TB, site D

Model TUB1 Site AB			
column			
(1)	(2)	(3)	(4)
Data Parameters		Hypothesis based on a Linear function	
R_d	b (slope)	Accept with 95% Confidence?	Accept with 99% Confidence?
1	-0.001	Accept	Accept
2	-0.001	Accept	Accept
4	-0.002	Accept	Accept
6	-0.002	Accept	Accept

Table 5.31 Likely hood of dependency of $Max\ \mu_x/Max\ \mu_{x0}$ for all fundamental periods and a specific R_d value on distance from the fault rupture zone for model TUB1, site AB

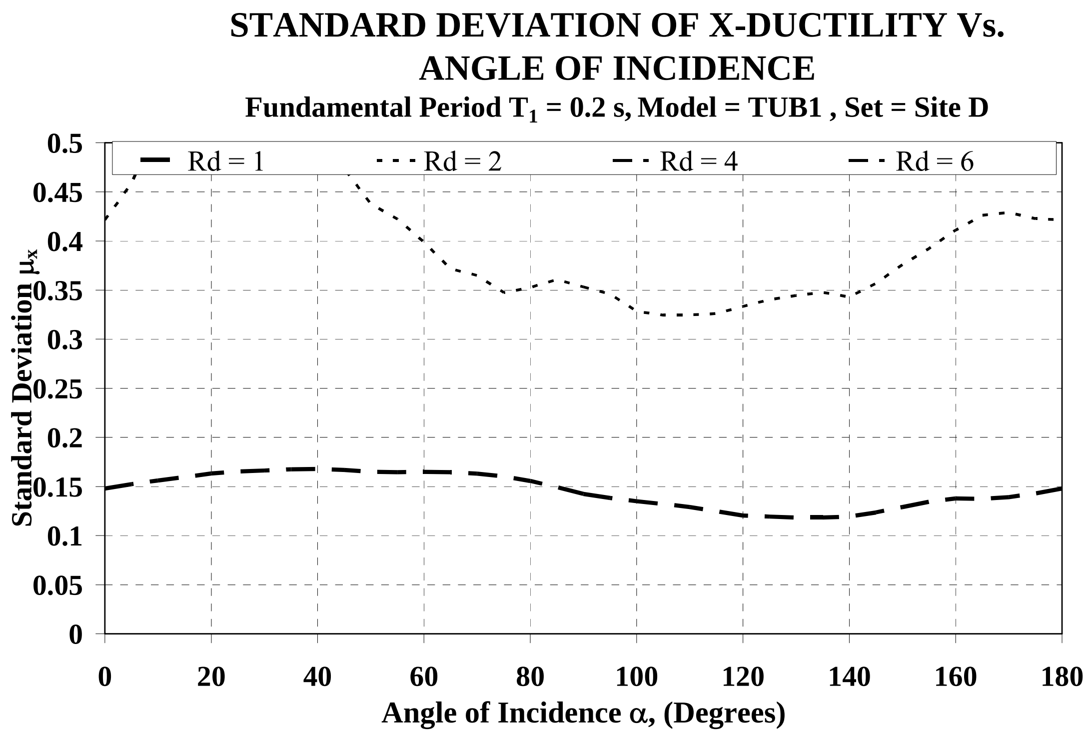

(Scale reduced for clarity)

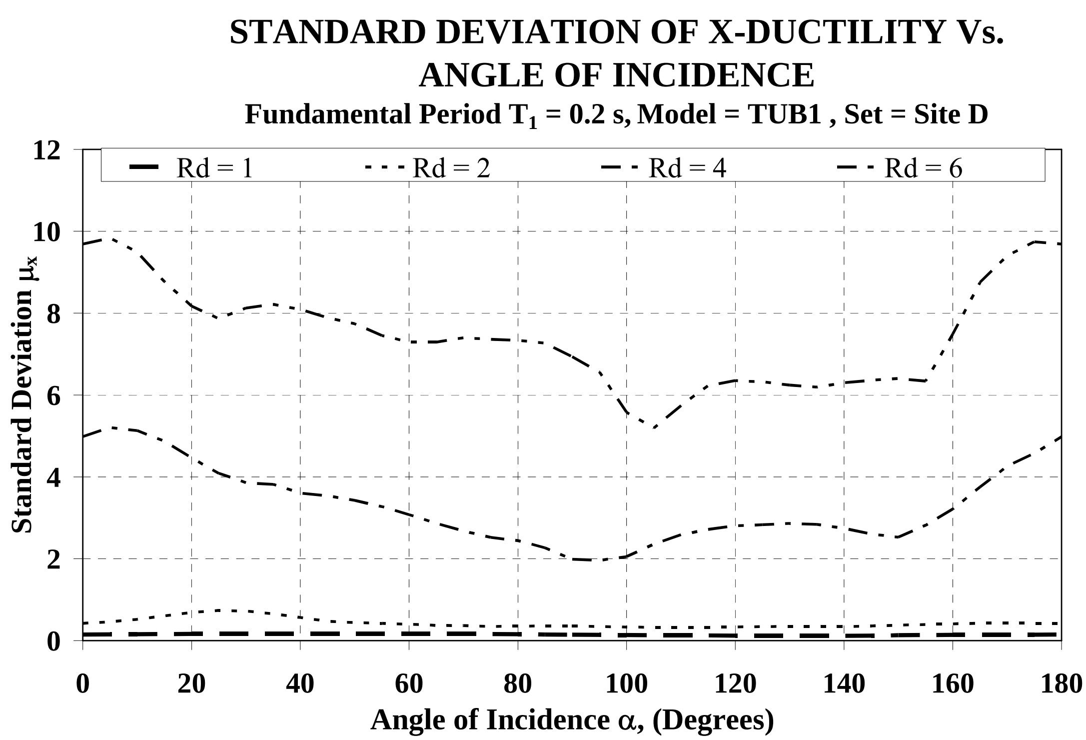

Figure 5.1 Standard deviation of X-ductilities and their dependence on angle of incidence at fundamental period of 0.2 s for Model TUB1

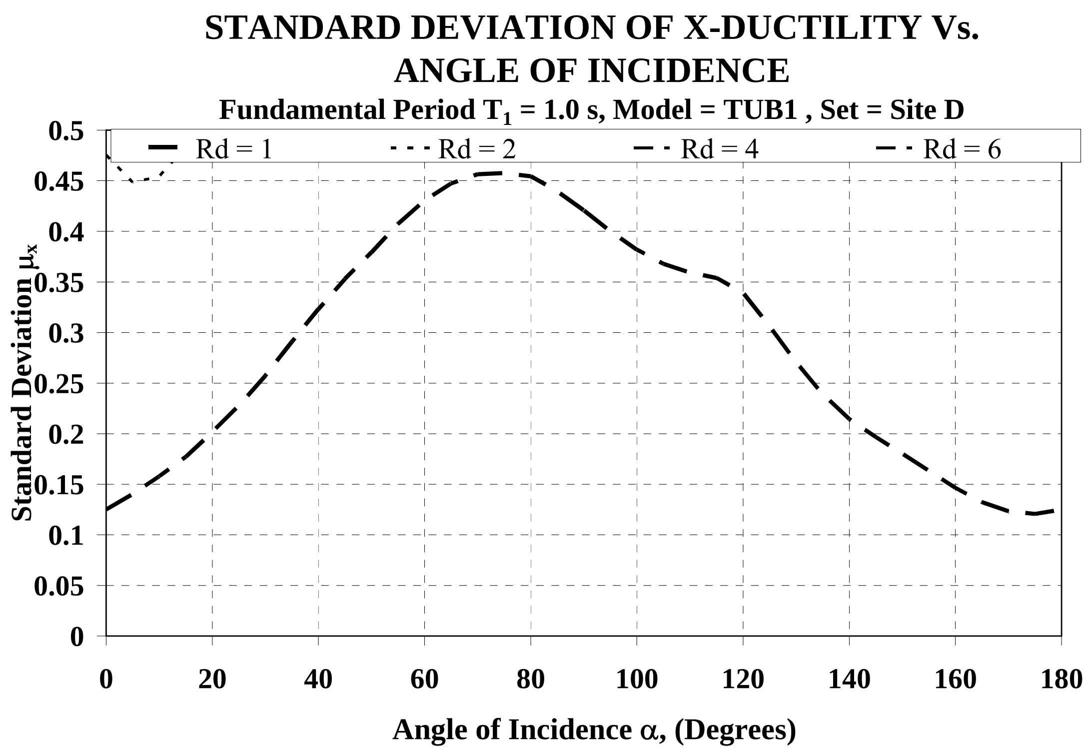

(Scale reduced for clarity)

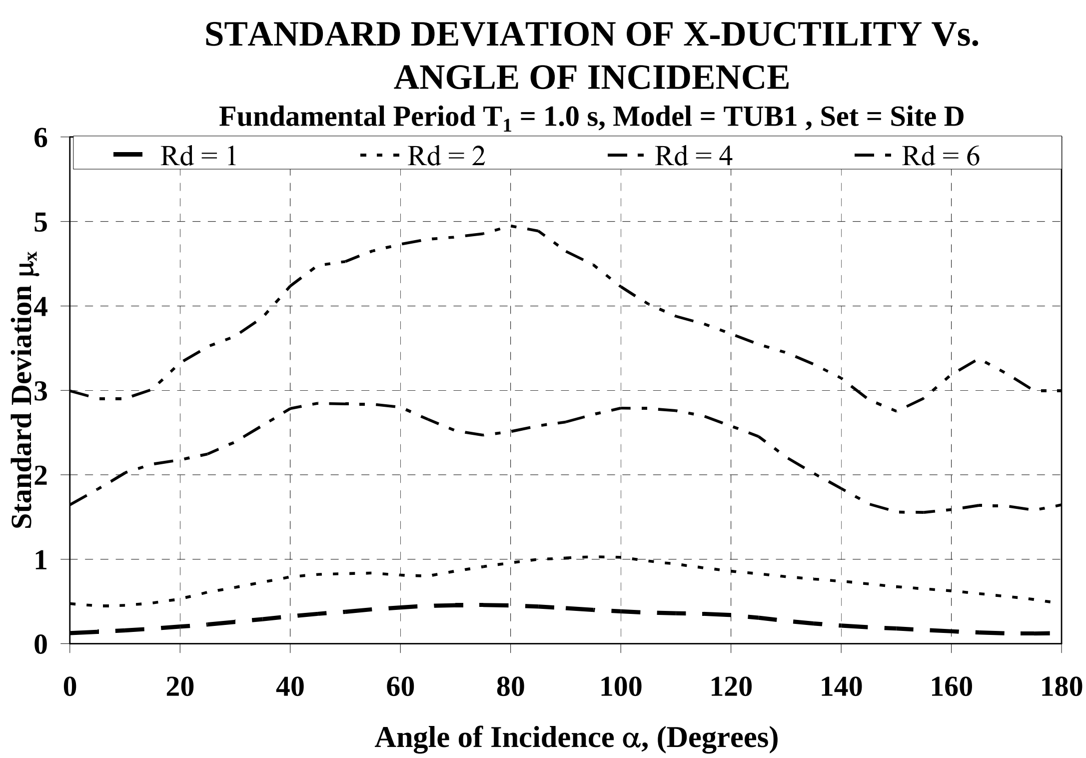

Figure 5.2 Standard deviation of X-ductilities and their dependence on angle of incidence at fundamental period of 1.0 s for Model TUB1

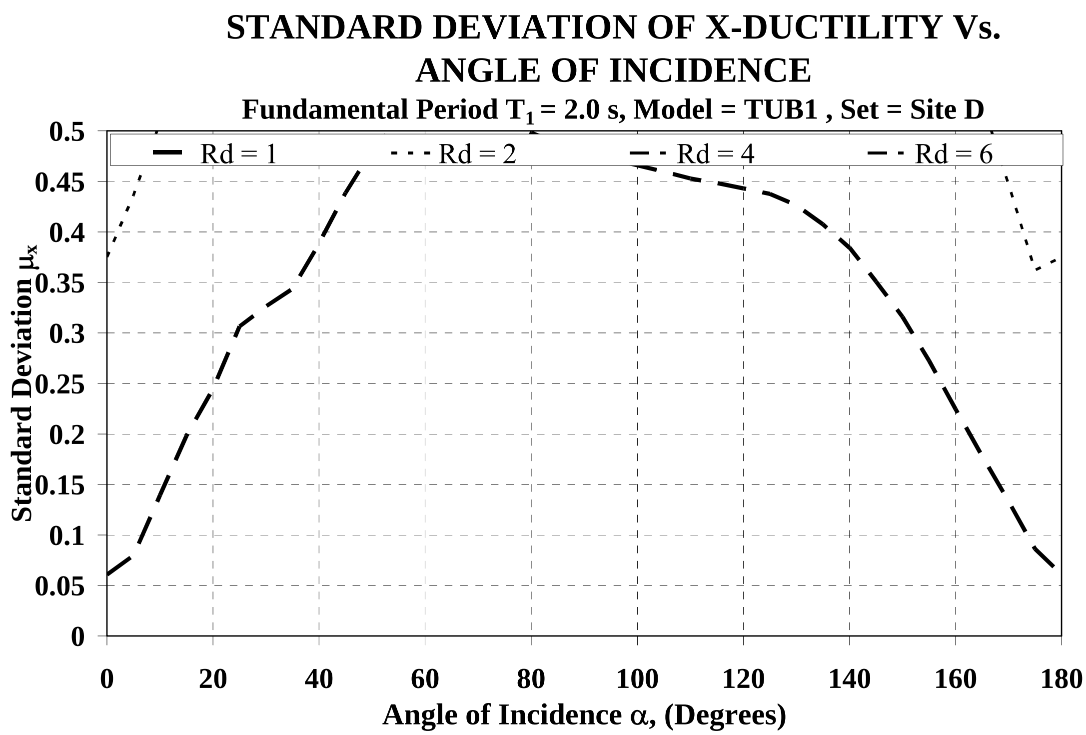

(Scale reduced for clarity)

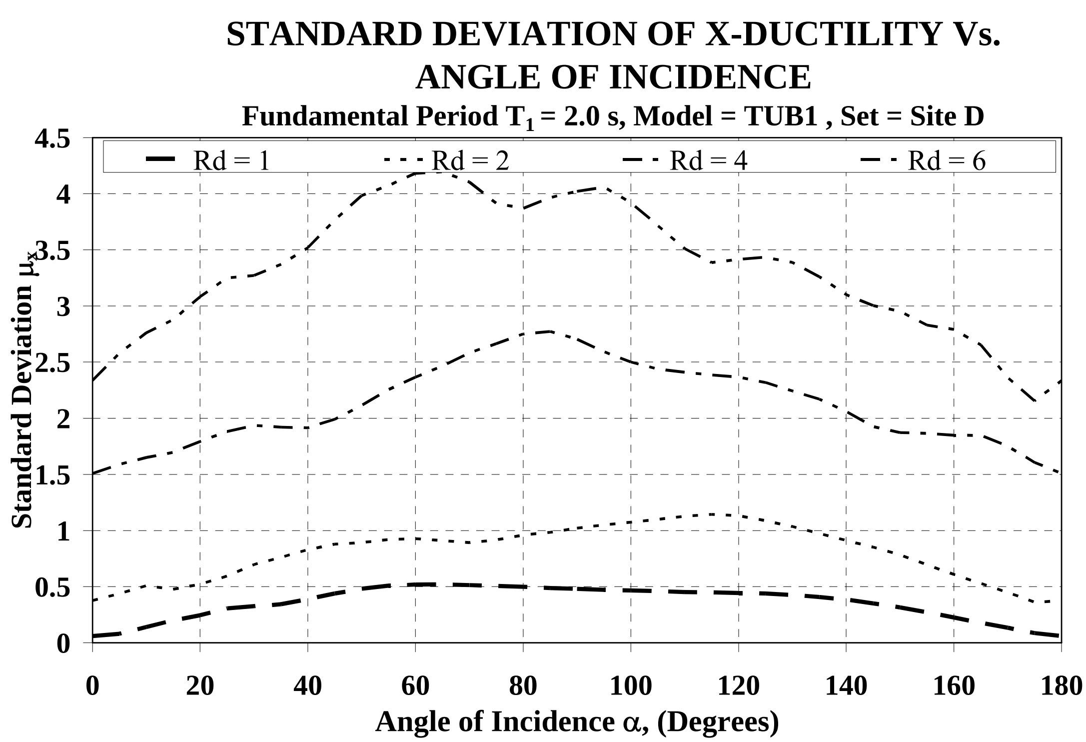

Figure 5.3 Standard deviation of X-ductilities and their dependence on angle of incidence at fundamental period of 2.0 s for Model TUB1

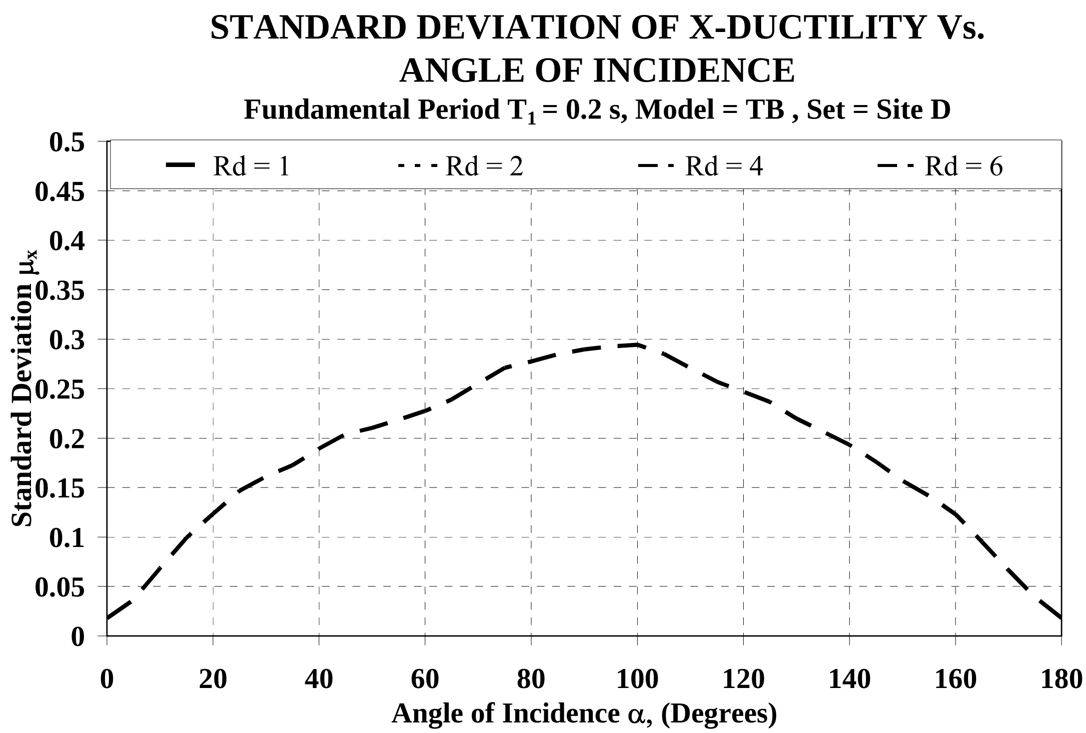

(Reduced scale for clarity)

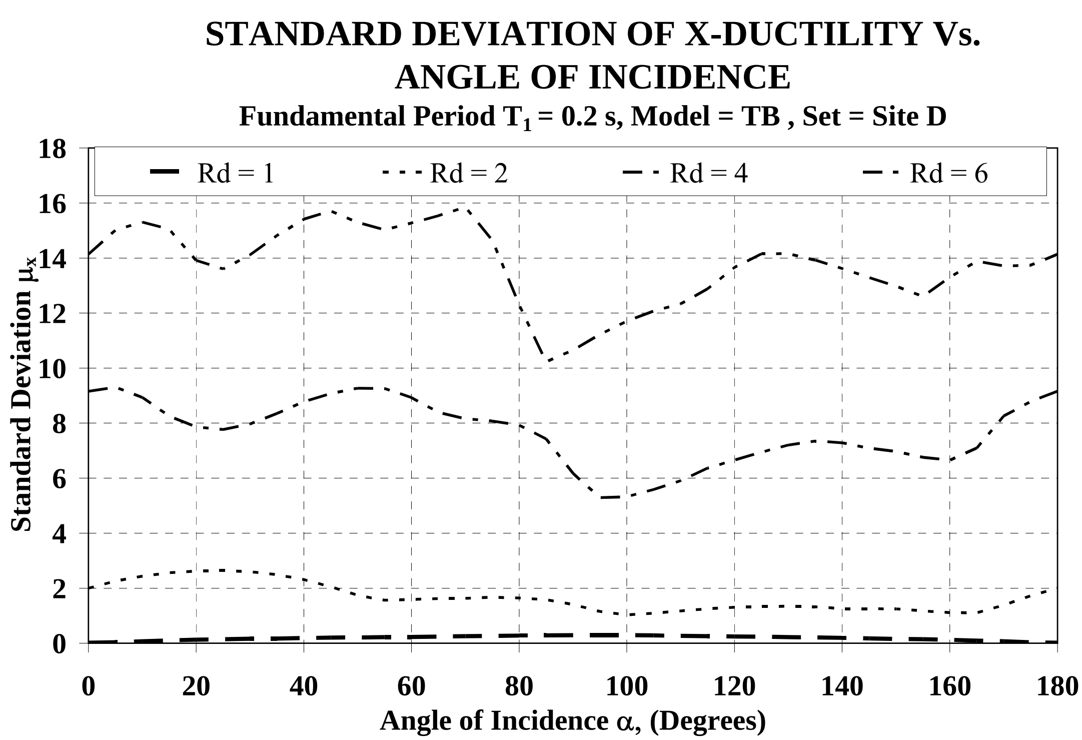

Figure 5.4 Standard deviation of X-ductilities and their dependence on angle of incidence at fundamental period of 0.2 s for Model TB

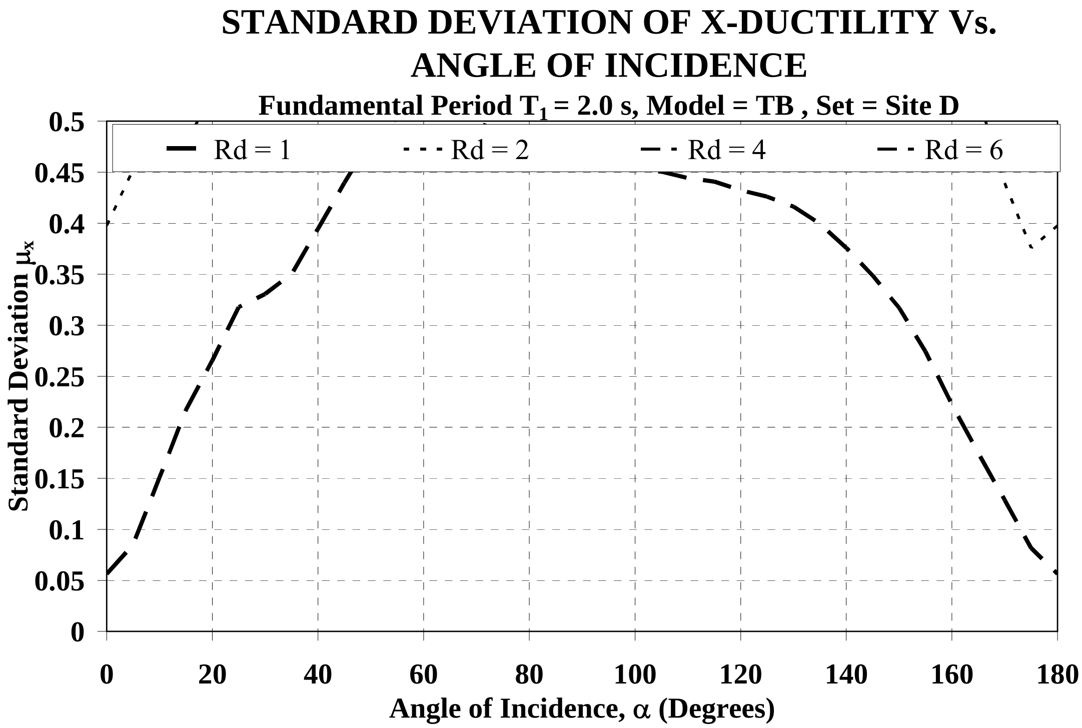

(Reduced scale for clarity)

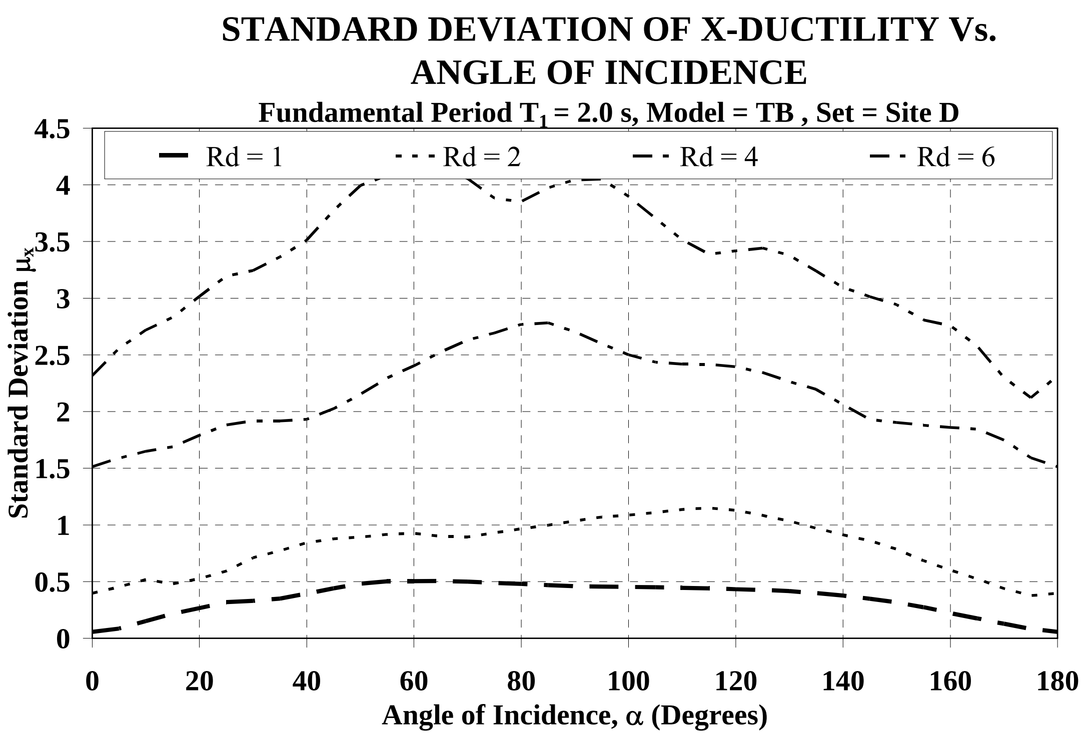

Figure 5.5 Standard deviation of X-ductilities and their dependence on angle of incidence at fundamental period of 2.0 s for Model TB

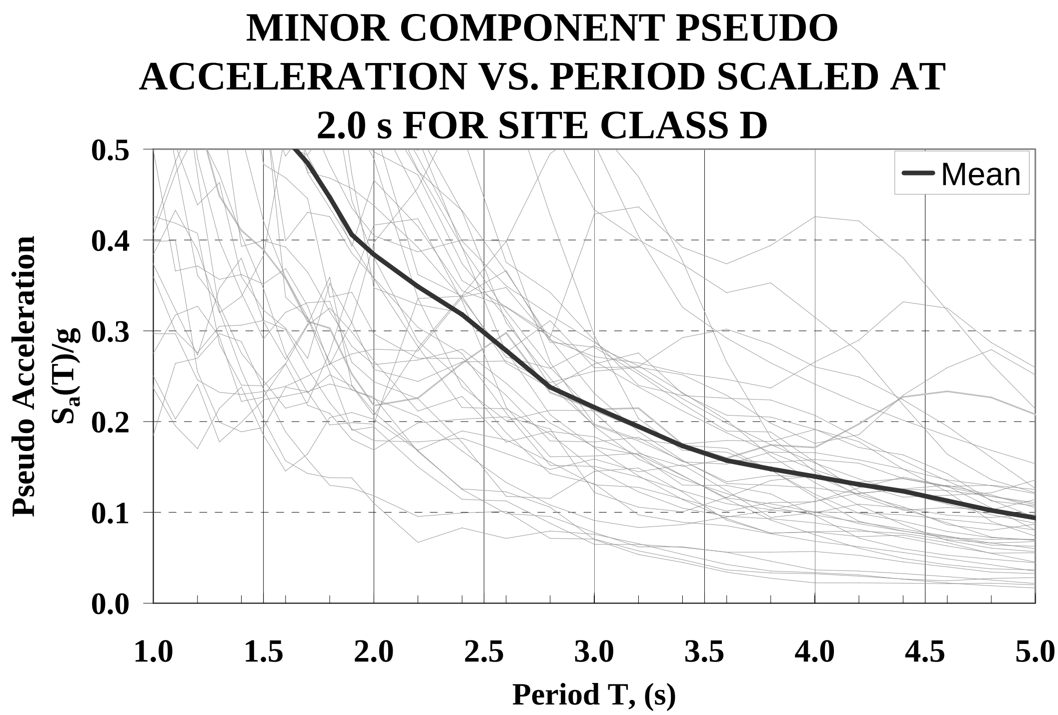

Figure 5.6 Scaled response spectra of minor component at 2.0 s, site D

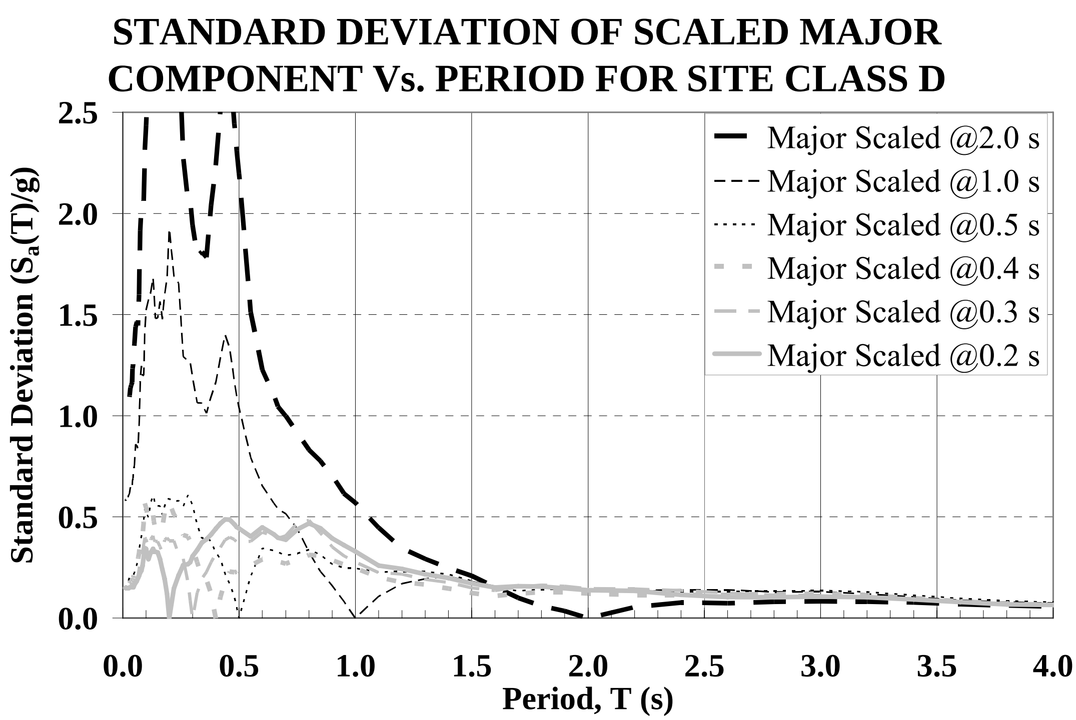

Figure 5.7 Dependency of scaled major component standard deviations on period for a given fundamental period for site class D

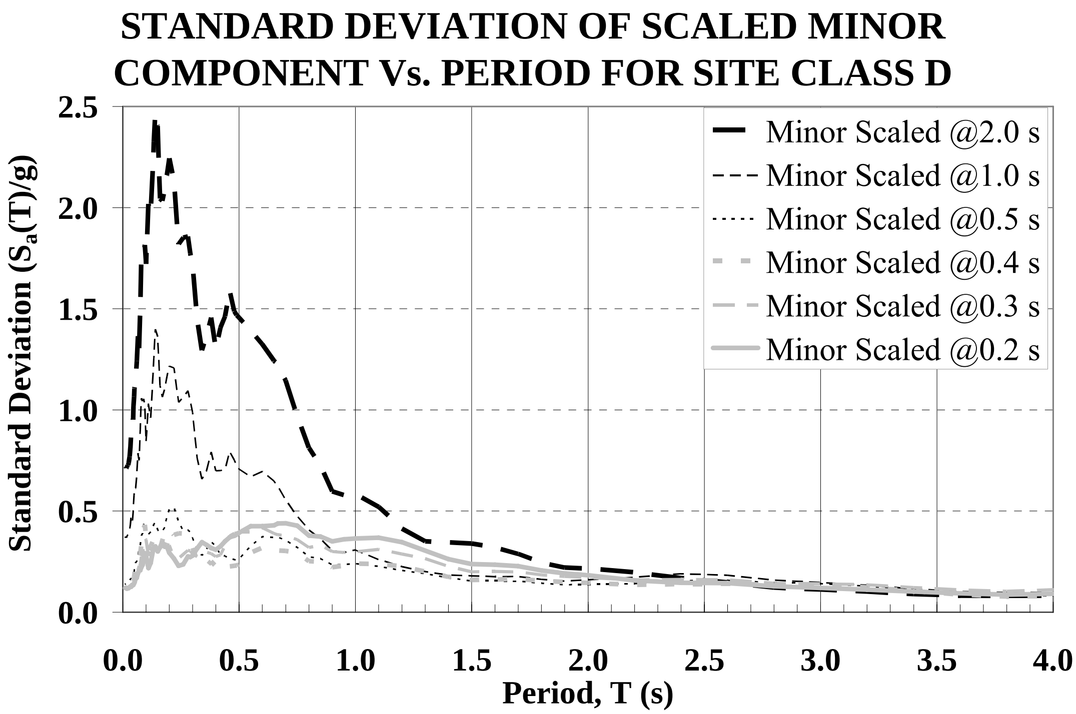

Figure 5.8 Dependency of scaled minor component standard deviations on period for a given fundamental period for site class D

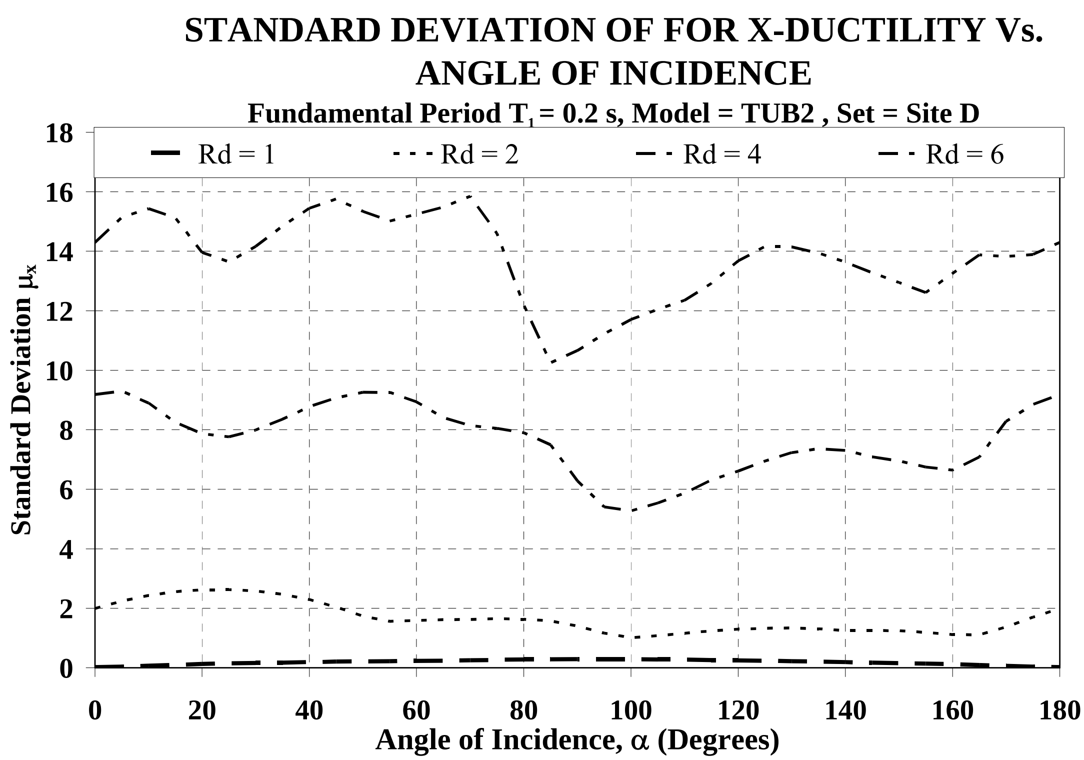

Figure 5.9 Standard deviation of X-ductilities and their dependence on angle of incidence at fundamental period of 0.2 s for Model TUB2

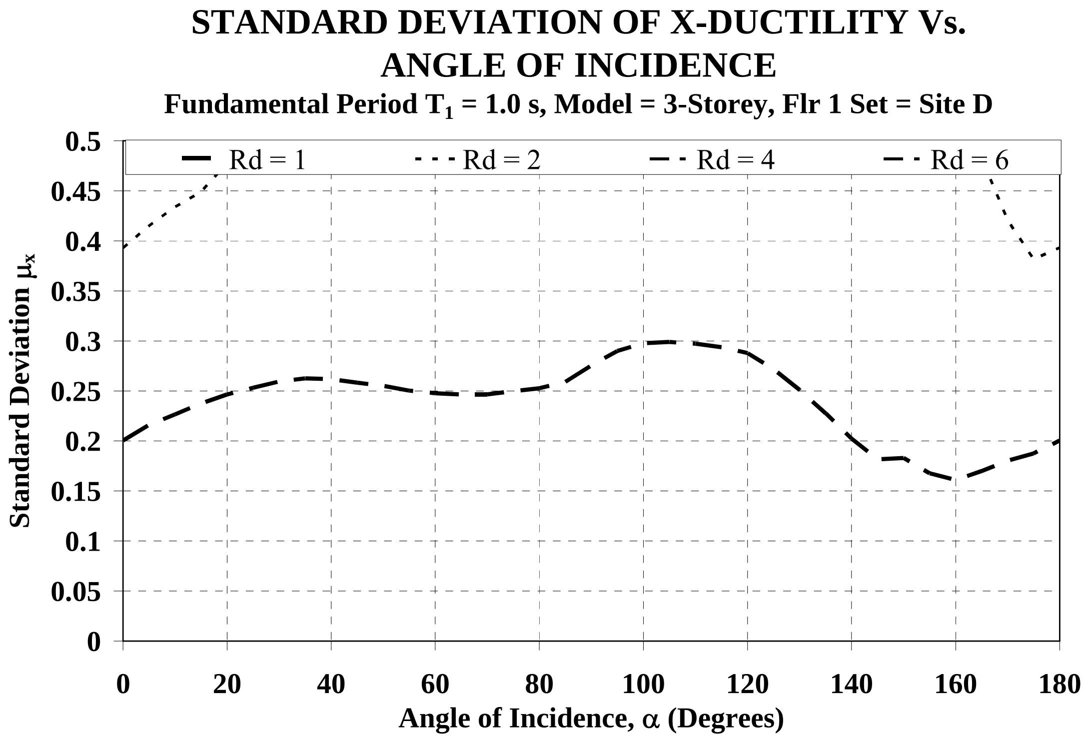

(Scale reduced for clarity)

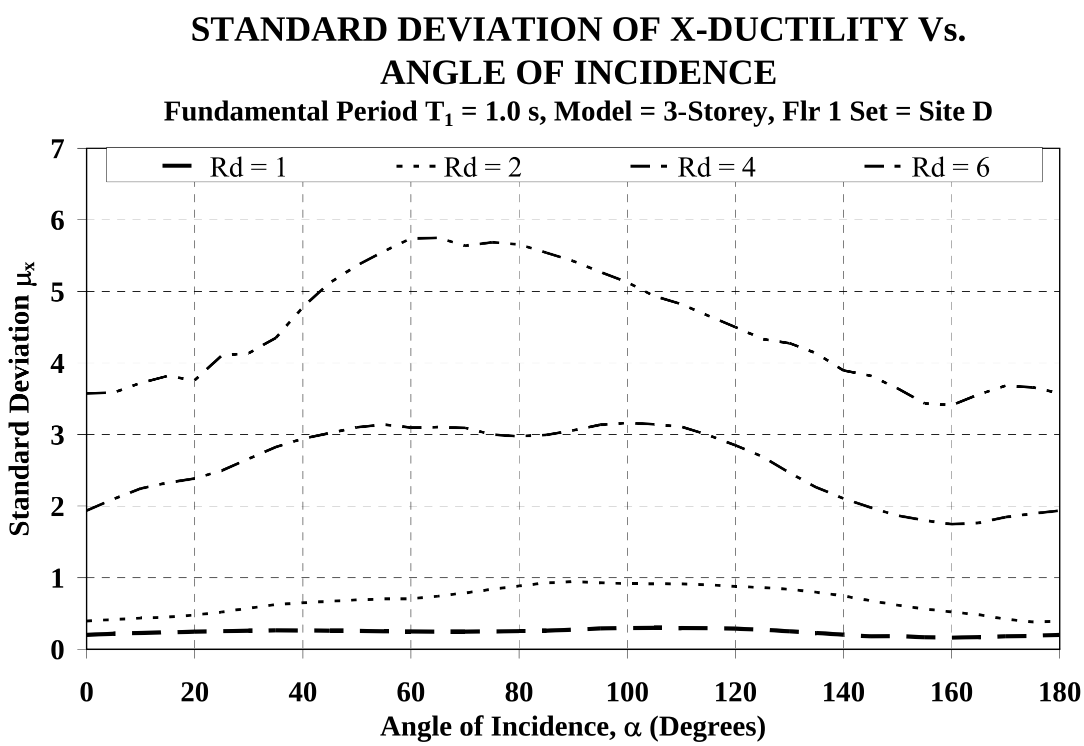

Figure 5.10 Standard deviation of X-ductilities and their dependence on angle of incidence at fundamental period of 1.0 s for the 3-storey model, Floor 1

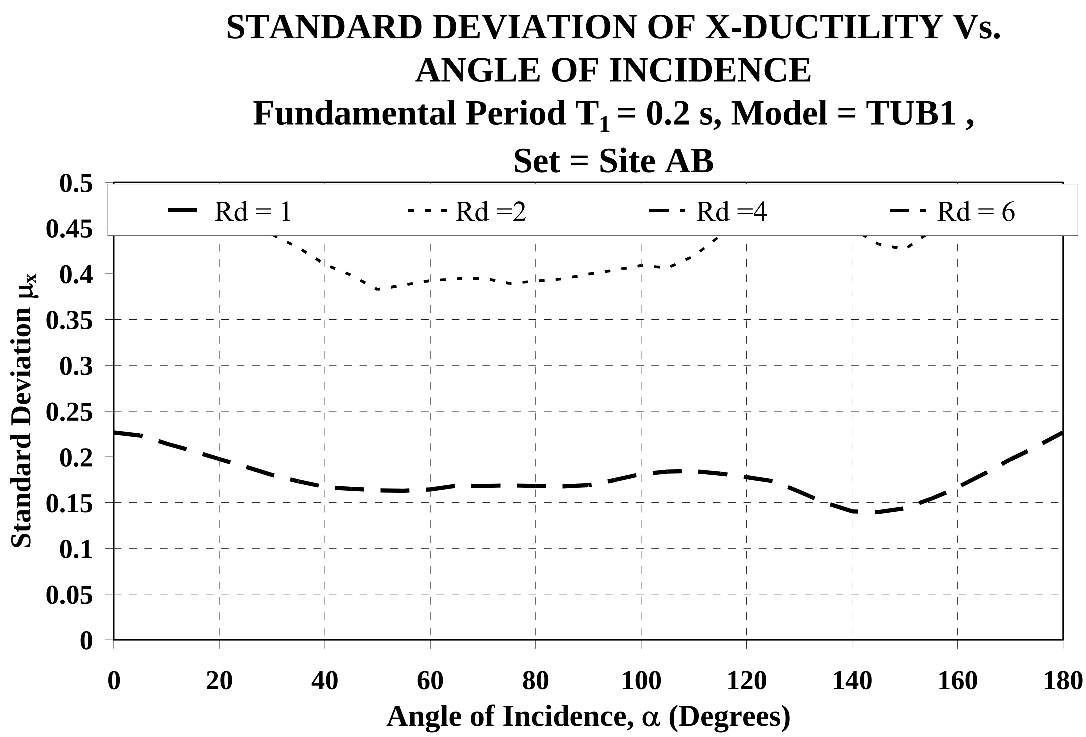

(Scale reduced for clarity)

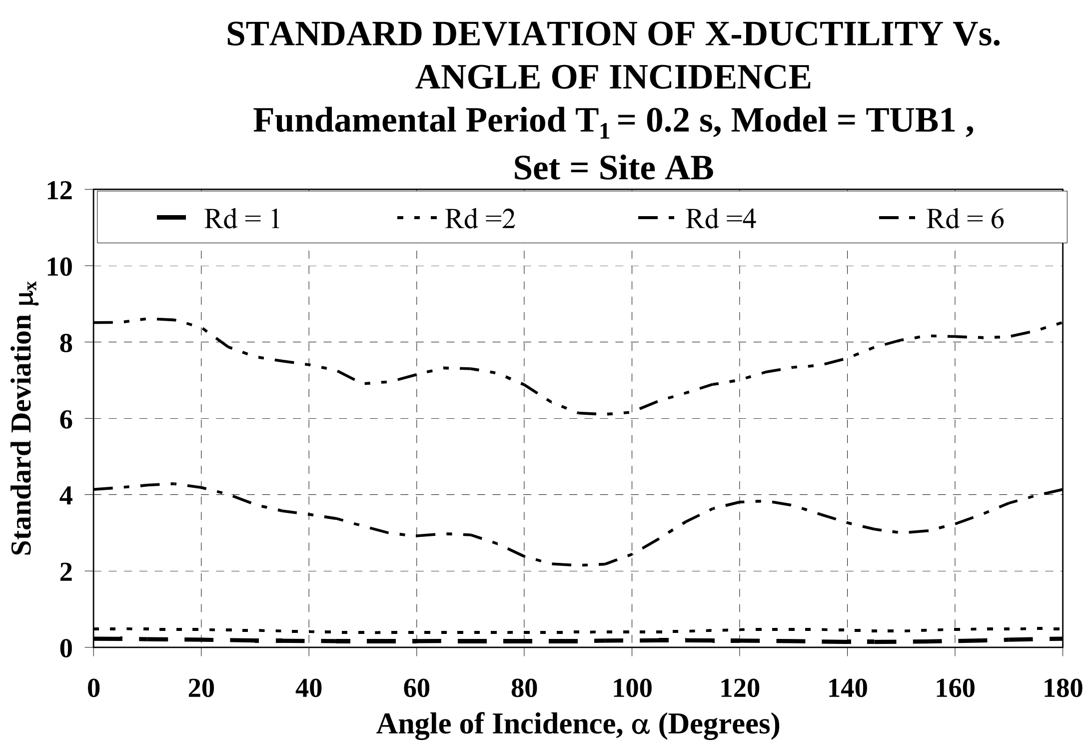

Figure 5.11 Standard deviation of X-ductilities and their dependence on angle of incidence at a fundamental period of 0.2 s for model TUB1 subjected to site AB ground motion pairs

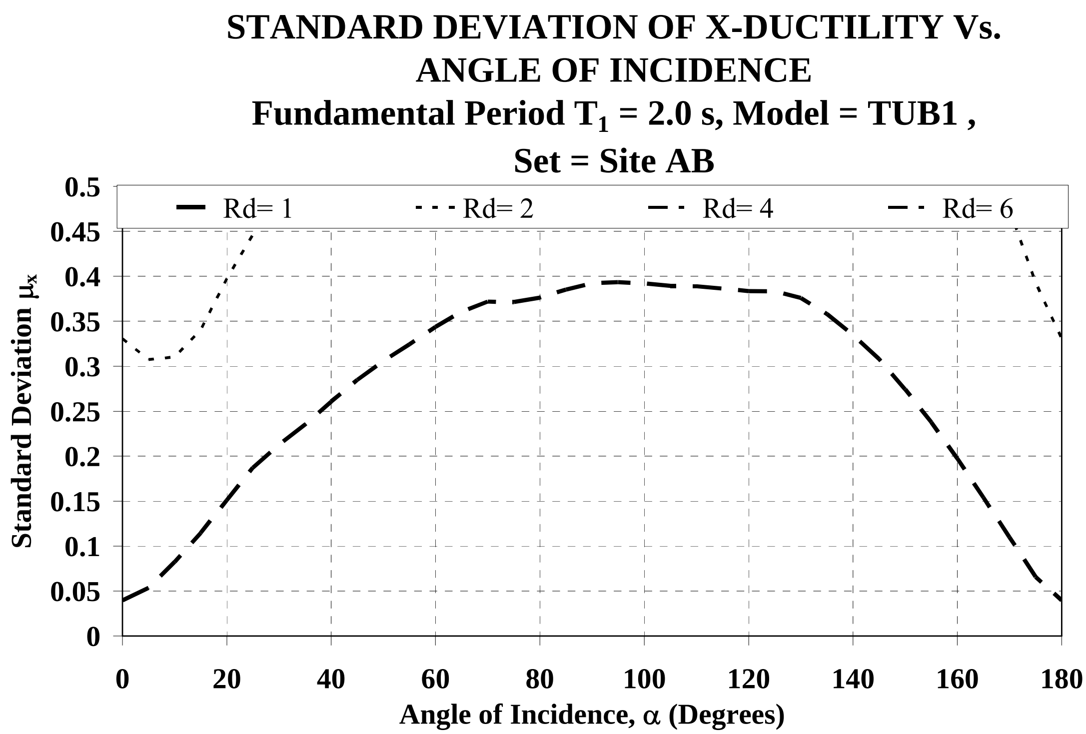

(scale reduced for clarity)

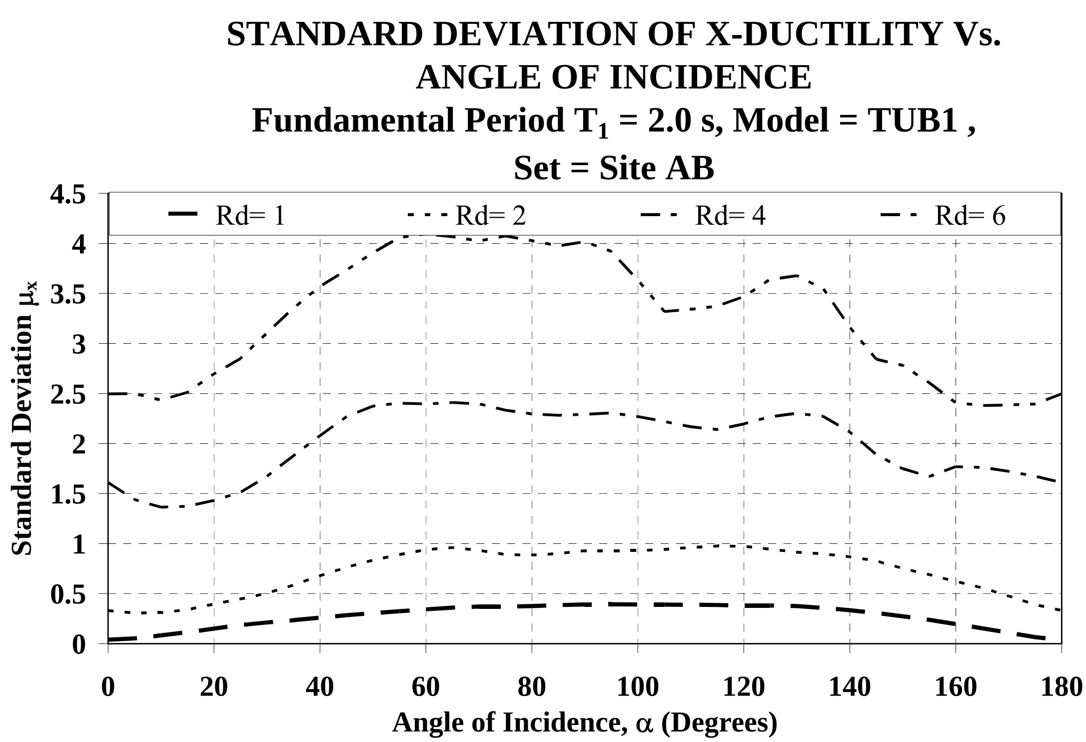

Figure 5.12 Standard deviation of X-ductilities and their dependence on angle of incidence at a fundamental period of 2.0 s for TUB1 model subjected to site AB ground motion pairs

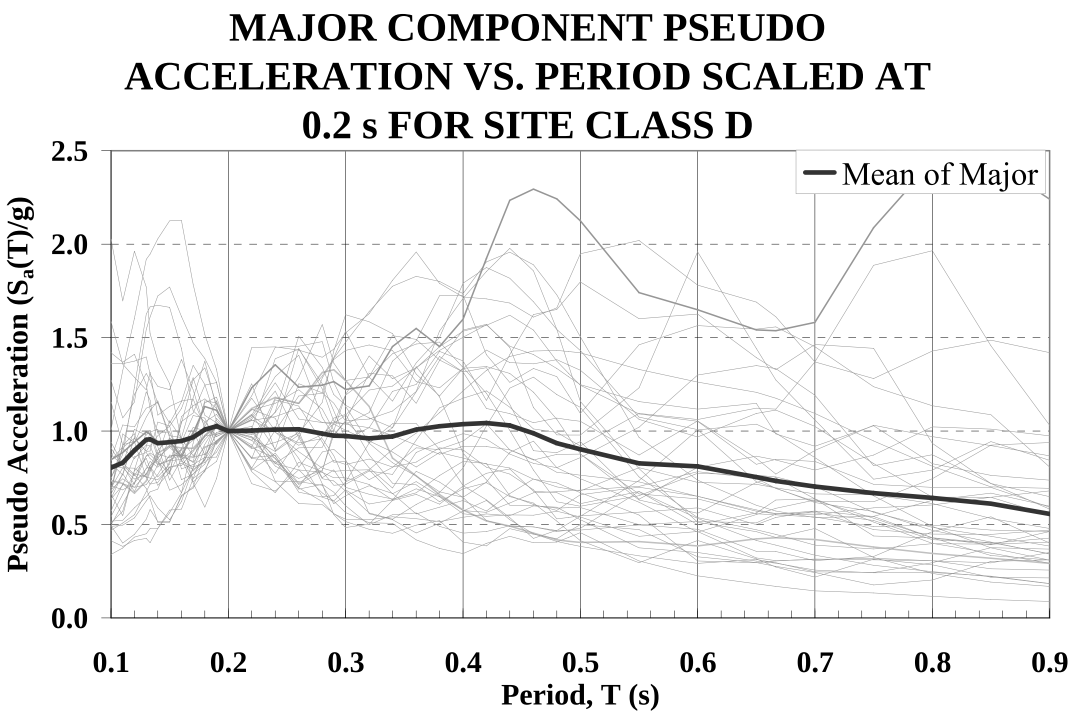

Figure 5.13 Major component spectra scaled at 0.2 s for site class D

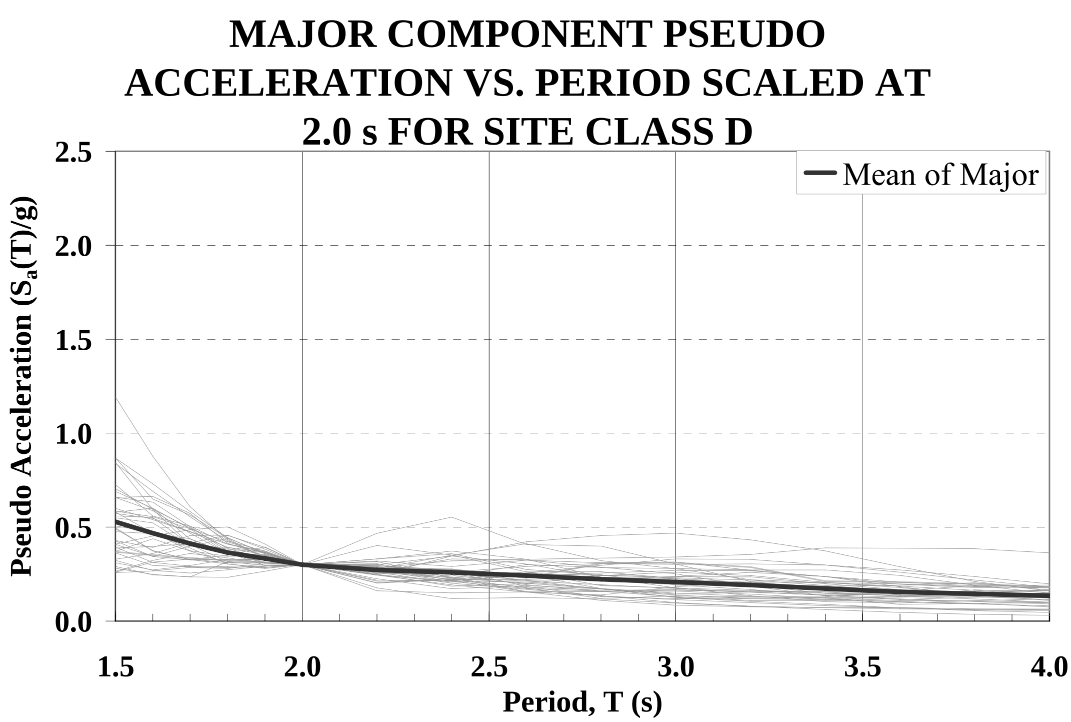

Figure 5.14 Major component spectra scaled at 2.0 s for site class D

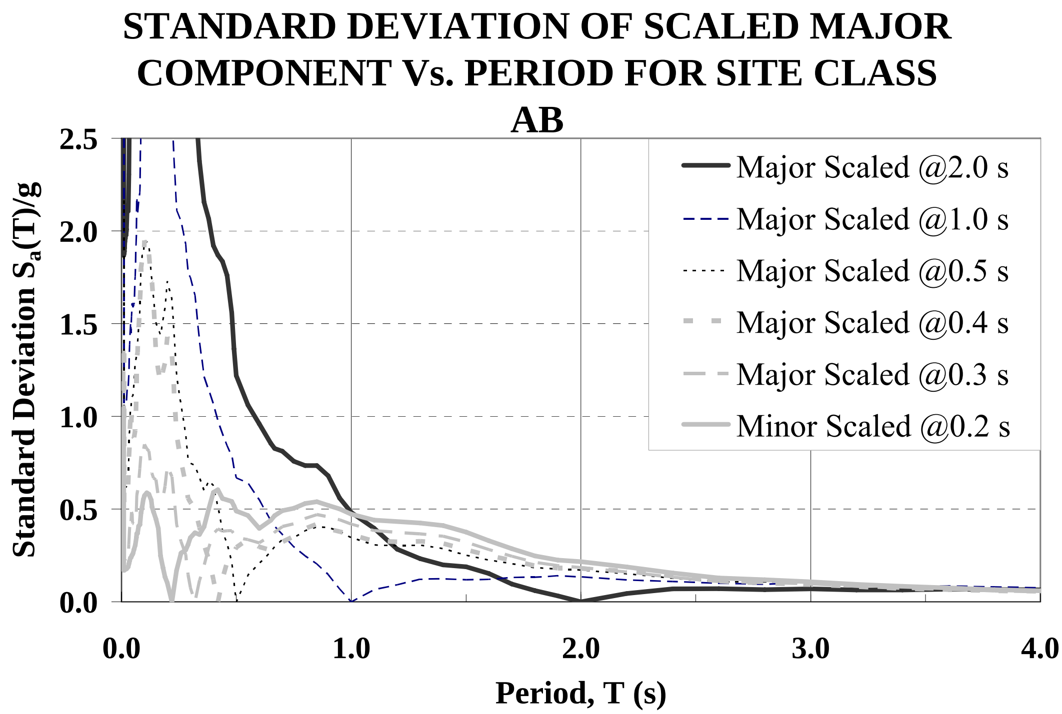

Figure 5.15 Dependency of scaled major component standard deviation on period for a given fundamental period for site class AB

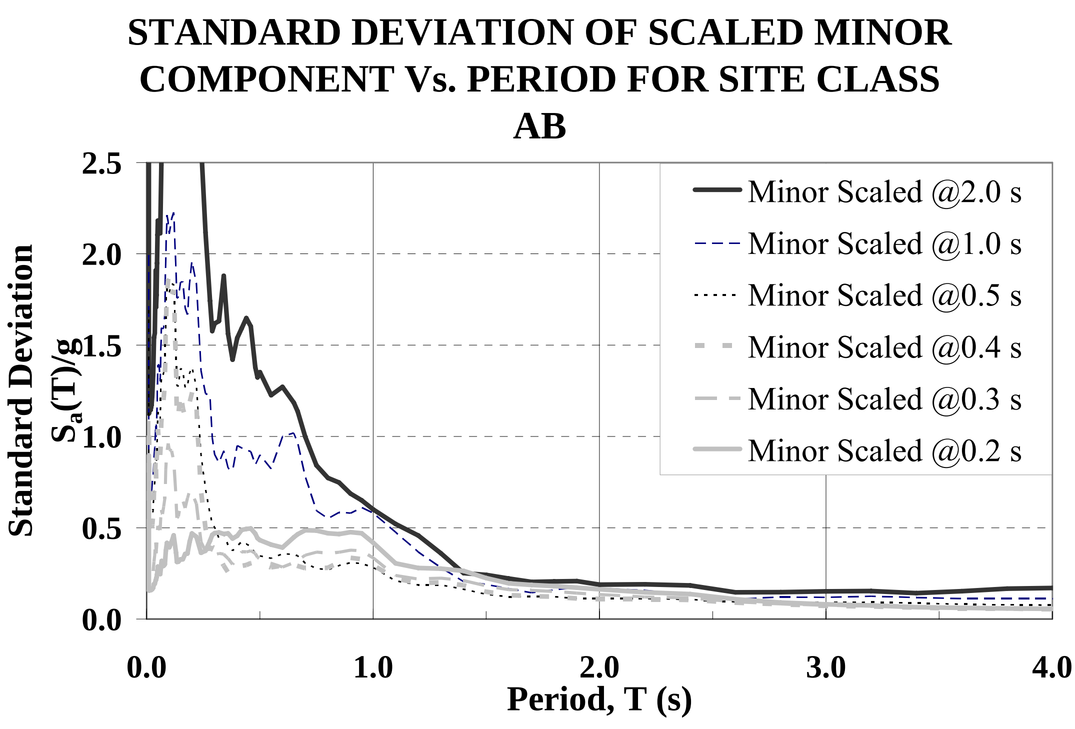

Figure 5.16 Dependency of scaled minor component standard deviation on period for a given fundamental period for site class AB

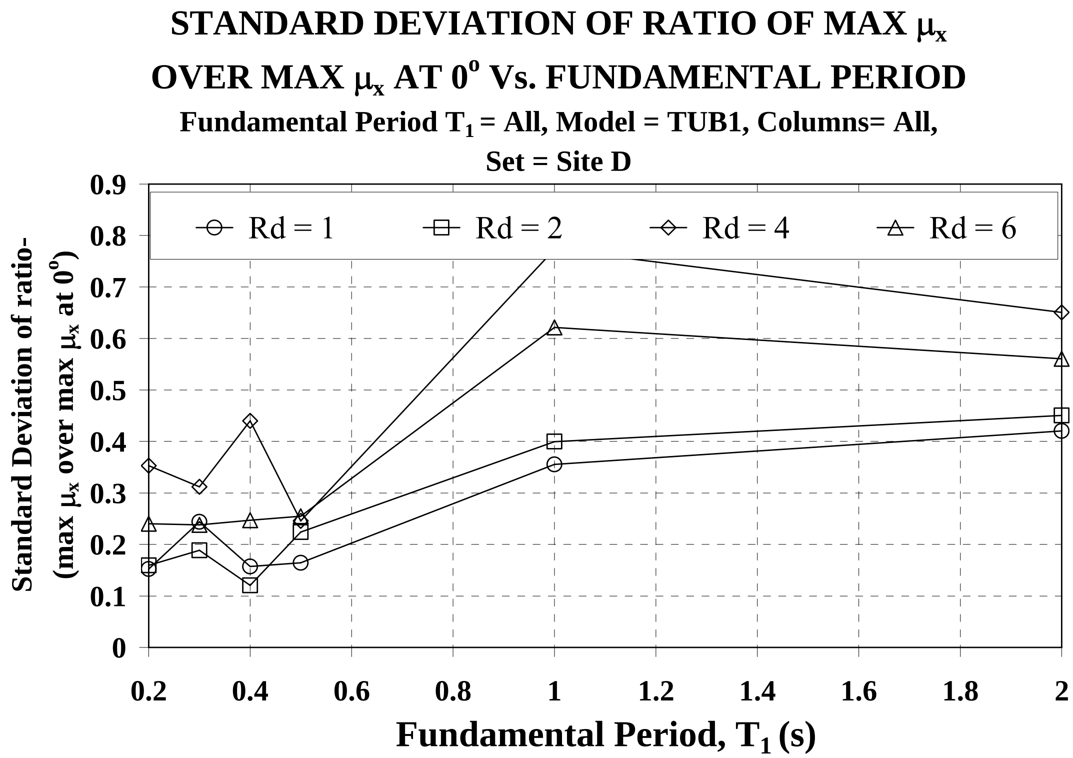

Figure 5.17 Standard deviations of *Max μ_x/Max μ_{x0}* and their dependence on fundamental period, model TUB1

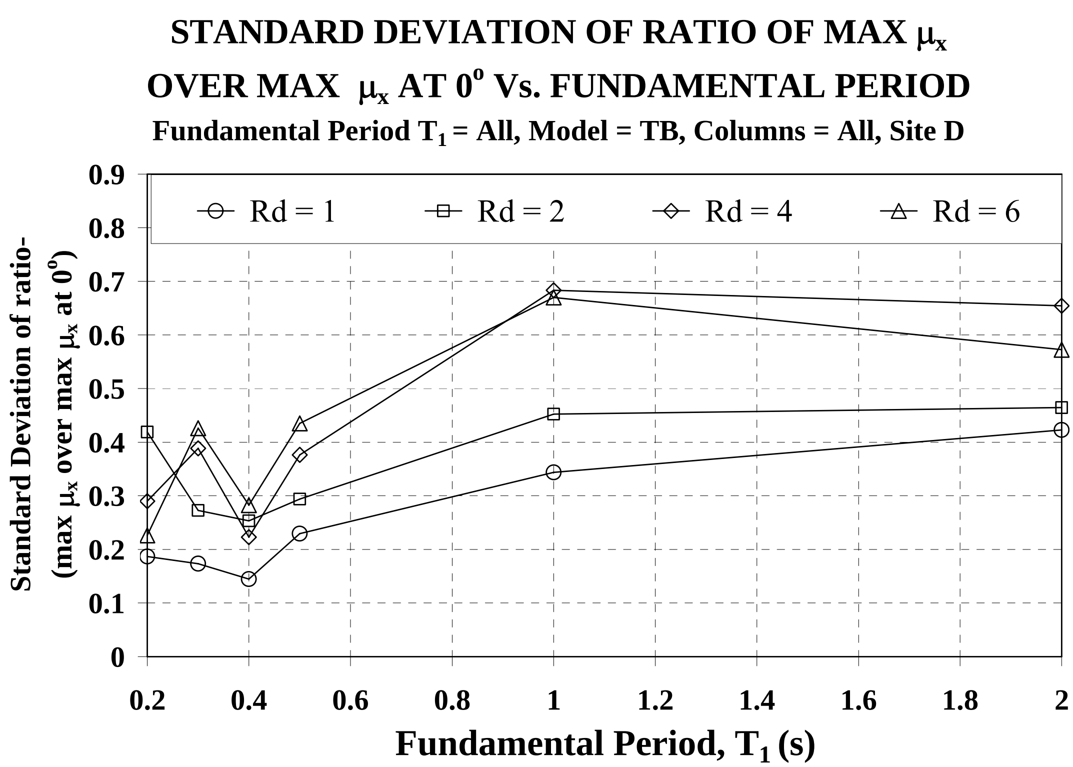

Figure 5.18 Standard deviations of *Max μ_x/Max μ_{x0}* and their dependence on fundamental period, model TB

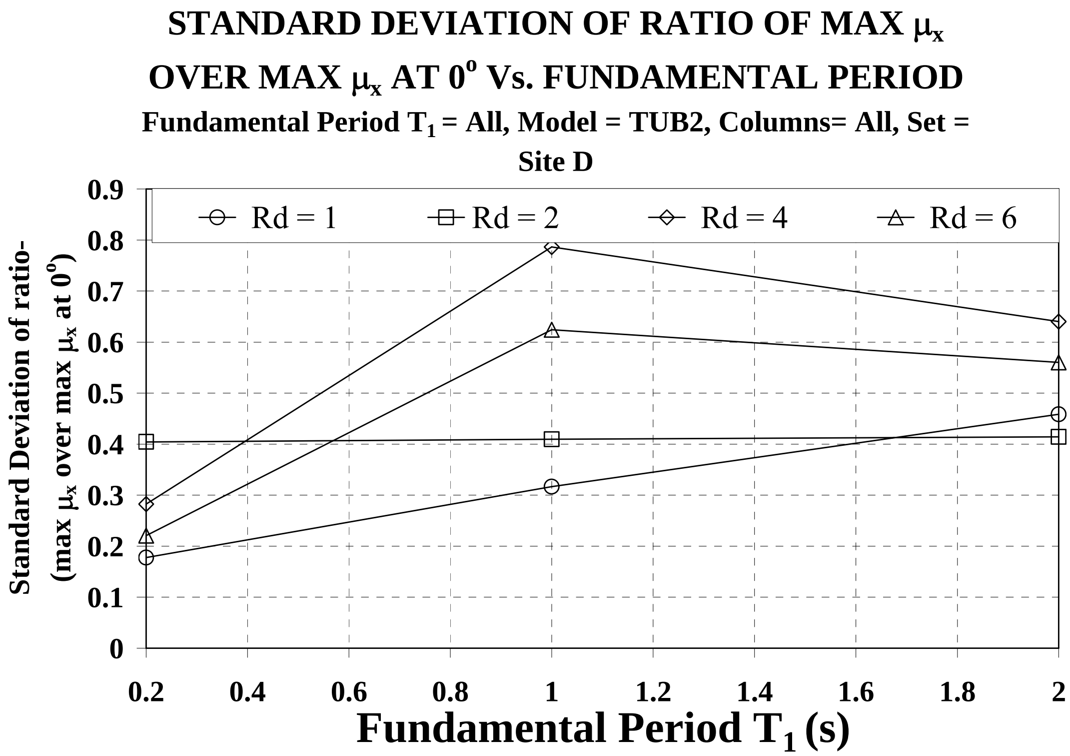

Figure 5.19 Standards deviation of *Max μ_x/Max μ_{x0}* and their dependence on fundamental period for site D, model TUB2

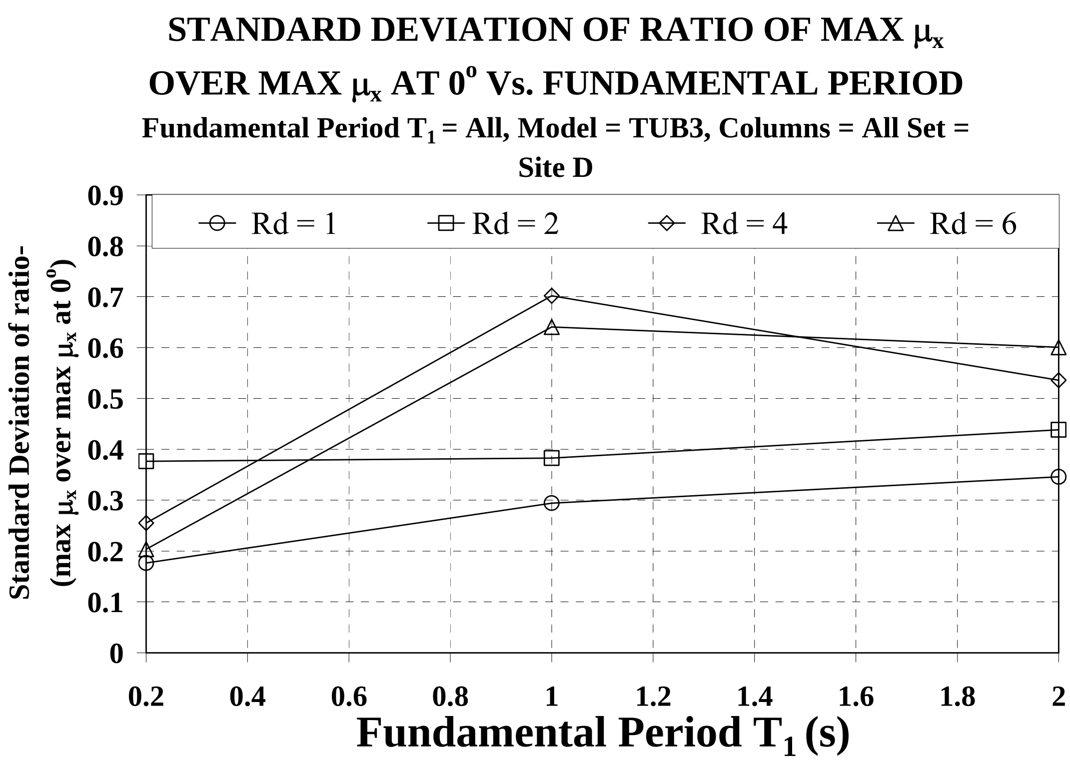

Figure 5.20 Standard deviations of *Max μ_x/Max μ_{x0}* and their dependence on fundamental period for site D, model TUB3

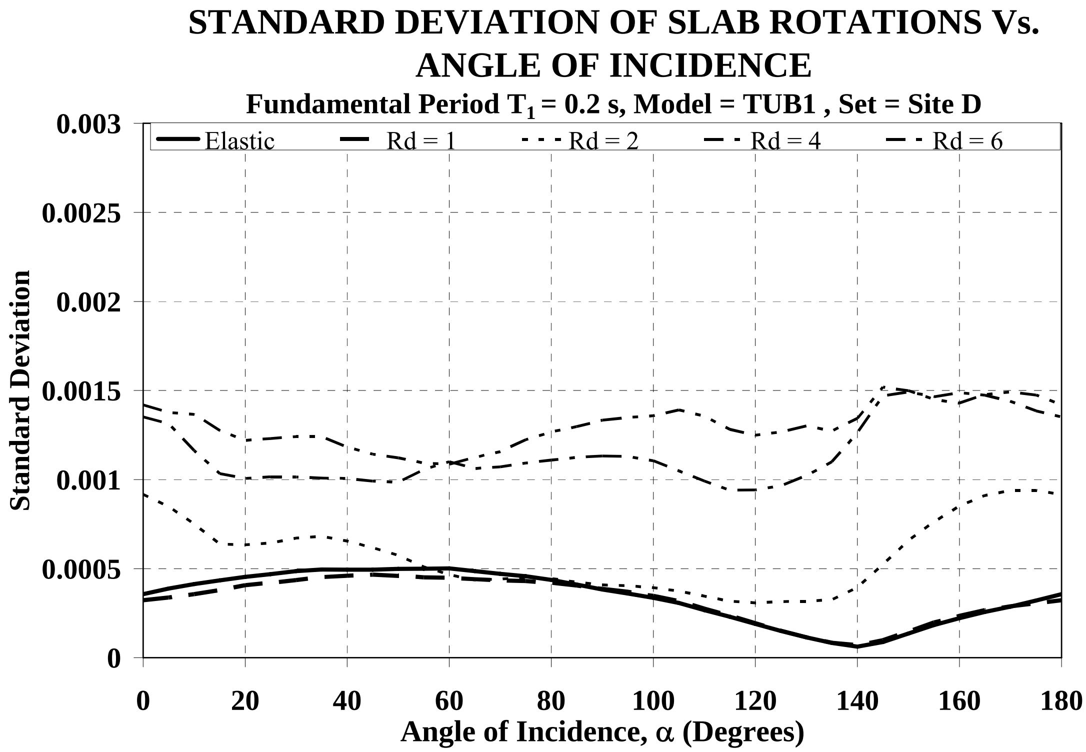

Figure 5.21 Standard deviation of slab rotations and their dependence on angle of incidence at fundamental period of 0.2 s for model TUB1

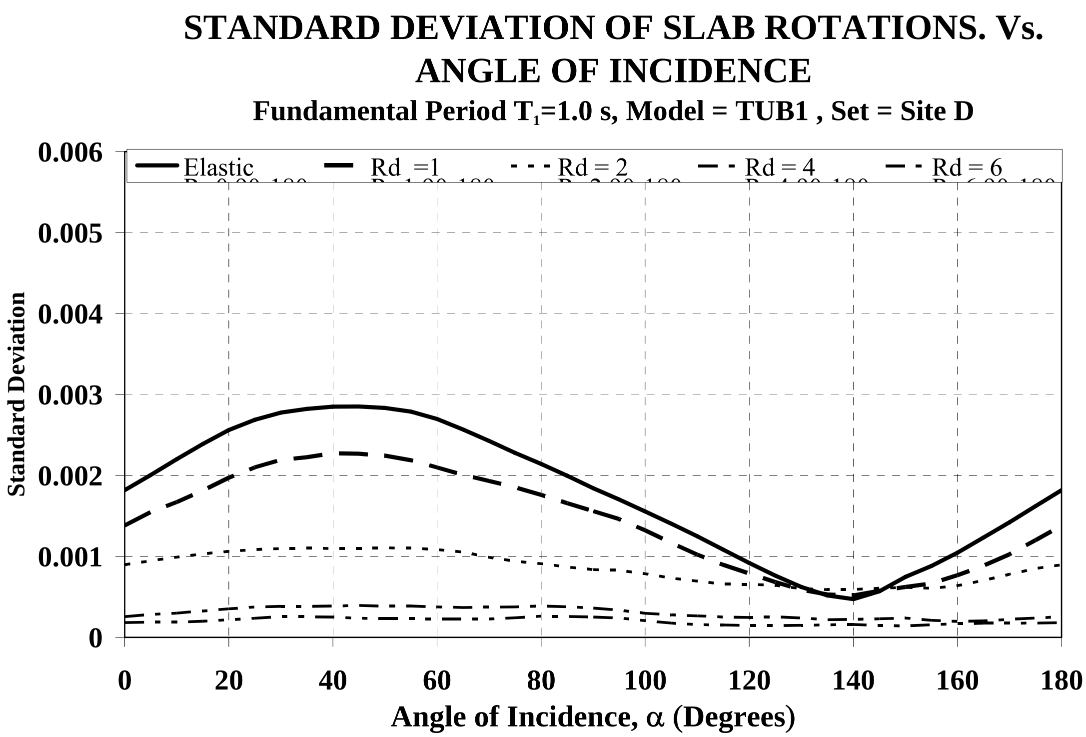

Figure 5.22 Standard deviation of slab rotations and their dependence on angle of incidence at fundamental period of 1.0 s for the model TUB1

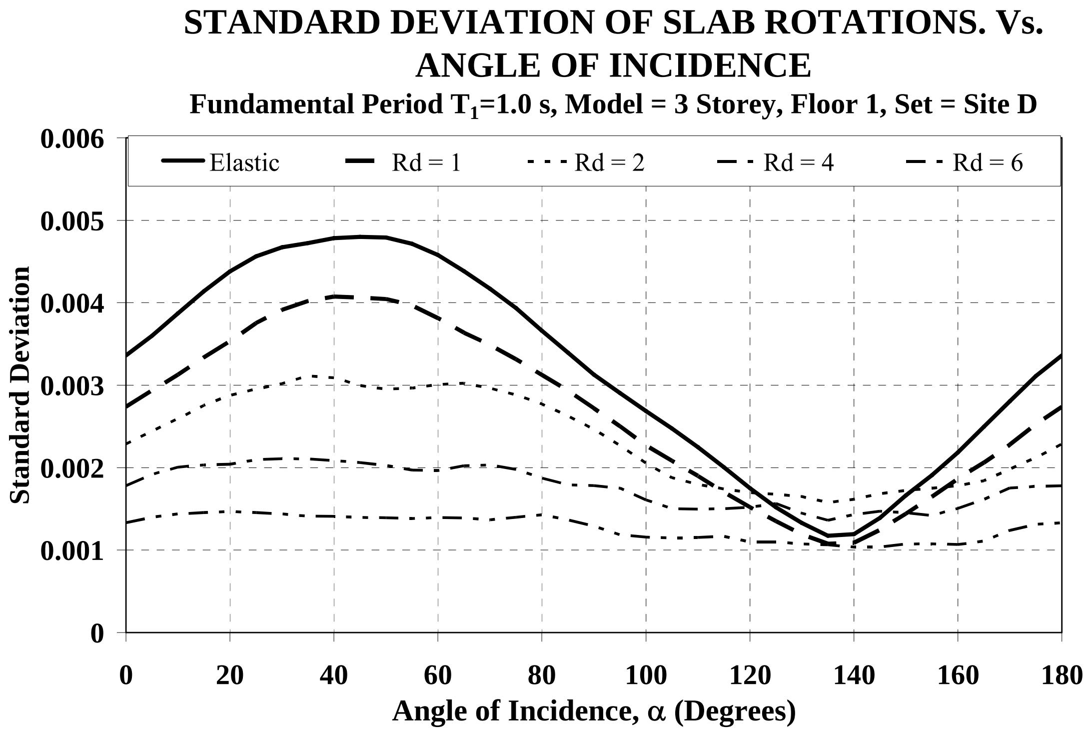

Figure 5.23 Standard deviation of slab rotations and their dependence on angle of incidence at fundamental period of 1.0 s for the 3-storey model

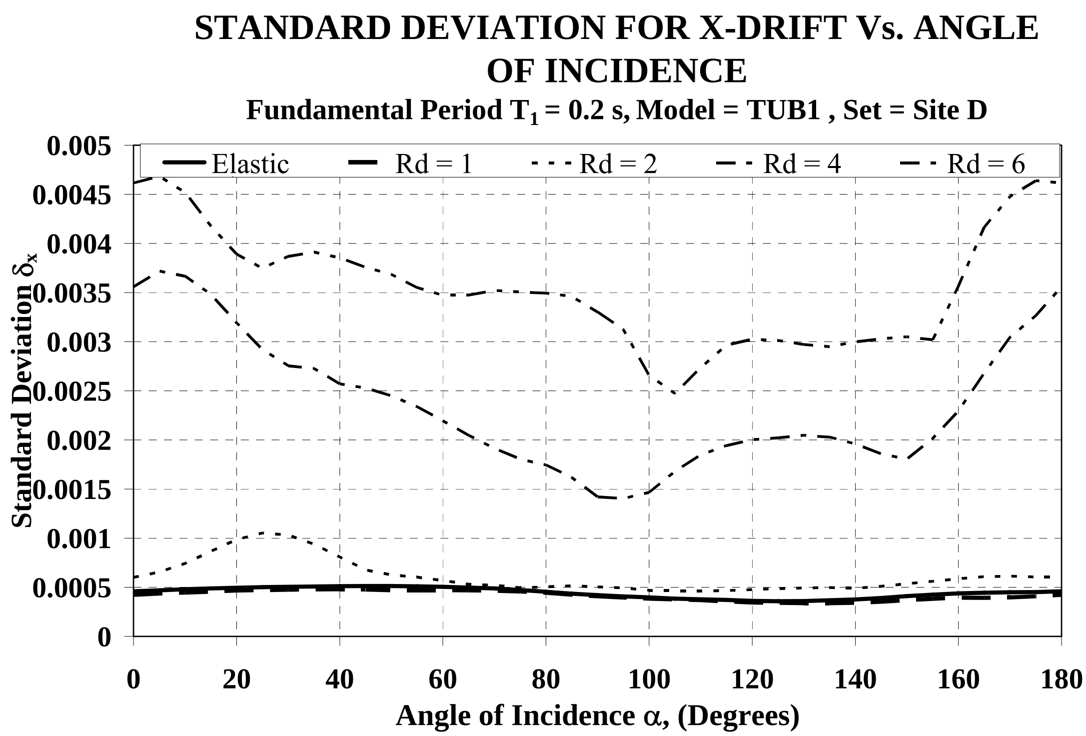

Figure 5.24 Standard deviation of X-drift and its dependence on angle of incidence at fundamental period of 0.2 s for Model TUB1

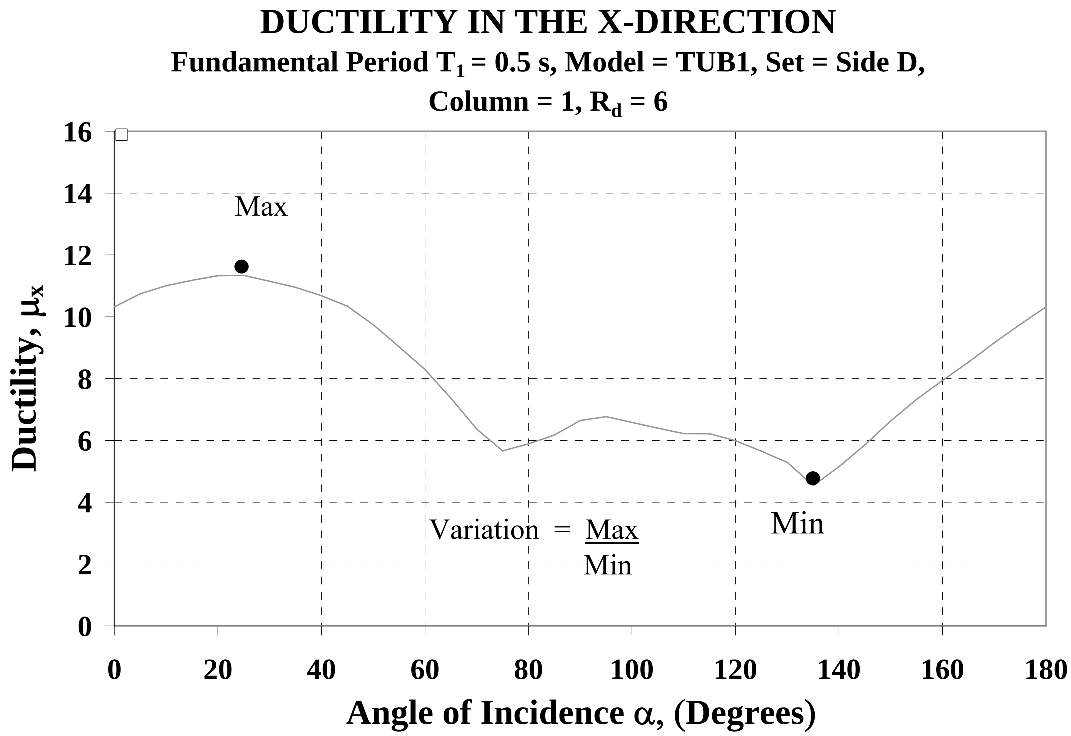

Figure 5.25 Definition of variation with regards to angle of incidence

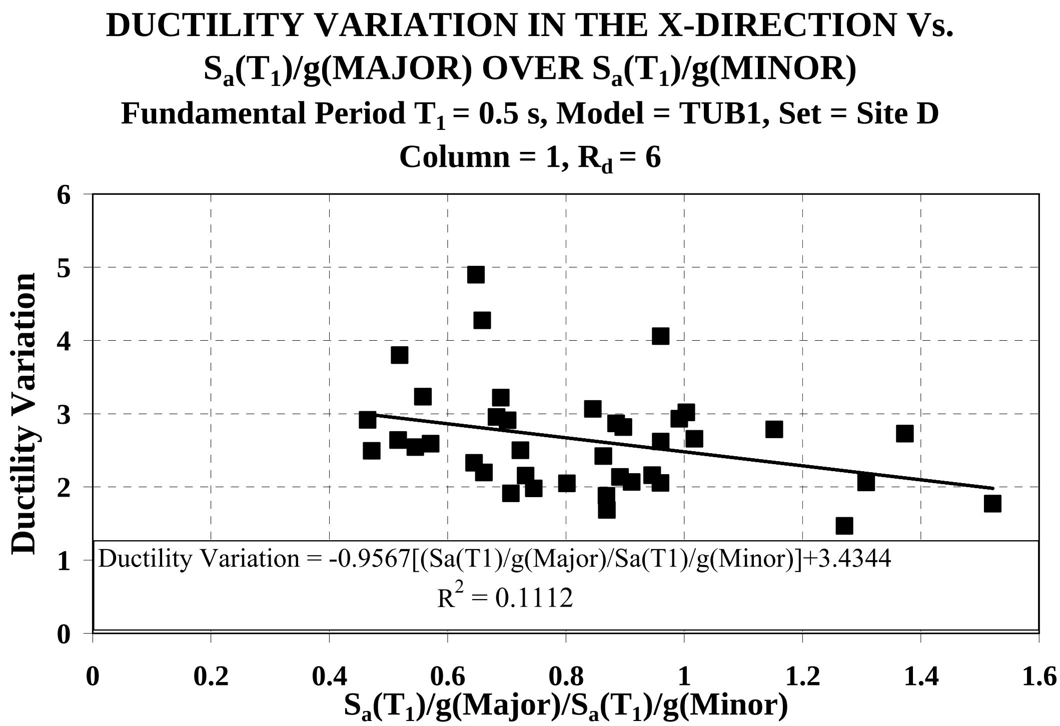

Figure 5.26 Dependence of the variation in column 1 ductility demands in the X-directions on the ratio of the major component and minor component ground motion input with a fitted linear model at a fundamental period of 0.5 s for Model TUB1

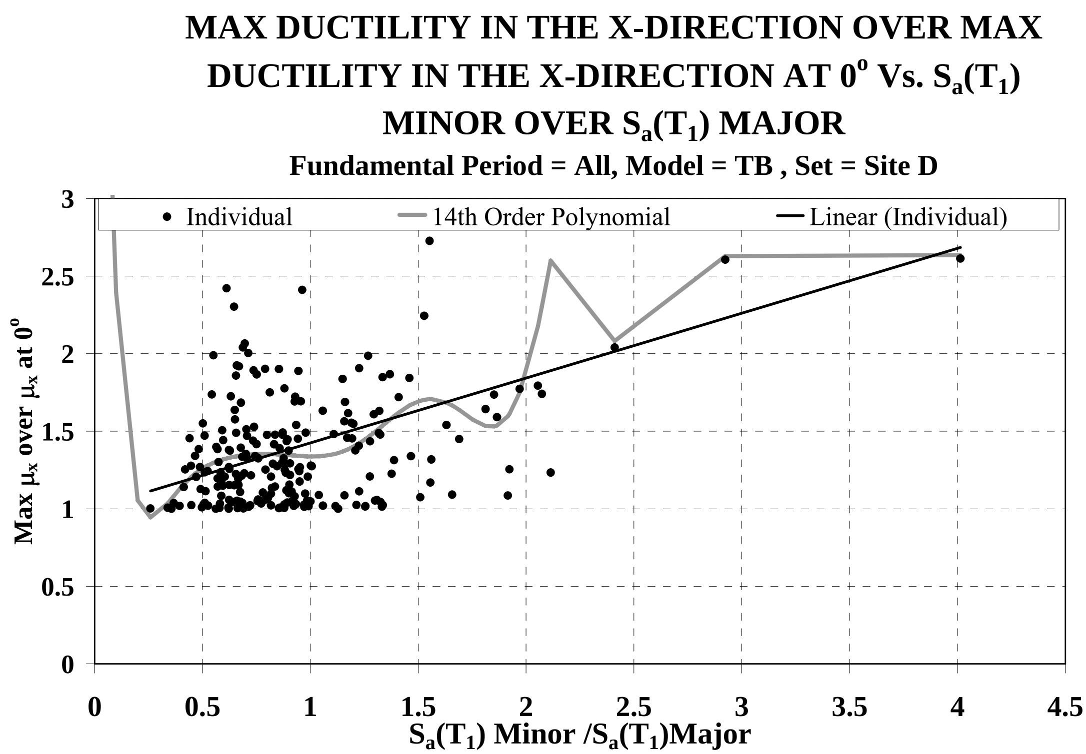

Figure 5.27 Dependence of *Max μ_x/Max μ_{x0}* vs. the ratio of the minor component and major component ground motion input along with fitted linear model and nonlinear model.

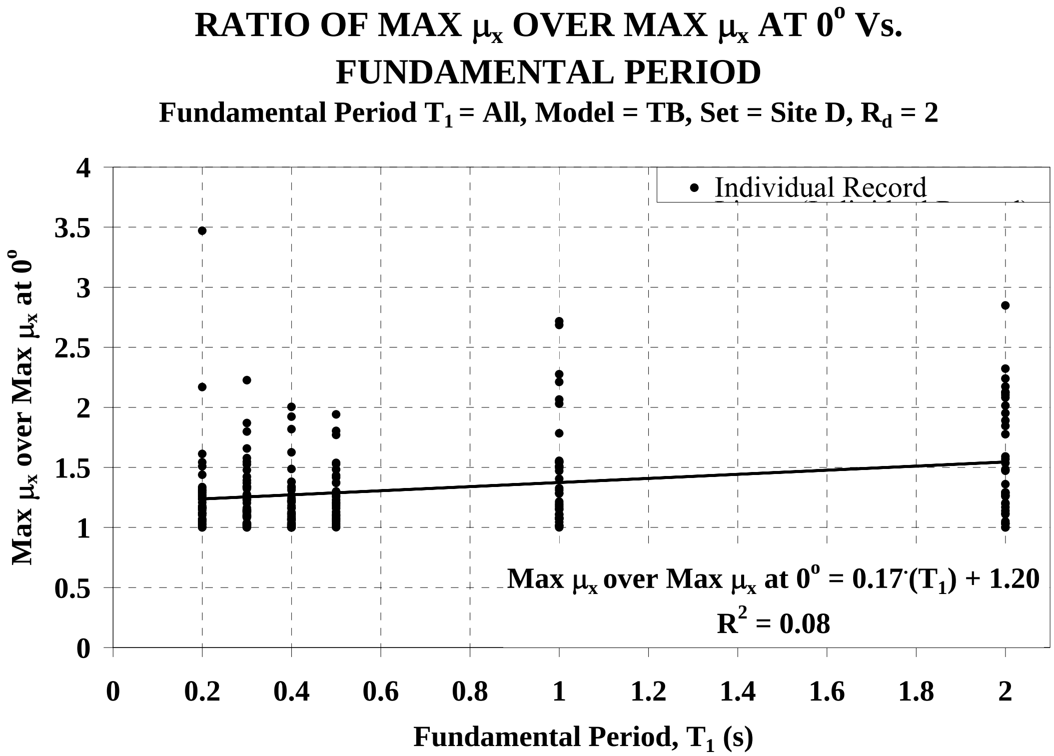

Figure 5.28 Dependence of $Max\ \mu_x/Max\ \mu_{x0}$ on fundamental period for model TB for R_d =2

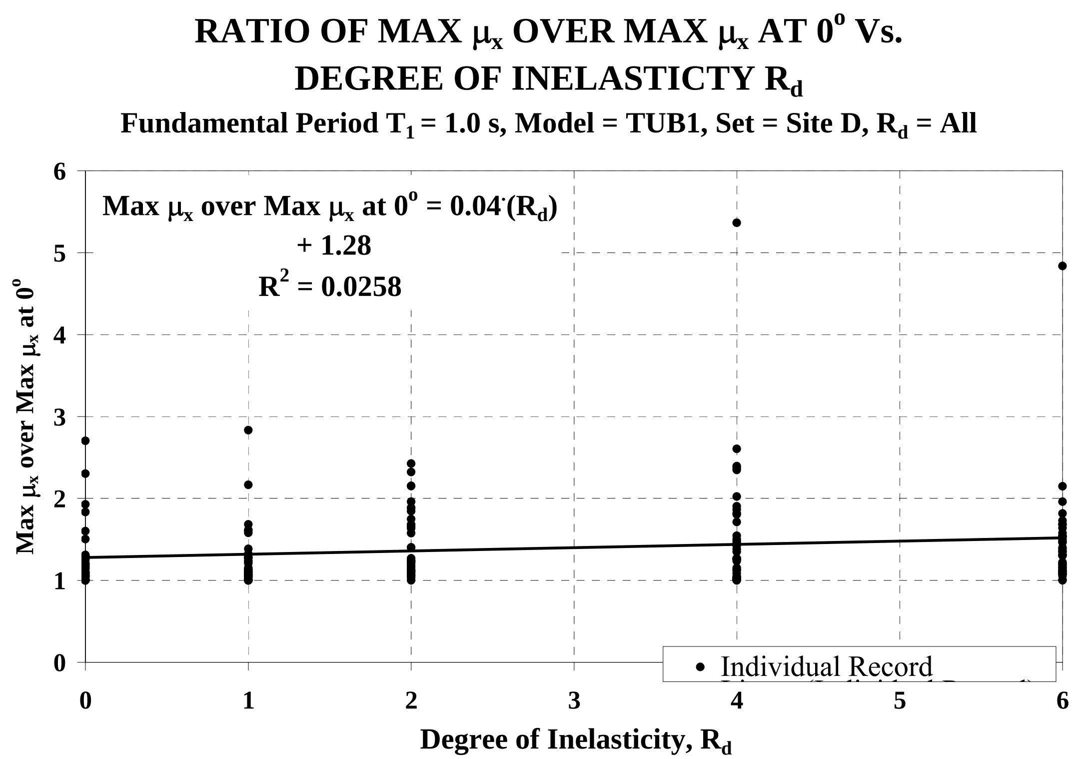

Figure 5.29 Dependence of $Max\ \mu_x/Max\ \mu_{x0}$ on R_d for model TUB1 for a fundamental period of 1.0 s

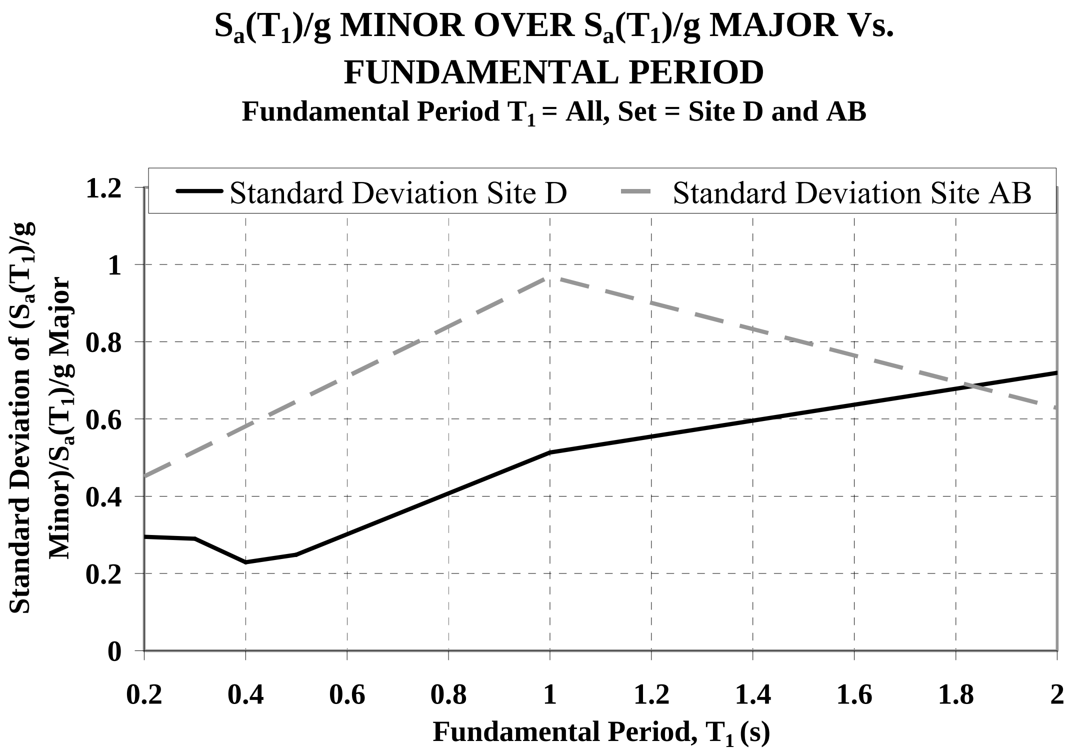

Figure 5.30 Dependence of standard deviations of $S_a(T_1)/g$ (minor)/ $S_a(T_1)/g$ (major) on fundamental period

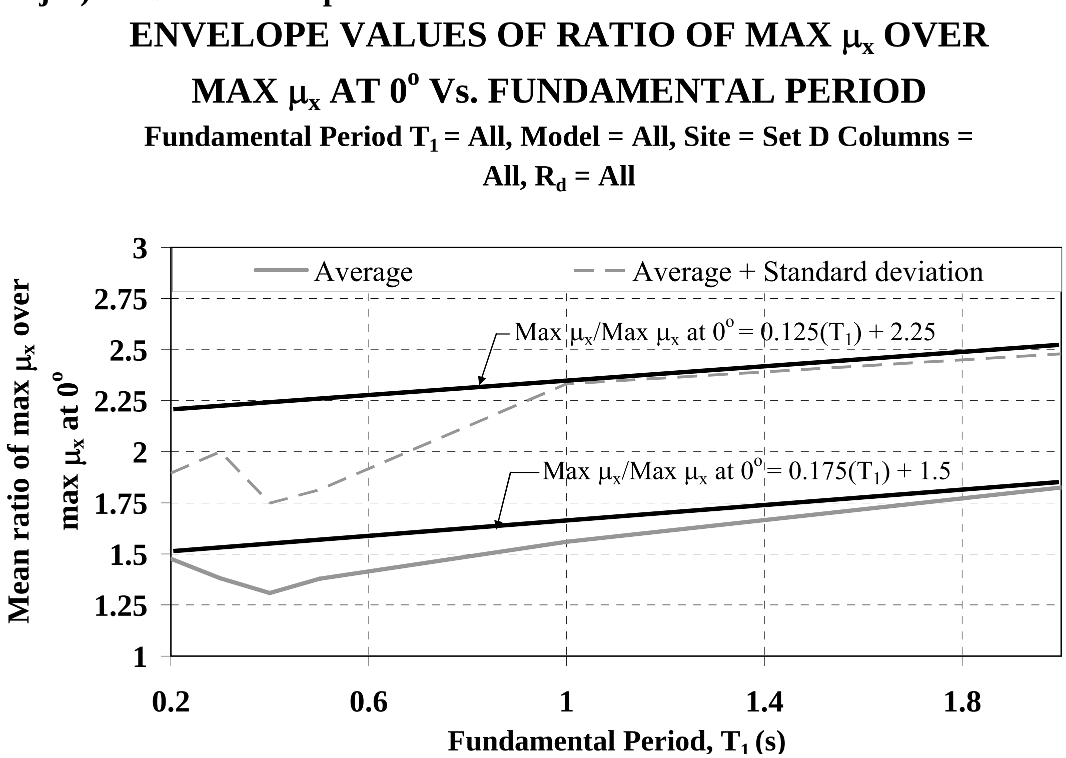

Figure 5.31 Envelope values of *Max μ_x/Max μ_{x0}* as a function of fundamental period

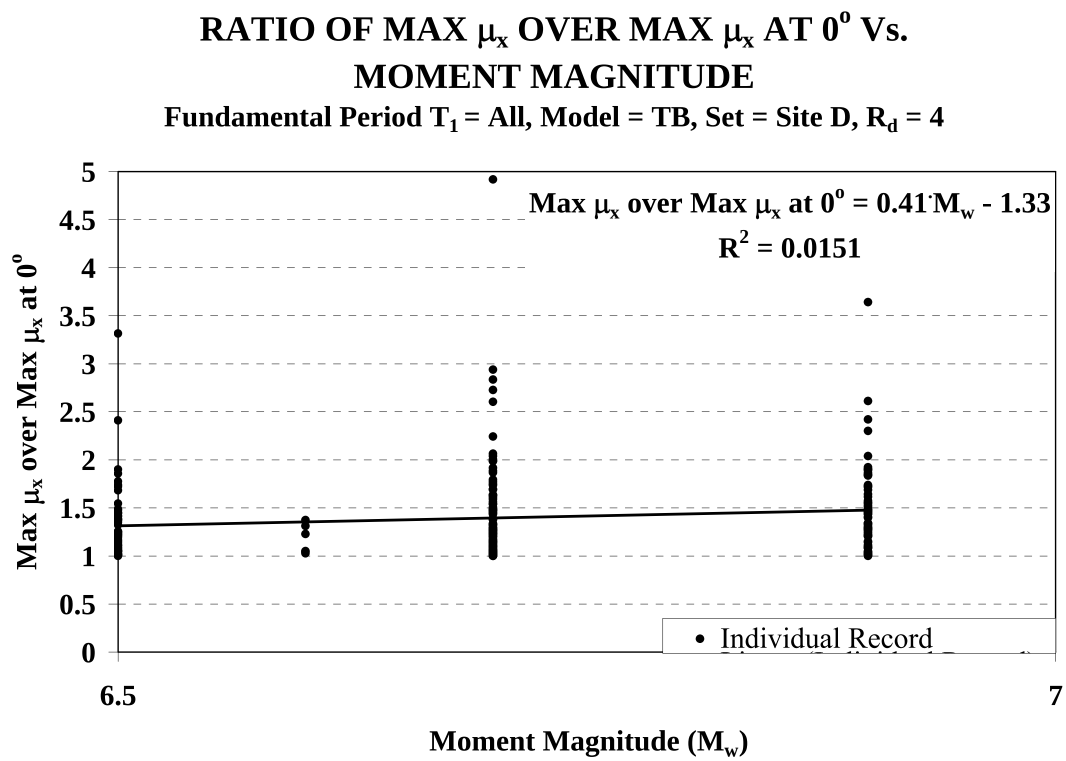

Figure 5.32 Dependence of $Max\ \mu_x/Max\ \mu_{x0}$ on moment magnitude for all fundamental periods and R_d = 4 model TB

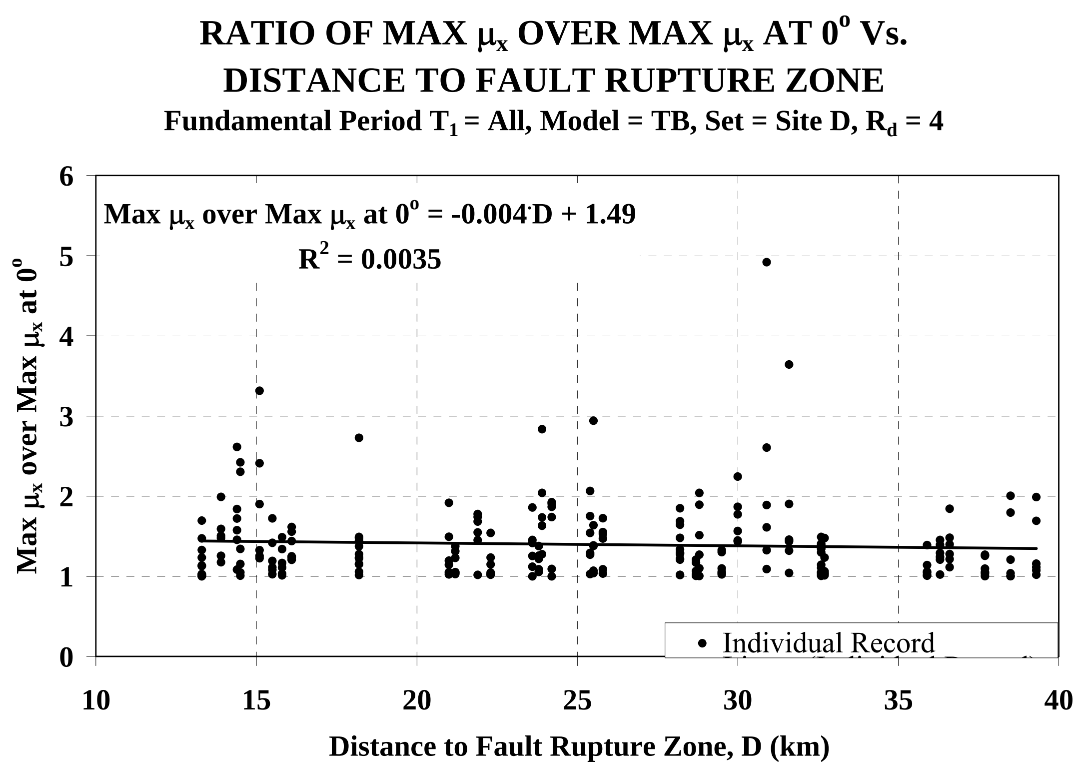

Figure 5.33 Dependence of $Max\ \mu_x/Max\ \mu_{x0}$ on distance to fault rupture zone for all fundamental periods and R_d = 4 model TB

Chapter 6 Summary and Conclusions

This work included systematic studies that investigate the influence of angle of incidence as a function of ground motion input, structural configuration, and fundamental period for primarily *inelastic* structural response. In particular, four types of single-storey structures were examined; one with off centered mass allowing torsional effects to be generated within the structure, model TUB1; one with no torsion, model TB; another model that exhibited co-centric strength and rigidity which were offset relative to the center of mass, model TUB2; and finally the balanced condition (model TUB3), where the center of strength was opposite of the center of rigidity relative to the center of mass which lied between the two. The 3-storey structure examined in this study was an extension of model TUB1 where each floor had the same amount of offset mass located at the same distance from the geometric center of the structure. Regarding the ground motion input, 39 pairs of horizontal components of bilateral non-near fault ground motions recorded on NEHERP site class D (stiff soil) were examined as well as 37 pairs of horizontal components of bilateral non-near fault ground motions recorded on NEHERP site class AB (rock) in addition to preliminary investigations that utilized a near-fault ground motion suite. A total of 5 degrees of inelasticity were utilized, and nonlinear time histories were conducted at 5^{o} increments with respect to the principal building orientation.

The goal of this study was to examine the effect that ground motion angle of incidence had on the response of several EDPs for the aforementioned structures with varying parameters as compared to ground motions applied at the principal building orientations. In general, the critical angle occurred when seismic loads were applied at orientations other than along the principal ones. Several conclusions were made and are summarized as follows:

- Although several parameters were examined such as fundamental period, degree of inelasticity, building configuration and ground motion frequency content, the majority of the models tended to exhibit the same behavior regardless of the EDP examined. Specifically, with respect to angle of incidence, the behavior of the mean of average ductility, mean of average drift and average slab rotations tended to vary mildly with angle of incidence and were not affected greatly by say, fundamental period or the amount of mass in the system. However, upper bound maximum values were slightly more sensitive to angle of incidence, while individual responses tended to be much more sensitive to angle of incidence. More realistic structures in previous work also exhibited individual ground motion sensitivity for a handful of records confirming that this phenomenon was not bound to generic models used in this work. On average, the same demands can be expected regardless of the angle of incidence of the seismic loads but when considered individually can vary greatly.

- On average, the ratio of $Max\ \mu_x/Max\ \mu_{x0}$ was a function of the ground motion suite and specifically the ratio $S_a(T_1)/g$ (minor component)/ $S_a(T_1)/g$ (major component) for a given fundamental period. The ratios of *Max* μ_x/*Max* μ_{x0} were also found to be weakly correlated to fundamental period (correlation coefficients from 0.1 to 0.4) and degree of inelasticity (correlation coefficients from 0.1 to 0.4) but correlated more strongly with $S_a(T_1)/g$ (minor component)/ $S_a(T_1)/g$ (major component). Little to no correlation was found with regards to moment magnitude and distance to fault rupture zone and the ratio of *Max* μ_x/*Max* μ_{x0}. The trends of this ratio are best anticipated by $S_a(T_1)/g$ (minor component)/ $S_a(T_1)/g$ (major component), followed by fundamental period and R_d. Moment magnitude and fault rupture distance need not be considered since they correlate poorly with the ratio of *Max* μ_x/*Max* μ_{x0} which has the potential to facilitate the analyses, as well as the record selection process as part of probabilistic seismic demand evaluation studies based on this ratio.

Standard deviations of *Max* μ_x/*Max* μ_{x0} correlated very well to the standard deviations of $S_a(T_1)/g$ (minor)/ $S_a(T_1)/g$ (major) allowing estimates of standard deviations of *Max* μ_x/*Max* μ_{x0} to be made prior to any analysis for low degrees of inelasticity based on spectral information only. Suggested envelope values of the average *Max* μ_x/*Max* μ_{x0} ratios varies from 1.5 to 1.85 while the average values plus a standard deviation varied from 2.25 to 2.5.

- Maximum ductility demand at any angle to the maximum ductility demand obtained at principal building orientation tended to be 10-80% greater than the demand based on the principal building orientation showing that on average, critical response typically occurred for ground motions that are applied at angles other than the principal building orientation for inelastic structures. The implication is that designs based on the principal building orientation alone tend to give non-conservative results. Indeed, individual responses were as much as 500% greater than those obtained at the principal building orientation. Confirmed by work with more “realistic” structures by Franklin and Volker (Franklin and Volker 1982) and Athanatopoulou (Athanatopoulou 2005), demands at angles of incidence not coinciding with the principal orientation had the largest critical response. Additionally, performance based damage assessment conveyed via fragilities indicated that the analysis should not rely only on ground motion angles of incidence that coincide with the principal building orientations.

- Critical response was found to occur at virtually any angle. The angles at which individual responses occur are quite dependent on the degree of inelasticity examined, but with no discernable pattern. Previous work by Franklin and Volker (Franklin and Volker 1982) and Athanatopoulou (Athanatopoulou 2005) analyzed more “realistic” structures for a single ground motion and illustrated that EDPs generally do not obtain maximums at the same angle of incidence, where this work observed the same occurrence for many ground motions. Regardless of the site and building configuration, trade-offs must be made regarding the minimization of demands in the design process when angle of incidence is considered.

- Contrary to previous research, the "balanced condition", the structural configuration with center of strength and rigidity at opposing locations with respect to the center of mass, on average, does not always induce smaller torsional demands when compared to a structural configuration with a similar moment arm.

- The ratio of inelastic slab rotations to elastic slab rotations tended to decrease with increasing fundamental period which was due to the shift that the center of rigidity underwent in a model when a pair of columns yielded, and was a function of the response spectra in the region after the initial fundamental period of the structure. Specifically, for a given fundamental period, if a column pair yielded during a time history analysis the distance (moment arm) from the center of mass and center of rigidity increased, which could induce larger slab rotations assuming the ground motion spectra beyond this fundamental period was also non-decreasing. If the ground motion spectra decreased however, slab rotations may decrease despite an increased moment arm. Increasing the degree of inelasticity for a given fundamental period further reduced slab rotations by as much as 65% for longer fundamental periods. If inelastic slab rotation demands are of concern, increasing the fundamental period of the structure or increasing the degree of inelasticity will reduce them.

- Generally speaking, the trends observed for the $R_d = 1$ case with respect to ratios of $Max\ \mu_x/Max\ \mu_{x0}$ provided an approximate measure of how this ratio will behave for inelastic demands as a function of fundamental period. Other trends for higher degrees of inelasticity regarding the EDPs examined generally could be approximated by the elastic case, however, the same could not be said with regards to standard deviations of those EDPs since they were sensitive to the degree of inelasticity. Trends of inelastic demands for the EDPs examined and *Max* μ_x/*Max* μ_{x0}, can be determined by a preliminary analysis with a small degree of inelasticity.

From this point, several paths could be taken in advancing this topic beyond its present state. Clearly, model restrictions such as P-delta and gravity loads moments could be lifted, while other material models that include degradation say, could be employed. The critical angle for a structure with such behavior might very well be different than without, and perhaps new trends may arise. With regards to the ground motion input, a 3rd component (vertical) could also be employed. Research that could further improve the estimation of the inelastic period of the structure for a given ground motion and degree of inelasticity would be of great interest for extending this work. This is so, given that the ratio of $S_a\,(T_1)/g$ (minor component)/ $S_a\,(T_1)/g$ (major component) which correlated best to *Max* μ_x/*Max* μ_{x0}, used in this work assumed the structure was *elastic*. A ratio such as $S_a\,(T_1)/g$ (minor component)/ $S_a\,(T_1)/g$ (major component) based on *inelastic* building periods might further improve the correlation of *Max* μ_x/*Max* μ_{x0} to $S_a\,(T_1)/g$ (minor component)/ $S_a\,(T_1)/g$ (major component). This perhaps would allow better demand predictions to be made relative to the principal orientation *a priori* for higher degrees of inelasticity. Of course, such estimates of inelastic period have to be relatively quick and easy to employ in order to reap the benefits of additional analyses. While this work dealt primarily with the demands of the structure itself, with respect to angle of incidence of the ground motions, a natural extension could possibly lend itself to building contents which may also be sensitive to angle of incidence.

Bibliography

Athanatopoulou, AM. Critical orientation of three seismic components. *Engineering Structures* 2005;27:301-312.

Aziminejad, A. Moghadam, AS. Behavior of asymmetric structures in near field ground motions. *Conference on Earthquake Engineering 2006*;Sept 3-8, Geneva, Switzerland, paper 399.

Bertero, R. Inelastic torsion for preliminary seismic design. *Journal of Structural Engineering* 1995;Vol 121, No. 8, Nov. pp. 1183-1189.

Chandler AM., Correnza JC. and Hutchinson GL. Seismic torsional provisions: Influence on element energy dissipation. *Journal of Structural Engineering* 1996;Vol 122, No. 5, May. pp. 494-500.

Chopra AK. *Dynamics of Structures: Theory and Applications to Earthquake Engineering*; 1st Edition. Prentice Hall: New Jersey 1995.

Clough RW. and Penzien J. *Dynamics of Structures,* 2nd Edition. McGraw Hill: Singapore 1993.

CSI. *SAP2000,* Computers and Structures Inc., Berkely, California.

Hyams D. G. *Curve Expert1.3* http://www.ebicom.net/~dhyams/cmain.htm, 1997

De-La-Colina, J. Effects of torsion factors on simple non-linear systems using fully bidirectional analyses. *Earthquake Engineering and Structural Dynamics* 1999;28: 691-706.

Donaldson B. K. *Introduction to Structural Dynamics,* 1st Edition. Cambridge University Press. New York 2006.

Fajfar, P., Marusic D., and Perus I. Influence of ground motion intensity on the inelastic torsional response of asymmetric buildings. 13th *World Conference on Earthquake Engineering.* 2004, Vancouver, Canada Aug 1-6, Paper 3496.

Fernandez-Davilla I., Cominetti S. and Cruz E.F. Considering the Bi-Direcional effects and the seismic angle variations in building design. 12th *World Conference on Earthquake Engineering.* 2000, Auckland, New Zealand Jan 30-Feb 4 Paper 0435.

Franklin CY, and Volker JA. Effect of various 3-D seismic input directions on inelastic building systems based on INRESB-3D-82 Computer Program. *Proceedings of the Seventh European Conference on Earthquake Engineering* 1982;Sept 20-25, Athens, Greece.

Fu Q. Modeling and prediction of fault-normal near-field ground motions and structural response. Department of Civil and Environmental Engineering. Stanford, CA, Stanford University. Doctoral Dissertation. 2005.

Ghersi, A. Rossi, PP. Influence of bi-directional ground motions on the inelastic response of one-storey in-plan irregular systems. *Engineering Structures* 2001;23:579-91.

Goel, RK. Seismic response of asymmetric systems: energy approach. *Journal of Structural Engineering* 1997;Vol 123, No. 11, Nov. pp. 1444-53.

Goel, RK and Chopra AK. Period Formulas for Moment-Resisting Frame Buildings. *Journal of Structural Engineering* 1997;Vol 123, No. 11, Nov. pp. 1454-1461.

Goel RK. Simplified analysis of asymmetric structures with supplemental damping. *Earthquake Engineering and Structural Dynamics* 2001:30:1399-1416.

Humar, JL. Kumar, P. Effect of orthogonal inplane structural elements on inelastic torsional response, *Earthquake Engineering and Structural Dynamics* 1999**;**28:1071-97.

ICC (2006). *International Building Code* (IBC-06) Whittier (CA); 2006 p. 663. International Code Council.

Khoshnoudian F., and Poursha M. Responses of three dimensional buildings under bi-directional and unidirectional seismic excitations. *Proceedings of the thirteenth World Conference on Earthquake Engineering 2004*;Aug 1-6 Vancouver, Canada.

Kramer SL. *Geotechnical Earthquake Engineering*; 3rd Edition. Pearson Education 1996.

Luco N. Probabilistic seismic demand analysis, smrf connections fractures, and near-source effects. Department of Civil and Environmental Engineering. Stanford, CA, Stanford University. Doctoral Dissertation. 2002.

Lopez, OA, Chopra, AK, Hernandez JJ. Critical response of structures to multi-component earthquake excitation. *Earthquake Engineering and Structural Dynamics* 2000;29:1759-78.

Lopez, OA, Torres R. The critical angle of seismic incidence and structural response. *Earthquake Engineering and Structural Dynamics* 1997;26:881-94.

Marusic D., I. Fajfar, P. On the inelastic torsional response of asymmetric buildings under bi-axial excitation. *Earthquake Engineering and Structural Dynamics* 2005;34:943-963.

MacRae, GA. Mattheis J. Three-dimensional steel building response to near-fault motions, *ASCE Journal of Structural Engineering* 2000;Vol 126, No 1, Jan. pp. 117-26.

Medina RA, Krawinkler H. Seismic demands for non-deteriorating frame structures and their dependence on ground motions. *PEER Report 2003/15*. Berkeley (CA): Pacific Earthquake Engineering Research Center; 2004.

Myslimaj, B. and Tso WK. A strength distribution criterion for minimizing torsional response of asymmetric wall-type systems. *Earthquake Engineering and Structural Dynamics* 2002:31:99-120.

Myslimaj, B. and Tso WK. A yield displacement distribution-based approach for strength assignment to lateral force-resisting elements having strength dependent stiffness. *Earthquake Engineering and Structural Dynamics* 2003:32:2319-2351.

Myslimaj, B. and Tso WK. A design-oriented approach to strength distribution in single-story asymmetric systems with elements having strength-dependent stiffness. *Earthquake Spectra* 2005;Vol 21, No. 1:197-212.

Myslimaj, B. and Tso WK. Response to: Discussion of: A design-oriented approach to strength distribution in single-story asymmetric systems with elements having strength-dependent stiffness. *Earthquake Spectra* 2005;Vol 21, No. 3:897-899.

Paulay T. Torsional mechanisms in ductile building systems. *Earthquake Engineering and Structural Dynamics* 1998; 27:1101-1121.

Paulay, T. Discussion of: A design-oriented approach to strength distribution in single-story asymmetric systems with elements having strength-dependent stiffness. *Earthquake Spectra* 2005;Vol 21, No. 3:893-895.

Paz M. and Leigh W. *Structural Dynamics: Theory and Computation.* 5th Edition. Kluwer Academic Publishers: Massachusetts 2004.

Penzien J. and Watabe. Characteristics of 3-dimensional earthquake ground motions. *Earthquake Engineering and Structural Dynamics* 1975;3:365-364.

Perus, I. Fajfar, P. On the inelastic torsional response of single-storey structures under bi-axial excitation. *Earthquake Engineering and Structural Dynamics* 2005;34:931-41.

Rigato, A. and Medina RA. Influence of angle of incidence on seismic demands for inelastic single-storey structures subjected to bi-directional ground motions. *Engineering Structures* 2007 Article in press.

Singh, P. and Singh G. On critical earthquake direction and treatment of accidental torsional response in 3D frame analysis. *Bulletin of the Indian Society of Earthquake technology*, 1992 Vol 29, No. 4, Dec. pp. 37-52.

Somerville, PG. (2003). Magnitude scaling of the near fault rupture directivity pulse. *Physics of the Earth and Planetary Interiors.* 137(1-4) pp. 201-212.

Somerville PG., Smith NF.Graves RW. And Abrahamson NA. Modifcation of empirical strong ground motion attenuation relations to include the amplitude and duration effects of rupture directivity. Seismological Research Letters 1997. 68(1):199-222

Stathopoulos and Anagnostopoulos SA. Inelastic torsion of multistory buildings under earthquake excitations. *Earthquake Engineering and Structural Dynamics* 2005;34:1449-1465.

Stathopoulos and Anagnostopoulos SA. Inelastic earthquake response of single-storey asymmetric buildings: an assessment of simplified shear-beam models.. *Earthquake Engineering and Structural Dynamics* 2003; 32:1813-1831.

Tezcan, SS. Alhan, C. Parametric analysis of irregular structures under seismic loading according to the new Turkish Earthquake Code. *Engineering Structures* 2001;23:600-9.

Tso, W. K. Smith, RSH. Re-evaluation of seismic tensional provisions. *Earthquake Engineering and Structural Dynamics* 1999;28: 899-917.

Wilson E.L. and M. Button, Three dimensional dynamic analysis for multi-component earthquake spectra. *Earthquake Engineering and Structural Dynamics* 1982;10:471-476.

Wilson E.L., Suhawardy I. and Habibullah A., A clarification of the orthogonal effects in a three-dimensional seismic analysis. *Earthquake Spectra* 1995;11:659-666.